N-HETEROCYCLIC CARBENES: STUDIES IN METALLATION, LIGAND MODIFICATION, AND PROPERTY DETERMINATION

A Thesis Submitted to the Committee on Graduate Studies
in Partial Fulfilment of the Requirements for the Degree of Master of Science
in the Faculty of Arts and Science.

TRENT UNIVERSITY

Peterborough, Ontario, Canada

Materials Science M.Sc. Graduate Program

January 2025

ABSTRACT

N-Heterocyclic Carbenes: Studies in Metallation, Ligand Modification, and Property Determination

Meilin Quiape Lim

N-Heterocyclic Carbenes (NHCs) have significantly impacted organometallic chemistry as ligands in transition metal catalysis, offering strong electron-donating properties and high bond dissociation energies. However, their structural versatility is limited by the scarcity of commercial precursors and challenging modification procedures. Furthermore, we have investigated its coordination to transition metals; copper, silver, and palladium. We further demonstrate the effects of its steric parameters by utilizing the Suzuki-Miyaura cross-coupling of aryl chlorides using [(RO-NHC)Pd(allyl)Cl] as precatalysts. This study demonstrates increased catalyst activity with bulkier ligands in Suzuki-Miyaura cross-coupling reactions. We also present simplified procedures for copper NHC complexes using triethylamine with no requirements for special equipment and techniques. Preliminary investigations towards a more economical approach to measuring the electron donating abilities of NHCs were conducted using Cu^{I} and Ag^{I} cyanide complexes as probes. The outcomes of this research may contribute to the growing research in the applications of NHCs as ligands in catalysis.

Acknowledgements

First and foremost, I would like to express my deepest gratitude to my supervisor, Dr. Eric Keske, for their continuous support, guidance, and encouragement throughout my research. Their invaluable advice and insights have been instrumental in the completion of this thesis.

I am also deeply grateful to my committee members, Dr. Andrew Vreugdenhil and Dr. Olena Zenkina for their time, effort, and constructive feedback, which greatly enhanced the quality of my work. I would like to thank Dr. Cathleen Crudden and again, Dr. Olena Zenkina for your NMR support.

A special thank you goes to my current colleagues and lab mates, Eric Fortin and Sterling Renzoni, for the stimulating discussions and for the long hours we spent in the lab together. Your support and friendship have made this journey a memorable one. Eric, thanks for the incredibly interesting music in the lab and Sterling, thanks for the debates and for helping me with mechanisms.

I would like to thank the former Keske members, Erin Cole, Hannah Girard, Nathalie Mapue, Eric Lind, Armaan Grewal, and Kasandra Brick. Every single one of you has made my experience at Trent exponentially better and for that I am so grateful to have worked with you.

I am also thankful to the Trent Chemistry Department for the stimulating conversations, the cat pictures, and for summer volleyball sessions.

On a personal note, I wish to thank my family and to my partner for their unwavering support and belief in me. I could not have completed this journey without your support.

Lastly, I want to extend my gratitude to all my friends and everyone else who supported me in any way during this journey. I would very much like to thank diet Coke for getting me through this rigorous writing process. Special thanks to Britney Spears and Halsey (specifically the Badlands album).

Table of Contents

List of Schemes

List of Figures

List of Tables

List of Abbreviations

acac	acetylacetonate
Ar	Aryl
BDE	Bond dissociation energy
Bu	butyl
°C	Celsius
CH_2Cl_2	Dichloromethane
COD	1,5-cyclooctadiene
Cp	cyclopentadienyl
DMF	Dimethylformamide
Equiv.	equivalent(s)
ESI-TOF	electrospray ionization
Et	Ethyl
EtOAc	Ethyl Acetate
EtOH	Ethanol
GC-MS	Gas Chromatography – Mass Spectrometry
HEP	Huynh electronic parameter
hr	hour(s)
HRMS	high-resolution mass spectrometry
Hz	hertz
IMes	1,3-*bis*(2,4,6-trimethylphenyl)imidazol-2-ylidene
iPr	isopropyl
IPr	1,3-*bis*(2,6-diisopropylphenyl)imidazol-2-ylidene

IPr*	1,3-*bis*(2,6-bis(diphenylmethyl)-4-methylphenyl)imidazo-2-ylidene
IR	Infrared spectroscopy
J	Coupling constant
KO^{t}Bu	Potassium tert-butoxide
LEP	Lever electronic parameter
LRMS	low-resolution mass spectrometry
Me	methyl
MeCN	acetonitrile
MeOH	Methanol
NaHMDS	Sodium *bis*(trimethylsilyl)amide
NEt_3	triethylamine
NHC	N-heterocyclic Carbenes
NMR	Nuclear Magnetic Resonance Spectroscopy
Ph	phenyl
PEPPSI	Pyridine Enhanced Precatalyst Preparation Stabilization and Initiation
Pr	propyl
ppm	parts per million
r.t.	room temperature
SIDEP	Saturated Imidazolium Diethoxyphenyl
SIDiPP	Saturated Imidazolium Diisopropoxyphenyl
SIDMP	Saturated Imidazolium Dimethoxyphenyl
SIDnBP	Saturated Imidazolium Di-*n*-butoxyphenyl
SIDnPP	Saturated Imidazolium Di-*n*-propoxyphenyl

SIMes	1,3-*bis*(2,4,6-trimethylphenyl)imidazolin-2-ylidene
SIPr	1,3-*bis*(2,6-diisopropylphenyl)imidazolin-2-ylidene
T	temperature
TEP	Tolman electronic parameter
THF	tetrahydrofuran
TLC	Thin-layer Chromatography
V_{Bur}	Volume buried

Chapter 1

Introduction to N-Heterocyclic Carbenes and Applications

1.1 Catalysis: General Background

Catalysis holds an extremely important place in chemical synthesis.[1] For decades, catalysis has revolutionized chemical reactions by offering enhanced selectivity and overall efficiency.[1] It has the capability to reduce energy barriers in reactions, facilitating fundamental processes that would otherwise be impractical or not feasible.[2] Furthermore, the development of new synthetic methodologies in catalysis can significantly reduce chemical waste, yielding substantial environmental benefits while also being cost-effective, time-saving, yield-boosting, and labor-efficient.[3] These factors have contributed to its rapid emergence and profound impact on organic chemistry.

Within the realm of catalytic reactions, transition metal catalysis has been extensively utilized in synthetic organic chemistry. In particular, the development of new ligands and the exploration of their coordination chemistry with late transition metals has been of great importance in this field.[4,5] Ligands play a crucial role in stabilizing catalytically active species, which in turn improves catalyst turnover and reduces the required catalyst loading (**Figure 1-1**).[6] Moreover, ligands can influence the chemo-,[7] regio-,[8] and enantioselectivity[9] of catalytic processes. However, there is no single ligand that is universally applicable; different catalytic reactions have different requirements. As a result, the availability of ligand diversity and modularity has become a key focus in the field of transition metal catalysis.

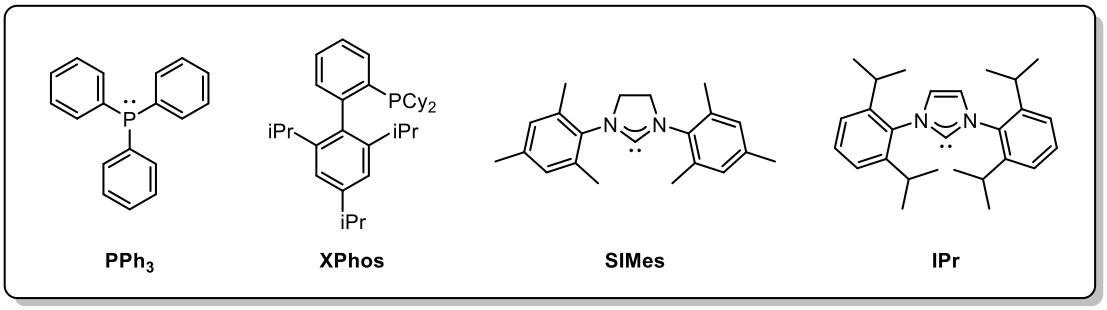

Figure 1-1: Select examples of common ligands used in transition metal catalysis

Phosphines are among the most widely used ligands in transition metal catalysis due to their tunable steric and electronic properties, as well as their ability to stabilize transition metal complexes in homogeneous catalysis (**Figure 1-1**).[10] Their popularity has led to the creation of various classes of phosphines, many of which are commercially available.[11] However, phosphines come with several limitations, including inherent toxicity and instability under oxidative conditions, which can make them challenging or potentially dangerous to work with.[12] Additionally, the general lability of their bonds to transition metals often results in reduced efficiency in catalytic reactions.

As a result, there has been significant research dedicated to improving phosphines making them more stable, more accessible, and stronger, with enhanced oxidative stability.[13,14] While the development of more active phosphine ligands continues, there has also been growing interest in other ligand classes that offer similar properties. One emerging alternative to phosphine ligands is the increasing development of N-Heterocyclic carbenes (NHCs).

1.2 N-Heterocyclic Carbenes

N-Heterocyclic carbenes (NHCs) have emerged as a pivotal class of ligands in homogeneous catalysis, renowned for their versatile reactivity and utility in a wide range of applications.[15,16] Indeed, these organometallic catalysts composed of these ligands have

revolutionized the field of homogeneous catalysis. Since the isolation of stable carbenes, the field has rapidly expanded from Bertrand and colleagues recognizing the first stable carbene in 1988,[17] followed by Arduengo *et al.* in 1991 with the first "bottle-able" free NHC.[18] NHCs have become indispensable tools in synthetic organic chemistry and transition metal catalysis.

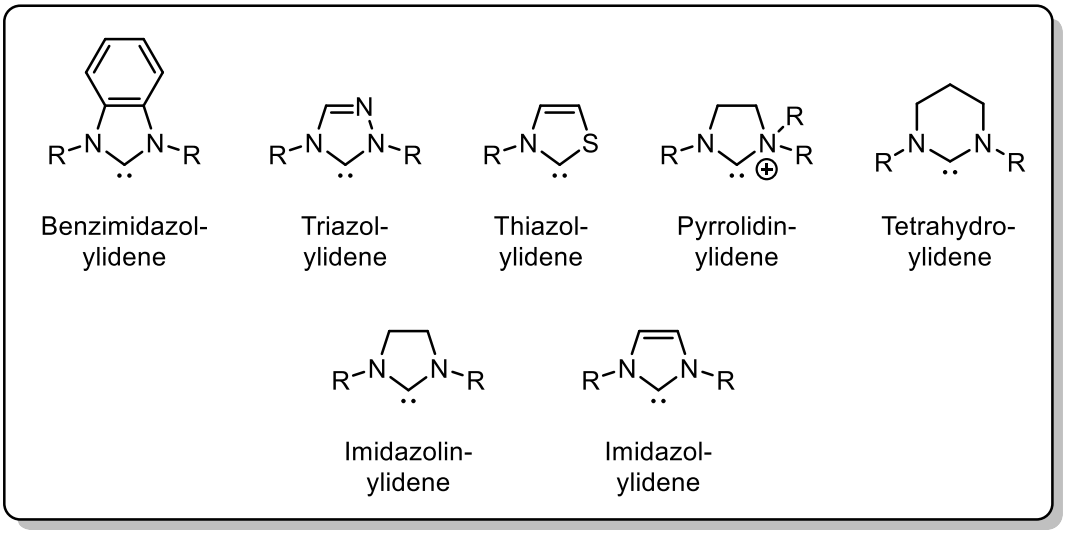

Figure 1-2: Examples of some commonly used NHC species in literature

NHCs are a class of carbenes, which are defined as divalent carbon atoms with only six valence electrons (**Figure 1-2**).[19] Carbenes are highly reactive species and typically exist as fleeting intermediates in organic chemistry with short lifetimes.[2] They can exist in either the singlet spin state or the triplet spin state depending on the substituents attached to the carbene carbon.[20] Carbenes that are stable in the singlet spin state are often flanked by electronegative substituents with donor electrons, while those stable in the triplet spin state typically have only hydrogen or alkyl groups.[2,20] Despite their inherent reactivity and instability, they make excellent ligands in homogeneous catalysis.

Initially NHCs were viewed as phosphine mimics,[21–23] but have since established their own unique identity in homogeneous catalysis. While phosphines have been common ligands in

transition metal catalysis, research over the years has sought to expand the range of ligands available for catalytic reactions.[22] Following the discovery and isolation of NHCs, they quickly attracted attention from researchers due to their distinct advantages over phosphines,[24] including increased stability of their metal complexes and reduced toxicity. NHCs possess a unique electronic structure that imparts both strong σ-donating nature and high bond dissociation energies towards transition metals.[22] This combination enables them to stabilize metal centers in a variety of oxidation states and coordinate geometries, thereby facilitating numerous catalytic processes.[25] The robustness and tunability of NHCs allows for modifications of their steric and electronic environments, making them highly adaptable for catalytic applications.[26]

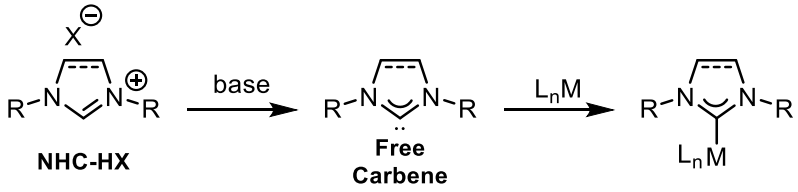

Scheme 1-1: General scheme of metallation via the free carbene route

Free NHCs are air-sensitive species however, they can be stabilized by the formation of complexes.[27] There are a number of preparative methods for synthesizing metal-NHC complexes have been reported in the literature. Typically, NHC-ligated transition metal complexes are synthesized using azolium salts (such as imidazolium, triazolium, tetrazolium, pyrazolium, benzimidazolium, oxazolium, and thiazolium salts) as precursors.[28] Most commonly NHC metal complexes are synthesized by treatment of a suitable metal complex with coordination a free NHC, activation of the azolium salt onto a metal with suitably basic ligands (such as $Pd(OAc)_2$), or transmetallation from silver.[22,26] A prominent strategy for synthesizing NHC-metal complexes is the free carbene route. In this approach, the azolium salt precursor is deprotonated with a base to generate a free carbene, which is then coordinated to a metal precursor (**Scheme 1-1**).[29] This

method often requires strong bases such as KOtBu or NaH, which are necessary for complete deprotonation, because the pKa of the azolium salt precursor typically ranges from 22 to 25.[30,31] However, there are reports of using weaker bases, such as K_2CO_3,[32] NEt_3,[33,34] or NaOAc,[35] to deprotonate the NHC salt precursors when in the presence of the metal precursor. Despite the beneficial nature of this weak base route, harsh conditions, including high temperatures and long reaction times are often required to successfully generate the metal-NHC complex. The deprotonation method has practical limitations, particularly the need for a glovebox due to the highly reactive nature of free carbenes. To overcome these challenges, alternative methods have been explored in the literature.[36]

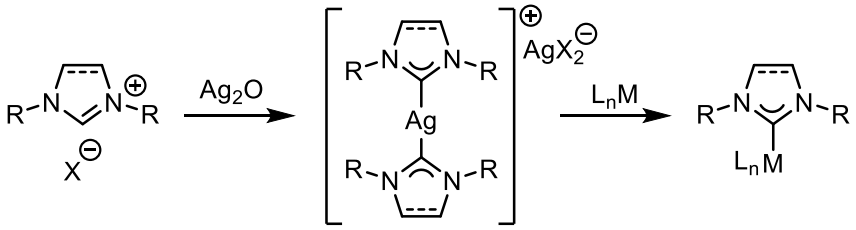

Scheme 1-2: General scheme for metallation using silver transmetallation

A prominent alternative approach is the transmetallation from silver route that was developed by Lin *et al.*,[37] which involves generating a stable Ag-NHC complex as a transfer agent. The Ag-carbene complex is synthesized by treating the azolium salt precursor with a basic silver(I) precursor, such as Ag_2O (**Scheme 1-2**).[38] Other silver precursors, including AgOAc[39] and Ag_2CO_3,[40–42] have also been used. The resulting Ag-NHC complex is then reacted with a metal precursor through a transmetallation reaction (**Scheme 1-2**).[38] The relatively labile nature of the silver-carbene complex allows this process to be effective for a variety of transition metals, such as palladium and gold. This method is convenient because it can be carried out under ambient conditions, producing a precursor that is typically stable to air and moisture. It is important to note,

however, that Ag-NHC complexes can display a wide range of complex structures, and exist in complex equilibria complicating analysis.[36] Furthermore, they are typically light sensitive. Nonetheless, the use of Ag-NHCs as transfer agents offers significant advantages, particularly when the free carbene route is not accessible.

1.3 Properties of NHCs

A highly regarded attribute of NHCs is their ability to produce electron rich metal complexes which is due to their strong σ-electron donating nature. Certain studies have been dedicated to quantifying their electron donating properties. One established method of measuring the electron donating ability of a ligand is the Tolman's electronic parameter (TEP) developed by Chadwick A. Tolman from the pioneering work of Strohmeier *et al.*[43] and Bigorgne *et al.*[44] TEP is a quantitative measurement used to describe the electronic properties of ligands, particularly with phosphines.[45] This method synthesizes a $[Ni(CO)_3(L)]$ complex as a direct probe to measure the electron donation of the ligand *trans* to the carbonyl group (**Figure 1-3**).[45] It is derived from the stretching frequency of the carbonyl group (ν_{CO}), which shifts based on the electron-donating or withdrawing nature of the attached ligand.[45] A lower TEP value indicates that the ligand is a strong electron donor (more electron-rich), which leads to greater back-donation from the metal to the carbonyl, resulting in a lower ν_{CO} stretching frequency.[45] Conversely, a higher TEP value suggests a weaker electron-donating ligand, correlating with a higher ν_{CO} frequency.[45] In 2005, Nolan and coworkers used nickel-based system to measure the electronics of a number of common bulky saturated and unsaturated NHCs to demonstrate that TEP can also work for NHC ligands.[46] Results showed that NHCs were more electron donating than even the most electron donating phosphines in Tolman's work.[46] Due to the noxious nature of the metal complex precursor, $[Ni(CO)_4]$, nickel-based probes are rarely used. The synthesis and analysis of other less toxic complex probes such

as $[IrCl(CO)_2(NHC)]$ and $[RhCl(CO)_2(NHC)]$ are preferred in recent years for the study of the electron donating properties of NHCs (**Figure 1-3**).

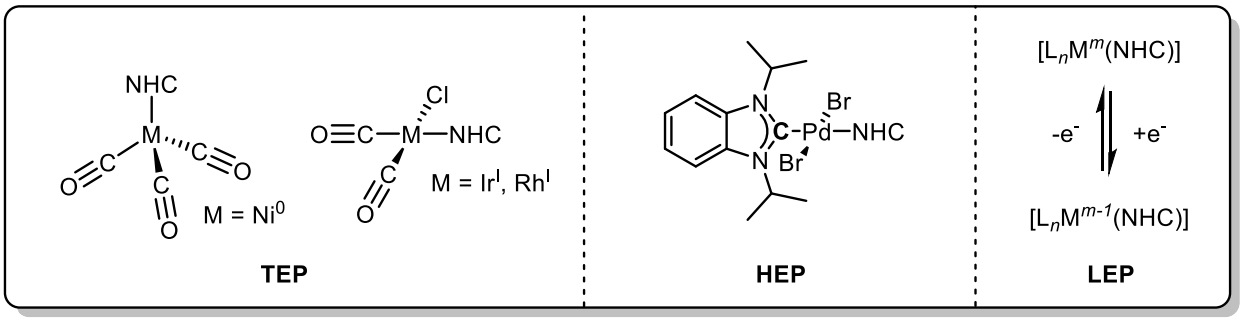

Figure 1-3: Different methods to measure electronics of NHCs in literature

Due to the high costs associated with rhodium or iridium, other avenues have also been explored in literature for studying ligand electronic properties. For example, the Hyunh electronic parameter (HEP), developed by Huynh and colleagues, utilizes the ^{13}C chemical shift of the carbene carbon of a palladium(II)-benzimidazolylidene complex probe (**Figure 1-3**).[47] This is a non-CO based system for investigations towards the electron donating properties of the NHC ligand of interest. Another useful method called Lever electronic parameter (LEP) was developed by Lever *et al.* and it is based on electrochemical E_0 value for redox couples in series of Ru^{III}/Ru^{II} complexes containing the ligands of interest (**Figure 1-3**).[48–51] This method is less explored as it requires the use of less common electrochemical devices.

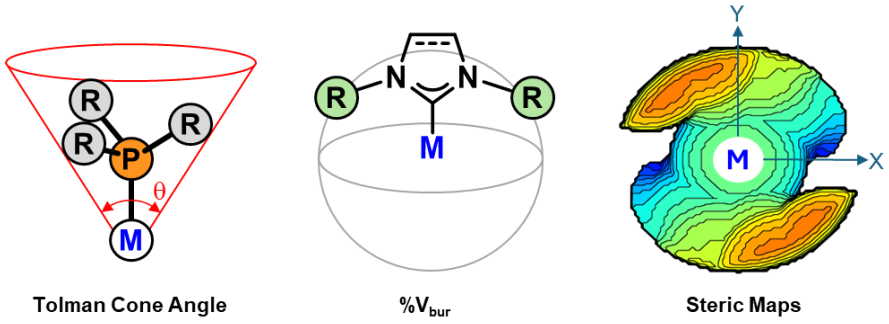

Figure 1-4: Steric descriptors for phosphines and NHCs

The steric parameters of phosphine ligands has historically been described by using the Tolman cone angle as they typically exhibit cone like geometries.[45] This requires a crystal structure to obtain data for this analysis. However, NHCs display a vastly different topography, and are harder to describe their exact steric impacts. Therefore, various other techniques have been developed to study the steric parameters of NHCs.[28] One of the earliest technique employed was single-crystal x-ray crystallography,[52] which allows for the measurement of bond lengths and bond angles around the carbene center. Additionally, computational analysis of structures has been utilized, with one prominent technique being the percent buried volume ($\%V_{Bur}$) developed by Cavallo and Nolan (**Figure 1-4**). The $\%V_{Bur}$ quantifies the steric bulk of the ligand by representing a ligand sphere that surrounds the metal center and determines the amount of space of this sphere that is occupied by the ligand. While this method allows for the direct comparisons between NHCs, the $\%V_{Bur}$ gives average measurements which are not necessarily representative of the ligand's conformation. Furthermore, comparisons must be made using metal very similar metal complexes consisting of the same metal, geometry and ancillary ligands for any meaningful results. Considering this limitation, the latest advancement in quantifying the steric bulk of an NHC has been the use of topographical steric maps (**Figure 1-4**). These maps provide a graphical representation of the spatial distribution of the ligand around the metal center, highlighting areas of steric hindrance rather than just a weighted average.[53] The data required to calculate the $\%V_{Bur}$ as well as to generate these 3D steric maps can be conveniently obtained either by density functional theory (DFT) studies or single-crystal x-ray crystallography data.[54–57] For direct comparisons, complexes of similar structures should ideally be compared and commonly linear complexes of Cu, Ag, or Au are used. One of the most important assets of the 3D steric maps is that it allows for a more accurate depiction of the ligands' behaviour during catalysis.[54–57]

Specifically, steric maps can give a better depiction of open coordination sites on a transition metal which is important for predicting catalytic activity.

Another significant feature of NHC metal complexes which differs from phosphine complexes is their exceptional thermal and air stability which enables them to stabilize highly reactive metal complexes. This is derived from their high bond dissociation energy (BDE), a parameter reflecting the strength of the bond between the ligands and the metal in a complex. The BDE of an NHC is crucial as it influences the stability, reactivity, and overall performance of the metal complex in catalysis and other applications. Higher BDE values indicate stronger bonds, contributing to the robustness and longevity of NHC-ligated complexes.

Table 1-1: BDE values (in kcal/mol) of select NHC and phosphine ligands in $[Ni(CO)_2(L)]$ and $[Ni(CO)_3(L)]$ complexes

Ligand	BDE of NHC in $[Ni(CO)_3(L)]$	BDE of NHC in $[Ni(CO)_2(L)]$
IMes	41.1	46.5
SIMes	40.2	47.2
ICy	39.6	46.3
IPr	38.5	45.4
SIPr	38.0	46.1
IAd	20.4	46.5
P^tBu_3	28.0	34.3
PPh_3	26.7	30.0
PH_3	22.7	25.7

As shown in **Table 1-1**, are measured BDE's of select NHCs and phosphines in literature. The experimental values in **Table 1-1**, displays higher BDE values consistently with NHCs compared to phosphines. This data was quantified by Nolan and coworkers using DFT calculations optimizing for each ligand.[46] These values can also be obtained using solution calorimetric studies which was demonstrated in 1999 by Nolan and coworkers.[58] BDE studies provides a clear picture of the differences between NHCs and phosphines as ligands in organometallic chemistry.

1.4 Important Catalytic Applications

As the exploration of transition metal-catalyzed reactions continues to advance, the demand for a diverse array of ligands becomes increasingly critical. As discussed in Section 1.1, ligands play an important role in influencing the activity of catalysts within these reactions. The field of NHCs has expanded significantly to meet the specific requirement of various catalytic processes. It is important to note that no single NHC ligand behaves uniformly across all reactions; each NHC exhibits unique characteristics depending on the reaction it is used in. Consequently, there is a growing need for a diverse and modular range of NHCs, prompting extensive research into how structural modifications impact their steric and electronic properties and in turn influence their catalytic performance. The following will provide an overview highlighting the influence of utilizing various NHCs, with a focus on how the properties of each NHC impact the specific reactions in which they are employed.

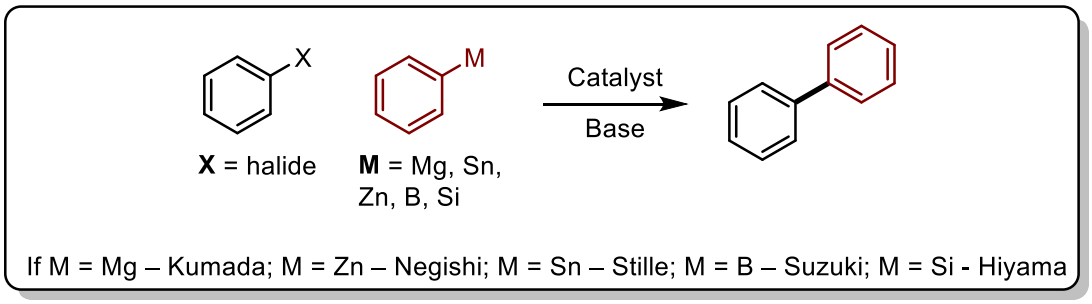

Scheme 1-3: General reaction scheme of Pd-catalyzed coupling reactions

From the initial reports of Herrmann and coworkers,[59,60] the use of Pd NHC complexes have been extensively studied in transition metal catalysis and have had numerous applications.[24] In particular, Pd NHC complexes have been demonstrated to be highly active precatalysts in several types of cross-coupling reactions.[22] In general, cross coupling reactions feature the use of aryl electrophiles such as aryl halides, and aryl organometallic nucleophiles (**Scheme 1-3**).[61]

Shown in **Scheme 1-4** is the simplified mechanism of cross-coupling reactions illustrated using a catalytic cycle. The mechanism begins with the activation of the Pd precatalyst (**A**) which is followed by the oxidative addition of the aryl halide which results in intermediate **B**.[22,61] This is then followed by transmetallation with an organometallic reagent, where a second aryl group is transferred to the palladium center resulting in intermediate **C**.[22,61] The cycle goes through reductive elimination generating the biaryl product and regenerating the catalyst (**A**).[22,61]

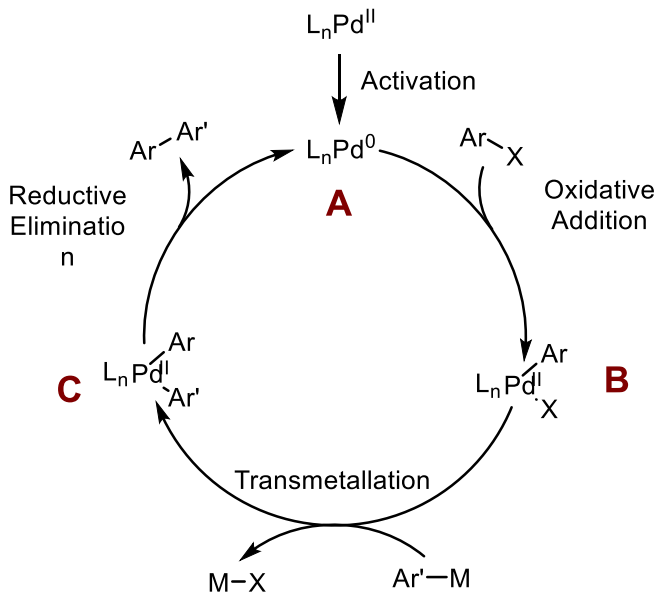

Scheme 1-4: General catalytic cycle for cross-coupling reactions

Of the different types of cross coupling reactions, the most commonly utilized in chemical synthesis is the Suzuki-Miyaura reaction (SMR). This coupling involves the use of aryl boronic acids or esters in the presence of a base, and a great amount of Pd-NHC catalysts have been studied in this reaction. An early example of a well-defined Pd-NHC catalyst used for SMR was reported in 2002 by Herrmann and colleagues using $[Pd(IAd)_2]$.[62] This study reported results of $[Pd(IAd)_2]$ catalyzing the production of 4-phenyltoluene from 4-chlorotoluene and phenylboronic acid with high turnover numbers (TON).[62] Their reports of a highly active and sterically demanding NHC-

ligated catalyst inspired the generation and investigations towards bulky NHCs in cross-coupling reactions. In 2006, Organ and coworkers reported a successful family of Pd-NHC complexes called the PEPPSI (pyridine enhanced precatalyst preparation stabilization and initiation) complexes (**Figure 1-5**).[32] The PEPPSI complexes features an NHC ligand as well as a 3-chloropyridine ligand which dissociates from the Pd centre after the reduction to Pd(0). These complexes can be easily prepared under air which avoids the use of tedious anhydrous conditions.

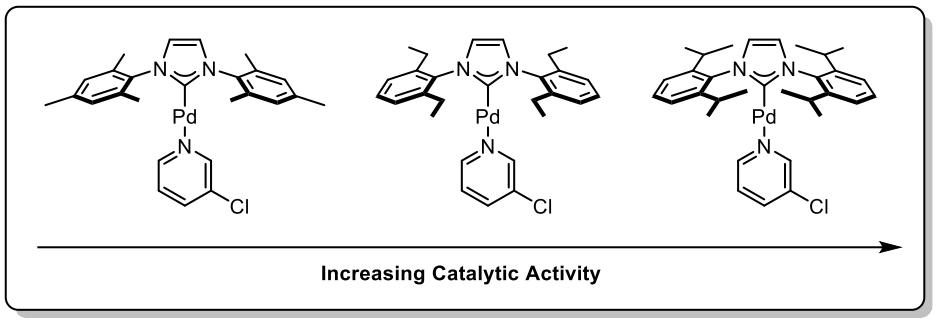

Figure 1-5: Organ and coworkers PEPPSI complexes developed in 2006 used in SMR

In their report, Organ and coworkers utilized the SMR to demonstrate the effects of various PEPPSI complexes coordinated to common sterically bulky NHC ligands (**Figure 1-5**).[32] They demonstrated that the sterically larger IPr-PEPPSI outperformed the less bulky NHC-ligated PEPPSI complexes such as IMes-PEPPSI and was able to facilitate the cross-coupling of challenging biaryls.[32] Furthermore, IPr-PEPPSI was demonstrated to be highly stable and even suitable for the challenging alkyl-alkyl SMR due to the bulky NHC ligand facilitating a fast reductive elimination.[32]

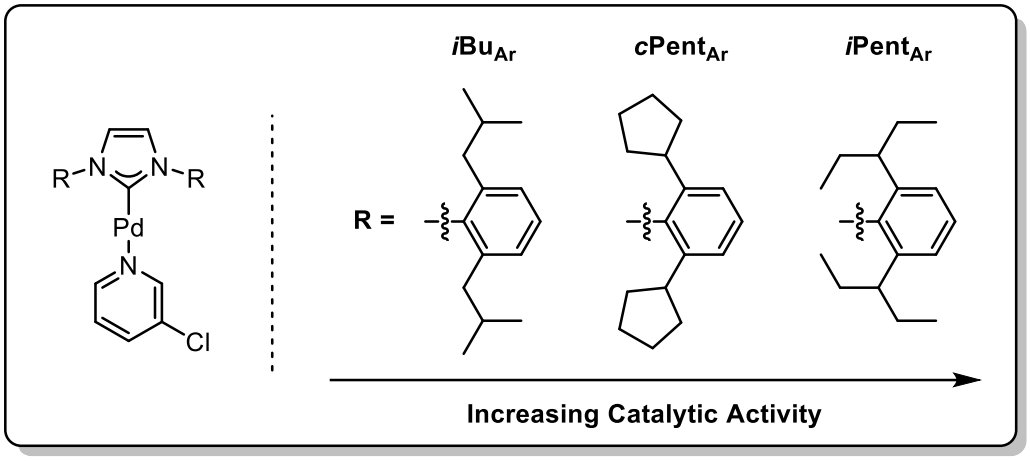

Figure 1-6: Organ and coworkers PEPPSI complexes developed in 2008 used in SMR

In 2008, Organ and coworkers developed IPent-Pd-PEPPSI which was an excellent catalyst for SMR of sterically demanding substrates generating tetra-*ortho*-substituted biaryls at mild temperatures.[63] IPent-Pd-PEPPSI features an even more sterically bulky NHC ligand that is reported to be larger than IPr-PEPPSI (**Figure 1-6**). [63] IPent was studied alongside ligands shown in **Figure 1-6**. The authors concluded that branched alkyl groups in the ortho-positions of the aryl ring was beneficial compared to the more linear IBu NHC.[63] They further supported their findings in 2006 that increasing the bulk of the ligand improves catalyst performance and lastly, the design of IPent with the branching alkyl groups allowed for conformational flexibility which was necessary compared to CPent, with a cyclopentane group.[63]

The discovery and success of the PEPPSI complexes generated a cascading report of bulkier catalysts featuring sterically hindered NHC ligands in literature. An excellent example of sterically hindered class of NHC ligands in literature is the IPr* family. First developed by Markò and coworkers, IPr* quickly became a staple in various catalytic applications that spans from an assortment of cross-coupling reactions to olefin metathesis[64] and semihydrogenations[65–68] to name a few. Similar to the PEPPSI complexes, the reactivity of this type of ligands has also been applied

to SMR. In 2012, Nolan and coworkers demonstrated the use of IPr* as an ancillary ligand in SMR demonstrating high activity towards the formation of tetra-ortho-substituted biaryls under mild conditions.[69] In the article, they also compared the steric bulk of IPr* compared to IPr, SIPr, and *anti*-(2,7)-SICyoctNap substituted complex that was reported by Dorta[70] as [Pd(NHC)(cin)Cl] analogues. The calculated $\%V_{Bur}$ are shown in **Table 1-2** and the $\%V_{Bur}$ of IPr* is significantly larger at 44.6%.[69] The applications of IPr* has exponentially expanded in cross-coupling reactions, [Pd(IPr*)(cin)Cl] is just one of several. Its use as ancillary ligands in well-defined transition metal catalysts have been demonstrated in reactions such as the Buchwald-Hartwig aminations (BHA) which is the formation of C-N bonds.[64,71–74]

Table 1-2: Comparison of $\%V_{Bur}$ with [Pd(NHC)(cin)Cl] analogues

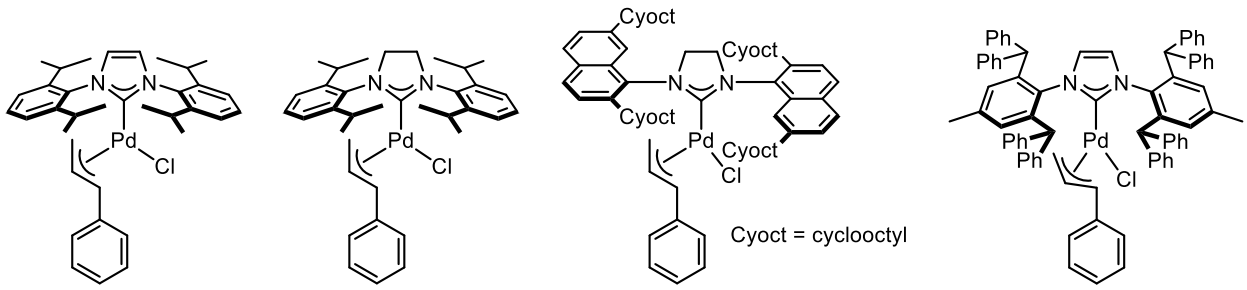

[(IPr)Pd(cin)Cl] [(SIPr)Pd(cin)Cl] [(*anti*-(2,7)-SICyoctNap)Pd(cin)Cl] [(IPr*)Pd(cin)Cl]

NHC	$\%V_{Bur}$[a]
IPr	36.7
SIPr	37.0
anti-(2,7)-SICyoctNap	42.0
IPr*	44.6

[a]Calculated experimentally.[69]

The quest for sterically hindered NHC ligands continues to grow in literature. The applications of NHCs in literature span several applications in transition metal catalysis. Further investigations to the design and tunability of NHC ligands are still being studied to this day.

1.5 Research Objectives

This chapter highlights the significance of the diverse array NHCs available in the literature. Our research group has focused on exploring the synthesis and coordination chemistry of NHC ligands with transition metals, aiming to leverage their potential in catalytic applications. Our primary objective was to develop a straightforward synthesis of synthetically accessible NHC ligands and to establish a practical approach for their metallation with transition metals. Chapter 2 describes our explorations into the synthesis of NHC copper complexes utilizing a weak base. The primary focus of this work lies in the reproducibility and simplicity of the synthetic procedure. This method avoids the use of a glovebox demonstrating a more accessible approach, making it more practical. Additionally, this method benefits from faster times and the use of mild temperatures, enhancing both efficiency and scalability. This chapter contributes to the burgeoning field of weak-base methodologies for the metallation of NHCs with transition metals, offering an alternative route that aligns with the growing demand for practical chemical processes.

Chapter 3 details our investigations into NHC ligands featuring 2,6-*bis*(alkoxyphenyl) groups. Our research focuses on the development of synthetic procedures for these ligands as well as the fine-tuning their steric parameters of these ligands, with a particular emphasis on increasing their bulk. The literature on this specific type of NHC is limited, primarily due to the challenges associated with their synthesis. Our exploration aims to develop a synthetic route that is both accessible and reproducible. Additionally, we explored the metallation of these NHCs with various transition metals, including copper, silver, and palladium. We further evaluated their catalytic applications, particularly investigating trends related to changes in ligand size.

Finally, Chapter 4 focuses on the study of the electronic parameters of NHCs using species that have been scarcely explored in the literature. Specifically, the use of (NHC)AgCN complexes

as probes for the electronic properties of NHCs through IR spectroscopy of the bound cyanide stretch, which would be trans to the NHC in this linear complex. This approach offers a cost-effective alternative to the more commonly used complexes involving nickel, iridium, and rhodium. Our research group has been working to develop a straightforward synthesis of (NHC)AgCN complexes that can be performed under ambient conditions, thereby enhancing its practicality and broadening its potential applications.

Chapter 2

Convenient Preparation of Copper (I) N-Heterocyclic Carbene Complexes under Mild Conditions

2.2 Introduction

Since their first report by Herrmann,[59] N-Heterocyclic carbenes (NHCs)[16,75,76] have been extensively utilized as ligands in homogeneous catalysis.[24] In particular, copper NHC complexes have been attractive as catalysts in a wide variety of transformations,[77] including catalytic hydrogenations,[78–80] reductions of carbonyls,[81,82] conjugate additions,[83,84] borylation of unsaturated species,[85–88] azide-alkyne cycloaddition reactions,[89–92] and functionalization of carbon dioxide.[93,94] Furthermore, Cu-NHC complexes have been demonstrated to act as carbene transfer agents to other metals.[95,96] Often, the active catalyst is generated in situ from a copper salt and an NHC-HX precursor; however, the benefits of a well-defined Cu-NHC catalyst have been previously reported.[82]

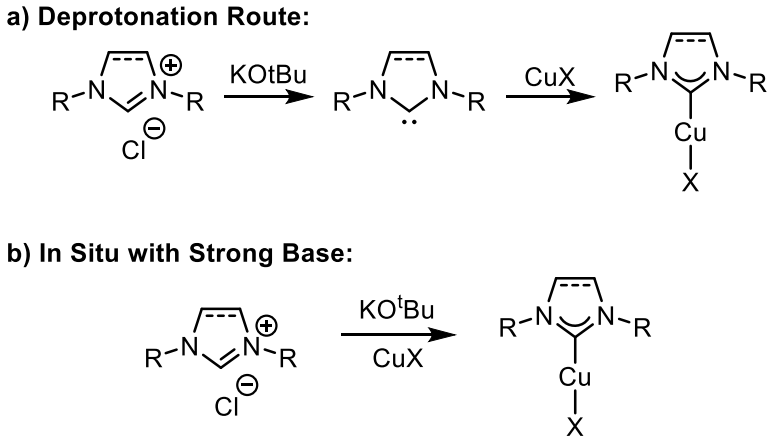

Scheme 2-1: Common synthetic routes of Cu-NHC complexes

While there have been many reported routes for the synthesis of (NHC) Cu(I) complexes, they are commonly prepared by deprotonating the NHC salt precursor with a strong base, such as

KO^{t}Bu, resulting in the free carbene product, which is air and moisture sensitive (**Scheme 2-1a**).[97] The free carbene is then reacted with a Cu precursor to form the Cu(I)NHC complex.[97] Similarly, the free carbene can be generated in situ in a one-pot method using a strong base in the presence of a Cu precursor to make the Cu(I)NHC complex (**Scheme 2-1b**). This method is particularly useful in catalytic transformations, as the Cu-NHC species does not need to be isolated in advance.[85,98–100] Furthermore, treatment of NHC-HX salts in the presence of Cu_2O[101] with a weaker base, NH_3, has also been reported in the literature to generate Cu(I)NHC complexes.[102]

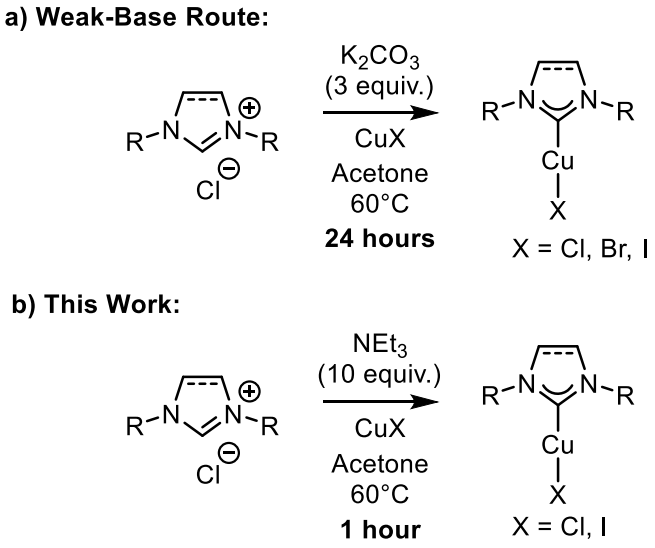

Scheme 2-2: Synthetic routes of Cu-NHC complexes using a weak base

A particularly attractive strategy to generate a variety of Cu(NHC)X (X = halide) type complexes was reported by Cazin and Nolan, which uses a weak base, K_2CO_3, under air in acetone solvent (**Scheme 2-2a**).[103] This method has also been reported for other metals, such as gold.[104] The appealing nature of this "weak-base route" is the absence of an inert atmosphere or any type of specialized equipment. This route allows for the facile synthesis of Cu-NHC complexes even on a large scale, as well as by continuous flow[105] or by ball milling.[106]

Although impressive, in some cases our group has observed inconsistent results with the methodology using K_2CO_3 as a base, often resulting in the re-isolation of the NHC-HX precursor by ^1H NMR spectroscopy. We hypothesized that this may be associated with the heterogeneous nature of K_2CO_3. As such, we reasoned that a homogeneous base may lead to higher reproducibility while also reducing reaction times. Accordingly, Nolan's group also reported the preparation of a variety of NHC complexes bound to different transition and main group metals, utilizing the inexpensive and convenient homogeneous base, triethylamine (NEt_3).[107] Despite its mild nature, NEt_3 has been extensively used in the metallation of different NHC ligands,[108–110] most notably in the formation of complexes possessing chelating functional groups or pincer-type complexes with a variety of metals.[111–113]

To further expand this weak-base methodology, we were interested in investigating the reactivity of Cu(I) halides with various NHC precursors using NEt_3 as a base under air (**Scheme 2-2b**). Herein, we report a convenient method to prepare [(NHC)CuX]-type complexes under mild conditions and in a short reaction time.

2.3 Results and Discussion

We began by investigating the use of homogeneous amine bases for the preparation of Cu-NHC complexes. Copper(I) chloride (CuCl) was treated with the commonly utilized NHC precursor IPr-HCl in acetone with 3.0 equivalents of NEt_3 at 60°C. The resulting homogeneous solution was stirred for 1 hour and [(IPr)CuCl] (**2-1**) was isolated in 38% yield after purification by silica gel chromatography (**Table 2-1,** Entry 1). Increasing the reaction time to 3 hours resulted in a yield increase to 70% (**Table 2-1,** Entry 2). Further extending the reaction time to 5 hours did not yield any significant improvement compared to the 3-hour reaction (**Table 2-1,** Entry 3). We then explored other reaction parameters, such as the equivalents of base. Increasing the base to 5.0

equivalents for 3 hours did not produce a significant change in yield (**Table 2-1,** Entry 4). However, increasing the base to 10.0 equivalents for 1 hour afforded a comparable 75% yield to the 3.0 equivalents reaction that had the reaction time of 3 hours (**Table 2-1,** Entry 5). Although the reaction required a large excess of base, the short reaction time proved to beneficial for convenience. These conditions were selected as optimal for further studies. Additionally, running the reaction in an inert atmosphere offered no benefit, therefore, all subsequent reactions were done under air.

Table 2-1: Generation of [(IPr)CuX] complexes with NEt_3 as a base

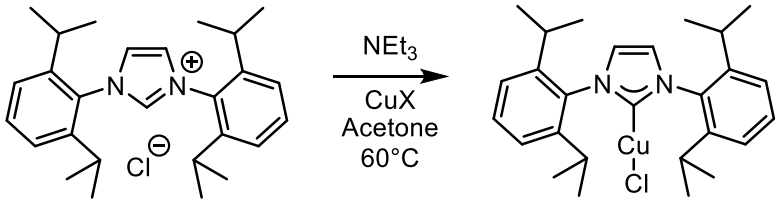

Entry	CuX	Product	NEt_3 (equiv.)	Time (h)	[a]Yield (%)
1	CuCl	(IPr)CuCl (**2-1**)	3	1	38
2	CuCl	(IPr)CuCl (**2-1**)	3	3	70
3	CuCl	(IPr)CuCl (**2-1**)	3	5	61
4	CuCl	(IPr)CuCl (**2-1**)	5	3	67
5	CuCl	(IPr)CuCl (**2-1**)	10	1	75
6	CuI	(IPr)CuI (**2-2**)	10	1	60
7[b]	CuI	(IPr)CuI (**2-2**)	2	24	39

Note: General Conditions: IPr-HCl (0.55 mmol), CuX (0.53 mmol), NEt_3 (indicated amount) in acetone (3.5 mL) at 60°C for the indicated time under air. [a]Isolated Yields. [b]Using K_2CO_3 as a base.

We found that copper(I) iodide (CuI) also works as a copper precursor in place of CuCl which resulted in achieving the product, [(IPr)CuI] (**2-2**), in 60% isolated yield (**Table 2-1,** Entry 6). For comparison, we tested Cazin and Nolan's procedure[103] using K_2CO_3 as a base for 24 hours (**Table 2-1,** Entry 7). This reaction resulted in a slightly lower yield. Moreover, other solvents such as MeOH, THF, DCE, and iPrOH were also tested in place of acetone. MeOH, THF, and DCE produced the product with comparable yield, whereas iPrOH failed to yield any product (**Table**

2-2). In all cases, ^{1}H NMR spectroscopy confirmed that the desired [(NHC)CuX] (X = Cl, I) complex was the sole product after purification by silica gel column chromatography.

Table 2-2: Generation of [(IPr)CuCl] in different solvents

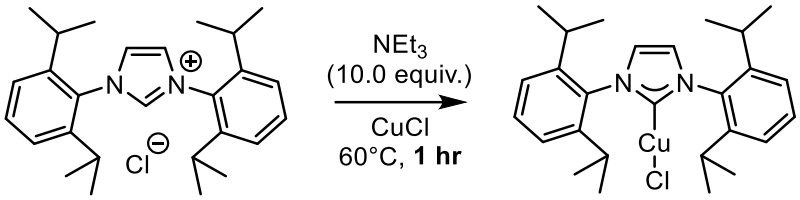

Entry	Solvent	[a]Yield (%)
1	MeOH	75
2	THF	57
3	DCE	68
4	iPrOH	0

Note: General Conditions: IPr-HCl (0.55 mmol), CuX (0.53 mmol), NEt_3 (5.3 mmol) in solvent (3.5 mL) at 60°C for the indicated time under air. [a]Isolated Yields.

We then tested the optimized procedure for generality with commonly utilized NHC precursors such as IMes-HCl, SIPr-HCl, and SIMes-HCl with both CuCl and CuI (**Table 2-3**). The reaction conditions were effective with IMes-HCl with CuCl giving [(IMes)CuCl] (**2-3**) in 92% yield (**Table 2-3,** Entry 1). The saturated NHC precursors, SIMes-HCl and SIPr-HCl, reacted with CuCl to give [(SIPr)CuCl] (**2-4**) and [(SIMes)CuCl] (**2-5**), however, we found that the yields for these were lower compared to the unsaturated NHC precursors (**Table 2-3,** Entry 2 and 3). We hypothesized that this may be due to the decreased acidity of the saturated NHC-HX precursors. Additionally, we tested the reaction with IMes-HBF_4 with CuCl and it resulted in [(IMes)CuCl] (**2-5**) which indicates that the reaction conditions are tolerant to non-halide NHC salt counterions, albeit with decreased yield (**Table 2-3,** Entry 4).

Table 2-3: Preparation of [(NHC)CuX]-type complexes

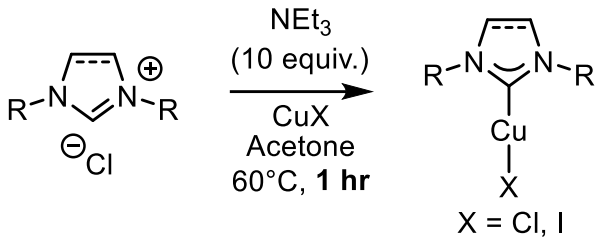

Entry	NHC-HX	CuX	Complex	[a]Yield (%)
1	IMes-HCl	CuCl	[(IMes)CuCl] (**2-3**)	92
2	SIPr-HCl	CuCl	[(SIPr)CuCl] (**2-4**)	61
3	SIMes-HCl	CuCl	[(SIMes)CuCl] (**2-5**)	25
4	IMes-HBF_4	CuCl	[(IMes)CuCl] (**2-5**)	44
5	SIPr-HCl	CuI	[(SIPr)CuI] (**2-6**)	46
6	IMes-HCl	CuI	[(IMes)CuI] (**2-7**) + $[(IMes)_2Cu][CuI_2]$ (**2-8**)	49[b]
7	SIMes-HCl	CuI	[(SIMes)CuI] (**2-9**) + $[(SIMes)_2Cu][CuI_2]$ (**2-10**)	33[b]

General Conditions: NHC-HX (0.55 mmol), CuX (0.53 mmol), NEt_3 (5.3 mmol), in acetone (3.5 mL) at 60°C under air. [a]Isolated yields. [b]Combined yield of [(NHC)CuI] and $[(NHC)_2Cu][CuI_2]$.

Moreover, the reaction conditions were effective with SIPr-HCl with CuI giving [(SIPr)CuI] (**2-6**) in 46% yield (**Table 2-3,** Entry 5). However, when CuI was reacted with the smaller ligands,[28] IMes-HCl and SIMes-HCl (**Table 2-3,** Entry 6 and 7), additional NHC-containing species was observed by ^{1}H NMR spectroscopy (**Figure 2-1** and **Figure 2-2**).[89] We hypothesized that this was due to the formation of $[(NHC)_2Cu][CuI_2]$ (**2-8** and **2-10**), which, have been previously observed in other procedures (**Figure 2-3**). Interestingly, a *bis*(NHC) species was never observed when instead using CuCl. We hypothesized that this may be related to the increased lability of iodide relative to chloride in combination with the decreased steric parameters associated with IMes and SIMes relative to IPr and SIPr, favouring a *bis*(NHC) product.

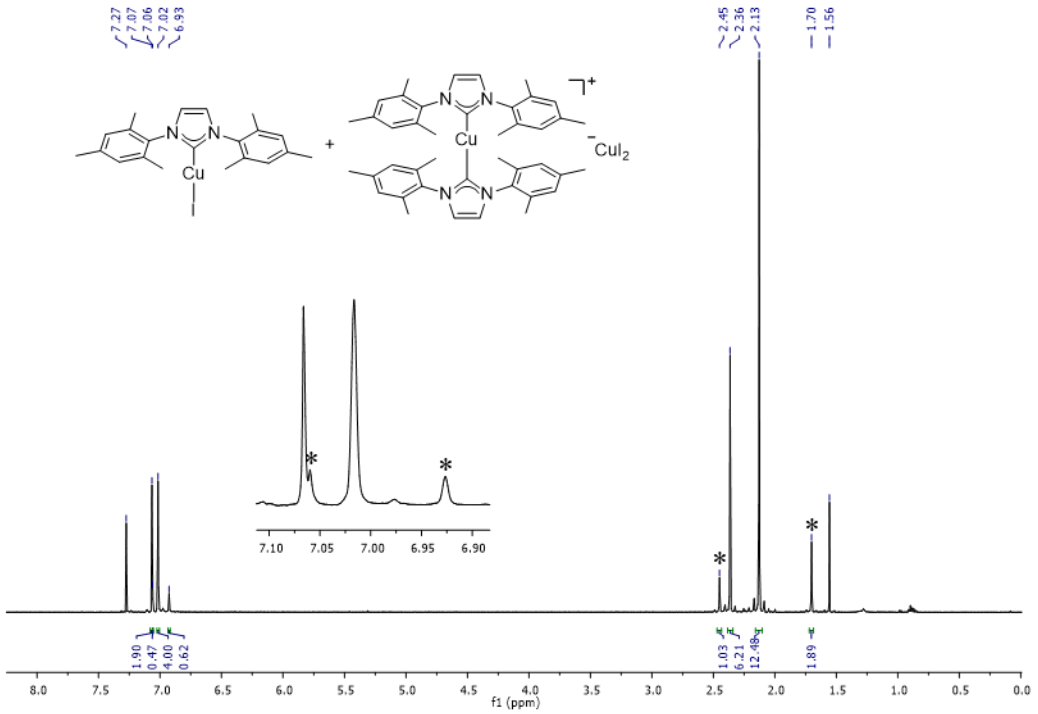

Figure 2-1: ^{1}H NMR spectrum of product mixture of [(IMes)CuI] and [(IMes)$_2$Cu][CuI$_2$]
**indicates [(IMes)$_2$Cu][CuI$_2$]*

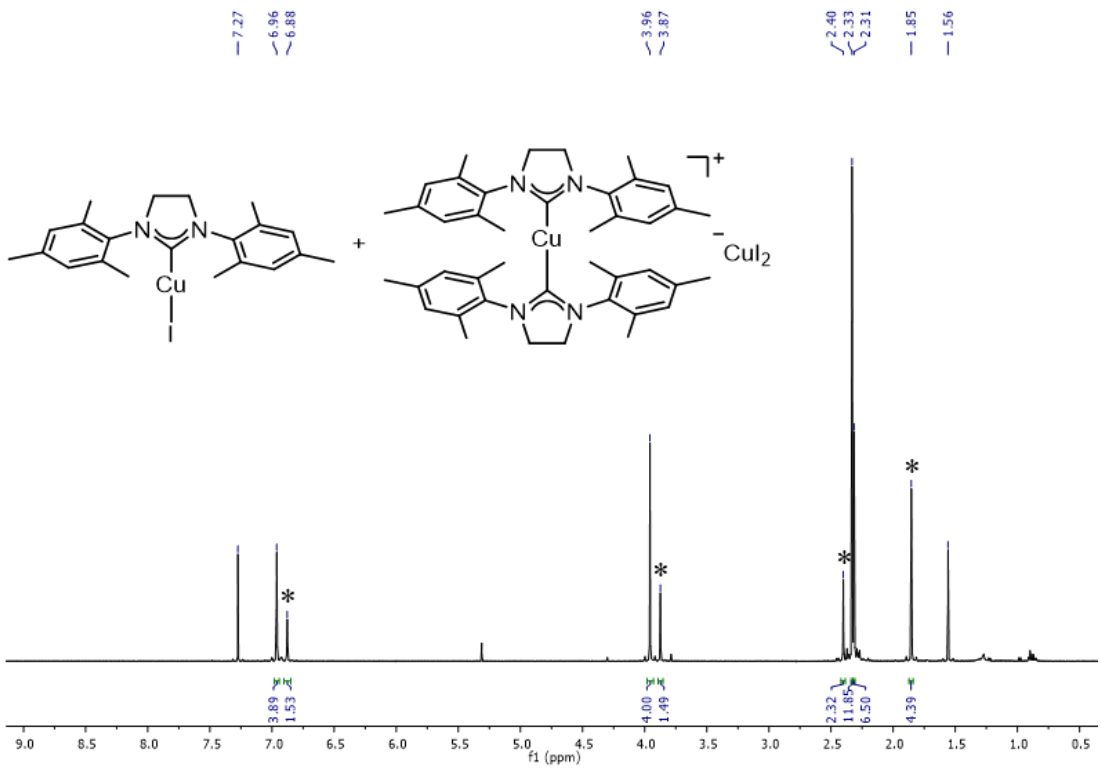

Figure 2-2: ^{1}H NMR spectrum of product mixture of [(SIMes)CuI] and [(SIMes)$_2$Cu][CuI$_2$].
**indicates [(SIMes)$_2$Cu][CuI$_2$]*

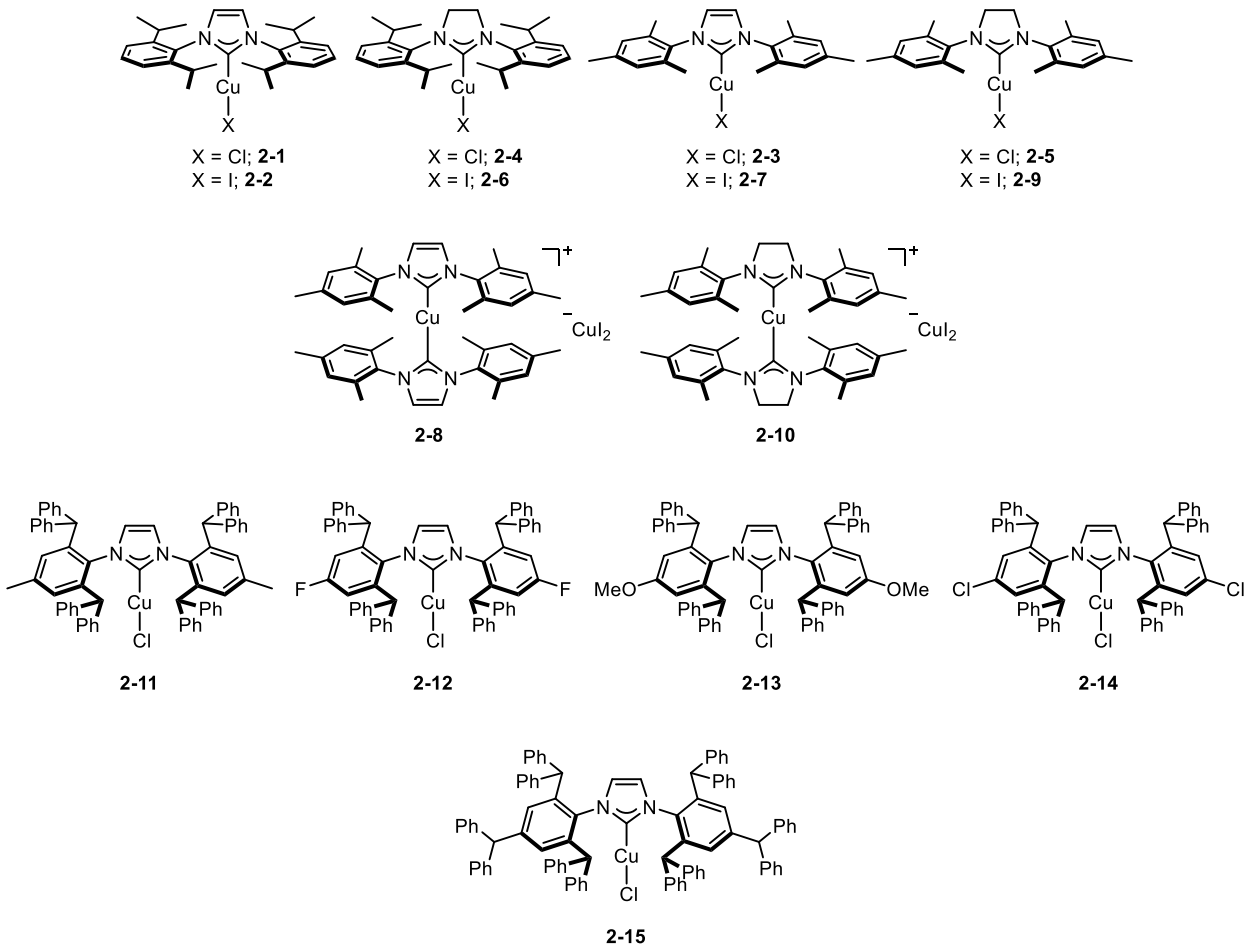

Figure 2-3: [Cu(NHC)X] complexes prepared in this study

We also investigated the reaction conditions on larger scale to indicate scalability of this reaction. Therefore, we tested the optimized conditions on 0.25 mmol of CuCl which represents a five-fold increase in scale and a slightly decreased yield of 75% was isolated after purification (**Scheme 2-3**). This result indicates general scalability of this reaction which illustrates its practicality for applications in catalysis.

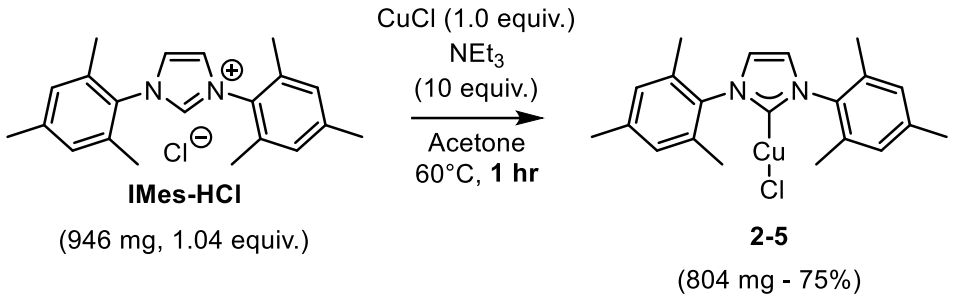

Scheme 2-3: Larger scale synthesis of complex **2-5**

To further test the limits of the ligand scope we also explored the use of the IPr* family of ligands[114] which are significantly sterically bulkier NHC precursors. As such, we explored the use of the remote functionalized NHC precursors IPr*-HCl, *p*-F-IPr*-HCl, *p*-OMe-IPr*-HCl, *p*-Cl-IPr*-HCl, IPr#-HCl, and *p*-morpholine-IPr*-HCl with CuCl (**Table 2-4**). Thus, also assessing any potential impacts based on the electronic parameters of the ligands. Importantly, this family of complexes have been found to be very active reduction catalysis,[65,67] as the high steric demand of these ligands help to stabilize monomeric (NHC)Cu-H type species.[68] Previous reports of the synthesis of CuCl complexes using these types of ligands involved harsh reagents, and an inert atmosphere.[65,115] Therefore, the conditions in this study would be a more suitable way to address potential limitations with synthesizing these complexes. Thus, we treated the sterically bulkier NHC precursors using the optimized conditions (**Table 2-4**) and in all cases, ^{1}H NMR spectroscopy confirmed the formation of the desired complexes; [(IPr*)CuCl] (**2-11**), [(*p*-F-IPr*)CuCl] (**2-12**), [(*p*-OMe-IPr*)CuCl] (**2-13**), [(*p*-Cl-IPr*)CuCl] (**2-14**), and [(IPr#)CuCl] (**2-15**), respectively in good to excellent yields (**Figure 2-3**). These results indicate that this procedure is truly general with no issues with sterically larger ligands, or those featuring remote electronic functionalization. Similar to the initial results, the general scalability of this reaction conditions was also applicable to these species of ligands which further demonstrates its practicality.

Table 2-4: Preparation of [(NHC)CuCl]-type complexes with sterically larger NHCs

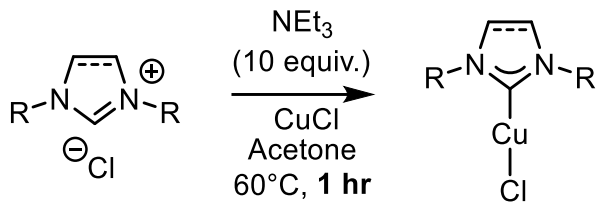

Entry	NHC-HX	Complex	[a]Yield (%)
1	IPr*-HCl	[(IPr*)CuCl] (**2-11**)	82
2	*p*-F-IPr*-HCl	[(*p*-F-IPr*)CuCl] (**2-12**)	91
3	*p*-OMe-IPr*-HCl	[(*p*-OMe-IPr*)CuCl] (**2-13**)	73
4	*p*-Cl-IPr*-HCl	[(*p*-Cl-IPr*)CuCl] (**2-14**)	76
5	IPr#-HCl	[(IPr#)CuCl] (**2-15**)	89

Note: General Conditions: NHC-HX (0.55 mmol), CuX (0.53 mmol), NEt_3 (5.3 mmol), in acetone (3.5 mL) at 60°C under air. [a]Isolated yields.

2.4 Conclusions and Future Work

In conclusion, we report a new convenient protocol for the preparation of [(NHC)CuX] (X = Cl, I) type complexes from simple copper salts and NHC precursors using NEt_3 as a base. The reaction was performed under air in acetone solvent in short reaction times. In general, unsaturated NHC precursors, regardless of steric or electronic parameters, generally performed better compared to the saturated NHC precursors, SIPr and SIMes. This may be associated with the decreased acidity of the saturated NHC-HX salts relative to the unsaturated ones. Furthermore, smaller ligands, IMes and SIMes, were found to have multiple products when reacted with CuI which were not the case for SIPr and IPr. This study contributes to the growing number of synthetic protocols for metal NHC complexes utilizing a weaker base which in turn results in milder reaction conditions. We believe that the use of a homogeneous base will lead to greater reproducibility in comparison to other protocols which may lead to widespread adoption. In particular, our method may find applications in automated synthesis or in-situ generation in catalytic reactions featuring NEt_3 as a base. Our group is currently pursuing the use of homogeneous bases in the preparation

of other metal NHC complexes as well as further expanding the scope of what these reaction conditions can achieve.

2.5 Experimental

General considerations: All manipulations were carried out under a nitrogen or argon atmosphere unless otherwise noted using standard Schlenk techniques. All reagents were purchased from commercial suppliers and used without further purification. Acetone, triethylamine, and copper chloride were purchased from Fisher Scientific and used as received without further purification. Copper iodide was purchased from Sigma–Aldrich. NHC precursors; IMes-HCl,[116] IMes-HBF_4,[116] SIMes-HCl,[117] IPr-HCl,[118] SIPr-HCl,[52] IPr*-HCl,[119] *p*-F-IPr*-HCl,[119] *p*-Cl-IPr*,[119] *p*-OMe-IPr*-HCl,[119] and IPr#-HCl,[119] were synthesized by published procedures. Column chromatography was performed using silica gel 60 (230–400 mesh) purchased from Sigma–Aldrich. Thin layer chromatography was performed using precoated Polygram® SIL G/UV_{254} TLC sheets, and spots were visualized using a UV light at 254 nm. ^{1}H NMR spectra were measured on a Varian INOVA 500 MHz or a Bruker Ascend 400 MHz spectrometer where noted at 298K. Chemical shifts are reported in delta (δ) units, expressed in parts per million (ppm) downfield from tetramethylsilane (TMS) using residual protonated solvent as an internal standard ($CDCl_3$ 7.27 ppm). $^{13}C\{^1H\}$ NMR spectra were recorded at 126 MHz or 101 MHz where noted. Chemical shifts are reported as above using the solvent as an internal standard ($CDCl_3$, 77.23 ppm). Metallation reactions were conducted in 16 × 125 culture tubes purchased from VWR. High-resolution mass spectrometry was performed by the Water Quality Centre at Trent University using a Thermo Qexactive Orbitrap ESI in the positive ion mode, with samples dissolved into a MeOH solution for analysis.

General procedure for the preparation of [(NHC)CuX]

A culture tube was charged with copper(I) chloride or copper(I) iodide (0.53 mmol), NHC-HCl salt (0.55 mmol) and acetone (3.5 mL) under air. The tube was sealed and heated to 60°C for 5 min, typically resulting in a homogeneous solution. The tube was then cooled to room temperature, and NEt_3 (740 µL, 5.3 mmol, 10 equiv.) was added via a micropipette. The tube was resealed and heated for an additional 60 min at 60°C. After returning the reaction to room temperature, all volatiles were removed *in vacuo*, and the residue was dispersed into CH_2Cl_2 and applied to a short pad of silica gel, washing with CH_2Cl_2.The CH_2Cl_2 was removed *in vacuo* using a rotary evaporator to give a solid product. **The product can be further purified by layering hexanes to a concentrated solution of CH_2Cl_2.*

Synthesis of [(IPr)CuCl] (2-1)

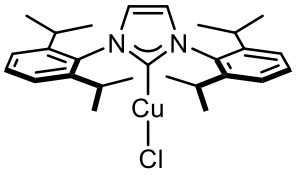

The general procedure was followed using CuCl (52.4 mg, 0.53 mmol) and IPr-HCl (233.8 mg, 0.55 mmol) in acetone (3.5 mL) with NEt_3 (740 µL, 5.30 mmol) for 60 min at 60°C, giving **2-1** in 194.3 mg (75%) as a white solid. **^{1}H NMR (500 MHz, $CDCl_3$):** δ 7.51 (t, *J* = 7.8 Hz, 2H), 7.31 (d, *J* = 7.8 Hz, 4H), 7.14 (s, 2H), 2.58 (s, *J* = 6.8 Hz, 4H), 1.32 (d, *J* = 6.8 Hz, 12H), 1.24 (d, *J* = 6.8 Hz, 12H) ppm. **^{13}C{^{1}H} NMR (126 MHz, $CDCl_3$):** δ 180.9, 145.8, 134.6, 130.8, 124.4, 123.3, 28.9, 25.0, 24.1 ppm. **HRMS (ESI+, *m/z*):** calc'd for $C_{27}H_{36}CuN_2$ $[M - Cl]^+$ 451.2175, found 451.2164.

Synthesis of [(IPr)CuI] (2-2)

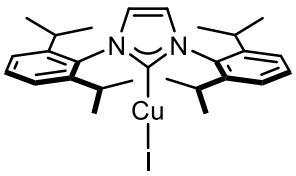

The general procedure was followed using CuI (100.9 mg, 0.53 mmol) and IPr-HCl (233.8 mg, 0.55 mmol) in acetone (3.5 mL) with NEt_3 (740 µL, 5.3 mmol) for 60 min at 60°C, giving **2-2** in 186.3 mg (60%) as a white solid. **^{1}H NMR (500 MHz, $CDCl_3$):** δ 7.51 (t, *J* = 7.8 Hz, 2H), 7.31 (d, *J* = 7.8 Hz, 4H), 7.15 (s, 2H), 2.60 (s, *J* = 6.9 Hz, 4H), 1.32 (d, *J* = 6.9 Hz, 12H), 1.24 (d, *J* = 6.9 Hz, 12H) ppm.

$^{13}C\{^1H\}$ NMR (126 MHz, $CDCl_3$): δ 182.6, 145.8, 134.4, 130.8, 124.4, 123.3, 28.9, 25.0, 24.1 ppm. **HRMS (ESI+, *m/z*):** calc'd for $C_{27}H_{36}CuN_2$ $[M - I]^+$ 451.2175, found 451.2164.

Synthesis of [(IMes)CuCl] (2-3)

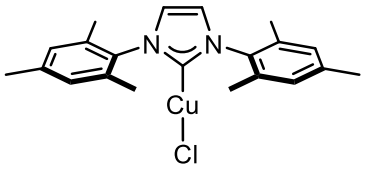

The general procedure was followed using CuCl (52.4 mg, 0.53 mmol) and IMes-HCl (187.5 mg, 0.55 mmol) in acetone (3.5 mL) with NEt_3 (740 μL, 5.3 mmol) for 60 min at 60°C, giving **2-3** in 197.0 mg (92%) as an off-white solid. **^1H NMR (500 MHz, $CDCl_3$):** δ 7.07 (br, 2H), 7.01 (s, 4H), 2.35 (s, 6H), 2.11 (s, 12H) ppm. **$^{13}C\{^1H\}$ NMR (126 MHz, $CDCl_3$):** δ 179.2, 139.7, 134.7, 129.7, 122.4, 21.3, 17.9 ppm. **HRMS (ESI+, *m/z*):** calc'd for $C_{42}H_{48}CuN_4$ $[(2M) - CuCl_2]^+$ 671.3175, found 671.3164.

Synthesis of [(SIPr)CuCl] (2-4)

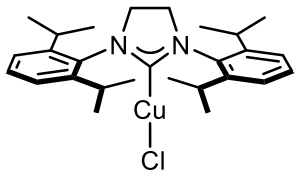

The general procedure was followed using CuCl (52.4 mg, 0.53 mmol) and SIPr-HCl (235.2 mg, 0.55 mmol) in acetone (3.5 mL) with NEt_3 (740 μL, 5.3 mmol) for 60 min at 60°C, giving **2-4** in 158.4 mg (61%) as a white solid. **^1H NMR (500 MHz, $CDCl_3$):** δ 7.42 (t, J = 7.7 Hz, 2H), 7.26 (d, J = 7.8 Hz, 4H), 4.03 (s, 4H), 3.08 (s, J = 6.9 Hz, 4H), 1.38 (d, J = 6.9 Hz, 12H), 1.36 (d, J = 6.9 Hz, 12H) ppm. **$^{13}C\{^1H\}$ NMR (126 MHz, $CDCl_3$):** δ 203.2, 146.8, 134.6, 130.1, 124.8, 53.9, 29.1, 25.7, 24.1 ppm. **HRMS (ESI+, *m/z*):** calc'd for $C_{27}H_{38}CuN_2$ $[M - Cl]^+$ 453.2331, found 453.2319.

Synthesis of [(SIMes)CuCl] (2-5)

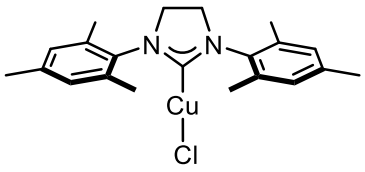

The general procedure was followed using CuCl (263.3 mg, 2.66 mmol) and SIMes–HCl (946.4 mg, 2.76 mmol) in acetone (17.5 mL) with NEt_3 (3.7 mL, 26.5 mmol) for 60 min at 60°C, giving **2-5** in 798.2 mg (74%) as a white solid. **^1H NMR (500 MHz, $CDCl_3$):** δ 6.97 (s, 4H), 3.96 (s, 4H),

2.33 (s, 12H), 2.31 (s, 6H) ppm. **$^{13}C\{^{1}H\}$ NMR (126 MHz, $CDCl_3$):** δ 202.8, 138.8, 135.6, 135.2, 130.0, 51.2, 21.2, 18.2 ppm. **HRMS (ESI+, *m/z*):** calc'd for $C_{42}H_{52}CuN_4$ $[(2M) - CuCl_2]^+$ 675.3488, found 675.3479.

Synthesis of [(SIPr)CuI] (2-6)

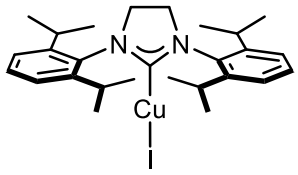

The general procedure was followed using CuI (100.9 mg, 0.53 mmol) and SIPr-HCl (235.4 mg, 0.55 mmol) in acetone (3.5 mL) with NEt_3 (740 μL, 5.3 mmol) for 60 min at 60°C, giving **2-6** in 144.4 mg (46%) as a white solid. **^{1}H NMR (500 MHz, $CDCl_3$):** δ 7.42 (t, *J* = 7.8 Hz, 2H), 7.26 (d, *J* = 7.8 Hz, 4H), 4.04 (s, 4H), 3.09 (s, *J* = 6.9 Hz, 1H), 1.39 (d, *J* = 6.9 Hz, 12H), 1.36 (d, *J* = 6.9 Hz, 12H) ppm. **$^{13}C\{^{1}H\}$ NMR (126 MHz, $CDCl_3$):** δ 204.7, 146.8, 134.4, 130.1, 124.9, 124.7, 53.9, 29.3, 29.1, 29.0, 28.9, 25.7, 25.6, 24.2 ppm. **HRMS (ESI+, *m/z*):** calc'd for $C_{27}H_{38}CuN_2$ $[M - Cl]^+$ 453.2331, found 453.2321.

Larger Scale Synthesis of [(IMes)CuCl]

The general procedure was followed using CuCl (263.3 mg, 2.66 mmol) and IMes–HCl (946.6 mg, 2.76 mmol) in acetone (17.5 mL) with NEt_3 (3.7 mL, 26.5 mmol) for 60 min at 60°C, giving **2-3** in 804.7 mg (75%) as an off-white solid. The spectral data were consistent with our other preparations of **2-3**.

Synthesis of [(IMes)CuCl] using IMes-HBF_4

The general procedure was followed using CuCl (52.4 mg, 0.53 mmol) and IMes–HBF_4 (215.6 mg, 0.55 mmol) in acetone (3.5 mL) with NEt_3 (740 μL, 5.3 mmol) for 60 min at 60°C, giving **2-3** in 94.1 mg (44%) as an off-white solid. The spectral data were consistent with our other preparations of **2-3**.

Synthesis of [(IPr*)CuCl] (2-11)

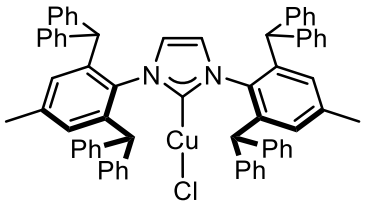

The general procedure was followed using CuCl (52.4 mg, 0.53 mmol) and IPr*-HCl (522.5 mg, 0.55 mmol) in acetone (3.5 mL) with NEt_3 (740 µL, 5.3 mmol) for 60 min at 60°C, giving **2-11** in 443.7 mg (82%) as an off-white solid. **^{1}H NMR (400 MHz, $CDCl_3$):** δ 7.22 – 7.14 (m, 24H), 7.02 (d, *J* = 6.65 Hz, 8H), 6.90 (dd, *J* = 6.47, 3.04 Hz, 8H), 6.85 (s, 4H), 5.82 (s, 2H), 5.21 (s, 4H), 2.23 (s, 6H) ppm. **^{13}C{^{1}H} NMR (126 MHz, $CDCl_3$):** δ 180.6, 143.3, 142.5, 141.1, 140.2, 134.4, 130.4, 129.8, 129.6, 128.8, 128.6, 126.8, 126.8, 123.4, 51.4, 22.0 ppm. Spectral data matches literature.[115] **HRMS (ESI+, *m/z*):** calc'd for $C_{69}H_{56}CuN_2$ $[M - Cl]^+$ 975.3740, found 975.3737.

Synthesis of [(*p*-F-IPr*)CuCl] (2-12)

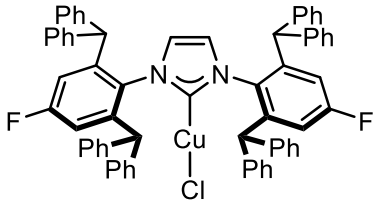

The general procedure was followed using CuCl (52.4 mg, 0.53 mmol) and *p*-F-IPr*-HCl (526.7 mg, 0.55 mmol) in acetone (3.5 mL) with NEt_3 (740 µL, 5.3 mmol) for 60 min at 60°C, giving **2-12** in 465.7 mg (91%) as an off-white solid. **^{1}H NMR (400 MHz, $CDCl_3$):** δ 7.25 – 7.16 (m, 24H), 7.05 – 6.97 (m, 8H), 6.93 – 6.83 (m, 8H), 6.78 (d, *J* = 8.97 Hz, 4H), 5.82 (s, 2H), 5.20 (s, 4H) ppm. **^{13}C{^{1}H} NMR (101 MHz, $CDCl_3$):** δ 181.2, 163.1 (d, *J* = 250.99 Hz), 144.4 (d, *J* = 7.96 Hz), 142.4, 141.6, 132.5 (d, *J* = 3.10 Hz), 129.6, 129.4, 129.1, 128.8, 127.3 (d, *J* = 2.25 Hz), 123.5, 117.0 (d, *J* = 23.95 Hz), 51.6 ppm. **HRMS (ESI+, *m/z*):** calc'd for $C_{67}H_{50}CuF_2N_2$ $[M - Cl]^+$ 983.3238, found 983.3240.

Synthesis of [(*p*-OMe-IPr*)CuCl] (2-13)

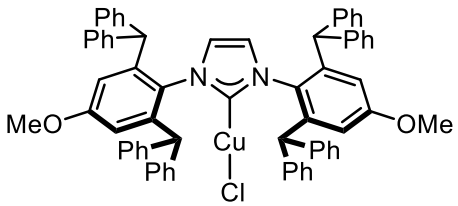

The general procedure was followed using CuCl (52.4 mg, 0.53 mmol) and *p*-OMe-IPr*-HCl (539.9 mg, 0.55 mmol) in acetone (3.5 mL) with NEt_3 (740 µL, 5.3 mmol) for 60 min at 60°C, giving **2-13** in 404.7 mg (73%) as a light brown solid. **^{1}H NMR (500 MHz, $CDCl_3$):** δ

7.2 – 7.1 (m, 24H), 7.1 – 7.0 (m, 8H), 6.9 – 6.9 (m, 8H), 6.6 (s, 4H), 5.8 (s, 2H), 5.2 (s, 4H), 3.6 (s, 6H) ppm. **$^{13}C\{^{1}H\}$ NMR (126 MHz, $CDCl_3$):** δ 181.3, 160.2, 143.1, 143.0, 142.3, 129.7, 129.5, 128.9, 128.6, 126.9, 123.6, 115.1, 55.3, 51.6 ppm. **HRMS (ESI+, *m/z*):** calc'd for $C_{69}H_{56}CuN_2O_2$ $[M - Cl]^+$ 1007.3638, found 1007.3621.

Synthesis of [(*p*-Cl-IPr*)CuCl] (2-14)

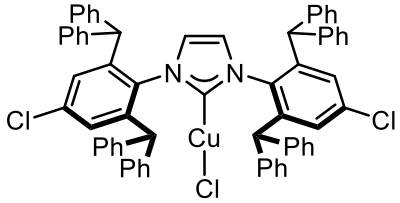

The general procedure was followed using CuCl (52.4 mg, 0.53 mmol) and *p*-Cl-IPr*-HCl (544.8 mg, 0.55 mmol) in acetone (3.5 mL) with NEt_3 (740 µL, 5.3 mmol) for 60 min at 60°C, giving **2-14** in 425.3 mg (76%) as an off-white solid. **^{1}H NMR (400 MHz, $CDCl_3$):** δ 7.3 – 7.1 (m, 24H), 7.0 (s, 4H), 7.0 – 7.0 (m, 8H), 6.9 – 6.8 (m, 8H), 5.8 (s, 2H), 5.2 (s, 4H) ppm. **$^{13}C\{^{1}H\}$ NMR (101 MHz, $CDCl_3$):** δ 180.7, 143.5, 142.3, 141.4, 136.7, 135.1, 130.0, 129.6, 129.4, 129.1, 128.8, 127.3, 127.3, 123.4, 51.5 ppm. **HRMS (ESI+, *m/z*):** calc'd for $C_{67}H_{50}Cl_2CuN_2$ $[M - Cl]^+$ 1015.2647, found 1015.2657.

Synthesis of [(IPr#)CuCl] (2-15)

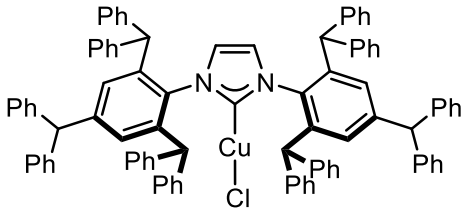

The general procedure was followed using CuCl (52.4 mg, 0.53 mmol) and IPr#-HCl (689.7 mg, 0.55 mmol) in acetone (3.5 mL) with NEt_3 (740 µL, 5.3 mmol) for 60 min at 60°C, giving **2-15** in 625.5 mg (89%) as an off-white solid. **^{1}H NMR (400 MHz, $CDCl_3$):** δ 7.2 – 7.0 (m, 36H), 7.0 – 6.9 (m, 16H), 6.8 – 6.8 (m, 12H), 5.9 (s, 2H), 5.4 (s, 2H), 5.2 (s, 4H) ppm. **$^{13}C\{^{1}H\}$ NMR (101 MHz, $CDCl_3$):** δ 180.6, 145.8, 143.2, 143.1, 142.2, 141.1, 134.8, 130.9, 129.5, 129.4, 129.4, 128.7, 128.5, 128.5, 126.8, 126.7, 126.5, 56.3, 51.5 ppm. **HRMS (ESI+, *m/z*):** calc'd for $C_{93}H_{72}CuN_2$ $[M - Cl]^+$ 1279.4992, found 1279.4982.

Chapter 3

Design and Synthesis of 2,6-*bis*-Alkoxyphenyl N-Heterocyclic Carbenes for Applications in Transition Metal Catalysis

3.1 Introduction

3.1.1 N-Heterocyclic Carbenes

As highlighted in Chapter 1, N-Heterocyclic carbenes (NHCs) are a class of ligand in organometallic chemistry that have been shown to possess stronger electron donating abilities than phosphine ligands, which renders their metal complexes very electron rich.[19] Furthermore, they have particularly high bond dissociation energies (BDE) to metals and this commonly results in air, moisture and often thermally stable metal complexes.[58] NHCs have been heavily utilized as ligands in transition metal catalysis, most notably in palladium[22,26] catalyzed cross coupling reactions and ruthenium[120] olefin metathesis. Similarly, as highlighted in Chapter 2, copper(I) NHC complexes have been heavily reported in a number of transformations in homogeneous catalysis.[121]

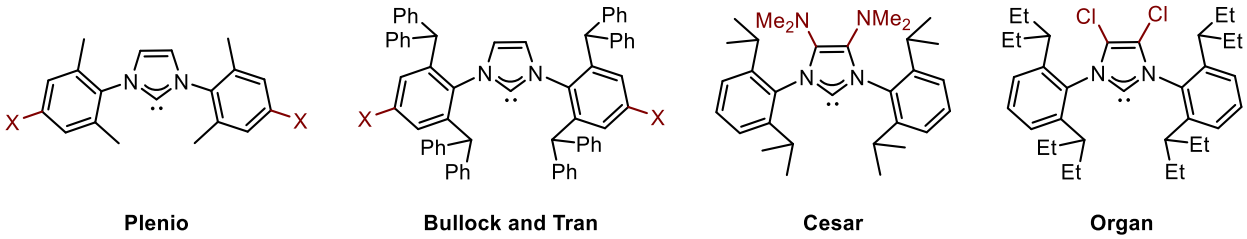

Figure 3-1: Select examples of electronically tuned NHCs in literature

NHCs are highly tunable and a major theme of research with NHCs has been dedicated to structural modifications to enhance or modify their properties in catalysis. In this regard, Plenio and coworkers demonstrated that the incorporation of various functional groups into the *para*-

position of the aryl wingtip groups allows for electronic tunability (**Figure 3-1**).[122] The incorporation of functional groups into the *para*- position has been further investigated by Bullock, Tran and coworkers who demonstrated the direct impacts of these modifications on the properties of the metal.[65–68] Consequently, Organ and coworkers have demonstrated that precatalysts featuring NHC ligands with electron withdrawing groups to the imidazolium ring display drastically higher catalytic activity in challenging Buchwald-Hartwig amination (BHA) reactions of aryl chlorides (**Figure 3-1**).[123] This was hypothesized to be related to the decrease in pK_a of an amine bound Pd(II) intermediate in the rate limiting deprotonation step of the reaction. Similarly, César and coworkers reported that the incorporation of electron donating dimethylamino groups similarly resulted in much higher catalytic activity in BHA reactions of aryl tosylates (**Figure 3-1**).[124] This was hypothesized to be associated with the facilitation of the rate limiting oxidative addition of the C-O bond in the substrate.

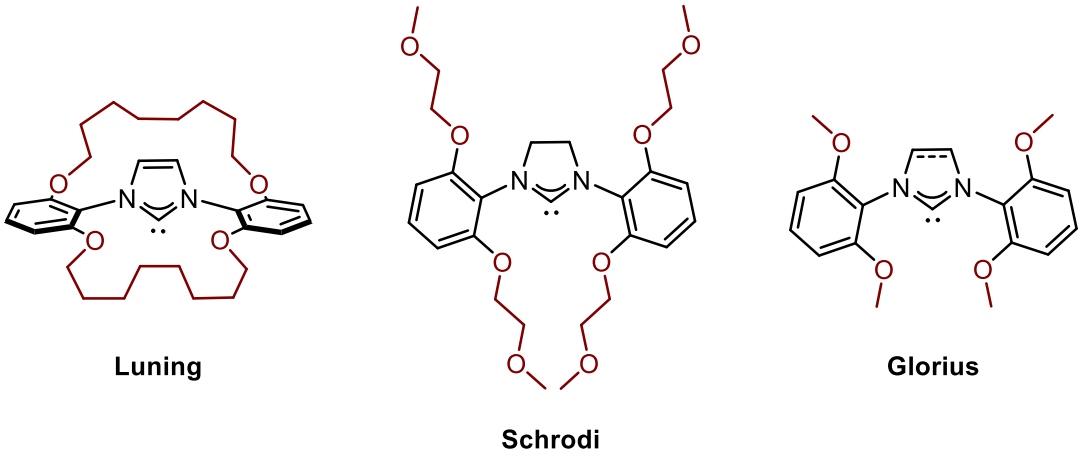

Figure 3-2: Select examples of 2,6-*bis*(alkoxyphenyl) substituted NHCs in literature

Modifications to the *ortho*- position of the aryl wingtip groups have also been reported to have beneficial impacts in catalysis. In this regard, Schrodi and coworkers reported that NHCs featuring methoxyethoxy substituents displayed rate enhancement in the ring closing metathesis reactions

(**Figure 3-2**).[125] In this report, hemilabile coordination was postulated to be the origin of increased catalyst activity.[125] Furthermore, reports by Glorius and coworkers[126] as well as Lüning and coworkers[127] of NHCs featuring 2,6-*bis*(alkoxyphenyl) substituents showed promising results in catalysis (**Figure 3-2**). Despite these examples, NHCs featuring 2,6-*bis*(alkoxyphenyl) wingtip groups have been scarcely explored as ligands for transition metals. Furthermore, sterically bulky and electron rich NHC ligands have been reported to be challenging to synthesize with lengthy procedures.[128,129] As such, we endeavored to develop new synthetic protocols for NHC ligands featuring 2,6-*bis*(alkoxyphenyl) wingtip groups and investigate their metallation for the preparation of transition metal complexes to be used in catalysis (**Figure 3-3**).

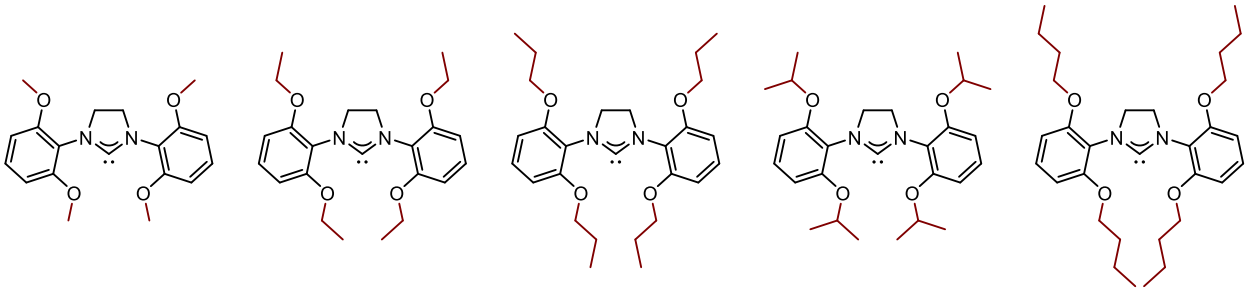

Figure 3-3: NHCs featuring 2,6-*bis*(alkoxyphenyl) substituents

This species of NHC ligands offer synthetic accessibility as we hypothesized that we could tune the steric parameters of the NHC by increasing or decreasing the size of the alkyl chains in the *ortho*- positions of the wingtip groups. Moreover, the addition of alkoxy substituents should increase the electron donating properties of the ligand resulting in more electron rich ligands which may find a unique place in catalysis.

3.1.2 Copper Hydrides for Reduction of Carbonyl Containing Compounds

The use of NHCs as ancillary ligands in copper-mediated catalysis has become a burgeoning field of research.[77,121] Since Arduengo's reports of the first NHC-ligated copper in

1993,[130] a diverse scope of reactions catalyzed by these complexes have been studied.[121] Ligated copper (I) hydride (Cu-H) generated from [Cu(NHC)X] (where X = halide) has been showed to be highly reactive in reduction of carbonyl containing compounds[68] and semihydrogenation of alkynes.[79] [Cu(NHC)X] type species have been reported to be air and moisture stable and suitable for long term storage under ambient conditions[121] and can be prepared by several routes.[103,131] It has been demonstrated that NHC ligands containing sterically bulky groups destabilize $[(NHC)CuH]_2$ dimers which form as off-cycle resting states in catalytic reactions by steric repulsion (**Scheme 3-1**).[67] Sterically hindered groups help push the equilibrium towards the [(NHC)CuH] monomeric species which has been shown to be more reactive than the $[(NHC)CuH]_2$ dimer species towards less electrophilic substrates.[68] In addition to steric bulk, the strong electron donating ability of the many NHC ligands has been shown to result in higher copper hydride migratory insertion reactivity into different unsaturated functionalities allowing for low catalyst loadings leading to milder reaction conditions.[132]

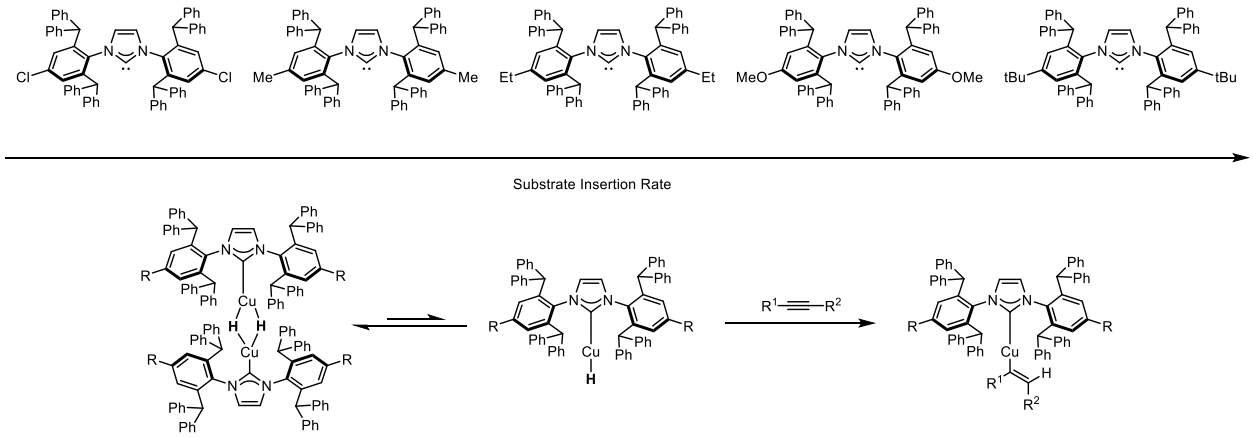

Scheme 3-1: Steric effects of the wingtip groups towards monomer-dimer equilibrium

These results demonstrate the importance of both steric and electronic tuning of NHCs for the optimal reactivity of metal complexes. As such, we propose to investigate the synthesis and coordination chemistry of NHC ligands containing 2,6-*bis*(alkoxyphenyl) wingtip groups as we

propose that these will not only result in very electron rich metal centers, but also provide a runway for steric modularity.

3.1.3 Pd-NHC Complexes for Homogeneous Catalysis

Due to their properties, NHCs have had a tremendous impact in the field of palladium catalyzed cross coupling reactions.[26] Their strong electron donating capabilities have helped to facilitate the activation of strong bonds through oxidative addition processes.[22,26] Furthermore, their high BDEs with metal centers result in transition metal complexes that are very stable to decomposition pathways, generally resulting in very high turnover numbers.[58]

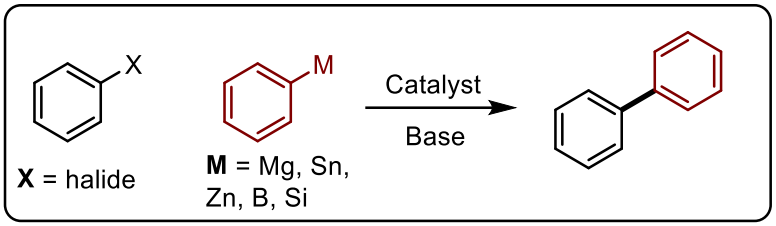

If M = Mg – Kumada; M = Zn – Negishi; M = Sn – Stille; M = B – Suzuki; M = Si - Hiyama

Scheme 3-2: General scheme of transition metal catalyzed cross coupling reactions

Palladium catalyzed cross coupling reactions has been a widely used method in the generation of new sp^2-sp^2 C-C bonds.[133] In general, these reactions feature the use of aryl electrophiles such as aryl halides, and aryl organometallic nucleophiles (**Scheme 3-2**).[134] The properties of the ligand have the capability to influence the catalyst performance of the reaction.[135] Specifically, the oxidative addition of the aryl electrophiles is facilitated by electron rich complexes, and the reductive elimination is facilitated by sterically bulky ligands. As a result of their strong σ-donating abilities, and large steric bulk, NHCs have been excellent ligands in Pd catalyzed cross coupling.

It is within our interest to study the properties of the 2,6-*bis*(alkoxyphenyl) substituted NHC ligands for its applications in Pd catalyzed cross coupling reactions. More specifically, we aim to investigate their effects in the widely used Suzuki-Miyaura reaction (SMR) which has become instrumental in the synthesis of pharmaceutical agents.[61] These ligands are expected to be more electron rich than the standard NHCs yet benefit from steric tunability by the incorporation of alkyl groups by simple alkylation reactions. The steric tunability provided by these novel NHC ligands would be ideal for their implementation in catalytic reactions.

3.2 Results and Discussion

3.2.1 Ligand Synthesis

Following a report by Lüning and coworkers,[136] we began by developing a synthetic route consisting of five steps to generate the RO-NHC-HX salts (**Scheme 3-3**). The proposed synthesis begins with the alkylation of commercially available 2-nitroresorcinol, followed by the reduction of the nitro functional group, thus synthesizing a 2,6-*bis*(alkoxy) aniline. The aniline would then be reacted with oxalyl chloride to synthesize a diamide, which would be reduced with lithium aluminum hydride ($LiAlH_4$). The resulting diamine would be ring closed with triethyl orthoformate under acidic conditions producing the RO-NHC-HX salt.

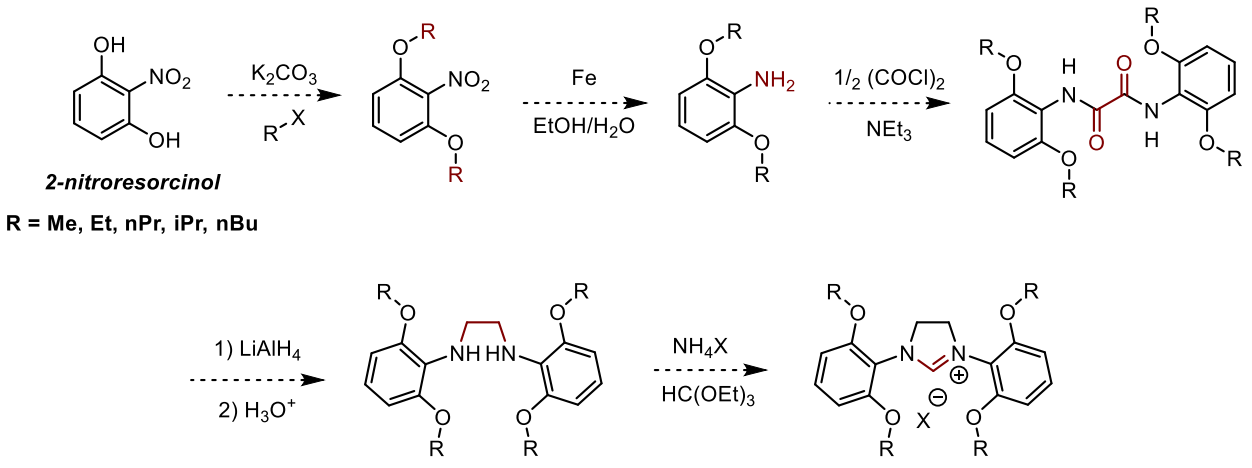

Scheme 3-3: Proposed synthesis of RO-NHC-HX salt

We began by reacting 2-nitroresorcinol with an excess of alkyl halide and using K_2CO_3 as a base at reflux in CH_3CN or DMF (**Scheme 3-4**). This procedure proved to be successful and applicable towards a variety of alkyl groups (methyl, ethyl, n-propyl, iso-propyl, and n-butyl) as well as high yielding with isolated yields ranging from 97-99%. The resulting products were characterized by using GC-MS, as well as ^{1}H and $^{13}C\{^{1}H\}$ NMR spectroscopy which confirmed the structure of the products that were isolated. We then proceeded to use the isolated products without further purification in the reduction of the nitro group using Fe metal as a reducing agent under acidic conditions.

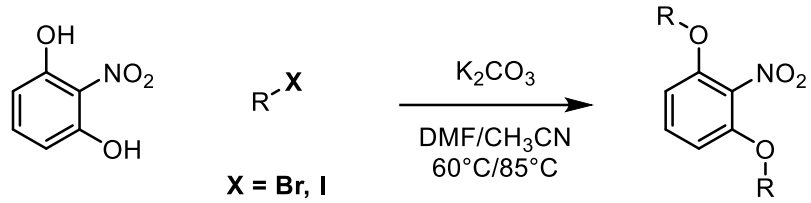

R = Me (**3-1**) 99%
Et (**3-2**) 99%
n-Pr (**3-3**) 99%
i-Pr (**3-4**) 97%
n-Bu (**3-5**) 99%

Scheme 3-4: Alkylation of 2-nitroresorcinol

The alkylated nitro aromatics **3-1** to **3-5** were reacted with excess Fe (4.0 equiv.) in the presence of an excess of NH_4Cl (4.0 equiv.) at 90°C in a 2:1 mixture of EtOH and H_2O for 18 hours (**Scheme 3-5**). While we successfully isolated product from this reaction, the initial isolated yields were unsatisfactory, ranging from 20-30%. This inefficiency represented a problem as this was early in the multistep synthesis. As full conversion of the starting material was observed by TLC, we hypothesized that our low yields stemmed from the workup process. Specifically, we proposed that the residual ethanol solvent proved challenging for separation and isolation of our

desired product during aqueous workup. As such, removal of the ethanol solvent *in vacuo* prior to aqueous workup was investigated, which dramatically increased our isolated yields to 70-90% of **3-6** to **3-10**. Moreover, we found that it was pertinent for the product to have minimal residual Fe in order to synthesize a clean product for the next steps of the synthesis. As such, careful filtration through Celite® along with careful purification using silica gel chromatography ensures the product's high purity.

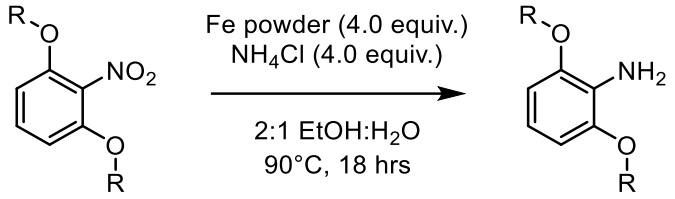

R = Me (**3-6**) 79%
Et (**3-7**) 85%
n-Pr (**3-8**) 85%
i-Pr (**3-9**) 77%
n-Bu (**3-10**) 90%

Scheme 3-5: Synthesis of 2,6-*bis*(alkoxy) aniline precursors by Fe reduction

Following the synthetic pathway in **Scheme 3-3**, we next reacted the sterically smaller anilines, **3-6** and **3-7**, with oxalyl chloride in the presence of the base, NEt_3, in anhydrous THF at room temperature for 18 hours (**Scheme 3-6**). We faced a major challenge with the isolation of **3-11** as it seems to be insoluble in common organic solvents such as EtOAc. This feat led to a difficult extraction, and we failed to isolate **3-11** for analysis. As for the reaction with **3-7**, were able to isolate product **3-12** by extracting it with EtOAc and washing it with H_2O. We observed inconsistent and low yielding results, likely related to solubility issues associated with the corresponding amide products.

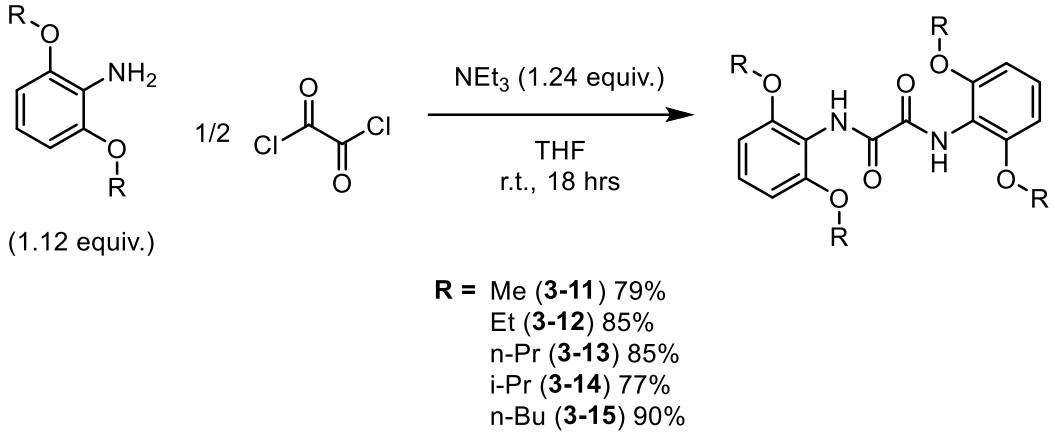

Scheme 3-6: Synthesis of the RO-amide precursors

We reviewed procedures from literature and examined a related procedure reported by Schrodi *et al.*[125] Precipitation of the product by slowly layering hexanes in a concentrated solution of CH_2Cl_2 afforded us **3-12** to **3-15**. However, this workup failed to successfully isolate compound **3-11**. In addition, analyses by ^1H NMR spectroscopy revealed minor impurities which we hypothesized to be residual ammonium salts. We therefore changed the workup process once more and we found that products **3-12** to **3-15** were not soluble in H_2O, but the ammonium salts were, thus, the crude mixture was dispersed in copious amounts of H_2O to dissolve the ammonium salts. The aqueous solution was filtered, and the product was washed with hexanes/Et_2O to remove further organic impurities leading us to good to excellent yields of compounds **3-12** to **3-15**.

Due to the success of the isolation of compounds **3-12** to **3-15**, we applied the same workup conditions, and successfully isolated **3-11** in excellent yields. Analyses of compounds **3-11** to **3-15** by GC-MS as well as ^1H and $^{13}C\{^1H\}$ NMR spectroscopy confirmed we have successfully synthesized our products with high purity.

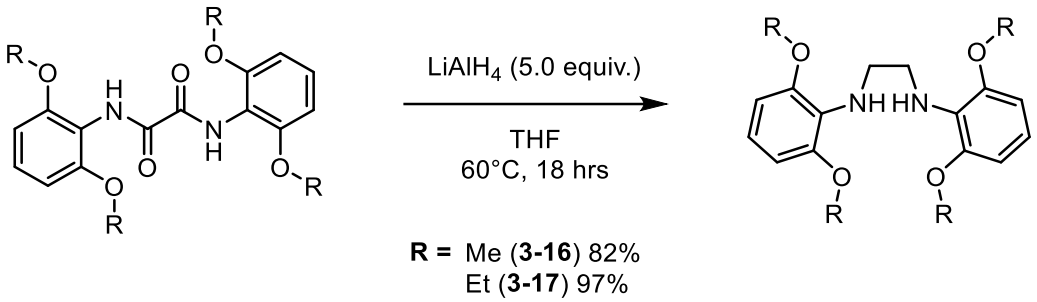

Scheme 3-7: Synthesis of RO-diamine precursor via $LiAlH_4$ reduction

The reduction of the amide precursors followed, and we were successful at reducing amide precursors, **3-11** and **3-12**, using 5.0 equivalents of $LiAlH_4$ in anhydrous THF at 60°C for 18 hours (**Scheme 3-7**). Upon completion of the reaction by TLC analysis, the excess $LiAlH_4$ was quenched with the slow addition of EtOAc and MeOH then H_2O resulting in the significant formation of insoluble salts. These salts were filtered through Celite® before extracting the product into EtOAc which resulted in an oil product which we opted to carry through without further purification. The oil product was characterized by ^{1}H NMR spectroscopy as well as GC-MS revealing the diamines **3-16** and **3-17**.

As we increased the steric bulk of the alkyl substituents, major challenges were encountered with this procedure. We first attempted to reduce **3-13** under the same conditions but unfortunately, full conversion of the starting material was not observed by TLC. This was confirmed further by GC-MS analysis of the reaction mixture which showed a peak for the residual amide precursor. Additionally, residual N*H* protons about the amide were observed in the ^{1}H NMR spectrum. Initially, we attempted to circumvent this issue by increasing the equivalents of $LiAlH_4$ (>10 equiv.) and extend heating times (48 – 72 hours). Unfortunately, in all cases we observed incomplete conversion. These results were also observed with amide precursors, **3-14** and **3-15**. We hypothesize the origin of this to be steric in nature, as the amide carbonyl is more sterically shielded by the increasing size of the R groups in precursors **3-13** to **3-15**.

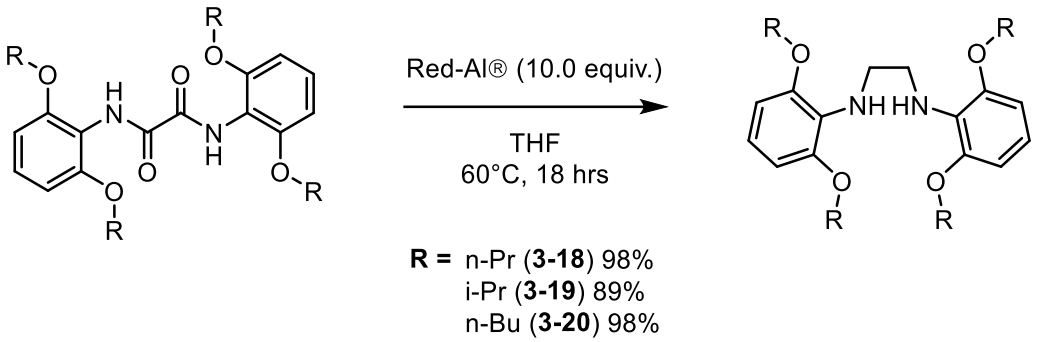

Scheme 3-8: Synthesis of RO-diamine precursor via Red-Al® reduction

To help mitigate this problem, we investigated the use of sodium *bis*(2-methoxyethoxy) aluminum hydride (Red-Al®) as an alternative reducing agent which was inspired by reports by Schrodi *et al*.[125] In contrast to $LiAlH_4$, Red-Al® is fully homogeneous in many organic solvents, which should facilitate this reaction kinetically, which may translate to higher reactivity. Indeed, Red-Al® successfully reduced **3-13**, along with **3-14** and **3-15** achieving compounds **3-18** to **3-20** in high yields (**Scheme 3-8**). In all cases, full conversion of the starting material to the product was observed by TLC as well as results from the analysis of the products using the GC-MS showed one peak which was the *m/z* values of the reduced products **3-18** to **3-20** which was 444.2, 444.2, and 501.3, representing the $[M]^+$ of these products respectively.

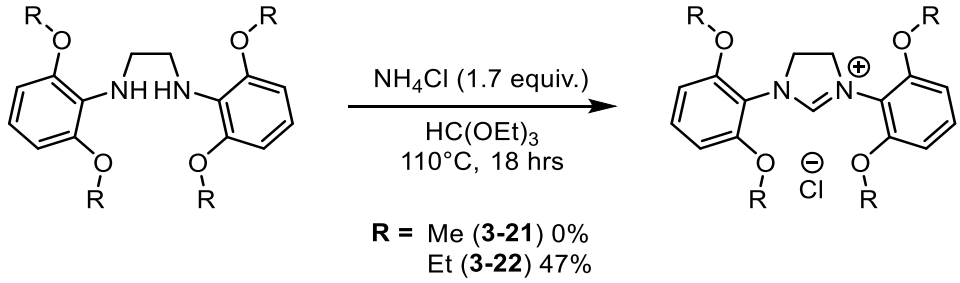

Scheme 3-9: Attempts to synthesize RO-NHC-HCl salts

With the diamine precursors in hand, **3-16** to **3-20**, we began the ring closing procedure with triethyl orthoformate under acidic conditions. We initially treated **3-16** and **3-17** with NH_4Cl

in triethyl orthoformate at 110°C for 18 hours to synthesize RO-NHC-HCl salts **3-21** and **3-22** (**Scheme 3-9**). Unfortunately, the isolation of **3-21** failed as we isolated an insoluble oily mixture which presented intractable mixtures by ^{1}H NMR spectroscopy.

Continuing to the isolation process of compound **3-22**, the product was isolated by extraction into CH_2Cl_2 and was characterized by ^{1}H NMR spectroscopy. The ^{1}H NMR spectrum of the chloride salt displayed multiple products and impurities. We attempted a myriad of ways to purify the crude compounds starting with recrystallization by layering hexanes onto a concentrated solution of CH_2Cl_2 which resulted in a minimal amount of product. Additionally, the ^{1}H NMR spectrum of the recrystallized product showed numerous impurities. We then tried to recrystallize the crude product by layering hexanes onto a concentrated solution of isopropanol. Unfortunately, no crystals were formed from this recrystallization attempt. We then proceeded to adjust the ratio of the solvents and tried a 4:1 as well as a 2:1 mixture of hexanes to isopropanol. The 4:1 mixture precipitated a small amount of product resulting in a 47% isolated yield. The ^{1}H NMR spectrum of the isolated product still showed baseline impurities, and the procedure was not reproducible. Therefore, we proposed changing the counter ion would influence the solubility, which may in turn translate to more facile purification. Schrodi *et al*. reported facile purification with similar species using a BF_4 counter ion.[125]

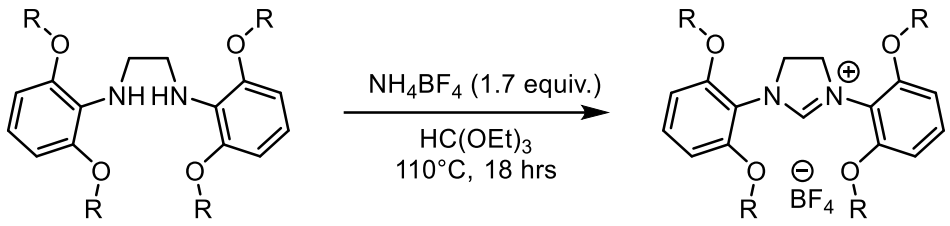

R = Me (**3-23**) 95% (SIDMP-HBF_4)
Et (**3-24**) 90% (SIDEP-HBF_4)
n-Pr (**3-25**) 90% (SIDnPP-HBF_4)
i-Pr (**3-26**) 70% (SIDiPP-HBF_4)
n-Bu (**3-27**) 75% (SIDnBP-HBF_4)

Scheme 3-10: Synthesis of RO-NHC-HBF_4 salts

Treatment of compounds **3-16** to **3-20** with NH_4BF_4 in triethyl orthoformate at 110°C for 18 hours under an inert atmosphere successfully resulted in compounds **3-23** to **3-27** (**Scheme 3-10**). This reaction had noticeable visual differences compared to NH_4Cl such as the formation of transparent crystals after 18 hours, around the round bottom flask, just above the solution. These clear crystals were used as an indication that the reaction has reached completion. In some cases, specifically with **3-27**, the reaction mixture solidifies as it was cooled to room temperature, and we treated this as an indication that the reaction has reached completion. For further confirmation, TLC analysis was utilized to observe the disappearance of the diamine starting material to indicate full conversion. The product was then extracted into CH_2Cl_2 and was precipitated out by layering hexanes into a concentrated solution of CH_2Cl_2. The RO-NHC-HBF_4 salt procedure was high yielding and the hypothesized solubility issue in the isolation process was resolved. ^1H and $^{13}C\{^1H\}$ NMR spectroscopy confirmed that we have successfully synthesized the target products and that we have successfully synthesized pure products as we acquired clean NMR spectra as well as high solution mass spectrometry (HRMS) for compounds **3-23** to **3-27**.

3.2.2 Metallation Studies

Metallation to Sulfur and Copper

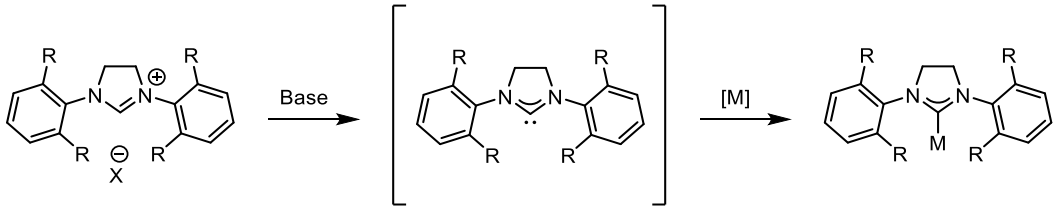

Scheme 3-11: General metallation path of NHCs in literature

In most cases in literature, the metallation of NHC ligands to transition metals is a two-step process that begins with the ligand being deprotonated with a strong base, such as KO^{t}Bu, to create the free carbene, followed by treatment with a suitable metal precursor to create the metal complex (**Scheme 3-11**).[26] However, because free carbenes are highly air and moisture-sensitive, the entire process is typically carried out in a glovebox. We viewed the requirement of a glovebox as a limitation at this stage of this thesis, and thus sought to develop methods which could be conducted on the benchtop.

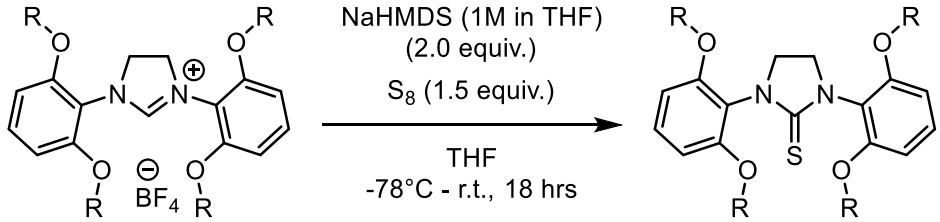

R = Me (**3-28**) 43%
Et (**3-29**) 53%
n-Pr (**3-30**) 29%
i-Pr (**3-31**) 15%
n-Bu (**3-32**) 61%

Scheme 3-12: Synthesis of RO-NHC sulfur complexes

To confirm the potential of **3-23** to **3-27** as ligands, we first explored metallation to sulfur in a one-pot procedure (**Scheme 3-12**), developed by our group.[137] Sulfur represents an ideal metal

to test the metallation of these ligands, as the resulting products are air and moisture stable and can easily be characterized to confirm successful metallation. Thus, treatment of **3-23** to **3-27** with 2.0 equivalents of a 1M solution of NaHMDS in anhydrous THF at -78°C which was gradually warmed to room temperature over the course of 18 hours resulted in the desired sulfur complexes in satisfactory yields. The structures of **3-28** to **3-32** were confirmed by ^{1}H NMR spectroscopy which showed the disappearance of the signal at δ 7.62 – 8.00 ppm corresponding to the C-H proton as well as GC-MS confirmed the masses of the complexes. These results indicated that **3-23** to **3-27** could act as suitable ligand precursors, and thus were investigated towards metallation with copper. We selected copper(I) halide salts as precursors as the expected products would be linear and therefore useful in the characterization of the steric parameters of the ligand.[54]

We first attempted to metallate **3-24** with a strategy we developed in our laboratories, using a one-pot procedure with the weak base NEt_3, in the presence of CuCl at 60°C for 1 hour.[131] Unfortunately, the desired product was isolated in very poor yields for **3-24** (<5%).[138] We then repeated this procedure with longer reaction times of 18 hours. The yield increased to 18% however, analysis by ^{1}H NMR spectroscopy showed an impure product with residual ligand and baseline impurities. Similar results were also observed using CuI. We hypothesized that the ineffectiveness of this procedure towards RO-NHC-HBF_4 salts may be due to their decreased acidity compared to other common NHCs that this method was effective with.

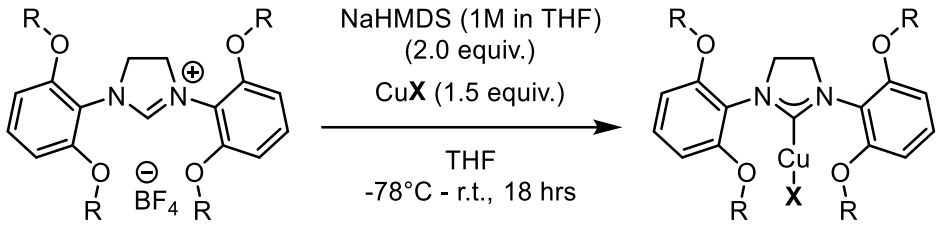

R =	X = Cl	X = Br	X = Cl
Me	(**3-33**) 11%	(**3-38**) 51%	(**3-43**) 32%
Et	(**3-34**) 50%	(**3-39**) 49%	(**3-44**) 44%
nPr	(**3-35**) 44%	(**3-40**) 53%	(**3-45**) 74%
iPr	(**3-36**) 16%	(**3-41**) 54%	(**3-46**) 65%
nBu	(**3-37**) 60%	(**3-42**) 76%	(**3-47**) 69%

Scheme 3-13: Metallation of RO-NHC-HBF_4 to copper(I) halides using a strong base

Thus, we employed the use of a stronger base, NaHMDS, using the same procedure we used to metallate the ligands to sulfur.[137] We subjected preligands, **3-23** to **3-27,** with 2.0 equivalents of NaHMDS under the presence of CuCl in THF at -78°C, which was gradually warmed to room temperature over the course of 18 hours (**Scheme 3-13**). This procedure resulted in the desired copper(I) complexes in satisfactory yields. The products were purified by simple filtration through basic alumina and then silica gel which gave the products in high purity as judged by ^{1}H NMR spectroscopy. Filtration using basic alumina was found to be essential to remove heterogeneous copper(I) salts whereas silica gel assures that residual ligand and other organic based impurities were removed. This procedure proved to be successful as well as reproducible which was transferable towards other copper precursors, CuBr and CuI, leading us to isolate [Cu(NHC)Br] (**3-38** to **3-42**) and [Cu(NHC)I] (**3-43** to **3-47**) complexes as well (**Scheme 3-13**). All the copper complexes were all characterized by ^{1}H and $^{13}C\{^{1}H\}$ NMR spectroscopy as well as high resolution mass spectrometry (HRMS).

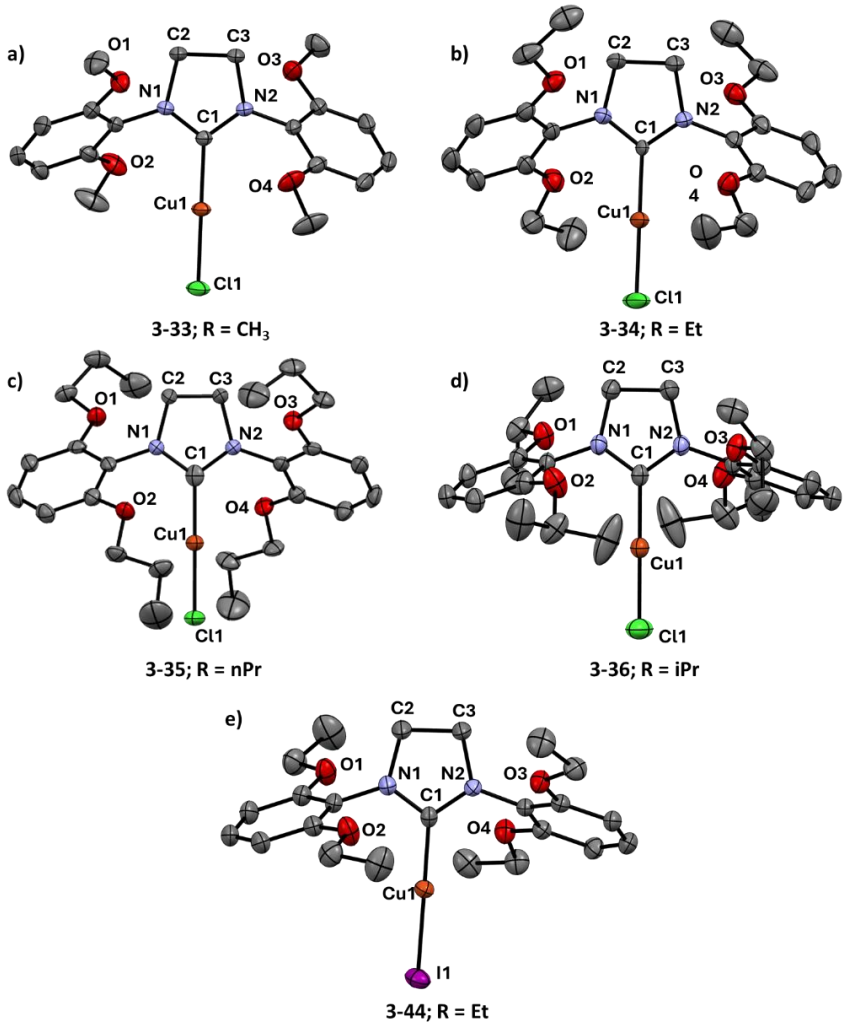

Figure 3-4: Crystallographically determined structure of a) [Cu(SIDMP)Cl] (**3-33**), b) [Cu(SIDeP)Cl] (**3-34**), c) [Cu(SIDnPP)Cl] (**3-35**), d) [Cu(SIDnPP)Cl] (**3-36**), and e) [Cu(SIDEP)I] (**3-44**) displaying thermal ellipsoids drawn at the 50% confidence level. Hydrogen atoms and solvent (THF/$CHCl_3$) are omitted for clarity. In complex **3-36**, disordered atoms are omitted for clarity. Selected interatomic distances [Å] and angles [deg] are detailed in **Table 3-1**. (*vide infra*)

Table 3-1: Selected interatomic distances [Å] and angles [deg] for crystallographic data in **Figure 3-4**.

Bonds	3-33	3-34	3-35	3-36	3-44
N(1)−C(1) [deg]	1.342(2)	1.330(9)	1.338(1)	1.332(8)	1.336(0)
C(1)−N(2) [deg]	1.342(2)	1.330(9)	1.338(1)	1.332(8)	1.332(4)
N(1)−C(1)−N(2) [Å]	107.8(1)	107.8(5)	107.5(8)	107.7(6)	108.0(3)
C(1)−Cu(1) [deg]	1.888(1)	1.885(2)	1.883(6)	1.891(1)	1.891(5)
Cu(1)−Cl(1) [deg]	2.109(9)	2.102(9)	2.105(9)	2.116(3)	2.401(6)
C(1)−Cu(1)−X(1) [Å]	180.0(0)	180.0(0)	180.0(0)	180.0(0)	176.1(3)

Furthermore, single crystals of **3-33** to **3-37** suitable for X-ray diffraction were grown from the slow diffusion of hexanes into a concentrated THF or $CHCl_3$ solutions to give definitive structural confirmation (**Figure 3-4**). The X-ray structure clearly demonstrates the successful ligation of these ligands about the copper center. In both cases, the copper exists in a linear geometry with the $C_{carbene}$-Cu bond lengths being closely resembled to the literature.[139]

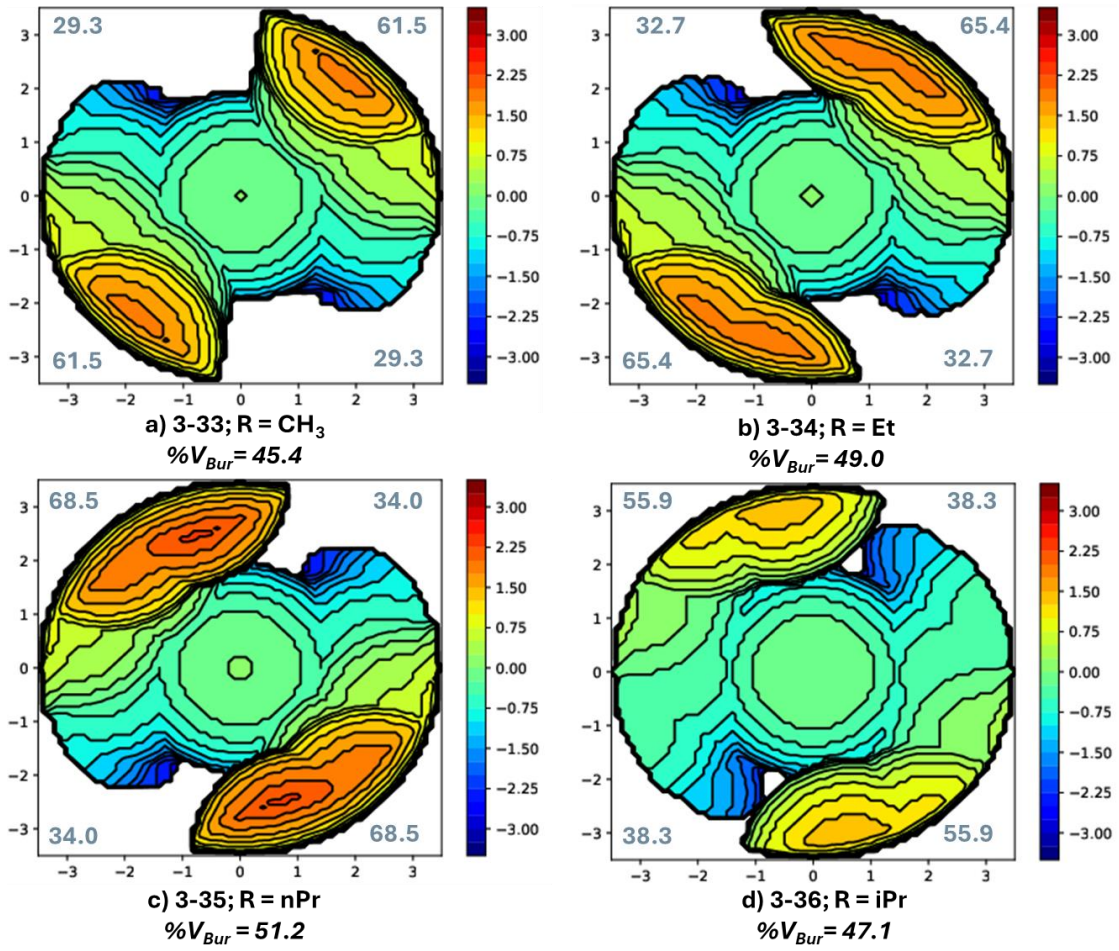

Figure 3-5: Topographical steric maps (along z-axis) of **3-33** to **3-36** showing $\%V_{Bur}$ values per quadrant and average $\%V_{Bur}$ for each complex

The steric parameters of the ligands from **3-23** to **3-27** were analyzed using the SambVca 2.1 web application to calculate the percent buried volume ($\%V_{Bur}$) and three-dimensional steric

maps of the linear [Cu(NHC)Cl] and [Cu(NHC)I] complexes **3-33** to **3-36**.[54] **Figure 3-5** displays the topography maps analyzing the $\%V_{Bur}$ in four different regions surrounding the metal center. All four complexes display two quadrants that are more sterically crowded and two that are less hindered characteristic of NHC ligands.[128,140] As predicted, an increase in the steric crowding was observed by increasing the size of the alkyl groups which is evident by the increase of in the averaged $\%V_{Bur}$ values. Interestingly, a different morphology can be observed when comparing isomers **3-35** and **3-36** as the longer linear chains in **3-35** results in distinct regions of steric strain while the secondary substituents in complex **3-36** appear more dispersed. When comparing the quadrant $\%V_{Bur}$ values of these two complexes **3-36** displays an increase in the NE and the SW quadrants while a decrease in the NW and SE quadrants relative to **3-35**. The topographical steric maps displayed in **Figure 3-5** demonstrates flexibility of such ligands that are promising for applications in catalysis.

Metallation to Silver, Palladium and Ruthenium

Preliminary Attempts

Following the success of metallating preligands, **3-23** to **3-27**, to sulfur and copper, we investigated the metallation to some other late transition metals such as palladium, ruthenium and silver.

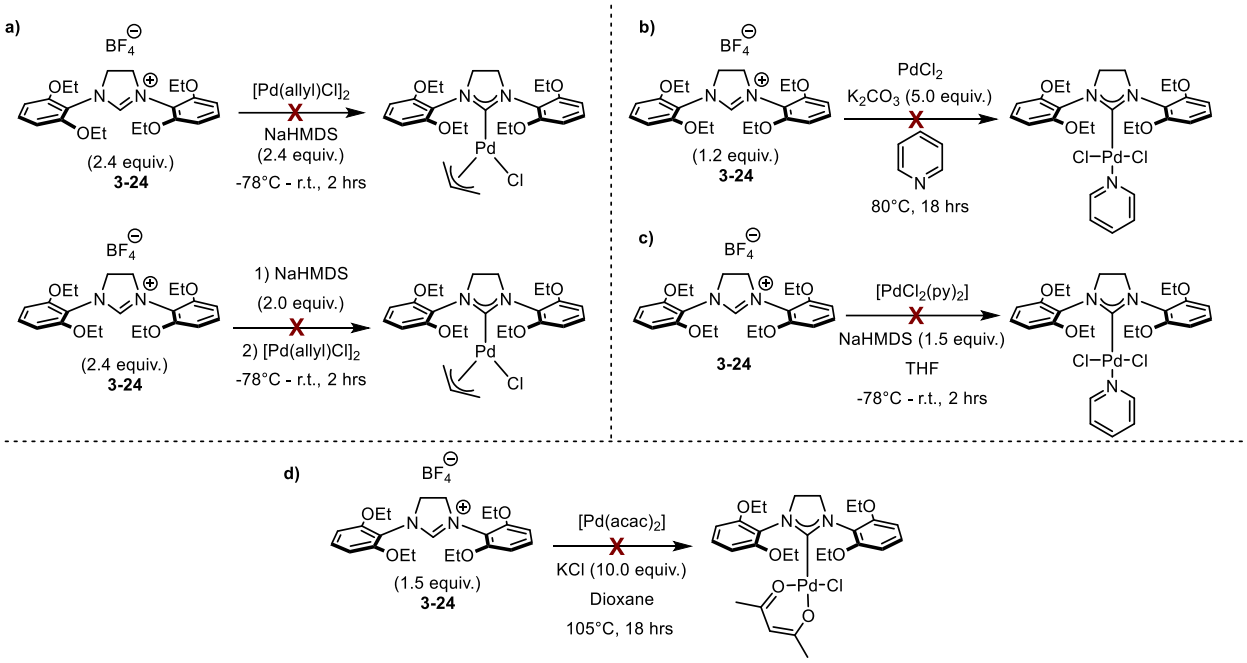

Scheme 3-14: Initial attempts at metallation to Pd using literature procedures

We first attempted to metallate **3-24** to palladium using a similar one-pot procedure that was successful with sulfur and copper.[137] Thus, we treated **3-24** with 2.4 equivalents of NaHMDS in the presence of $[Pd(allyl)Cl]_2$ in anhydrous THF at -78°C, which was gradually warmed to room temperature over the course of 2 hours (**Scheme 3-14a**). The reaction mixture was then quenched with the addition of CH_2Cl_2, and the product was isolated using silica gel chromatography and precipitated with hexanes. Analysis by ^1H NMR spectroscopy revealed that the reaction was unsuccessful as both the ligand and the Pd dimer were present in the spectrum with no evidence of a Pd coordinated ligand due to the remaining $C_{carbene}$-H peak at δ 7.86 ppm.

After the failed attempts with $[Pd(allyl)Cl]_2$, we sought out other metallation procedure of NHC ligands to palladium in literature. First, we attempted the preparation of a PEPPSI-type complex (PEPPSI = pyridine enhanced precatalysts preparation stabilization and initiation) which was developed by Professor Michael Organ and colleagues.[32] Thus, we treated 1.2 equivalents of **3-24** with $PdCl_2$ and 5.0 equivalents of K_2CO_3 in pyridine at 80°C for 18 hours under air (**Scheme**

3-14b). Unfortunately, this method was also met with failure and analysis by ^{1}H NMR spectroscopy showed multiple compounds which includes the presence of an unreacted NHC salt as indicated by the $C_{carbene}$-H peak at δ 7.86 ppm. We hypothesized that the weak base, K_2CO_3, may be ineffective at deprotonating the ligand due to the increased pK_a of the ligand precursor. Therefore, we changed the conditions treating **3-24** with NaHMDS with a pre-formed Pd precursor, $[PdCl_2(py)_2]$, in anhydrous THF at -78°C which was gradually cooled to room temperature during the course of 2 hours (**Scheme 3-14c**). ^{1}H NMR spectroscopy results showed that the reaction had failed once again. Multiple undiscernible compounds were observed leading us to the assumption that the ligand may have decomposed under these conditions. Finally, we attempted to metallate 1.5 equivalents of **3-24** to $[Pd(acac)_2]$ with 10.0 equivalents of KCl in anhydrous dioxane at 105°C for 18 hours (**Scheme 3-14d**).[141] Unfortunately, this reaction was also met with failure. Analysis of the isolated product by ^{1}H NMR spectroscopy revealed trace amounts of the ligand and majority of the peaks were from the Pd precursor. Similarly, as before, coordination of the ligand to Pd was not observed as we did not see the disappearance of the $C_{carbene}$-H peak at δ 7.86 ppm.

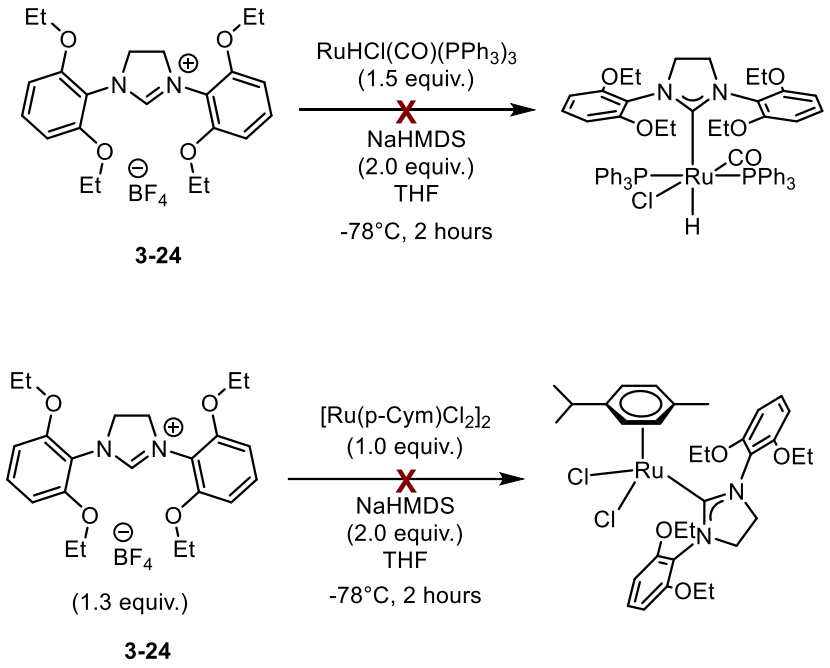

Scheme 3-15: Attempts at metallation of 3-24 to Ru using literature procedure

As shown in **Scheme 3-15**, attempts to metallate RO-NHC-HBF_4 to ruthenium precursors,[137] $[RuHCl(CO)(PPh_3)_3]$ and $[Ru(p\text{-}cym)Cl_2]_2$ were met with the same fate as our initial attempts with palladium. In both cases, multiple compounds that were difficult to identify and ascertain were observed by ^1H NMR spectroscopy.

Table 3-2: Synthesis of complex **3-48** using procedures from literature

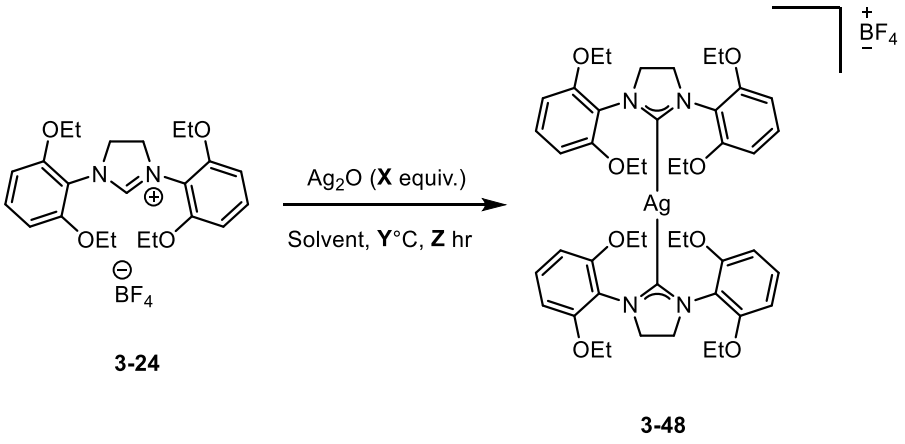

Entry	Temperature (°C)	Solvent	Ag_2O (equiv.)	Time (h)
1	85	CH_3CN	1.75	3
2	85	CH_3CN	1.75	24
3	85	CH_3CN	1.75	48
4	45	CH_2Cl_2	1.15	24

General Consideration: 3-24 (0.10-0.21 mmol) and Ag_2O (0.18-0.37 mmol) in solvent (1-2 mL).

As all other methods attempted to metallate ligand **3-24** to palladium and ruthenium failed, we instead pivoted towards other common NHC metallation routes. As such, we investigated the direct metallation of **3-24** to Ag_2O.[37] NHC complexes of Ag have been demonstrated to be labile in nature and undergo facile transmetallation to other transition metals.[36,142] Furthermore, metallation onto Ag_2O is commonly reported to occur under air giving bench-stable complexes. We first attempted procedures from literature[143,144] which involved refluxing conditions in acetonitrile, resulting in complex **3-48** (**Table 3-2**, Entry 1). Upon analysis of the ^1H NMR spectrum, a new species we attributed to successful metallation appeared to form. However residual ligand was also observed indicating incomplete conversion. Therefore, we attempted the optimization of this reaction with longer reactions times, higher temperatures, and solvent changes (**Table 3-2**, Entry 2 to 4).

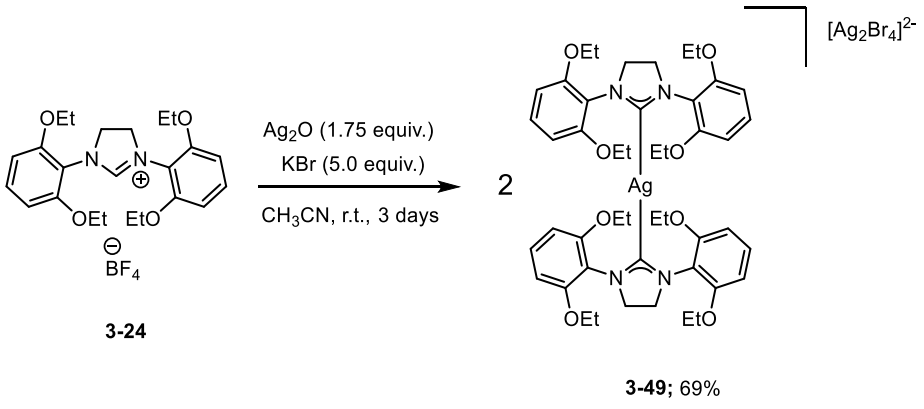

Scheme 3-16: Metallation of **3-24** to silver using literature procedure

Unfortunately, these modifications resulted in the apparent decomposition of Ag_2O in solution as indicated by a silver mirror forming around the reaction flask after every reaction. We hypothesize that the silver mirror formed via the consumption of Ag_2O, preventing further conversion. As such, we attempted another procedure from literature[145] which operated under milder conditions which hopefully would hinder silver mirror formation. The procedure was followed verbatim, and we successfully synthesized complex **3-49** in full conversion and in good yield (**Scheme 3-16**). The disappearance of the $C_{carbene}$-H peak as well as the shift in the position of the backbone peak of the ligand in the ^{1}H NMR spectrum, was indicative of the formation of complex **3-49**.

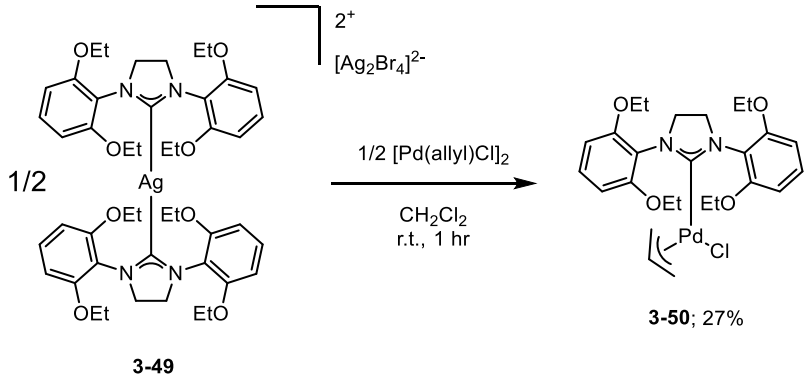

Scheme 3-17: Synthesis of Pd complex through transmetallation

We proceeded to attempt transmetallation of **3-49** to Pd and Ru with the silver complex in hand. Treatment of **3-49** with $[Pd(allyl)Cl]_2$ in CH_2Cl_2 under air resulted in the immediate formation of a white precipitate, likely indicative of AgX salts. Upon filtration and removal of all volatiles *in vacuo*, an off-white solid tentatively assigned complex **3-50** was isolated (**Scheme 3-17**). Although analysis by ^{1}H NMR spectroscopy was consistent with the structure of **3-50**, additional byproducts were also observed. Upon further analysis with TLC, multiple spots were observed which confirmed that the product was impure, and purification was attempted by column

chromatography which clearly resulted in the formation of our desired product in relatively low isolated yield of 27%.

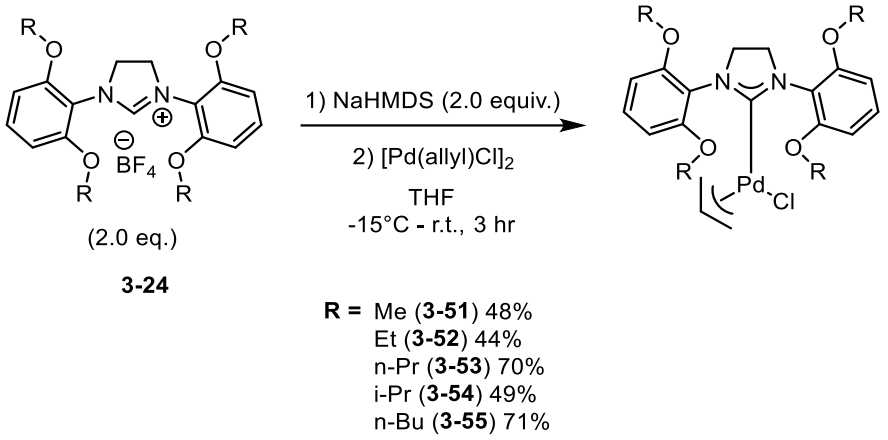

Scheme 3-18: Synthesis of RO-NHC Pd complexes using the glovebox

During the late stages of this project, our research group acquired a nitrogen atmosphere glovebox. We were then able to test the most common metallation method for NHCs precursors, including a two-step deprotonation then metallation method. Thus, in a nitrogen filled glovebox, we treated **3-23** to **3-27** with NaHMDS for 2 hours at -15°C, which, was gradually warmed to room temperature (**Scheme 3-18**). After the 2 hours, a solution of $[Pd(allyl)Cl]_2$ in THF was added to the solution containing the free ligand, and this stirred at room temperature for 1 hour. The reaction mixture was then taken out of the glovebox and worked up in the fumehood. It was quenched with MeOH, and the solvent was removed *in vacuo*. The residue was dispersed in CH_2Cl_2 and filtered through Celite® on a frit to remove heterogeneous Pd black. Analysis by TLC revealed three spots which we were able to separate via flash column chromatography. The ^1H NMR spectroscopy and HRMS was consistent with the structures of **3-51** to **3-55** with higher yields compared to the transmetallation route. Upon analysis of their ^1H spectra, we observed broad peaks for the allyl region which was sharpened when cooled to 278K suggesting thermally fluxional behaviour.[146] We hypothesized that this behaviour could potentially be indicative of hemilability of the NHC

wingtip groups which was most evident in complex **3-51**, the smallest ligand of the series. Complexes **3-51** to **3-55** were observed to exhibit decomposition as indicated by slow discoloration upon standing and were store under N_2.

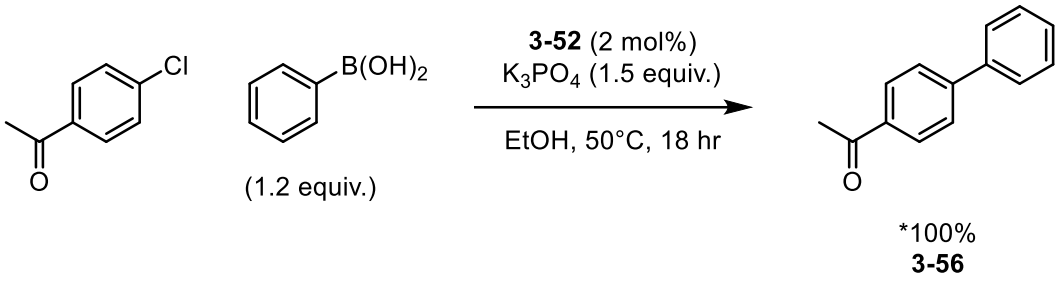

Scheme 3-19: Suzuki-Miyaura coupling with **3-52** as the catalyst. **denotes conversion by GC-MS*

With pure Pd complexes in hand, we investigated their activity in a benchmark Suzuki-Miyaura reaction (SMR) of aryl chlorides (**Scheme 3-19**). Aryl chlorides represent challenging substrates in cross coupling reactions such as the SMR, and use of highly electron rich and sterically hindered ligands such as NHCs have been previously demonstrated to be highly effective in this transformation.[22,32] Thus, this transformation would allow us to evaluate the potential synthetic applications of complexes **3-51** to **3-55**. Full conversion by GC-MS of the starting material to the product was achieved using 2 mol% of the **3-52** using 4-chloroacetophenone as our electrophile. This demonstrates that the catalyst, **3-52**, was indeed active in catalysis. Moreover, we were interested at investigating the influence of sterics in catalyst activity. Therefore, the non-activated and subsequently very challenging substrate, 4-chloroanisole, was used instead investigated as a starting material with catalysts **3-51** to **3-55**, run under otherwise identical conditions. As shown in **Table 3-3**, an obvious pattern emerges with the more sterically bulky the ligands giving higher the conversions by GC-MS. Additionally, for catalyst comparison with a known catalyst, we used [(SIMes)Pd(allyl)Cl] and found that catalyst **3-55** was more active (**Table**

3-3, Entry 6). This trend helps to demonstrate the influence of a ligand on catalytic results and helps to signify the importance of steric tunability and modularity in ligand design.

While a trend can be observed with the higher steric parameters and the yields, the catalytic performance of complex **3-55** is lower compared to reported Pd-NHC precatalysts in literature.[147] Palladium catalysts bound to a single monodentate ligand are typically reported to have higher catalytic performance. Thus, we hypothesize that the lower catalytic activity of precatalysts **3-51** to **3-55** may be due to non-productive hemilabile coordination of the RO-NHC ligand to the palladium center under these conditions. We believe that these ligands may be more effective in other catalytic transformations and are currently exploring alternative applications in our laboratories.

Table 3-3: Suzuki-Miyaura reaction with 4-chloroanisole comparing the Pd catalysts

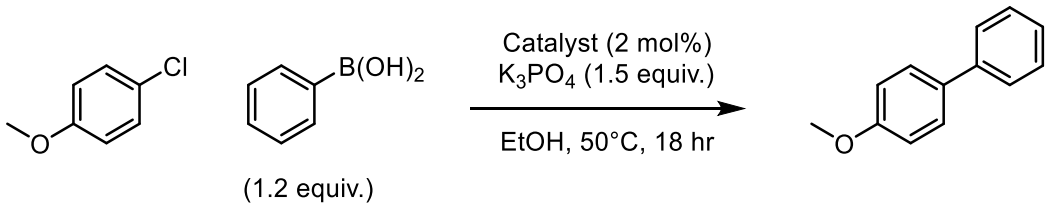

(1.2 equiv.)

Entry	Catalyst	*Conversion (%)
1	3-51	16
2	3-52	26
3	3-53	46
4	3-54	47
5	3-55	60
6	[(SIMes)Pd(allyl)Cl]	45

General Consideration: 4-chloroanisole (0.3 mmol), phenyl boronic acid (0.36 mmol), K_3PO_4 (0.45 mmol), catalyst (0.006 mmol), in solvent (1.5 mL) at 50°C for 18 hours. **denotes conversion by GC-MS, average of 2 replicates*.

3.3 Conclusions and Future Work

In conclusion, we have established the synthesis of several new sterically modular and very electron rich NHCs, which are conveniently prepared in high yield with little purification in

between steps. We have further demonstrated that these ligands can be metallated to sulfur, copper, palladium and silver. The highest yields and purities were obtained using the strong base NaHMDS, but we demonstrated that a transmetallation route via Ag-NHCs is also viable, which does not require inert conditions or a glovebox. Modulation of the alkyl groups installed into the NHC-HX salts in the first step of their metallation ultimately results in different steric parameters of the ligands which can be structurally observed via X-ray crystallography. The direct impact of the steric environment provided by the ligand was made evident in the SMR of aryl chlorides using [(RO-NHC)Pd(allyl)Cl] type precatalysts, with the highest conversions being observed by the sterically largest ligand (SIDnBP). This proof of principle helps to indicate the significance of being able to sterically manipulate ligands in catalysis.

Future work on this project will be dedicated to the further investigations of these ligands in catalysis. Additionally, we propose the synthesis of several new ligands, which would further push their steric boundaries. As these ligands represent sterically tunable and very electron rich spectator ligands, we anticipate that they will find use in a variety of different catalytic transformations. The steric modularity made possible for these ligands will help to decouple electronic vs steric consideration in ligand/catalyst design which would otherwise have been very challenging to consider.

3.4 Experimental

General Considerations: All manipulations were carried out under a nitrogen or argon atmosphere unless otherwise noted using standard Schlenk techniques or in a nitrogen filled glovebox (Vigor technologies) with O_2 and H_2O levels below 0.1 ppm. Anhydrous N,N'-dimethylformamide (DMF) and acetonitrile (MeCN) were purchased from Acros Organics and stored under argon prior to use. Anhydrous tetrahydrofuran was purchased from Sigma Aldrich and stored on 3Å molecular sieves under an atmosphere of Argon. Sodium hexamethyldisilazide (NaHMDS) was purchased as 1M solutions in THF and stored under Argon at 5°C. NaHMDS as a solid at 95% purity was purchased from Sigma Aldrich All reagents were purchased from commercial suppliers and used without further purification. $[Pd(allyl)Cl]_2$ and [(SIMes)Pd(allyl)Cl] were synthesized by our previous literature procedures.[137] Catalytic reactions were performed in 16x125 culture tubes purchased from VWR. ^1H NMR spectra were measured on a Varian INOVA 500 MHz, Nanalysis 60 MHz, or a Bruker Ascend 400 MHz spectrometer where noted at 298K. Chemical shifts are reported in delta (δ) units, expressed in parts per million (ppm) downfield from tetramethylsilane (TMS) using residual protonated solvent as an internal standard ($CDCl_3$ 7.27 ppm). $^{13}C\{^1H\}$ NMR spectra were recorded at 126 MHz or 101 MHz where noted. Chemical shifts are reported as above using the solvent as an internal standard ($CDCl_3$, 77.23 ppm). Low resolution mass spectrometry was determined by GCMS using an Agilent 7890B GC equipped with a HP-5MS UI column and a 5977A MSD. High resolution mass spectrometry was performed at the Water Quality Centre at Trent University using a Thermo Qexactive Orbitrap ESI in the positive ion mode. Reaction progress was monitored by thin layer chromatography, using pre-coated Polygram® SIL G/UV_{254} TLC sheets, and spots were visualized using a UV light at 254 nm. Silica gel and basic alumina filtrations were performed with silica gel

60 (230-400-mesh) and aluminum oxide (99%, metals basis) purchased from Sigma Aldrich. Purifications of [(NHC)Pd(allyl)Cl] complexes were completed using a Buchi C-805 automated chromatography system using Buchi irregular silica gel cartridges.

Synthesis of RO-NHC-HBF$_4$ Precursors:

Synthesis of 1,3-dimethoxy-2-nitrobenzene (3-1)

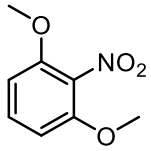

2-nitroresorcinol (4.0 g, 25.8 mmol, 1.0 equiv.), and K_2CO_3 (8.8 g, 64.5 mmol, 2.5 equiv.), were combined in anhydrous acetonitrile (20 mL) in a 50 mL pressure tube under argon. Methyl iodide (3.4 mL, 54.2 mmol, 2.1 equiv.) was injected via syringe and the pressure tube was sealed and heated at 85°C (oil bath temperature) for 18 hours. The consumption of the starting material was confirmed by TLC analysis. The solution was then cooled to room temperature then extracted into EtOAc, washed with distilled H_2O and saturated aqueous solution of NaCl. The organic layers were combined and dried with $MgSO_4$, filtered, and concentrated *in vacuo* giving 4.7 g (99%) of an orange solid. The product was used in further transformation without purification. **^{1}H NMR (400 MHz, CDCl$_3$):** δ 7.34 (t, *J* = 8.6 Hz, 1H), 6.63 (d, *J* = 8.5 Hz, 2H), 3.89 (s, 6H) ppm. **^{13}C{^{1}H} NMR (101 MHz, CDCl$_3$):** δ 152.1, 131.3, 104.7, 56.6 ppm. **LRMS** (EI, *m/z*): calc'd for $C_8H_9NO_4$: 183.1 (M^+); found: 183.1.

General Procedure for the Synthesis of RO-Nitrobenzene Precursors (Et, iPr, nPr, nBu):

Under Ar, a 150 mL round bottom flask equipped with a condenser was charged with 2-nitroresorcinol, K_2CO_3, and anhydrous DMF. The haloalkane was injected via syringe into the solution. The reaction mixture was heated at 60°C (oil bath temperature) for 18 hours. The consumption of the starting material was confirmed by TLC analysis. The solution was then cooled to room temperature then extracted into EtOAc, washed with distilled H_2O and saturated aqueous

solution of NaCl. The organic layers were combined and dried with $MgSO_4$, filtered, and concentrated *in vacuo*. The product was used in further transformation without purification.

Synthesis of 1,3-diethoxy-2-nitrobenzene (3-2)

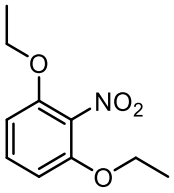

The general procedure was followed with 2-nitroresorcinol (4.0 g, 25.8 mmol) and K_2CO_3 (14.2 g, 103 mmol), in 40 mL of anhydrous DMF with bromoethane (7.6 mL, 102 mmol) giving 5.3 g (99%) as a light yellow microcrystalline solid. **^{1}H NMR (500 MHz, $CDCl_3$)**: δ 7.28 (t, *J* = 8.5 Hz, 1H), 6.59 (d, *J* = 8.5 Hz, 2H), 4.12 (q, *J* = 7.0 Hz, 4H), 1.40 (t, *J* = 7.0 Hz, 6H) ppm. **^{13}C{^{1}H} NMR (126 MHz, $CDCl_3$):** δ 151.4, 131.0, 105.5, 65.4, 14.7 ppm. **LRMS** (EI, *m/z*): calc'd for $C_{10}H_{13}NO_4$: 211.1 (M^+); found: 211.1.

Synthesis of 1,3-dipropoxy-2-nitrobenzene (3-3)

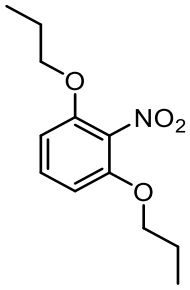

The general procedure was followed with 2-nitroresorcinol (4.0 g, 25.8 mmol) and K_2CO_3 (14.2 g, 103 mmol), in 40 mL of anhydrous DMF with 1-bromopropane (10.7 mL, 117 mmol) giving 6.2 g (99%) as a dark yellow oil. **^{1}H NMR (400 MHz, $CDCl_3$):** δ 7.27 (t, *J* = 8.4 Hz, 1H), 6.59 (d, *J* = 8.5 Hz, 2H), 4.00 (t, *J* = 6.4 Hz, 4H), 1.79 (sext, *J* = 7.4 Hz, 4H), 1.00 (t, *J* = 7.4 Hz, 6H) ppm. **^{13}C{^{1}H} NMR (101 MHz, $CDCl_3$):** δ 151.6, 131.0, 105.4, 71.1, 22.5, 10.5 ppm. **LRMS** (EI, *m/z*): calc'd for $C_{12}H_{17}NO_4$: 239.1 (M^+); found: 239.1.

Synthesis of 1,3-diisopropoxy-2-nitrobenzene (3-4)

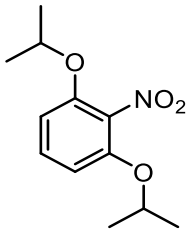

The general procedure was followed with 2-nitroresorcinol (4.0 g, 25.8 mmol) and K_2CO_3 (14.2 g, 103 mmol), in 40 mL of anhydrous DMF with 2-iodopropane (10.4 mL, 104 mmol) giving 6.0 g (97%) as a dark yellow crystalline solid. **^{1}H NMR (400 MHz, $CDCl_3$):** δ 7.25 (t, *J* = 8.5 Hz, 1H), 6.58 (d, *J* = 8.5 Hz, 2H), 4.59 (sept, *J* = 6.1 Hz, 2H), 1.33 (d, *J* = 6.1 Hz, 12H) ppm. **^{13}C{^{1}H} NMR (101 MHz, $CDCl_3$):** δ

150.6, 134.8, 130.6, 106.8, 72.6, 22.0 ppm. **LRMS** (EI, *m/z*): calc'd for $C_{12}H_{17}NO_4$: 239.1 (M^+); found: 239.1.

Synthesis of 1,3-dibutoxy-2-nitrobenzene (3-5)

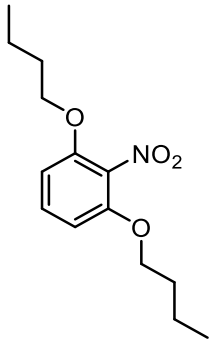

The general procedure was followed with 2-nitroresorcinol (4.0 g, 25.8 mmol) and K_2CO_3 (14.2 g, 103 mmol), in 40 mL of anhydrous DMF with 1-iodobutane (13.2 mL, 116 mmol) giving 6.9 g (99%) as a yellow microcrystalline solid. **^{1}H NMR (400 MHz, $CDCl_3$):** δ 7.27 (t, *J* = 8.5 Hz, 1H), 6.59 (d, *J* = 8.5 Hz, 2H), 4.04 (t, *J* = 6.4 Hz, 4H), 1.75 (pent, *J* = 6.4 Hz, 4H), 1.45 (sext, *J* = 7.4 Hz, 4H), 0.95 (t, *J* = 7.4 Hz, 6H) ppm. **^{13}C{^{1}H} NMR (101 MHz, $CDCl_3$):** δ 151.6, 131.0, 105.4, 69.4, 31.1, 19.2, 13.9 ppm. **LRMS** (EI, *m/z*): calc'd for $C_{14}H_{21}NO_4$: 267.1 (M^+); found: 267.1.

General Procedure for the Synthesis of the RO-Aniline Precursors:

Under air, a 250 mL round bottom flask was charged with the nitrobenzene precursor, NH_4Cl (4 equiv.), Fe powder (4 equiv.), EtOH, and distilled H_2O. The solution was stirred and heated at 90°C (oil bath temperature) for 18 hours. The consumption of the starting material was confirmed by TLC analysis. The solution was cooled to room temperature, diluted with EtOAc, and filtered over Celite® on a frit. The filtrate was then extracted into EtOAc and washed with distilled H_2O and a saturated solution of $NaHCO_3$. The organic layers were combined and dried with $MgSO_4$ and filtered. The solvent was then removed under reduced pressure to give a black oil which was allowed to solidify. The resulting solid was purified by silica gel flash column chromatography using a 4:1 mixture of hexane to EtOAc as the eluent. The product was used in further transformation without purification.

Synthesis of 2,6 – dimethoxyaniline (3-6)

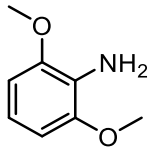

The general procedure was followed with **3-1** (3.0 g, 16.4 mmol), NH_4Cl (3.5 g, 65.5 mmol), Fe powder (3.7 g, 65.5 mmol) in 30 mL of EtOH and 15 mL of distilled H_2O giving 2.0 g (79%) as an amethyst-coloured crystalline solid. **^{1}H NMR (400 MHz, $CDCl_3$)**: δ 6.71 (t, *J* = 7.7 Hz, 1H), 6.55 (d, *J* = 8.2 Hz, 2H), 3.87 (s, 6H), 3.78 (s, 2H) ppm. **^{13}C{^{1}H} NMR (101 MHz, $CDCl_3$):** δ 151.8, 126.8, 120.4, 104.8, 56.1, 47.2 ppm. **LRMS** (EI, *m/z*): calc'd for $C_8H_{11}NO_2$: 153.1 (M^+), found: 153.1.

Synthesis of 2,6 – diethoxyaniline (3-7)

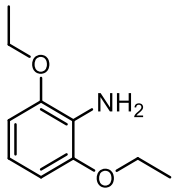

The general procedure was followed with **3-2** (3.0 g, 14.2 mmol), NH_4Cl (3.04 g, 56.8 mmol), and Fe powder (3.2 g, 56.8 mmol) in 30 mL of EtOH and 15 mL of distilled H_2O giving 2.2 g (85%) as a pale mauve flaky solid. **^{1}H NMR (400 MHz, $CDCl_3$)**: δ 6.65 (t, *J* = 7.6 Hz, 1H), 6.51 (d, *J* = 7.9 Hz, 2H), 4.08 (q, *J* = 7.0 Hz, 4H), 3.95 (s, 2H), 1.44 (t, *J* = 7.0 Hz, 6H) ppm. **^{13}C{^{1}H} NMR (101 MHz, $CDCl_3$):** δ 147.1, 125.8, 117.1, 105.3, 64.3, 15.3 ppm. **LRMS** (EI, *m/z*): calc'd for $C_{10}H_{15}NO_2$: 181.1 (M^+), found: 181.1.

Synthesis of 2,6 – dipropoxyaniline (3-8)

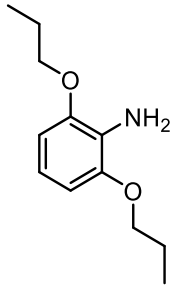

The general procedure was followed with **3-3** (4.4 g, 18.6 mmol), NH_4Cl (3.97 g, 74.2 mmol), and Fe powder (4.1 g, 74.2 mmol) in 7.0 mL of EtOH and 3.5 mL of distilled H_2O giving 3.3 g (85%) as a dark brown crystalline solid. **^{1}H NMR (400 MHz, $CDCl_3$)**: δ 6.66 (d, *J* = 7.9 Hz, 1H), 6.52 (d, *J* = 8.2 Hz, 2H), 3.98 (t, *J* = 6.5 Hz, 4H), 3.85 (s, 2H), 1.85 (sext, *J* = 7.1 Hz, 4H), 1.07 (t, *J* = 7.4 Hz, 6H) ppm. **^{13}C{^{1}H} NMR (101 MHz, $CDCl_3$):** δ 147.1, 126.1, 116.9, 105.2, 70.3, 22.9, 10.8 ppm. **LRMS** (EI, *m/z*): calc'd for $C_{12}H_{19}NO_2$: 209.1 (M^+), found: 209.2.

Synthesis of 2,6 – diisopropoxyaniline (3-9)

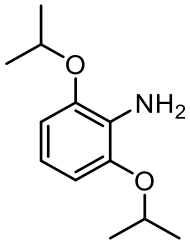

The general procedure was followed with **3-4** (3.0 g, 12.7 mmol), NH_4Cl (2.7 g, 50.8 mmol), and Fe powder (2.8 g, 50.8 mmol) in 30 mL of EtOH and 15 mL of distilled H_2O giving 2.0 g (77%) as a black oil. **^{1}H NMR (400 MHz, $CDCl_3$)**: δ 7.25 (t, *J* = 8.5 Hz, 1H), 6.58 (d, *J* = 8.5 Hz, 2H), 4.59 (sept, *J* = 6.1 Hz, 2H), 1.33 (d, *J* = 6.1 Hz, 12H) ppm. **^{13}C{^{1}H} NMR (101 MHz, $CDCl_3$):** δ 146.1, 128.1, 116.8, 107.1, 71.0, 22.6 ppm. **LRMS** (EI, *m/z*): calc'd for $C_{12}H_{19}NO_2$: 209.1 (M^+); found: 209.2.

Synthesis of 2,6 – dibutoxyaniline (3-10)

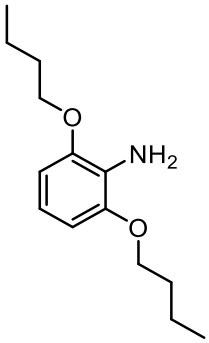

The general procedure was followed with **3-5** (709 mg, 2.65 mmol), NH_4Cl (568 mg, 10.6 mmol), and Fe powder (593 g, 10.6 mmol) in 7 mL of EtOH and 3.5 mL of distilled H_2O giving 572 mg (90%) as a dark brown crystalline solid. **^{1}H NMR (400 MHz, $CDCl_3$)**: δ 6.66 (t, *J* = 7.6 Hz, 1H), 6.53 (d, *J* = 8.2 Hz, 2H), 4.02 (t, *J* = 6.5 Hz, 4H), 3.80 (s, 2H), 1.81 (pent, *J* = 6.5 Hz, 4H), 1.53 (sext, *J* = 7.4 Hz, 4H), 1.00 (t, *J* = 7.4 Hz, 6H) ppm. **^{13}C{^{1}H} NMR (101 MHz, $CDCl_3$):** δ 147.1, 126.0, 116.9, 105.2, 68.4, 31.7, 19.5, 14.0 ppm. **LRMS** (EI, *m/z*): calc'd for $C_{14}H_{23}NO_2$: 237.3 (M^+); found: 237.1.

General Procedure for the Synthesis of the RO-Diamide Precursors:

Following a modified literature procedure,[125] the RO-aniline precursor was dispersed into anhydrous THF in a 150 mL round bottom flask under Ar. NEt_3 was added via syringe. The flask was cooled on an ice bath and oxalyl chloride (2M in CH_2Cl_2) was injected dropwise to the solution. The solution was then stirred at room temperature for 18 hours. The consumption of the starting material was confirmed by TLC analysis. The reaction was quenched with MeOH, and the solvent was removed under reduced pressure. The residue was washed with distilled H_2O and filtered, then it was rinsed with hexane or ether.

Synthesis of *N*[1],*N*[2]-*bis*(2,6-methoxyphenyl)-oxalamide (3-11)

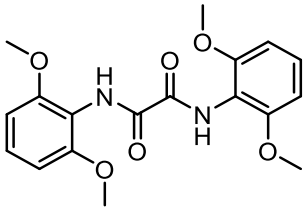

The general procedure was followed with **3-6** (2.0 g, 13.1 mmol) in 40 mL of THF with NEt_3 (2.0 mL) and oxalyl chloride (2M in CH_2Cl_2 – 5.8 mL, 11.6 mmol). The resulting product was rinsed with hexane giving 2.2 g (93%) of a course white solid. **^{1}H NMR (500 MHz, $CDCl_3$)**: δ 8.73 (s, 1H), 7.24 (t, *J* = 8.4 Hz, 2H), 6.63 (d, *J* = 8.5 Hz, 4H), 3.87 (s, 12H) ppm. **^{13}C{^{1}H} NMR (101 MHz, $CDCl_3$):** δ 158.2, 155.4, 128.3, 113.1, 104.5, 56.2 ppm. **LRMS** (EI, *m/z*): calc'd for $C_{18}H_{20}N_2O_6$: 360.1 (M^+), found: 360.1.

Synthesis of *N*[1],*N*[2]-*bis*(2,6-ethoxyphenyl)-oxalamide (3-12)

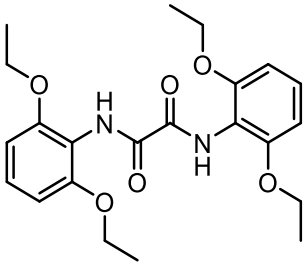

The general procedure was followed with **3-7** (1.0 g, 5.52 mmol) in 20 mL of THF with NEt_3 (850 μL) and oxalyl chloride (2M in CH_2Cl_2 – 2.5 mL, 5.0 mmol). The resulting product was rinsed with ether giving 1.0 g (87%) of a fine white solid. **^{1}H NMR (500 MHz, $CDCl_3$)**: δ 8.75 (s, 2H), 7.17 (t, *J* = 8.4 Hz, 2H), 6.59 (d, *J* = 8.4 Hz, 4H), 4.09 (q, *J* = 7.0 Hz, 8H), 1.40 (t, *J* = 7.0 Hz, 12H) ppm. **^{13}C{^{1}H} NMR (126 MHz, $CDCl_3$):** δ 158.1, 154.8, 128.0, 113.7, 105.5, 64.7, 15.0 ppm. **LRMS** (EI, *m/z*): calc'd for $C_{22}H_{28}N_2O_6$: 416.2 (M^+), found: 416.1.

Synthesis of *N*[1],*N*[2]-*bis*(2,6-propoxyphenyl)-oxalamide (3-13)

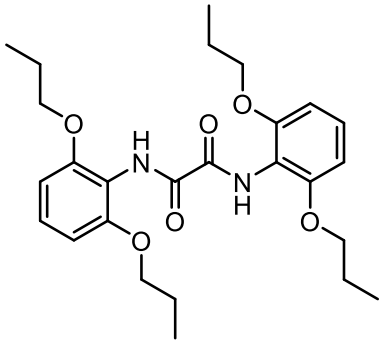

The general procedure was followed with **3-8** (550 mg, 2.63 mmol) in 15 mL of THF with NEt_3 (410 μL) and oxalyl chloride (2M in CH_2Cl_2 – 1.2 mL, 2.4 mmol). The resulting product was rinsed with ether giving 561 mg (90%) of an off white solid. **^{1}H NMR (400 MHz, $CDCl_3$)**: δ 8.75 (s, 2H), 7.17 (t, *J* = 8.4 Hz, 2H), 6.59 (d, *J* = 8.4 Hz, 4H), 3.97 (t, *J* = 6.5 Hz, 8H), 1.79 (sext, *J* = 7.1 Hz, 8H), 1.02 (t, *J* = 7.4 Hz,

12H) ppm. **^{13}C{^{1}H} NMR (101 MHz, $CDCl_3$):** δ 158.0, 155.1, 129.1, 113.7, 105.4, 70.5, 22.8, 10.7 ppm. **LRMS** (EI, *m/z*): calc'd for $C_{26}H_{36}N_2O_6$: 472.3 (M^+), found: 472.2.

Synthesis of *N*^{1},*N*^{2}-*bis*(2,6-isopropoxyphenyl)-oxalamide (3-14)

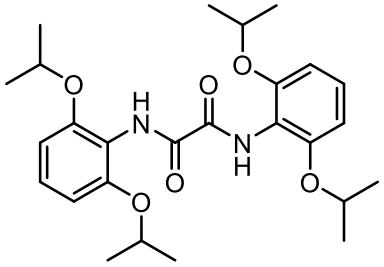

The general procedure was followed with **3-9** (2.04 g, 9.75 mmol) in 40 mL of THF with NEt_3 (1.5 mL) and oxalyl chloride (2M in CH_2Cl_2 – 4.4 mL, 8.8 mmol). The resulting product was rinsed with hexane giving 1.6 g (71%) of an off white solid. **^{1}H NMR (500 MHz, $CDCl_3$)**: δ 8.71 (s, 2H), 7.15 (t, *J* = 8.4 Hz, 2H), 6.59 (d, *J* = 8.8 Hz, 4H), 4.52 (sept, *J* = 6.2 Hz, 4H), 1.33 (d, *J* = 6.8 Hz, 24H) ppm. **^{13}C{^{1}H} NMR (101 MHz, $CDCl_3$):** δ 158.0, 154.1, 127.8, 115.9, 107.3, 71.6, 22.4 ppm. **LRMS** (EI, *m/z*): calc'd for $C_{26}H_{36}N_2O_6$: 472.3 (M^+), found: 472.2.

Synthesis of *N*^{1},*N*^{2}-*bis*(2,6-butoxyphenyl)-oxalamide (3-15)

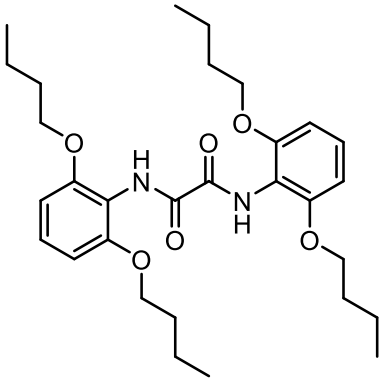

The general procedure was followed with **3-10** (3.08 g, 13.0 mmol) in 60 mL of THF with NEt_3 (2.0 mL) and oxalyl chloride (2M in CH_2Cl_2 – 5.8 mL, 11.6 mmol). The resulting product was rinsed with ether giving 2.7 g (77%) of a light fine pale yellow solid. **^{1}H NMR (400 MHz, $CDCl_3$):** δ 8.74 (s, 2H), 7.17 (t, *J* = 8.4 Hz, 2H), 6.59 (d, *J* = 8.4 Hz, 4H), 4.01 (t, *J* = 6.5 Hz, 8H), 1.76 (d, *J* = 6.7 Hz, 8H), 1.48 (sext, *J* = 7.3 Hz, 8H), 0.95 (t, *J* = 7.4 Hz, 12H) ppm. **^{13}C{^{1}H} NMR (101 MHz, $CDCl_3$):** δ 158.0, 154.9, 128.0, 113.7, 105.4, 77.5, 77.2, 76.9, 68.7, 31.5, 25.6, 19.3, 14.0 ppm. **HRMS** (ESI+, *m/z*)**:** calc'd for $C_{30}H_{44}N_2O_6$: 529.3251 $[M + H]^+$, found: 529.3276.

General Procedure for the Synthesis of the RO-Diamine Precursors:

A 150 mL round bottom flask under Ar was charged with RO-diamide precursor and anhydrous THF. The reaction flask was cooled on an ice bath and $LiAlH_4$ was added in portions. The mixture stirred at 0°C for 20 minutes then at room temperature for another 20 minutes. The reaction was heated at 60°C for 18 hours. The consumption of the starting material was confirmed by TLC analysis. The reaction was quenched with careful addition of EtOAc then MeOH. Distilled H_2O was then added, and the solution was filtered through Celite®. The filtrate was extracted into EtOAc and washed with distilled H_2O followed by a saturated aqueous solution of NaCl. The organic layer was dried with $MgSO_4$, filtered, and the solvent was removed under vacuum. The product was used in further transformation without purification.

Synthesis of the *N*[1],*N*[2]-*bis*(2,6-dimethoxyphenyl)ethane-1,2-diamine (3-16)

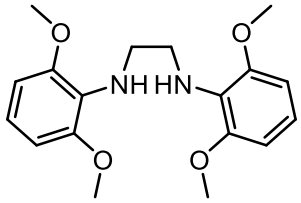

The general procedure was followed with **3-11** (1.0 g, 2.77 mmol) in 20 mL of THF with $LiAlH_4$ (526 mg, 13.9 mmol) giving 764 mg (82%) as a black oil. **^{1}H NMR (500 MHz, $CDCl_3$):** δ 6.84 (t, *J* = 8.3 Hz, 2H), 6.56 (d, *J* = 8.1 Hz, 4H), 3.84 (s, 12H), 3.28 (s, 4H) ppm. **^{13}C{^{1}H} NMR (101 MHz, $CDCl_3$):** δ 151.6, 126.7, 120.2, 104.6, 55.9, 47.0 ppm. **LRMS** (EI, *m/z*): calc'd for $C_{18}H_{24}N_2O_4$: 332.2 (M^+), found: 332.2.

Synthesis of the *N*[1],*N*[2]-*bis*(2,6-diethoxyphenyl)ethane-1,2-diamine (3-17)

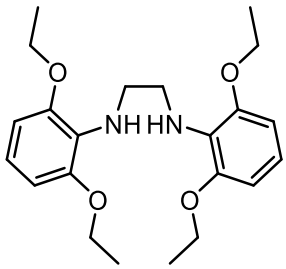

The general procedure was followed with **3-12** (1.0 g, 2.40 mmol) in 20 mL of THF with $LiAlH_4$ (460 mg, 12.0 mmol) giving 910 mg (97%) as a copper-coloured crystalline solid. **^{1}H NMR (400 MHz, $CDCl_3$)**: δ 6.65 (t, *J* = 7.6 Hz, 1H), 6.51 (d, *J* = 7.9 Hz, 2H), 4.08 (q, *J* = 7.0 Hz, 4H), 3.95 (s, 2H), 1.44 (t, *J* = 7.0 Hz, 6H) ppm. **^{13}C{^{1}H} NMR (126 MHz, $CDCl_3$):** δ 159.3, 142.5, 131.4,

127.3, 113.2, 43.1, 31.1, 15.1 ppm. **LRMS** (EI, *m/z*): calc'd for $C_{22}H_{32}N_2O_4$: 388.2 (M^+), found: 388.1.

General Procedure for the Synthesis of the RO-Diamine Precursors:

Following a modified literature procedure,[4] a 150 mL round bottom flask under Ar was charged with RO-diamide precursor and anhydrous THF. The reaction flask was cooled on an ice bath and a solution of 70w% Red Al® in toluene was added dropwise. The mixture stirred at 0°C for 20 minutes then at room temperature for another 20 minutes. The reaction was heated at 60°C for 18 hours. The consumption of the starting material was confirmed by TLC analysis. The reaction was quenched with careful addition of aqueous 20w% KOH and the solution was filtered through Celite®. The filtrate was extracted into EtOAc and washed with distilled H_2O followed by a saturated aqueous solution of NaCl. The organic layer was dried with $MgSO_4$, filtered, and the solvent was removed under vacuum. The product was used in further transformation without purification.

Synthesis of the *N*^{1},*N*^{2}-*bis*(2,6-dipropoxyphenyl)ethane-1,2-diamine (3-18)

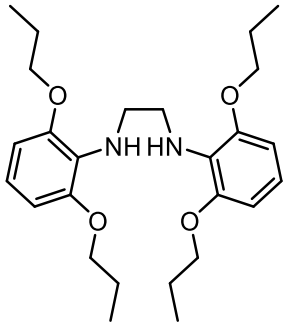

The general procedure was followed with **3-13** (500 mg, 1.06 mmol) in 10 mL of THF with Red Al® (70% in Toluene – 3.0 mL, 10.6 mmol) giving 384 mg (81%) as a brown crystalline solid. **^{1}H NMR (400 MHz, $CDCl_3$)**: δ 6.78 (t, *J* = 8.2 Hz, 2H), 6.52 (d, *J* = 8.2 Hz, 4H), 3.93 (t, *J* = 6.7 Hz, 8H), 3.40 (s, 4H), 1.81 (sext, *J* = 7.2 Hz, 8H), 1.01 (t, *J* = 7.4 Hz, 12H) ppm. **^{13}C{^{1}H} NMR (101 MHz, $CDCl_3$):** δ 150.7, 127.7, 119.6, 105.7, 70.4, 47.6, 22.9, 10.8 ppm. **LRMS** (EI, *m/z*): calc'd for $C_{26}H_{40}N_2O_4$: 444.3 (M^+), found: 444.2.

Synthesis of the *N*^{1},*N*^{2}-*bis*(2,6-diisopropoxyphenyl)ethane-1,2-diamine (3-19)

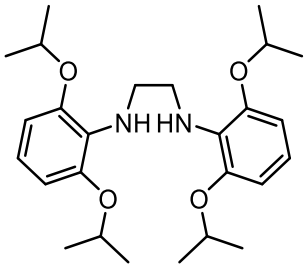

The general procedure was followed with **3-14** (1.09 g, 2.31 mmol) in 20 mL of THF with Red Al® (70% in Toluene – 6.5 mL, 23.1 mmol) giving 915 mg (89%) as a black oil. **^{1}H NMR (500 MHz, $CDCl_3$):** δ 6.73 (t, *J* = 8.21 Hz, 2H), 6.51 (d, *J* = 8.21 Hz, 4H), 4.54 (sept, *J* = 6.10 Hz, 4H), 3.36 (s, 4H), 1.34 (d, *J* = 6.09 Hz, 24H) ppm. **^{13}C{^{1}H} NMR (101 MHz, $CDCl_3$):** δ 149.4, 129.9, 119.4, 107.7, 70.8, 47.5, 22.5, 22.4, 22.3 ppm. **LRMS** (EI, *m/z*): calc'd for $C_{26}H_{40}N_2O_4$: 444.3 (M^+), found: 444.2.

Synthesis of the *N*^{1},*N*^{2}-*bis*(2,6-dibutoxyphenyl)ethane-1,2-diamine (3-20)

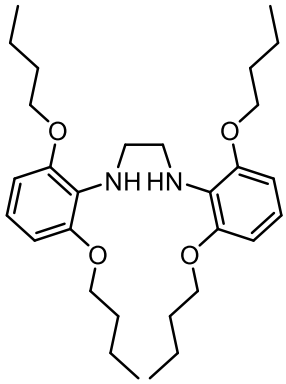

The general procedure was followed with **3-15** (350 mg, 0.66 mmol) in 5 mL of THF with Red Al® (70% in Toluene – 1.9 mL, 6.60 mmol) giving 266 mg (80%) as a brown crystalline solid. **^{1}H NMR (400 MHz, $CDCl_3$)**: δ 6.77 (t, *J* = 8.2 Hz, 2H), 6.52 (d, *J* = 8.3 Hz, 4H), 3.97 (t, *J* = 6.6 Hz, 8H), 3.38 (s, 4H), 1.77 (pent, *J* = 6.4 Hz, 8H), 1.46 (sext, *J* = 7.4 Hz, 8H), 0.94 (t, *J* = 7.4 Hz, 12H) ppm. **^{13}C{^{1}H} NMR (101 MHz, $CDCl_3$):** δ 150.7, 127.8, 119.5, 105.7, 68.6, 47.6, 31.6, 19.5, 14.0 ppm. **HRMS** (ESI+, *m/z*): calc'd for $C_{30}H_{48}N_2O_4$: 501.3666 $[M + H]^+$, found: 501.3691.

General Procedure for the Synthesis of the RO-NHC-HBF_4 Salt:

To a reaction flask containing RO-diamine, NH_4BF_4, and triethyl orthoformate were added. The solution was heated at 110°C for 18 hours. Transparent crystals formed around the sides of the flask indicating the reaction was successful. The solution was extracted into CH_2Cl_2 and washed with distilled H_2O. The organic layer was dried with $MgSO_4$ and filtered and dried *in vacuo*. The residue was dissolved in minimal CH_2Cl_2 and layered with hexanes. The precipitate was filtered through a frit and washed with cold hexanes then EtOAc.

Synthesis of the *N*[1],*N*[2]-*bis*(2,6-dimethoxyphenyl)imidazolinium BF_4 (3-23)

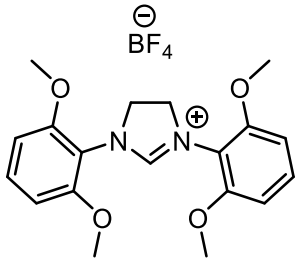

The general procedure was followed with **3-16** (521 mg, 1.57 mmol) in 5 mL of triethyl orthoformate with NH_4BF_4 (279 mg, 2.66 mmol) giving 645 mg (95%) as a dark brown solid. **^{1}H NMR (500 MHz, $CDCl_3$):** δ 8.00 (s, 1H), 7.36 (t, *J* = 8.5 Hz, 2H), 6.68 (d, *J* = 8.5 Hz, 4H), 4.53 (s, 4H), 3.94 (s, 12H) ppm. **^{13}C{^{1}H} NMR (126 MHz, $CDCl_3$):** δ 160.3, 155.2, 155.2, 131.3, 112.7, 104.7, 56.6, 51.2 ppm. **HRMS** (ESI+, *m/z*): calc'd for $C_{19}H_{23}BF_4N_2O_4$: 343.1652 $[M - BF_4]^+$, found: 343.1654.

Synthesis of the *N*[1],*N*[2]-*bis*(2,6-dimethoxyphenyl)imidazolinium BF_4 (3-24)

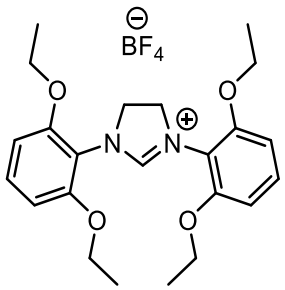

The general procedure was followed with **3-17** (1.4 g, 3.57 mmol) in 20 mL of triethyl orthoformate with NH_4BF_4 (636 mg, 6.06 mmol) giving 1.6 g (90%) as a white solid. **^{1}H NMR (500 MHz, $CDCl_3$):** δ 7.28 (t, *J* = 8.5 Hz, 1H), 6.59 (d, *J* = 8.5 Hz, 2H), 4.12 (q, *J* = 7.0 Hz, 4H), 1.40 (t, *J* = 7.0 Hz, 6H) ppm. **^{13}C{^{1}H} NMR (126 MHz, $CDCl_3$):** δ 160.4, 154.9, 131.5, 113.0, 105.4, 65.2, 51.5, 14.8 ppm. **HRMS** (ESI+, *m/z*): calc'd for $C_{23}H_{31}BF_4N_2O_4$: 399.2278 $[M - BF_4]^+$, found: 399.2275.

Synthesis of the *N*[1],*N*[2]-*bis*(2,6-dipropoxyphenyl)imidazolinium BF_4 (3-25)

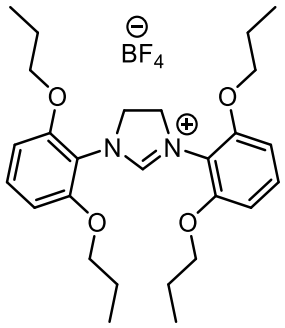

The general procedure was followed with **3-18** (1.1 g, 2.36 mmol) in 10 mL of triethyl orthoformate with NH_4BF_4 (421 mg, 4.01 mmol) giving 1.2 g (90%) as a white solid. **^{1}H NMR (400 MHz, $CDCl_3$)**: δ 7.85 (s, 1H), 7.33 (t, *J* = 8.5 Hz, 2H), 6.64 (d, *J* = 8.5 Hz, 4H), 4.53 (s, 4H), 4.03 (t, *J* = 6.6 Hz, 8H), 1.84 (sext, *J* = 7.1 Hz, 8H), 1.03 (t, *J* = 7.4 Hz, 12H) ppm. **^{13}C{^{1}H} NMR (101 MHz, $CDCl_3$):** δ 160.5, 155.0, 131.5, 113.0, 105.3, 71.0, 51.7, 22.5, 10.6 ppm. **HRMS** (ESI+, *m/z*) calc'd for $C_{27}H_{39}BF_4N_2O_4$: 455.2904 $[M - BF_4]^+$, found: 455.2906.

Synthesis of the *N*^{1},*N*^{2}-*bis*(2,6-diisopropoxyphenyl)imidazolinium BF_4 (3-26)

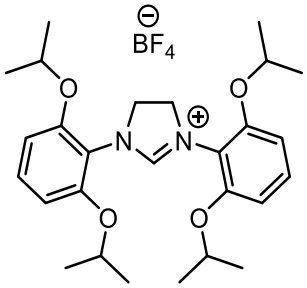

The general procedure was followed with **3-19** (1.4 g, 3.15 mmol) in 10 mL of triethyl orthoformate with NH_4BF_4 (562 mg, 5.36 mmol) giving 1.2 g (70%) as a pale yellow microcrystalline solid. **^{1}H NMR (400 MHz, $CDCl_3$)**: δ 7.62 (s, 1H), 7.32 (t, *J* = 8.5 Hz, 2H), 6.62 (d, *J* = 8.6 Hz, 4H), 4.64 (sept, *J* = 6.1 Hz, 4H), 4.49 (s, 4H), 1.39 (d, *J* = 6.0 Hz, 24H) ppm. **^{13}C{^{1}H} NMR (101 MHz, $CDCl_3$):** δ 160.2, 154.2, 131.2, 114.7, 106.3, 72.2, 51.8, 22.2 ppm. **HRMS** (ESI+, *m/z*): calc'd for $C_{27}H_{39}BF_4N_2O_4$: 455.2904 $[M - BF_4]^+$, found: 455.2903.

Synthesis of the *N*^{1},*N*^{2}-*bis*(2,6-dibutoxyphenyl)imidazolinium BF_4 (3-27)

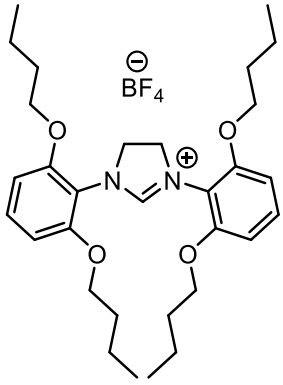

The general procedure was followed with **3-20** (1.0 g, 1.99 mmol) in 10 mL of triethyl orthoformate with NH_4BF_4 (355 mg, 3.38 mmol) giving 894 mg (75%) as a white solid. **^{1}H NMR (400 MHz, $CDCl_3$)**: δ 7.83 (s, 1H), 7.33 (t, *J* = 8.5 Hz, 2H), 6.64 (d, *J* = 8.5 Hz, 4H), 4.52 (d, *J* = 1.4 Hz, 4H), 4.07 (t, *J* = 6.7 Hz, 8H), 1.81 (pent, *J* = 6.9 Hz, 8H), 1.46 (sext, *J* = 7.4 Hz, 8H), 0.97 (t, *J* = 7.4 Hz, 12H) ppm. **^{13}C{^{1}H} NMR (101 MHz, $CDCl_3$)**: δ 160.5, 155.0, 131.4, 113.0, 105.3, 69.3, 51.7, 31.2, 19.4, 14.0 ppm. **HRMS** (ESI+, *m/z*): calc'd for $C_{31}H_{47}BF_4N_2O_4$: 511.3530 $[M - BF_4]^+$, found: 511.3533.

Synthesis of RO-NHC Sulfur Complexes:

A flame dried 50 mL round bottom flask under argon was charged with RO-NHC-HBF_4, S_8 (1.5 equiv.) and anhydrous THF. The flask was cooled to -78°C and NaHMDS (1M in THF – 2.0 equiv.) was injected via syringe dropwise. The solution was stirred at this temperature and was allowed to gradually warm to room temperature over the course of 18 hours. The colour of the reaction mixture darkening over time was typically observed. At this time, the flask was exposed

to air, 1 mL of MeOH was added and the THF was removed *in vacuo*. The residue was then dispersed in EtOAc and run through a short pad of basic alumina and then silica gel eluting with EtOAc.

Synthesis of Complex 3-28

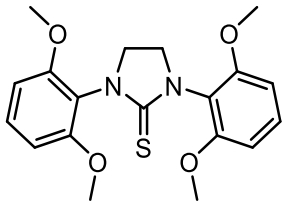

Following the general procedure using S_8 (11.2 mg, 0.35 mmol) and **3-23** (100 mg, 0.23 mmol), in 5 mL of anhydrous THF with 460 uL of NaHMDS (1M in THF) giving 37.7 mg (43%) as a brown solid. **^{1}H NMR ($CDCl_3$, 400 MHz):** δ 7.27 (d, *J* = 8.40 Hz, 2H), 6.65 (d, *J* = 8.44 Hz, 4H), 3.99 (s, 4H), 3.90 (s, 12H) ppm. **^{13}C{^{1}H} NMR (101 MHz, $CDCl_3$):** δ 184.7, 157.8, 129.4, 118.8, 105.6, 56.7, 48.2 ppm. **LRMS** (EI, *m/z*): calc'd for $C_{19}H_{22}N_2O_4S$: 374.1 (M^+), found: 374.1.

Synthesis of Complex 3-29

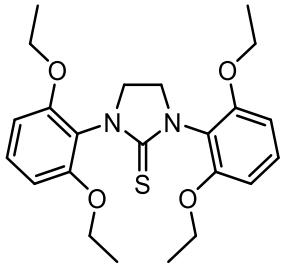

Following the general procedure using S_8 (10.3 mg, 0.32 mmol) and **3-24** (100 mg, 0.21 mmol), in 5 mL of anhydrous THF with NaHMDS (1M in THF – 0.42 mL, 0.42 mmol) giving 48.3 mg (53%) as a pale yellow solid. **^{1}H NMR (500 MHz, $CDCl_3$):** δ 7.21 (t, *J* = 8.4 Hz, 2H), 6.63 (d, *J* = 8.4 Hz, 4H), 4.20 – 4.05 (m, 8H), 3.99 (s, 4H), 1.43 (t, *J* = 7.0 Hz, 12H) ppm. **^{13}C{^{1}H} NMR (126 MHz, $CDCl_3$):** δ 184.3, 157.3, 129.1, 119.6, 106.9, 65.1, 48.2, 15.3 ppm. **LRMS** (EI, *m/z*): calc'd for $C_{23}H_{30}N_2O_4S$: 430.1 (M^+), found: 430.1.

Synthesis of Complex 3-30

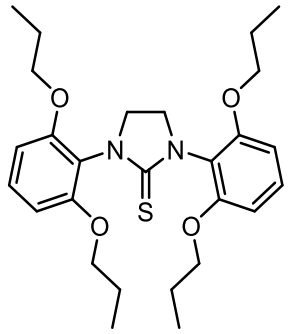

Following the general procedure using S_8 (8.98 mg, 0.28 mmol) and **3-25** (100 mg, 0.18 mmol), in 5 mL of anhydrous THF with 360 μL of NaHMDS (1M in THF) giving 26.2 mg (29%) as a white solid. **^{1}H NMR ($CDCl_3$, 400 MHz):** δ 7.21 (t, *J* = 8.38 Hz, 2H), 6.61 (d, *J* = 8.40 Hz, 4H), 4.10 – 4.03 (m, 4H), 3.99 – 3.91 (m, 8H), 1.90 – 1.78 (m, 8H), 1.06 (t, *J* = 7.44 Hz, 12H) ppm. **^{13}C{^{1}H} NMR (101 MHz, $CDCl_3$):** δ 184.2, 157.4, 129.1, 119.0, 106.1, 70.7, 48.2, 22.9, 10.9 ppm. **LRMS** (EI, *m/z*): calc'd for $C_{27}H_{38}N_2O_4S$: 486.2 (M^+), found: 486.1.

Synthesis of Complex 3-31

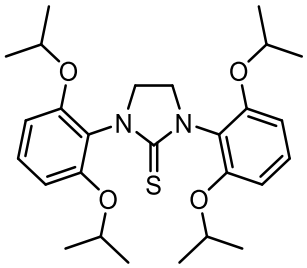

Following the general procedure using S_8 (8.98 mg, 0.28 mmol) and **3-26** (100 mg, 0.18 mmol), in 5 mL of anhydrous THF with NaHMDS (1M in THF – 0.36 mL, 0.36 mmol) giving 13.5 mg (15%) as a yellow oily product. **^{1}H NMR (400 MHz, $CDCl_3$):** δ 7.18 (t, *J* = 8.39 Hz, 2H), 6.59 (d, *J* = 8.38 Hz, 4H), 4.60 (sept, *J* = 6.12 Hz, 4H), 3.96 (s, 4H), 1.38 (dd, *J* = 13.05, 6.04 Hz, 24H) ppm. **^{13}C{^{1}H} NMR (101 MHz, $CDCl_3$):** δ 183.7, 156.5, 128.8, 120.4, 107.1, 77.5, 77.2, 76.8, 71.0, 48.0, 22.7, 22.7 ppm. **LRMS** (EI, *m/z*): calc'd for $C_{27}H_{38}N_2O_4S$: 486.2 (M^+), found: 486.2.

Synthesis of Complex 3-32

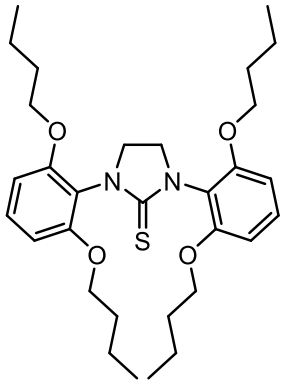

Following the general procedure using S_8 (8.0 mg, 0.25 mmol) and **3-27** (100 mg, 0.17 mmol), in 5 mL of anhydrous THF with NaHMDS (1M in THF – 0.3 mL, 0.3 mmol) giving 57 mg (61%) as a yellow oily product. **^{1}H NMR (400 MHz, $CDCl_3$):** δ 7.21 (t, *J* = 8.39 Hz, 2H), 6.62 (d, *J* = 8.37 Hz, 4H), 4.13 – 3.98 (m, 8H), 3.97 (s, 4H), 1.90 – 1.74 (m, 8H), 1.62 – 1.42 (m, 8H), 0.98 (t, *J* = 7.39 Hz, 12H) ppm. **^{13}C{^{1}H} NMR (101 MHz,**

$CDCl_3$): δ 184.0, 157.3, 129.0, 119.0, 106.2, 68.8, 48.1, 31.5, 19.3, 14.0 ppm. **LRMS** (EI, *m/z*): calc'd for $C_{31}H_{46}N_2O_4S$: 542.3 (M^+), found: 542.2.

Synthesis of RO-NHC Copper Complexes

Weak Base Route

Following a procedure we previously reported,[131] a culture tube was charged with copper(I) chloride (28 mg, 0.28 mmol), **3-24** (146 mg, 0.3 mmol), and acetone (1.6 mL) under air. The tube was sealed and heated at 60°C for 5 minutes which resulted in a homogeneous reaction solution. The tube was then cooled to room temperature and NEt_3 (390 μL, 2.8 mmol) was added via a micropipette. The tube was resealed and heated for an additional 60 minutes at 60°C. After returning to room temperature, all volatiles were removed *in vacuo* and the residue was dispersed into CH_2Cl_2 and applied to a short pad of silica gel washing with CH_2Cl_2. The CH_2Cl_2 was removed *in vacuo* using a rotary evaporator to give an off-white solid product (4.9 mg, 3%) which was triturated with hexanes and isolated by filtration. Analysis by ^1H NMR spectroscopy gave identical results to the strong base route below.

Strong Base Route

A flame dried 50 mL round bottom flask under argon was charged with RO-NHC-HBF_4 (1.0 equiv.) and CuX (1.5 equiv.) and was dissolved into anhydrous THF. The flask was cooled to -78°C and NaHMDS (1M in THF – 2.0 equiv.) was injected via syringe dropwise. The solution was stirred at this temperature and was allowed to gradually warm to room temperature over the course of 18 hours. The colour of the reaction mixture darkening over time was typically observed. At this time, the flask was exposed to air, 1 mL of MeOH was added and the THF was removed *in vacuo*. The residue was then dispersed in CH_2Cl_2 and run through a short pad of basic alumina and then silica gel eluting with CH_2Cl_2.

Synthesis of 3-33 [Cu(SIDMP)Cl]

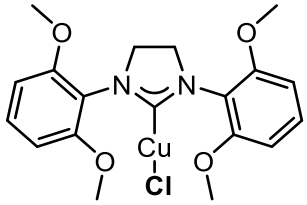

Following the general procedure using CuCl (68.3 mg, 0.69 mmol) and **3-23** (200 mg, 0.46 mmol), in 10 mL of anhydrous THF with NaHMDS (1M in THF – 0.92 mL, 0.92 mmol) giving 23.4 mg (11%) as an off-white solid. Single crystals suitable for X-ray diffraction were grown by slow diffusion of hexanes into a concentrated solution of $CHCl_3$. **^{1}H NMR (400 MHz, $CDCl_3$):** δ 7.26 (t, *J* = 8.50 Hz, 2H), 6.63 (d, *J* = 8.47 Hz, 4H), 4.00 (s, 4H), 3.90 (s, 12H) ppm. **^{13}C{^{1}H} NMR (101 MHz, $CDCl_3$):** δ 156.7, 129.0, 118.6, 104.8, 56.2, 50.3 ppm. *Despite our best efforts, the carbene carbon could not be located.* **HRMS** (ESI+, *m/z*)**:** calc'd for $C_{38}H_{44}CuN_4O_8$ $[M - Cl]^+$ 747.2455, found: 747.2454.

Synthesis of 3-34 [Cu(SIDEP)Cl]

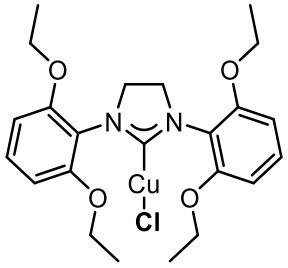

Following the general procedure using CuCl (31.2 mg, 0.32 mmol) and **3-24** (100 mg, 0.21 mmol), in 10 mL of anhydrous THF with NaHMDS (1M in THF – 0.42 mL, 0.42 mmol) giving 52.3 mg (50%) as an off-white solid. Single crystals suitable for X-ray diffraction were grown by slow diffusion of hexanes into a concentrated solution of THF. **^{1}H NMR (500 MHz, $CDCl_3$):** δ 7.20 (t, *J* = 8.39 Hz, 2H), 6.60 (d, *J* = 8.38 Hz, 4H), 4.15 – 4.07 (m, 8H), 3.99 (s, 4H), 1.44 (t, *J* = 6.95 Hz, 12H) ppm. **^{13}C{^{1}H} NMR (126 MHz, $CDCl_3$):** δ 205.2, 156.5, 129.2, 119.3, 106.0, 64.8, 50.6, 15.2 ppm. **HRMS** (ESI+, *m/z*)**:** calc'd for $C_{46}H_{60}CuN_4O_8$ $[M - Cl]^+$ 859.3707, found: 859.3694.

Synthesis of 3-35 [(CuSIDnPP)Cl]

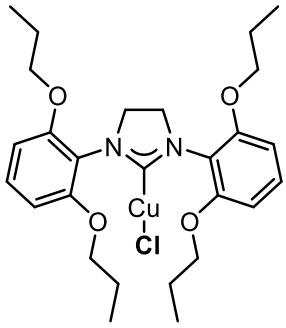

Following the general procedure using CuCl (55.4 mg, 0.56 mmol) and **3-25** (200 mg, 0.37 mmol), in 10 mL of anhydrous THF with NaHMDS (1M in THF – 0.74 mL, 0.74 mmol) giving 91.0 mg (44%) as an off-white solid. Single crystals suitable for X-ray diffraction were grown by slow diffusion of hexanes into a concentrated solution of $CHCl_3$. **^{1}H NMR (400 MHz, $CDCl_3$):** δ 7.17 (t, *J* = 8.49 Hz, 2H), 6.38 (d, *J* = 8.42 Hz, 4H), 3.80 – 3.64 (m, 12H), 1.68 (sext, *J* = 7.09 Hz, 8H), 0.98 (t, *J* = 7.40 Hz, 12H) ppm. **^{13}C{^{1}H} NMR (101 MHz, $CDCl_3$):** δ 204.2, 156.0, 129.4, 118.0, 105.3, 70.0, 50.9, 22.7, 10.9 ppm. **HRMS** (ESI+, *m/z*)**:** calc'd for $C_{54}H_{76}CuN_4O_8$ $[M - Cl]^+$ 971.4959, found: 971.4961.

Synthesis of 3-36 [Cu(SIDiPP)Cl]

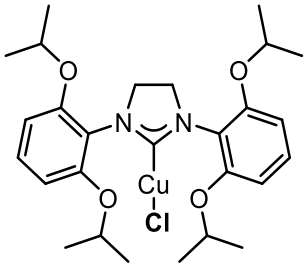

Following the general procedure using CuCl (26.7 mg, 0.27 mmol) and **3-26** (100 mg, 0.18 mmol), in 5 mL of anhydrous THF with NaHMDS (1M in THF – 0.36 mL, 0.36 mmol) giving 34.0 mg (16%) as an off-white solid. Single crystals suitable for X-ray diffraction were grown by slow diffusion of hexanes into a concentrated solution of $CHCl_3$. **^{1}H NMR (400 MHz, $CDCl_3$):** δ 7.18 (t, *J* = 8.41 Hz, 2H), 6.57 (d, *J* = 8.46 Hz, 4H), 4.60 (sept, *J* = 6.06 Hz, 4H), 3.93 (s, 4H), 1.41 (d, *J* = 6.0 Hz, 12H), 1.36 (d, *J* = 6.1 Hz, 12H). **^{13}C{^{1}H} NMR (101 MHz, $CDCl_3$):** δ 205.0, 155.7, 128.9, 120.4, 106.7, 71.1, 50.6, 22.8, 22.6 ppm. **HRMS** (ESI+, *m/z*)**:** calc'd for $C_{54}H_{76}CuN_4O_8$ $[M - Cl]^+$ 971.4959, found: 971.4975.

Synthesis of 3-37 [Cu(SIDnBP)Cl]

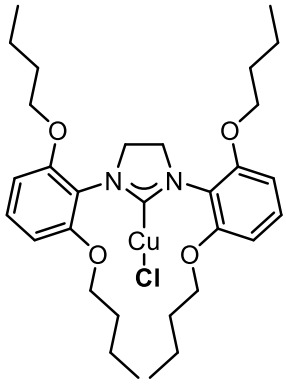

Following the general procedure using CuCl (49.5 mg, 0.50 mmol) and **3-27** (200 mg, 0.33 mmol), in 10 mL of anhydrous THF with NaHMDS (1M in THF – 0.66 mL, 0.66 mmol) giving 122.5 mg (61%) as an off-white solid. Single crystals suitable for X-ray diffraction were grown by slow diffusion of hexanes into a concentrated solution of $CHCl_3$. **^{1}H NMR (400 MHz, $CDCl_3$):** δ 7.63 (t, *J* = 8.41 Hz, 2H), 7.02 (d, *J* = 8.43 Hz, 4H), 4.54 – 4.39 (m, 8H), 4.38 (s, 4H), 2.23 (pent, *J* = 6.70 Hz, 8H), 1.93 (q, *J* = 7.44 Hz, 8H), 1.40 (t, *J* = 7.38 Hz, 12H) ppm. **^{13}C{^{1}H} NMR (101 MHz, $CDCl_3$):** δ 205.4, 156.5, 129.1, 118.8, 105.5, 68.6, 50.6, 31.5, 19.5, 14.1 ppm. **HRMS** (ESI+, *m/z*)**:** calc'd for $C_{62}H_{92}CuN_4O_8$ $[M - Cl]^+$ 1083.6211, found: 1083.6222.

Synthesis of 3-38 [Cu(SIDMP)Br]

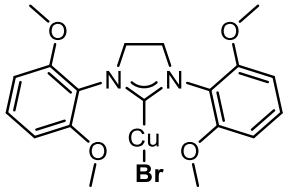

Following the general procedure using CuBr (99.0 mg, 0.69 mmol) and **3-23** (200 mg, 0.46 mmol), in 10 mL of anhydrous THF with NaHMDS (1M in THF – 0.92 mL, 0.92 mmol) giving 114.6 mg (51%) as an off-white solid. **^{1}H NMR (400 MHz, $CDCl_3$):** δ 7.25 (t, *J* = 8.53 Hz, 2H), 6.63 (d, *J* = 8.44 Hz, 4H), 4.00 (s, 4H), 3.90 (s, 12H) ppm. **^{13}C{^{1}H} NMR (101 MHz, $CDCl_3$):** δ 206.5, 156.7, 129.1, 118.6, 104.9, 56.3, 50.4 ppm.

Synthesis of 3-39 [Cu(SIDEP)Br]

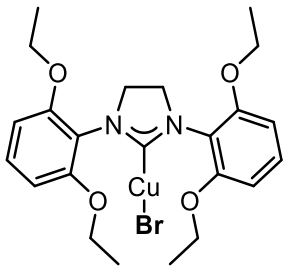

Following the general procedure using CuBr (88.9 mg, 0.62 mmol) and **3-24** (200 mg, 0.41 mmol), in 10 mL of anhydrous THF with NaHMDS (1M in THF – 0.82 mL, 0.82 mmol) giving 110 mg (49%) as an off-white solid. **^{1}H NMR (400 MHz, $CDCl_3$):** δ 7.20 (t, *J* = 8.39 Hz, 2H), 6.60 (d,

J = 8.44 Hz, 4H), 4.15 – 4.08 (m, 8H), 3.99 (s, 4H), 1.44 (t, *J* = 6.97 Hz, 12H) ppm. **$^{13}C\{^{1}H\}$ NMR (101 MHz, $CDCl_3$):** δ 205.8, 156.4, 129.1, 119.1, 105.6, 64.7, 50.5, 15.2 ppm.

Synthesis of 3-40 [Cu(SIDnPP)Br]

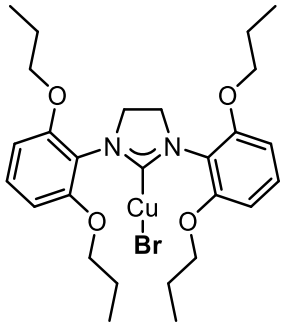

Following the general procedure using CuBr (80.3 mg, 0.56 mmol) and **3-25** (200 mg, 0.37 mmol), in 10 mL of anhydrous THF with NaHMDS (1M in THF – 0.74 mL, 0.74 mmol) giving 119.5 mg (53%) as an off-white solid. **^{1}H NMR (400 MHz, $CDCl_3$):** δ 7.20 (t, *J* = 8.39 Hz, 2H), 6.58 (d, *J* = 8.45 Hz, 4H), 4.09 – 3.91 (m, 12H), 1.83 (sext, *J* = 7.05 Hz, 8H), 1.05 (t, *J* = 7.41 Hz, 12H) ppm. **$^{13}C\{^{1}H\}$ NMR (101 MHz, $CDCl_3$):** δ 205.9, 156.5, 129.1, 118.6, 105.4, 70.3, 50.6, 22.9, 10.9 ppm.

Synthesis of 3-41 [Cu(SIDiPP)Br]

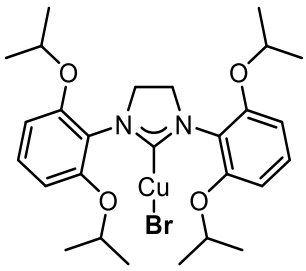

Following the general procedure using CuBr (38.7 mg, 0.27 mmol) and **3-26** (100 mg, 0.18 mmol), in 5 mL of anhydrous THF with NaHMDS (1M in THF – 0.36 mL, 0.36 mmol) giving 59.0 mg (54%) as an off-white solid. **^{1}H NMR (400 MHz, $CDCl_3$):** δ 7.18 (t, *J* = 8.40 Hz, 2H), 6.57 (d, *J* = 8.43 Hz, 4H), 4.60 (sept, *J* = 5.99 Hz, 4H), 3.93 (s, 4H), 1.41 (d, *J* = 6.0 Hz, 12H), 1.36 (d, *J* = 6.1 Hz, 12H) ppm. **$^{13}C\{^{1}H\}$ NMR (101 MHz, $CDCl_3$):** δ 205.6, 155.7, 129.0, 120.4, 106.7, 71.1, 50.6, 22.9, 22.5 ppm.

Synthesis of 3-42 [Cu(SIDnBP)Br]

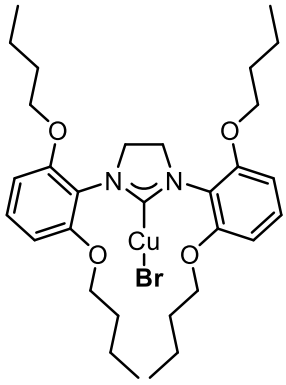

Following the general procedure using CuBr (71.7 mg, 0.50 mmol) and **3-27** (200 mg, 0.33 mmol), in 10 mL of anhydrous THF with NaHMDS (1M in THF – 0.66 mL, 0.66 mmol) giving 164.6 mg (76%) as an off-white solid. **^{1}H NMR (400 MHz, $CDCl_3$):** δ 7.20 (t, *J* = 8.43 Hz, 2H), 6.59 (d, *J* = 8.42 Hz, 4H), 4.12 – 3.99 (m, 8H), 3.96 (s, 4H), 1.81 (pent, *J* = 6.5 Hz, 8H), 1.50 (sext, *J* = 7.40 Hz, 8H), 0.97 (t, *J* = 7.39 Hz, 12H) ppm. **^{13}C{^{1}H} NMR (101 MHz, $CDCl_3$):** δ 206.0, 156.4, 129.1, 118.8, 105.4, 68.6, 50.6, 31.5, 19.4, 14.1 ppm.

Synthesis of 3-43 [Cu(SIDMP)I]

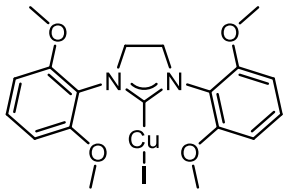

Following the general procedure using CuI (131 mg, 0.69 mmol) and **3-23** (200 mg, 0.46 mmol), in 10 mL of anhydrous THF with NaHMDS (1M in THF – 0.92 mL, 0.92 mmol) giving 79.2 mg (32%) as an off-white solid. **^{1}H NMR (400 MHz, $CDCl_3$):** δ 7.25 (t, *J* = 8.36 Hz, 2H), 6.63 (d, *J* = 8.54 Hz, 4H), 4.01 (s, 4H), 3.91 (s, 12H) ppm. **^{13}C{^{1}H} NMR (101 MHz, $CDCl_3$):** δ 207.5, 156.7, 129.1, 118.5, 104.9, 56.4, 50.4 ppm.

Synthesis of 3-44 [Cu(SIDEP)I]

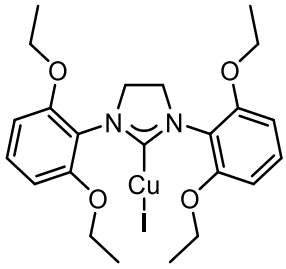

Following the general procedure using CuI (118 mg, 0.62 mmol) and **3-24** (200 mg, 0.41 mmol), in 10 mL of anhydrous THF with NaHMDS (1M in THF – 0.82 mL, 0.82 mmol) giving 159.6 mg (65%) as a white solid. Single crystals suitable for X-ray diffraction were grown from a slow diffusion of hexanes into a concentrated THF solution. **^{1}H NMR (500 MHz, $CDCl_3$):** δ 7.21 (t, *J* = 8.42 Hz, 2H), 6.60 (d, *J* = 8.42 Hz, 4H), 4.18 – 4.06 (m, 8H), 4.00 (s, 4H), 1.44 (t, *J* = 6.96 Hz,

12H) ppm. **^{13}C{^{1}H} NMR (126 MHz, $CDCl_3$):** δ 206.9, 156.4, 129.1, 119.0, 106.0, 106.0, 105.9, 64.8, 50.5, 15.3 ppm.

Synthesis of 3-45 [Cu(SIDnPP)I]

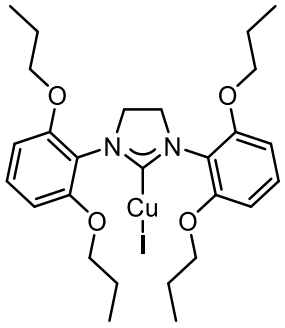

Following the general procedure using CuI (107 mg, 0.56 mmol) and **3-25** (200 mg, 0.37 mmol), in 10 mL of anhydrous THF with NaHMDS (1M in THF – 0.74 mL, 0.74 mmol) giving 178.1 mg (74%) as a white solid. **^{1}H NMR (400 MHz, $CDCl_3$):** δ 7.20 (t, *J* = 8.43 Hz, 2H), 6.59 (d, *J* = 8.47 Hz, 4H), 4.09 – 3.91 (m, 12H), 1.84 (sext, *J* = 7.10 Hz, 8H), 1.05 (t, *J* = 7.43 Hz, 12H) ppm. **^{13}C{^{1}H} NMR (101 MHz, $CDCl_3$):** δ 207.0, 156.4, 129.1, 118.6, 105.4, 70.3, 50.6, 22.9, 11.0 ppm.

Synthesis of 3-46 [Cu(SIDiPP)I]

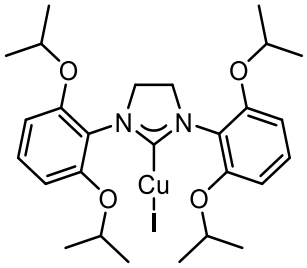

Following the general procedure using CuI (51.4 mg, 0.27 mmol) and **3-26** (100 mg, 0.18 mmol), in 5 mL of anhydrous THF with NaHMDS (1M in THF – 0.36 mL, 0.36 mmol) giving 75.7 mg (65%) as a white solid. **^{1}H NMR (400 MHz, $CDCl_3$):** δ δ 7.19 (t, *J* = 8.40 Hz, 2H), 6.58 (d, *J* = 8.44 Hz, 4H), 4.60 (sept, *J* = 6.05 Hz, 4H), 3.94 (s, 4H), 1.42 (d, *J* = 6.03 Hz, 12H), 1.36 (d, *J* = 6.06 Hz, 12H) ppm. **^{13}C{^{1}H} NMR (101 MHz, $CDCl_3$):** δ 206.7, 155.7, 129.0, 120.2, 106.7, 71.1, 50.6, 23.1, 22.5 ppm.

Synthesis of 3-47 [(SIDnBP)CuI]

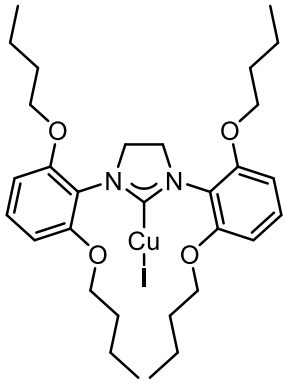

Following the general procedure using CuI (95.2 mg, 0.50 mmol) and **3-27** (200 mg, 0.33 mmol), in 10 mL of anhydrous THF with NaHMDS (1M in THF – 0.66 mL, 0.66 mmol) giving 159.8 mg (69%) as a white solid. **^{1}H NMR (400 MHz, $CDCl_3$):** δ 7.20 (t, *J* = 8.40 Hz, 2H), 6.59 (d, *J* = 8.44 Hz, 4H), 4.11 – 3.99 (m, 8H), 3.97 (s, 4H), 1.81 (pent, *J* = 6.60 Hz, 8H), 1.50 (sext, *J* = 7.43 Hz, 8H), 0.97 (t, *J* = 7.40 Hz, 12H) ppm. **^{13}C{^{1}H} NMR (101 MHz, $CDCl_3$):** δ 207.1, 156.4, 129.1, 105.4, 68.6, 50.6, 31.6, 19.5, 14.1 ppm.

Synthesis of RO-NHC Palladium Complexes

Transmetallation Route

Under air, Ag_2O (100 mg, 0.43 mmol), **3-24** (119 mg, 0.245 mmol), and KBr (145 mg, 1.25 mmol) were added as solids to culture tube and dissolved in anhydrous acetonitrile (20 mL) and stirred with the exclusion of light for 3 days at room temperature. A white precipitate was observed in the reaction mixture. The opaque solution was then diluted with CH_2Cl_2 and filtered through Celite® on a frit, and all volatiles were removed *in vacuo*. Precipitation was induced with the addition of hexanes, followed by filtration resulting in an off-white powder in 99.5 mg in (69%) yield. The formation of the Ag-NHC complex was confirmed by ^{1}H NMR spectroscopy and was carried through directly to the next step without any purification. **^{1}H NMR (60 MHz, $CDCl_3$):** δ 7.5 – 7.0 (m, 4H), 6.8 – 6.4 (m, 8H), 4.4 – 3.8 (m, 24H), 1.4 (t, *J* = 6.77 Hz, 24H). *(see Figure A113)*

A solution of Ag-NHC complex (99.5 mg, 0.17 mmol) in CH_2Cl_2 (3 mL) was added to a stirring solution of $[Pd(allyl)Cl]_2$ (62.1 mg, 0.17 mmol) in CH_2Cl_2 (3 mL) under air. A white precipitate was observed immediately. The resulting solution was stirred at room temperature for 1 hour, then diluted with CH_2Cl_2 and filtered through Celite® on a frit, rinsed with CH_2Cl_2 and all

volatiles were removed *in vacuo*. The crude product was purified by silica gel flash chromatography with an eluent of hexanes/EtOAc, giving 25.1 mg (27%) as a white microcrystalline solid. Analysis by ^{1}H NMR matched the spectra obtained from the carbene route below.

Free Carbene Route: General Procedure

In a nitrogen-filled glovebox, a solution of NaHMDS (2.1 equiv.) in THF (2 mL) was added to a stirring solution of RO-NHC-HBF_4 (2.1 equiv.) in THF (2 mL) in a 4-dram vial at -15°C. This reaction solution was stirred for 2 hours while gradually warming to room temperature. After the 2 hours, a solution of $[Pd(allyl)Cl]_2$ (1 equiv.) in THF (2 mL) was added to the free carbene solution. This reaction mixture continued to stir for 1 hour at room temperature. The vial was then exposed to air, diluted with CH_2Cl_2 and filtered through Celite® on a frit and all volatiles were removed *in vacuo*. The crude product was purified by silica gel flash column chromatography with an eluent of hexanes/EtOAc gradient solution. The resulting products were stable under air for days, but displayed discolouring upon extended timeframes, and were stored under N_2 at -15 °C.

Synthesis of 3-51 [(SIDMP)Pd(allyl)Cl]

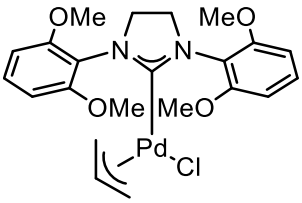

Following the general procedure using NaHMDS (42.6 mg, 0.23 mmol), **3-23** (100 mg, 0.23 mmol), $[Pd(allyl)Cl]_2$ (42.5 mg, 0.12 mmol) in THF (6 mL) giving 55.0 mg (48%) as a white solid. **^{1}H NMR (400 MHz, $CDCl_3$, 298K):** δ 7.23 (t, *J* = 8.41 Hz, 2H), 6.56 (d, *J* = 8.43 Hz, 4H), 4.70 – 4.56 (m, 1H), 4.06 – 3.76 (m, 17H), 3.37 – 3.20 (m, 1H), 2.66 – 2.53 (m, 1H), 1.79 – 1.70 (m, 1H) ppm. **^{1}H NMR (400 MHz, $CDCl_3$, 278K):** δ 7.23 (t, *J* = 8.43 Hz, 2H), 6.57 (d, *J* = 8.39 Hz, 4H), 4.68 – 4.59 (m, 1H), 4.04 – 3.73 (m, 17H), 3.31 – 3.12 (m, 1H), 2.56 (d, *J* = 13.44 Hz, 1H), 1.71 (d, *J* = 12.16 Hz, 1H) ppm. **^{13}C{^{1}H} NMR (101 MHz, $CDCl_3$, 298K):** δ 157.8, 129.3, 114.3, 104.5, 104.4, 70.7, 56.3,

51.0, 48.7 ppm. *Despite our best efforts, the carbene peak was not observed.* **HRMS** (ESI+, *m/z*)**:** calc'd for $C_{22}H_{27}N_2O_4Pd$ $[M\text{-}Cl]^+$ 489.1006, found: 489.1007.

Synthesis of 3-52 [(SIDEP)Pd(allyl)Cl]

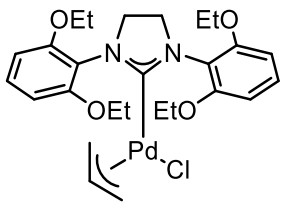

Following the general procedure using NaHMDS (38.5 mg, 0.21 mmol), **3-24** (100 mg, 0.21 mmol), $[Pd(allyl)Cl]_2$ (40.2 mg, 0.11 mmol) in THF (6 mL) giving 53.5 mg (44%) as a white solid. **^{1}H NMR (400 MHz, $CDCl_3$, 298K):** δ 7.17 (t, *J* = 8.38 Hz, 2H), 6.54 (d, *J* = 8.41 Hz, 4H), 4.74 – 4.60 (m, 1H), 4.18 – 3.94 (m, 12H), 3.66 (d, *J* = 7.42 Hz, 1H), 3.42 – 3.19 (m, 1H), 2.59 (d, *J* = 13.38 Hz, 1H), 1.87 – 1.69 (m, 1H), 1.49 (t, *J* = 6.94 Hz, 12H) ppm. **^{1}H NMR (400 MHz, $CDCl_3$, 278K):** δ 7.17 (t, *J* = 8.38 Hz, 2H), 6.53 (d, *J* = 5.16 Hz, 4H), 4.73 – 4.59 (m, 1H), 4.15 – 3.92 (m, 12H), 3.65 (d, *J* = 6.03 Hz, 1H), 3.32 (d, *J* = 4.88 Hz, 1H), 2.58 (d, *J* = 13.38 Hz, 1H), 1.77 – 1.73 (m, 1H), 1.50 (d, *J* = 6.20 Hz, 12H) ppm. **^{13}C{^{1}H} NMR (101 MHz, $CDCl_3$, 298K):** δ 211.8, 157.5, 129.1, 119.2, 114.1, 105.0, 70.7, 64.4, 50.8, 48.9, 15.3 ppm. **HRMS** (ESI+, *m/z*)**:** calc'd for $C_{26}H_{35}N_2O_4Pd$ $[M\text{-}Cl]^+$ 545.1632; found: 545.1633.

Synthesis of 3-53 [(SIDnPP)Pd(allyl)Cl]

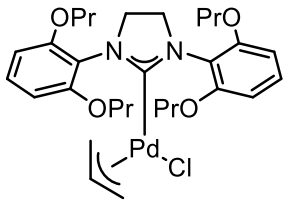

Following the general procedure using NaHMDS (33.8 mg, 0.18 mmol), **3-25** (100 mg, 0.18 mmol), $[Pd(allyl)Cl]_2$ (33.7 mg, 0.09 mmol) in THF (6 mL) giving 82.7 mg (70%) as a white solid. **^{1}H NMR (400 MHz, $CDCl_3$, 298K):** δ 7.17 (t, *J* = 8.40 Hz, 2H), 6.53 (d, *J* = 8.42 Hz, 4H), 4.73 – 4.60 (m, 1H), 4.12 – 3.87 (m, 12H), 3.66 (d, *J* = 7.40 Hz, 1H), 3.40 – 3.19 (m, 1H), 2.59 (d, *J* = 13.40 Hz, 1H), 1.92 (dh, *J* = 14.05, 7.00 Hz, 8H), 1.80 – 1.67 (m, 1H), 1.06 (t, *J* = 7.44 Hz, 12H) ppm. **^{1}H NMR (400 MHz, $CDCl_3$, 278K):** δ 7.19 (t, *J* = 8.40 Hz, 2H), 6.54 (d, *J* = 5.37 Hz, 4H), 4.76 – 4.59 (m, 1H), 4.14 – 3.83 (m, 12H), 3.66 (d, *J* = 1.42 Hz, 1H), 3.31 (d, *J* = 6.30 Hz, 1H), 2.59 (d, *J* = 13.35 Hz,

1H), 2.01 – 1.83 (m, 8H), 1.75 (d, *J* = 12.71 Hz, 1H), 1.07 (t, *J* = 7.43 Hz, 12H) ppm. **^{13}C{^{1}H} NMR (101 MHz, $CDCl_3$, 298K):** δ 212.0, 157.5, 129.1, 119.1, 114.1, 104.8, 70.6, 70.2, 50.9, 48.9, 22.9, 10.9 ppm. **HRMS** (ESI+, *m/z*)**:** calc'd for $C_{30}H_{43}N_2O_4Pd$ $[M\text{-}Cl]^+$ 601.2258; found: 601.2264.

Synthesis of 3-54 [(SIDiPP)Pd(allyl)Cl]

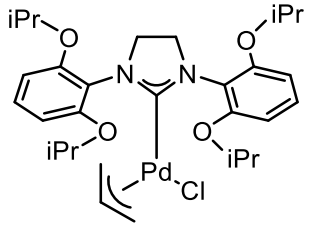

Following the general procedure using NaHMDS (33.8 mg, 0.18 mmol), **3-26** (100 mg, 0.18 mmol), $[Pd(allyl)Cl]_2$ (33.7 mg, 0.09 mmol) in THF (6 mL) giving 57.1 mg (49%) as a white solid. **^{1}H NMR (400 MHz, $CDCl_3$, 298K):** δ 7.14 (t, *J* = 8.40 Hz, 2H), 6.51 (d, *J* = 8.41 Hz, 4H), 4.81 – 4.70 (m, 1H), 4.65 – 4.54 (m, 4H), 3.94 (s, 4H), 3.68 (d, *J* = 7.42 Hz, 1H), 3.44 – 3.20 (m, 1H), 2.65 (d, *J* = 13.37 Hz, 1H), 1.86 – 1.69 (m, 1H), 1.47 (d, *J* = 6.03 Hz, 12H), 1.36 (d, *J* = 6.00 Hz, 12H) ppm. **^{1}H NMR (400 MHz, $CDCl_3$, 278K):** δ 7.15 (t, *J* = 8.39 Hz, 2H), 6.51 (d, *J* = 8.43 Hz, 4H), 4.83 – 4.69 (m, 1H), 4.59 (s, 4H), 4.05 – 3.81 (m, 4H), 3.67 (d, *J* = 1.31 Hz, 1H), 3.36 (d, *J* = 6.16 Hz, 1H), 2.63 (d, *J* = 13.39 Hz, 1H), 1.77 (d, *J* = 12.29 Hz, 1H), 1.47 (d, *J* = 6.05 Hz, 12H), 1.35 (d, *J* = 6.01 Hz, 12H) ppm. **^{13}C{^{1}H} NMR (101 MHz, $CDCl_3$, 298K):** δ 210.9, 156.4, 128.7, 120.9, 114.1, 106.0, 70.8, 70.6, 50.7, 49.7, 22.8, 22.6 ppm. **HRMS** (ESI+, *m/z*)**:** calc'd for $C_{30}H_{43}N_2O_4Pd$ $[M\text{-}Cl]^+$ 601.2258; found: 601.2262.

Synthesis of 3-55 [(SIDnBP)Pd(allyl)Cl]

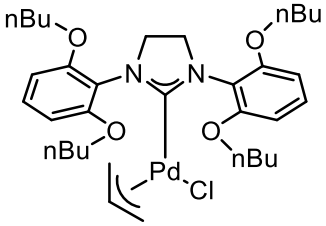

Following the general procedure using NaHMDS (31.2 mg, 0.17 mmol), **3-27** (100 mg, 0.17 mmol), $[Pd(allyl)Cl]_2$ (31.1 mg, 0.085 mmol) in THF (6 mL) giving 84.1 mg (71%) as a white solid. **^{1}H NMR (400 MHz, $CDCl_3$, 298K):** δ 7.09 (t, *J* = 8.38 Hz, 2H), 6.45 (d, *J* = 8.40 Hz, 4H), 4.64 – 4.51 (m, 1H), 4.06 – 3.83 (m, 12H), 3.57 (d, *J* = 7.40 Hz, 1H), 3.31 – 3.09

(m, 1H), 2.50 (d, *J* = 13.37 Hz, 1H), 1.89 – 1.71 (m, *J* = 6.57 Hz, 8H), 1.65 (d, *J* = 6.44 Hz, 1H), 1.49 – 1.36 (m, 8H), 0.92 (t, *J* = 7.40 Hz, 12H) ppm. **^{1}H NMR (400 MHz, $CDCl_3$, 278K):** δ 7.17 (t, *J* = 8.39 Hz, 2H), 6.53 (d, *J* = 6.75 Hz, 4H), 4.66 (ddd, *J* = 18.24, 13.37, 7.56 Hz, 1H), 4.12 – 3.90 (m, 12H), 3.64 (d, *J* = 1.42 Hz, 1H), 3.32 – 3.23 (m, 1H), 1.97 – 1.78 (m, 8H), 1.72 (d, *J* = 1.60 Hz, 1H), 1.50 (q, *J* = 7.40 Hz, 8H), 0.99 (t, *J* = 7.40 Hz, 12H) ppm. **^{13}C{^{1}H} NMR (101 MHz, $CDCl_3$, 298K):** δ 211.9, 157.5, 129.1, 119.1, 114.1, 104.8, 70.5, 68.5, 50.9, 48.8, 31.5, 19.4, 14.1 ppm. **HRMS** (ESI+, *m/z*)**:** calc'd for $C_{34}H_{51}N_2O_4Pd$ $[M\text{-}Cl]^+$ 657.2884; found: 657.2887.

Chapter 4

N-Heterocyclic Carbene Complexes of Ag Bound Cyanides: An Economical Approach to Studying Electronic Properties

4.1 Introduction

Since the discovery of the first isolable N-heterocyclic carbenes (NHCs) by Arduengo and coworkers,[18] a variety of structurally distinct NHCs have been reported with attempts to modulate steric and electronic parameters as well as incorporate chelating functional groups or chirality.[28] Due to the numerous different NHC species reported in the literature, extensive studies have been conducted to investigate and benchmark their properties. In any catalytic situation, ligands for homogeneous catalysts are not necessarily suitable towards other metals or other applications. As such, the design and discovery of new ligands is a common theme in organometallic chemistry. Thus, researchers require methods to bench mark the properties of new ligands for their comparisons. Understanding the specific properties of ligands will help to build trends and optimize catalysts for their applications.

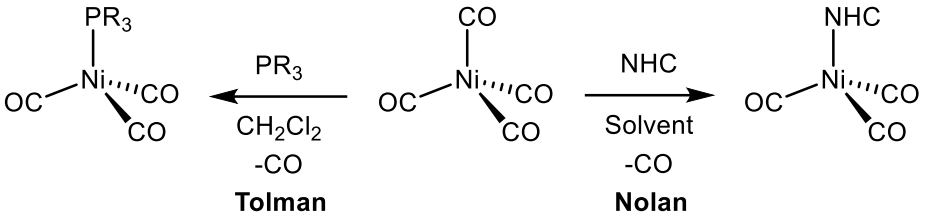

Figure 4-1: Preparation of [Ni(CO)$_3$(PR$_3$/NHC)] complexes for TEP measurements

The σ-donating and π-accepting electronic properties of a ligand can be studied by their Tolman electronic parameters (TEP). One of the most common methods utilized was TEP to study the electronic parameters of NHC ligands, and this originated from phosphine ligand studies (**Figure 4-2**).[45]

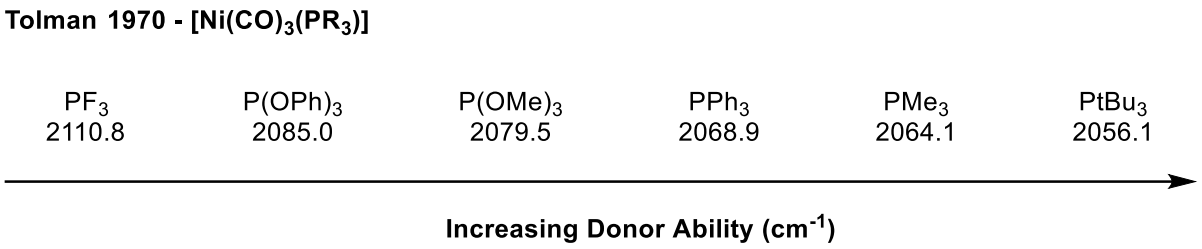

Figure 4-2: Electronic studies of select phosphine ligands using TEP by IR spectroscopy

In Tolman's original report, $[Ni(CO)_4]$ was treated with one equivalent of a phosphine ligand liberating one molecule of CO and resulting in a tetrahedral $[(PR_3)Ni(CO)_3]$ complex (**Figure 4-1**). This complex is then analyzed by the infrared (IR) spectroscopy looking at the stretching frequency of carbonyl ligands. Essentially, the more electron density the ligand donates to the metal, in this case Ni, the more electron rich the metal becomes which weakens the C-O bond eliciting a lower IR frequency.[45,46] As shown in **Figure 4-2**, are select examples of phosphine ligands demonstrating the effectiveness of TEP by showing a trend in which the most electron donating ligand gives the lowest IR frequency.[45]

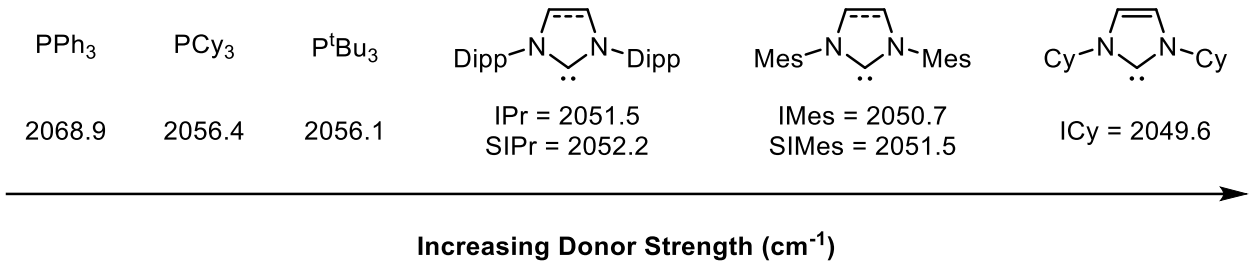

Figure 4-3: Electronic studies of select NHC ligands compared to select electron rich phosphine ligands by Nolan and coworkers using IR spectroscopy

Nolan and coworkers demonstrated the efficacy of this method in some common NHCs (**Figure 4-3**).[46] This method helped benchmark NHCs as more donating ligands compared to most phosphines and is therefore very significant. While this method utilizing $[Ni(CO)_4]$ is effective,

$[Ni(CO)_4]$ is a volatile and highly toxic reagent which also not economical making its use very impractical. As a result, alternative methods have been developed which operate by the same basic principles which instead employ the use transition metals such as iridium and rhodium to study the electronic donating abilities of NHCs.[28]

Herrmann 2006

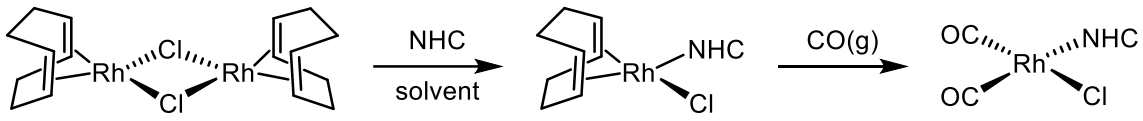

Scheme 4-1: TEP using rhodium square planar complex by Herrman and coworkers

Herrmann and coworkers reported the use of square planar rhodium carbonyl complexes of general formula $[(NHC)Rh(CO)_2Cl]$ comparing the electronics of select NHC ligands.[148] These complexes can easily be prepared by the treatment of bench stable $[Rh(COD)Cl]_2$ with a free NHC ligand, followed by treatment with CO(g) (**Scheme 4-1**). Similarly, $[(NHC)Ir(CO)_2Cl]$ have also been utilized which can be prepared by the same manner. Although effective, there are still practical limitations of this method as rhodium or iridium complexes are very costly limiting their practicality. Furthermore, the presence of two CO ligands leads to two CO stretching frequencies by the *trans* and *cis* carbonyls which can complicate analysis. Finally, studies using this method have demonstrated that these species do not exhibit large differences in between different ligands, which can result in experimental errors in comparisons.

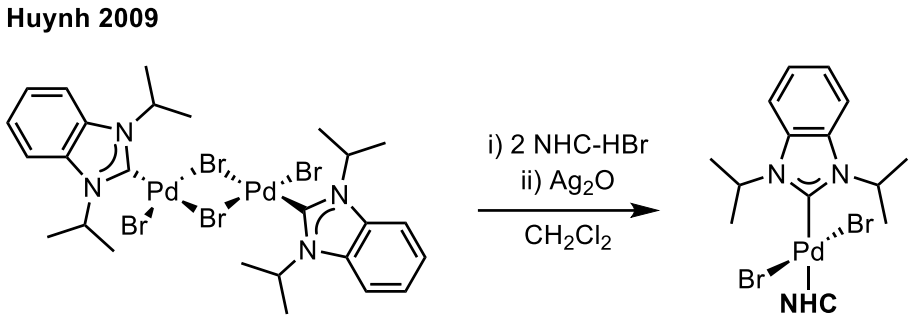

Scheme 4-2: Synthesis of HEP complex probe for NHC electronic studies

As such, alternative methods for the analysis of the electronic properties of NHCs have been reported. Most notably, the Huynh electronic parameter (HEP) which was introduced by Huynh and colleagues in 2009 (**Scheme 4-2**). This utilizes ^{13}C NMR studies on Pd-NHC complexes.[47,149] HEP evaluates the influence of a ligand, such as an NHC, that is *trans* to a reporter ligand, IPr_2-bimy, on its $^{13}C_{carbene}$ NMR signal.[27] In essence, a strongly donating ligand will induce a downfield shift on the $^{13}C_{carbene}$ of the reporter ligand and a weakly donating ligand will induce a upfield shift on the $^{13}C_{carbene}$ of the reporter ligand.[27] Although this HEP avoids the use of CO systems, it has its limitations. This method requires lengthy experiment times and can be problematic when 'super strong' electron donating ligand is *trans* to IPr_2-bimy, it can dissociate. Additionally, increased steric bulk has been shown to be a limitation.[27]

To combat these practical problems of the above experimental studies, computational analysis has been recently utilized. By measuring the energies of the HOMO and LUMO of the free carbenes, the σ-donating and π-accepting capabilities of a ligand can be probed.[140] However, as this method is not experimental in nature, the predicted geometries of ligands by DFT may not be structurally accurate. Furthermore, no benchmark conditions have been reported for the use of basis sets or DFT functionals, making comparisons between different reports challenging. As such, we believe that a more practical experimental method for the determination of electronic properties

of NHCs is needed, ideally using easily available and inexpensive reagents, and widely accessible forms of spectroscopy. Furthermore, the analysis should be free of experimental error and display large experimental differences where possible.

In this study, we propose the use of Cu(I) and Ag(I) NHC complexes bound to cyanide ligands may be ideal study the electronic effects of NHC ligands using the same principle as TEP. Both copper and silver precursors are more cost-effective transition metals compared to iridium or rhodium, and there have been many practical syntheses reported for [(NHC)CuX][121] or [(NHC)AgX][142] type complexes (X = halide). Additionally, these complexes generally display linear 2-coordinate geometries indicating that the NHC ligand will be directly *trans* to the CN without any additional competing ligands. This will likely give a more accurate depiction of electronic properties of NHCs while reducing variables such as *cis*- and *trans*- isomers involved when studying these complexes through IR spectroscopy. The choice of CN was due to its characteristic region in IR spectroscopy, typically giving distinct signals. Furthermore, the use of [(NHC)AgCN] complexes have been shown to be diagnostic towards electronic activities of an NHC ligand.[143]

4.2 Results and Discussion

4.2.1 Electronic Parameter Studies: An Attempt

As our group has extensive experience working with copper complexes of general type [(NHC)CuX], we hypothesized that these might be ideal precursors to begin investigating electronic properties of the NHC. Gaillard and coworkers reported the straightforward synthesis of [(NHC)CuCN] complexes by treating [(NHC)CuCl] complexes with KCN (**Scheme 4-3**).[150]

Following their procedure, [(IPr)CuCl] was treated with 1.0 equivalents of KCN in MeOH at 50°C for 4 hours.

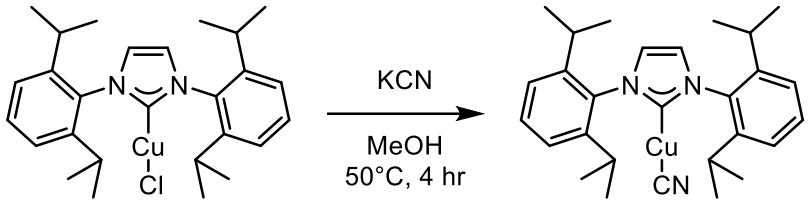

Scheme 4-3: Synthesis of [(IPr)CuCN] (**4-1**)

Following this reaction, the product was isolated in 88% yield and was characterized by ^{1}H NMR spectroscopy however, it bears a near identical spectrum to the ^{1}H NMR spectrum of [(IPr)CuCl], rendering this characterization method of little value. Similarly, high-resolution mass spectrometry (HRMS) was also ineffective, as the CN group, like Cl, would dissociate, resulting in an *m/z* value corresponding to either the $[(NHC)Cu]^{+}$ or the *bis*-NHC $[(NHC)_2Cu]^{+}$ species,[131,151] indistinguishable from the (NHC)CuCl complex. Therefore, to confirm the coordination of CN, we utilized IR spectroscopy for the presence of a CN stretching frequency around ~2200 cm^{-1}. For complex **4-1**, we observed a sharp signal at 2136.7 cm^{-1} which was tentatively assigned to be a CN stretch (**Figure 4-4**).[152] Additionally, the CN can be observed using ^{13}C{^{1}H} NMR spectroscopy, however, this requires several scans resulting in long experiments.

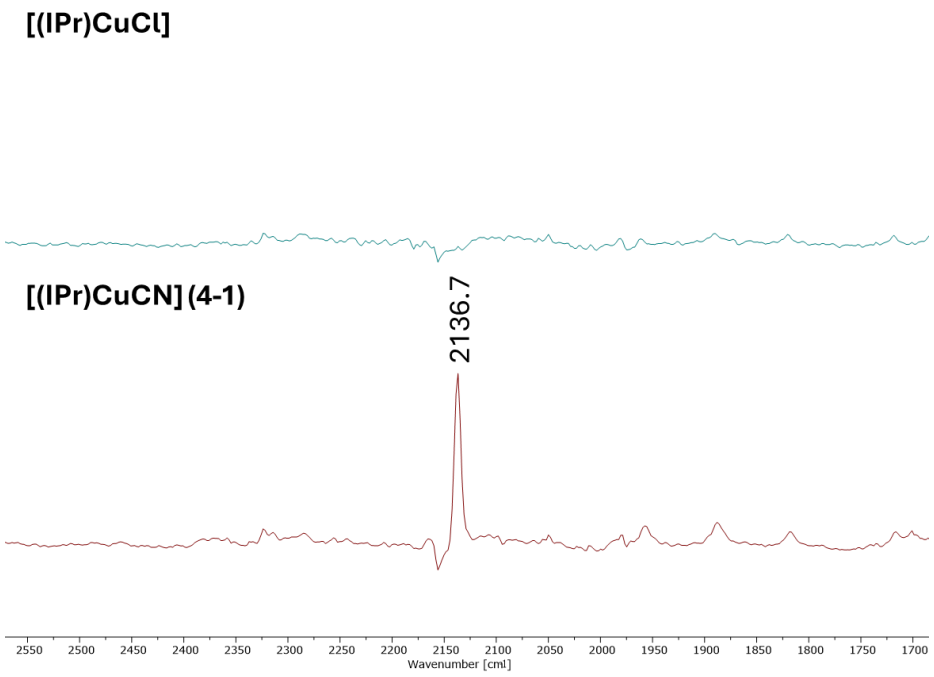

Figure 4-4: Section of the IR spectrum of complex **4-1** showing the CN stretching frequency

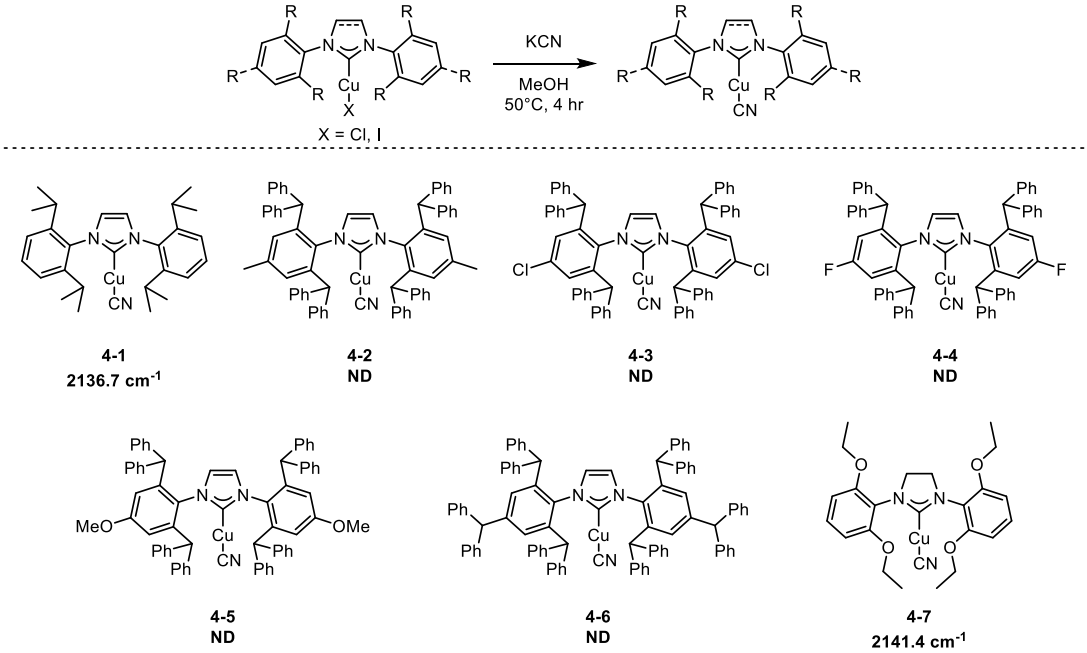

Figure 4-5: Series of CuCN complexes attempted. *ND denotes none detected*

From this result, we proceeded to attempt to synthesize a variety of [(NHC)CuCN] complexes with the more sterically hindered ligands, but electronically distinct X-IPr* derivatives,

as well as SIDEP-HBF_4 (**Figure 4-5**). Unfortunately, the distinctive sharp signals corresponding to a CN stretch were not observed with the series of [(X-IPr*)CuCN] complexes (**4-2** to **4-6**). Furthermore, the IR stretching frequency that we observed for [(SIDEP)CuCN] (**4-7**) was at 2141.4 cm^{-1} which was higher compared to complex **4-1**, suggesting a less donating NHC. Based on the principles of TEP, this result was unexpected as it suggests that IPr as a ligand is more electron-donating than the SIDEP. As SIDEP contains aromatic wingtip groups bearing electron donating substituents in the *ortho-* position of the wingtip groups, it was expected to exhibit a stretching frequency lower than **4-1**. This was further supported by our DFT studies.[153] To help explain our experimental results, we hypothesized potential macromolecular structures may be present, potentially with bridging CN ligands complicating analysis. This phenomenon has been reported before for phosphine ligands.[154] Due to the insoluble nature of KCN in the reaction mixture, we hypothesized that the reaction was largely unsuccessful and the crude product mixture may only contain a small percentage of the desired [(NHC)CuCN] complex. As such, attempts to isolate single crystals suitable for X-ray diffraction (XRD) of the presumed CuCN complexes (**4-1** to **4-6**) to support this hypothesis for our results were met with failure.

Given the inconsistent results we encountered with [(NHC)CuCN] type complexes, we shifted our focus to studying Ag(I) complexes. Following reports by Albrecht and coworkers,[143] we aimed to synthesize and investigate [(NHC)AgCN] complexes as these species have been previously reported and structurally characterized as monomolecular species. The preparation of [(NHC)AgCN] type complexes was reported to occur from the treatment of an NHC-HX precursor with Ag_2O in CH_3CN at elevated temperature via a C-C bond activation process along with the formation of CH_3OH. However, this procedure was only demonstrated with a limited ligand set, all of which were not sterically demanding. We tested the procedure to various ligands from the

more common, SIMes-HCl, IMes-HCl, IPr-HCl, SIPr-Cl and the sterically hindered X-IPr* series and analyzed all of the products obtained by IR spectroscopy. The values obtained are presented in **Table 4-1**.

Table 4-1: Synthesis of [(NHC)AgCN] complexes using Albrecht's procedure

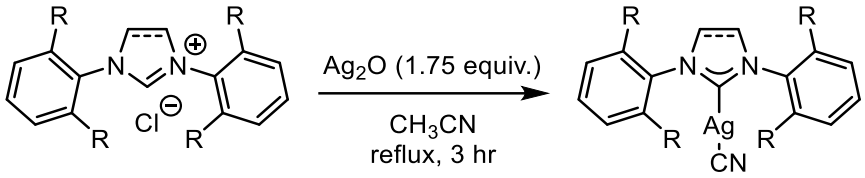

Entry	[(NHC)AgCN]	ν_{CN} (cm^{-1})
1	IPr (**4-8**)	ND
2	IMes (**4-9**)	2211.8 (br), 2137.8 (s)
3	SIMes (**4-10**)	2133.2 (s)
4	SIPr (**4-11**)	2202.3 (br), 2139.1 (s)
5	IPr* (**4-12**)	ND
6	*p*-F-IPr* (**4-13**)	ND
7	*p*-MeO-IPr* (**4-14**)	ND
8	*p*-Morpholine-IPr* (**4-15**)	ND

General Conditions: NHC-HX (0.05-0.15 mmol), Ag_2O (0.09-0.20 mmol) in CH_3CN (1-2 mL) at refluxed under air for 3 hours. *ND means none detected*.

In our hands, we received curious results. Complex **4-8** appeared to have no signal in the characteristic CN region (**Figure 4-6**). However, when the same procedure was used instead with the smaller IMes-HCl, producing complex **4-9**, two signals were present in the CN region (**Figure 4-6**). Specifically we observed a relatively broad signal at 2211.8 cm^{-1}, whose wavenumber approximately aligned with Albrecht's results,[143] and a second sharper signal at 2137.8 cm^{-1} (**Figure 4-6**). With regards to complex **4-10**, which contained the saturated SIMes ligand, surprisingly only a single sharp signal at 2133.2 cm^{-1} was observed (**Figure 4-6**). Next, we synthesized another complex, **4-11**, containing SIPr, which gave a spectrum similar to **4-9**, with two signals, a broad one at 2202.3 cm^{-1} and another sharper signal at 2139.1 cm^{-1} (**Figure 4-6**).

Single crystals of complex **4-11** were grown from the slow diffusion of hexanes into a concentrated CH_3Cl solution. Complex **4-11** co-crystallized with the desired [(SIPr)Ag-CN] and [(SIPr)Ag-Cl] complex in approximately 1:1 ratio (**Figure 4-7**). The [(SIPr)AgCl][144] analog likely forms as an intermediate on route to the desired cyanide complex. Of note, while this structure helps to confirm the structure of our desired product, it is not necessarily representative of the bulk sample as it does not explain the second IR stretching frequency observed.

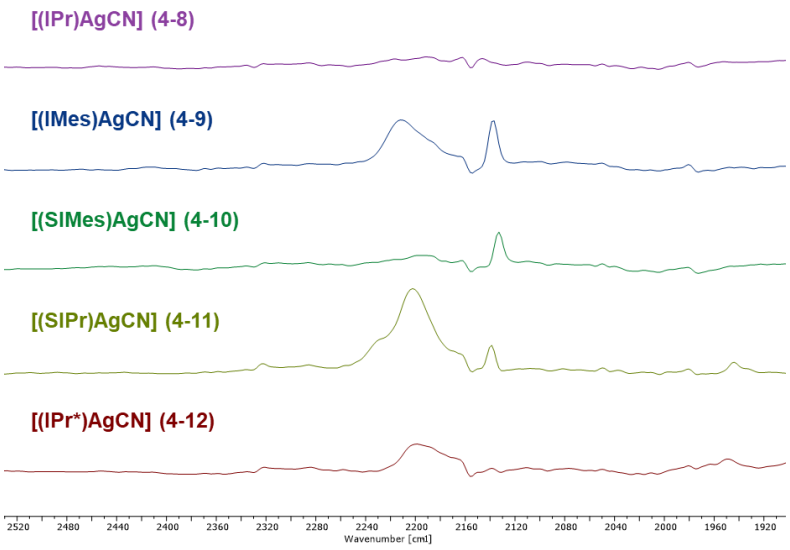

Figure 4-6: IR spectra associated with the complexes made in **Table 4-1**

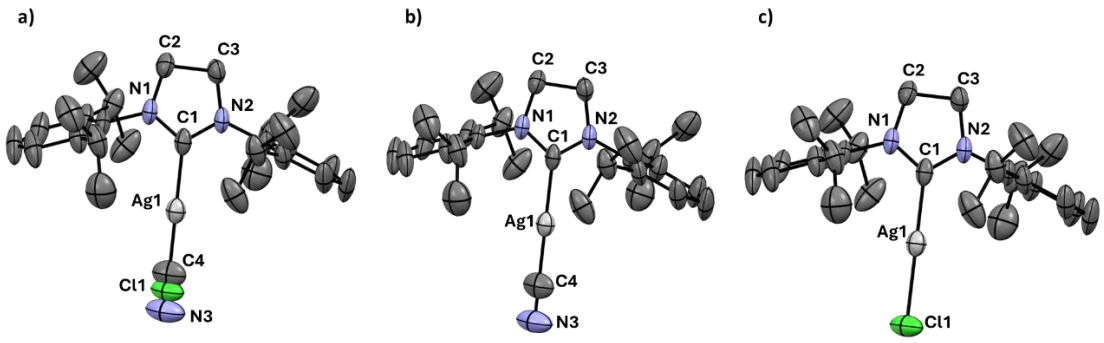

Figure 4-7: Crystallographically determined structure of **4-11** a) as a co-crystal (~50% occupancy of CN^-, ~50% occupancy of Cl^-), b) separated [(SIPr)AgCN] complex, and c) separated [(SIPr)AgCN] displaying thermal ellipsoids drawn at the 50% confidence level. Hydrogen atoms and solvent ($CHCl_3$) are omitted for clarity. interatomic distances [Å] and

angles [deg] (identical for both complexes with exceptions to AgCN and AgCl bonds): N(1)−C(1), 1.327(9); C(1)−N(2), 1.327(9); N(1)−C(1)−N(2), 108.4(3); C(1)−Ag(1), 2.081(1); Ag(1)−C(4), 1.899(2); C(4)−N(3), 1.115(0); Ag(1)−Cl(1), 2.403(3); C(1)−Ag(1)−C(4), 180.0(0); C(1)−Ag(1)−Cl(1), 180.0(0).

Our attempts to synthesize [(NHC)AgCN] complexes with X-IPr* derivatives were unsuccessful (**4-12** to **4-15**). In all cases, analysis by ^{1}H NMR spectroscopy of all complexes showed that the ligand successfully coordinated to silver due to the disappearance of the $C_{carbene}$-H peak indicating successful metallation. Though complex **4-12** appears to have a peak in the CN region (**Figure 4-6**), this was very broad and not characteristic of a CN stretch, therefore, we concluded that no CN stretching frequencies were observed in any of the X-IPr* complexes made by IR spectroscopy. We hypothesized that this may be due to the complicated nature of the reaction, which likely produces multiple Ag-NHC type complexes.[142] In terms of complexes, **4-9** and **4-11**, which both gave two signals in the IR spectrum we hypothesized the presence of a second CN containing product. As such, we explored alternative procedures from the literature in the hopes of generating pure [(NHC)AgCN] type complexes. We hypothesized that the formation of a [(NHC)AgCl] type complex could then be followed with treatment of KCN to generate [(NHC)AgCN] type complexes.

Table 4-2: Two-step method of generating AgCN complexes

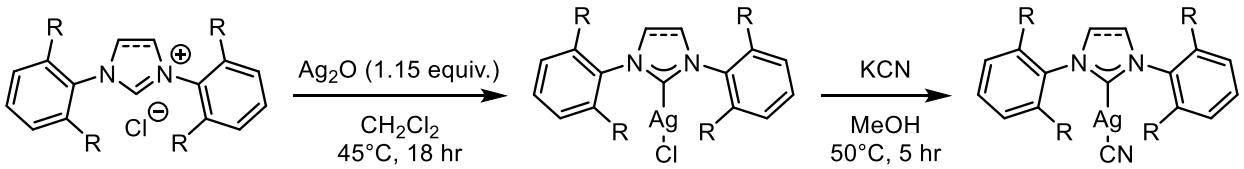

Entry	[(NHC)AgCN]	ν_{CN} (cm^{-1})
1	IPr (**4-16**)	2143.4
2	IMes (**4-17**)	2138.4
3	SIMes (**4-18**)	2133.3
4	SIPr (**4-19**)	2139.6
5	IPr* (**4-20**)	ND
6	*p*-F-IPr* (**4-21**)	ND
7	*p*-MeO-IPr* (**4-22**)	ND
8	*p*-Morpholine-IPr* (**4-23**)	ND
9	IPr# (**4-24**)	ND

General Considerations: NHC-HX (0.05-0.15 mmol), Ag_2O (0.06-0.17 mmol) in CH_2Cl_2 (1 mL) at 45°C under air. [(NHC)AgCl] (0.04-0.48 mmol), KCN (0.04-0.48 mmol) in MeOH (1-10 mL) at 50°C under air. *ND means none detected*.

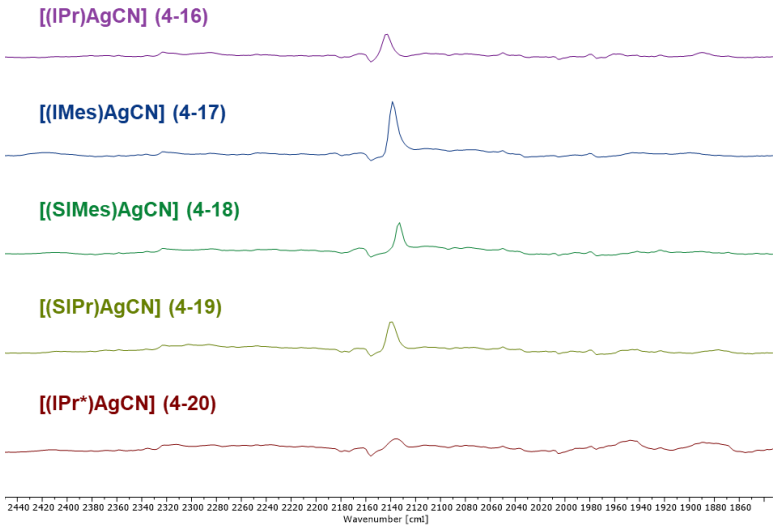

Figure 4-8: IR spectra associated with the complexes in **Table 4-2**

We attempted conditions from the literature reported by Nolan for the formation of [(NHC)AgCl] complexes followed by Gaillard's method by treating with KCN in MeOH (**Table 4-2**).[144,150] We then measured the obtained crude samples (**4-16** to **4-24)** using IR spectroscopy, and the results are summarized in **Table 4-2**. Unfortunately, our attempts to synthesize [(NHC)AgCN] type complexes with the sterically large X-IPr* NHC ligands (**4-20** – **4-24**) were unsuccessful once again (**Table 4-2**). However, a single sharp peak characteristic of a CN stretching frequency was observed for complexes **4-16** to **4-19** which contained smaller NHC

ligands (**Table 4-2**). Most notably, in all cases with the smaller ligands, the observed stretching frequency appeared at 2133 – 2144 cm^{-1} (**Figure 4-8**). In the case of SIPr (**4-19**) and IMes (**4-17**) the signal observed closely resembled the sharp signals from the previous procedure (**Figure 4-8**).

Curiously, the stretching frequencies obtained for **4-16** – **4-19** differs from those reported by Albrecht and coworkers[143] by more than 50 cm^{-1} and leads to the questions regarding the specific structural identity of these species. As with the copper species, NMR and HRMS analysis was unfortunately not informative as [(NHC)AgCl] and [(NHC)AgCN] appear to have near identical spectra. Furthermore, we failed to observe the CN ligand by ^{13}C NMR spectroscopy, presumably due to a very slow relaxation of the metal bound CN ligand, which would be further impacted by the Ag, as it exists as two NMR active nuclei ^{107}Ag and ^{109}Ag likely resulting in multiple doublets of lower intensity, combined with low concentration from incomplete product formation. In our hands, all attempts to grow single crystals suitable for x-ray diffraction of these species obtained by this procedure have failed.

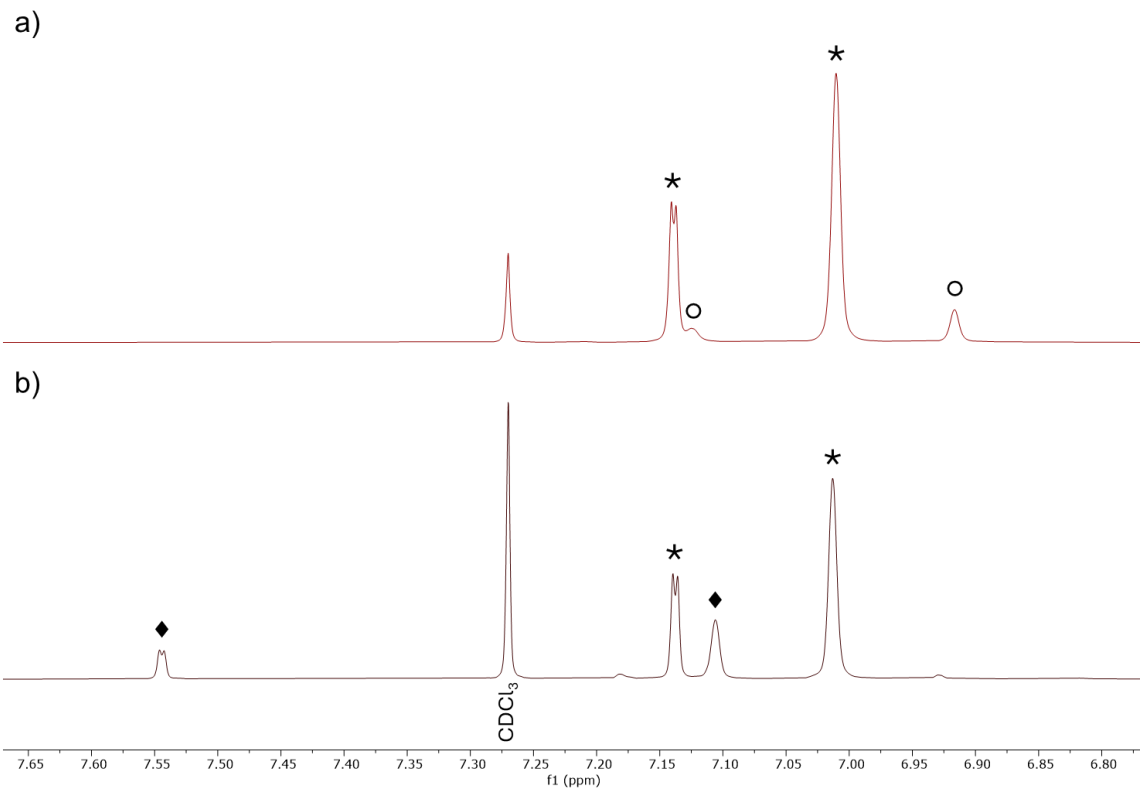

Figure 4-9: Aromatic region of a) complex **4-9** and b) complex **4-17** using ^{1}H NMR spectroscopy. *(* was tentatively assigned to be [(IMes)AgCN], ° and ♦ were unknown compounds observed)*

While our structural assignments of complexes **4-16** to **4-19** are tentative, it appears that our two-step procedure in **Table 4-2** is a cleaner route to what we believe to be the desired [(NHC)AgCN] products, possessing a single sharp IR stretching frequency in the anticipated region of a CN moiety. It is worth noting that while analogous phosphine silver cyanide complexes are rare,[155] their reported IR spectra are more consistent with our results in **Table 4-2** than those reported by Albrecht. Upon analysis by ^{1}H NMR spectroscopy, the presence of another compound was observed for complexes **4-17** to **4-19**. An example of this is represented in **Figure 4-9** which shows [(IMes)AgCN] produced from Albrecht's procedure (**Figure 4-9a**) and the two-step procedure (**Figure 4-9b**). Unfortunately, for complexes **4-17** and **4-18** the identity of the other compound was unknown as we could not isolate a single crystal suitable for X-ray crystallography.

For complex **4-19**, we hypothesized that the identity of the other compound observed was [(SIPr)AgCl] which we observed in the X-ray crystallography analysis of complex **4-11** as well as in literature.[143]

While the exact structural identity of complexes **4-16** to **4-19** are still ambiguous, the stretching frequencies observed clearly show an obvious trend, which is particularly interesting when compared to the literature. Analysis of the results obtained indicated that SIMes (**4-18**) had the lowest stretching frequency, indicating it was the most electron-donating ligand, followed by IMes (**4-17**), SIPr (**4-19**), and IPr (**4-16**), which was the least electron-donating ligand. This overall trend can be rationalized as both IMes and SIMes have wingtip groups with three electron donating substituents in the *ortho*- and *para*- positions, where as IPr and SIPr only have two in the ortho positions. Furthermore, in contrast to IMes and IPr, SIMes and SIPr are not aromatic heterocycles, and one could reasonably predict that would directly impact the electron donating abilities of the NHCs.

Notably, there was also a clear distinction between the ligands' stretching frequencies compared to examples of literature studies (**Table 4-3**). We further hypothesize that the failure to form [(NHC)AgCN] type complexes with the X-IPr* type ligands result from the increased steric parameters of these ligands, hindering substitution at the Ag.

Table 4-3: Comparison of literature electronic studies to this study

NHC	**[(NHC)Ni(CO)$_3$] (cm^{-1})[a]**	**[(NHC)Ir(CO)$_2$Cl] (cm^{-1})[a]**	**[(NHC)AgCN] (cm^{-1})**
IMes	2050.7	2023.1	2138.4
IPr	2051.5	2023.9	2143.4
SIMes	2051.5	2024.6	2133.3
SIPr	2052.5	2024.9	2139.6

[a] Determined experimentally.[28,46]

In the literature electronic measurement studies, IMes was identified as the most electron-donating ligand.[28,46,148] In the nickel study, IPr and SIMes showed no distinguishable differences in electron-donating abilities (2051.5 and 2051.5 respectively), while SIPr was the least donating. In the iridium study, the differences in stretching frequencies between IMes and IPr (2050.7 and 2051.5 cm^{-1} respectively), as well as between SIMes and SIPr (2051.5 and 2052.5 cm^{-1} respectively), were minimal, essentially falling within the margin of error. However, in our system, a clear distinction between the stretching frequencies of each ligand was observed. Specifically, the differences in IR frequencies between the ligands were all greater than 1.0 cm^{-1}. We hypothesize that this is due to the lack of competing back-bonding ligands on the [(NHC)AgCN] type complex, with the CN directly trans to the NHC ligand. This would render the CN ligand more susceptible to changes with to the NHC ligand. Ultimately, our study proposes a different trend relative to electron donating ability than previous studies.

Our study shows a promising start for a cost effective and user-friendly method of studying NHC ligands, however our study has been hampered by synthetic methods either resulting in poor yields or multiple products complicating our analysis We hypothesize if new synthetic procedures can be developed for the preparation of [(NHC)Ag-CN] type complexes in high yield and purity, these complexes may be ideal to be used for this purpose.

4.3 Conclusions and Future Work

Though, we initially focused on Cu-NHC complexes to investigate the electronic properties and the impact of NHC ligands, the results from this system were largely inconclusive. This was particularly the case when comparing observed results of the IR studies with [(IPr)CuCN] and [(SIDEP)CuCN] which gave counter intuitive results. Our shift to Ag(I) complexes, shows a promising start in studying the electron-donating abilities of the ligands by their CN stretching

frequencies. While our results indicate a clear obvious trend with the electronic properties of common NHC ligands, structural ambiguity and problematic synthetic procedures have hindered progress. Significantly, despite our best efforts, we were unable to synthesize pure [(NHC)AgCN] complexes with larger NHC ligands such as the X-IPr* family, indicating the narrow operating window for this method.

In conclusion, our study highlights the potential of Ag(I) cyanide complexes as a cost-effective and user-friendly method for exploring the electronic donating properties of NHC ligands. The distinct differences in IR frequencies among the ligands suggest that Ag(I) systems may offer clearer differentiation in electronic properties when compared to the iridium and nickel systems. Future work will focus on refining these methods to successfully coordinate the more sterically bulky ligands to AgCN to further elucidate the electronic effects in these systems. Specifically, we will explore the use of homogeneous sources of cyanide such as TMS-CN to help improve our synthetic procedures.

4.4 Experimental

General Considerations: All manipulations were carried out under a nitrogen or argon atmosphere unless otherwise noted using standard Schlenk techniques. All reagents were purchased from commercial suppliers and used without further purification. Acetonitrile was purchased from Sigma Aldrich and stored on 3Å molecular sieves. [(NHC)CuCl] precursors were synthesized by procedures from Chapter 2. [(SIDEP)CuCl] was synthesized by procedures from Chapter 3. Celite® was purchased from Sigma–Aldrich. ^{1}H NMR spectra were measured on a Varian INOVA 500 MHz, Bruker Ascend 400 MHz, or a Nanalysis 60 MHz benchtop spectrometer where noted at 298K. Chemical shifts are reported in delta (δ) units, expressed in parts per million (ppm) downfield from tetramethylsilane (TMS) using residual protonated solvent as an internal

standard ($CDCl_3$, 7.27 ppm). $^{13}C\{^1H\}$ NMR spectra were recorded at 126 MHz or 101 MHz where noted. Chemical shifts are reported as above using the solvent as an internal standard ($CDCl_3$, 77.23 ppm).

Synthesis of [(NHC)CuCN] Complexes

Under Ar, an oven-dried culture tube was charged with [(NHC)CuX] (0.3 mmol), KCN (0.3 mmol), and degassed MeOH. The tube was sealed and heated at 50°C for 4 hours. The reaction solution was then cooled to room temperature and the solvent was removed *in vacuo*. The residue was dissolved in CH_2Cl_2 and filtered through a small plug of silica gel. The filtrate was evaporated to remove excess solvent and the product was precipitated in hexanes under vacuum.

Synthesis of [(IPr)CuCN] (4-1)

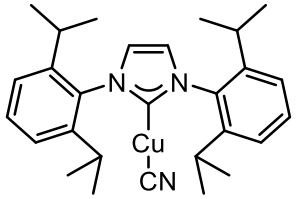

The general procedure was followed with [(IPr)CuCl] (150 mg, 0.3 mmol) and KCN (19 mg, 0.3 mmol), in 5 mL of degassed MeOH giving 127.1 mg (88%) as an off-white solid. *Spectra matches literature.*[152] **^{1}H NMR (400 MHz, $CDCl_3$):** δ 7.52 (t, *J* = 7.80 Hz, 2H), 7.31 (d, *J* = 7.76 Hz, 4H), 7.15 (s, 2H), 2.51 (sept, *J* = 6.89 Hz, 4H), 1.28 (d, *J* = 6.88 Hz, 12H), 1.23 (d, *J* = 6.90 Hz, 12H) ppm. **$^{13}C\{^1H\}$ NMR (101 MHz, $CDCl_3$):** δ 180.6, 145.7, 143.5, 134.1, 131.0, 124.4, 123.5, 28.9, 25.1, 24.0 ppm.

Synthesis of [(SIDEP)CuCN] (4-7)

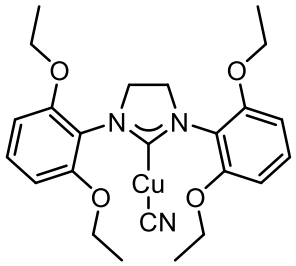

The general procedure was followed with [(SIDEP)CuI] (176.7 mg, 0.3 mmol) and KCN (19 mg, 0.3 mmol), in 5 mL of degassed MeOH giving 22.7 mg (15%) as an off-white solid. **NMR spectra pending.*

Synthesis of [(NHC)AgCN] Complexes using Albrecht *et al.* Procedure

Under air, a culture tube equipped with a stirbar was charged with NHC-HX, Ag_2O, and CH_3CN. The tube was sealed and heated at reflux for 3 hours in the absence of light.[143] A white precipitate was typically observed after the reaction. The solution was then cooled to room temperature and the solvent was removed *in vacuo*. The residue was dissolved in CH_2Cl_2 and filtered through Celite® on a frit. The filtrate was evaporated to dryness and the crude residue was dissolved in minimal amounts of CH_2Cl_2 and layered with hexanes to precipitate the product out. The precipitate was collected by filtration and washed with Et_2O.

Synthesis of [(IMes)AgCN] (4-9)

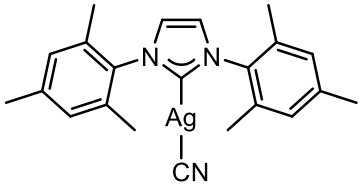

The general procedure was followed with IMes-HCl (50 mg, 0.15 mmol) and Ag_2O (60.3 mg, 0.26 mmol), in 1.5 mL of CH_3CN giving 50.5 mg (76%) as an off-white solid. **^{1}H NMR (400 MHz, $CDCl_3$):** δ 7.14 (d, *J* = 1.57 Hz, 2H), 7.01 (s, 4H), 2.37 (s, 6H), 2.06 (s, 12H) ppm. **^{13}C{^{1}H} NMR (101 MHz, $CDCl_3$):** δ 184.6 (d, *J* = 212.3 Hz), 140.0, 134.7, 129.7, 122.9 (d, *J* = 6.51 Hz), 21.3, 17.8 ppm. *Carbene peak found by ^{1}H-^{13}C HMBC experiment.*

Synthesis of [(SIMes)AgCN] (4-10)

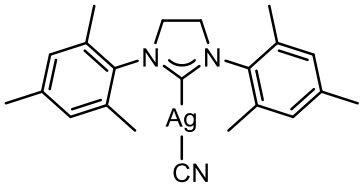

The general procedure was followed with IPr-HCl (50 mg, 0.15 mmol) and Ag_2O (59.1 mg, 0.26 mmol), in 1.5 mL of CH_3CN giving 50.3 mg (76%) as an off-white solid. **^{1}H NMR (400 MHz, $CDCl_3$):** δ 6.96 (s, 4H), 4.00 (s, 4H), 2.32 (s, 6H), 2.28 (s, 12H) ppm. **^{13}C{^{1}H} NMR (101 MHz, $CDCl_3$):** δ 139.2, 135.6, 130.0, 51.3 (d, *J* = 7.58 Hz), 21.2, 18.1 ppm. *Despite our best efforts, the carbene carbon was not observed.*

Synthesis of [(SIPr)AgCN] (4-11)

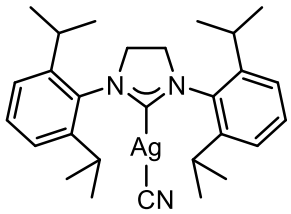

The general procedure was followed with SIPr-HCl (50 mg, 0.12 mmol) and Ag_2O (47.5 mg, 0.20 mmol), in 1.2 mL of CH_3CN giving 33.4 mg (53%) as an off-white solid. Single crystals suitable for X-ray diffraction were grown by slow diffusion of hexanes into a concentrated solution of $CHCl_3$. **^{1}H NMR (400 MHz, $CDCl_3$):** δ 7.43 (t, *J* = 7.77 Hz, 2H), 7.26 (d, *J* = 7.78 Hz, 4H), 4.07 (s, 4H), 3.13 – 2.90 (m, 4H), 1.39 – 1.22 (m, 24H) ppm. **^{13}C{^{1}H} NMR (101 MHz, $CDCl_3$):** δ 146.5, 130.1, 124.7, 53.9 (d, *J* = 7.82 Hz), 28.9, 25.4, 24.0 ppm. *Despite our best efforts, the carbene carbon was not observed.*

Synthesis of [(NHC)AgCN] Complexes using Nolan *et al.* and Gaillard *et al.* Procedure

Under air, a culture tube equipped with a stirbar was charged with NHC-HX, Ag_2O, and CH_2Cl_2. The tube was sealed and heated at 45°C for 18 hours in the absence of light.[144] A precipitate was typically observed at the end of the reaction. The solution was then cooled to room temperature and the solvent was removed *in vacuo*. The residue was dissolved in CH_2Cl_2 and filtered through Celite® on a frit. The filtrate was evaporated to dryness and the product was precipitated in hexanes under vacuum. The formation of the Ag-NHC complex was confirmed by ^{1}H NMR spectroscopy and was carried through directly to the next step without any purification.

Synthesis of [(IPr)AgCl]

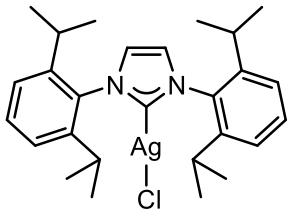

The general procedure was followed with IPr-HCl (50 mg, 0.12 mmol) and Ag_2O (31.3 mg, 0.14 mmol), in 1 mL of CH_2Cl_2 giving 44.8 mg (70%) as an orange solid. *Spectra matches literature.*[144] **^{1}H NMR (60 MHz, $CDCl_3$):** δ 7.5 – 6.9 (m, 8H), 2.8 – 2.1 (m, 4H), 1.4 – 0.8 (m, 24H) ppm.

Synthesis of [(IMes)AgCl]

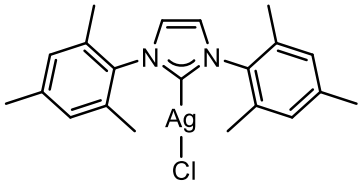

The general procedure was followed with IMes-HCl (50 mg, 0.15 mmol) and Ag_2O (39.1 mg, 0.17 mmol), in 1 mL of CH_2Cl_2 giving 54.9 mg (81%) as a white solid. *Spectra matches literature.*[144] **^{1}H NMR (60 MHz, $CDCl_3$):** δ 7.14 (s, 2H), 7.01 (s, 4H), 2.36 (s, 6H), 2.08 (s, 12H) ppm.

Synthesis of [(SIMes)AgCl]

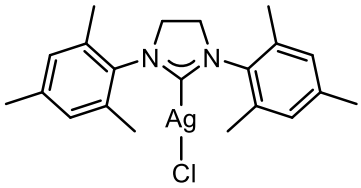

The general procedure was followed with SIMes-HCl (50 mg, 0.15 mmol) and Ag_2O (38.9 mg, 0.17 mmol), in 1 mL of CH_2Cl_2 giving 49.6 mg (73%) as a white solid. *Spectra matches literature.*[144] **^{1}H NMR (60 MHz, $CDCl_3$):** δ 7.0 (s, 4H), 4.0 (s, 4H), 2.3 (s, 18H) ppm.

Synthesis of [(SIPr)AgCl]

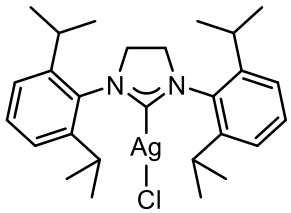

The general procedure was followed with SIPr-HCl (50 mg, 0.12 mmol) and Ag_2O (31.2 mg, 0.13 mmol), in 1 mL of CH_2Cl_2 giving 55.5 mg (86%) as a white solid. *Spectra matches literature.*[144] **^{1}H NMR (60 MHz, $CDCl_3$):** δ 7.7 – 7.0 (m, 6H), 4.1 (s, 4H), 3.4 – 2.7 (m, 4H), 1.4 (d, J = 6.90 Hz, 24H) ppm.

Under Ar, an oven-dried culture tube was charged with [(NHC)AgCl], KCN, and degassed MeOH. The tube was sealed and heated at 50°C for 18 hours in the absence of light. The reaction solution was then cooled to room temperature and the solvent was removed *in vacuo*. The residue was dissolved in CH_2Cl_2 and filtered through Celite® on a frit. The filtrate was evaporated to remove excess solvent and the product was precipitated in hexanes under vacuum.

Synthesis of [(IPr)AgCN] (4-16)

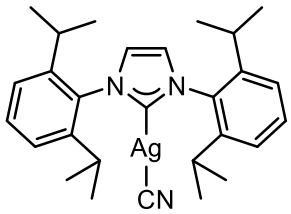

The general procedure was followed with [(IPr)AgCl] (44.8 mg, 0.08 mmol) and KCN (5.5 mg, 0.08 mmol), in 2 mL of degassed MeOH giving 37.7 mg (90%) as a white solid. **^{1}H NMR (400 MHz, $CDCl_3$):** δ 7.52 (t, *J* = 7.81 Hz, 2H), 7.31 (d, *J* = 7.78 Hz, 4H), 7.22 (d, *J* = 1.54 Hz, 2H), 2.50 (sept, *J* = 6.91 Hz, 4H), 1.26 (d, *J* = 6.86 Hz, 12H), 1.23 (d, *J* = 6.83 Hz, 12H) ppm. **^{13}C{^{1}H} NMR (101 MHz, $CDCl_3$):** δ 186.4 (d, *J* = 15.26 Hz), 145.7, 134.5, 131.0, 124.5, 123.8 (d, *J* = 6.39 Hz), 28.9, 24.9, 24.2 ppm.

Synthesis of [(IMes)AgCN] (4-17)

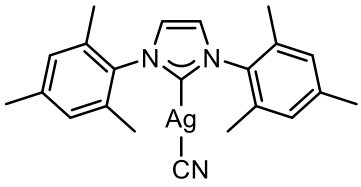

The general procedure was followed with [(IMes)AgCl] (54.9 mg, 0.12 mmol) and KCN (7.9 mg, 0.12 mmol), in 2 mL of degassed MeOH giving 49.5 mg (94%) as a white solid. **^{1}H NMR (400 MHz, $CDCl_3$):** δ 7.14 (d, *J* = 1.56 Hz, 2H), 7.01 (s, 4H), 2.37 (s, 6H), 2.07 (s, 12H) ppm. **^{13}C{^{1}H} NMR (101 MHz, $CDCl_3$):** δ 140.0, 134.7, 129.8, 122.9 (d, *J* = 6.57 Hz), 21.3, 17.8 ppm.

Synthesis of [(SIMes)AgCN] (4-18)

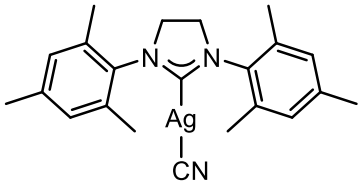

The general procedure was followed with [(SIMes)AgCl] (49.6 mg, 0.11 mmol) and KCN (7.2 mg, 0.11 mmol), in 2 mL of degassed MeOH giving 39.2 mg (80%) as an off-white solid. **^{1}H NMR (400 MHz, $CDCl_3$):** δ 6.95 (s, 4H), 4.00 (s, 4H), 2.32 (s, 6H), 2.28 (s, 12H) ppm. **^{13}C{^{1}H} NMR (101 MHz, $CDCl_3$):** δ 209.1 (d, *J* = 14.20 Hz), 139.0, 135.4, 129.9, 51.2 (d, *J* = 7.44 Hz), 21.0, 17.9 ppm.

Synthesis of [(SIPr)AgCN] (4-19)

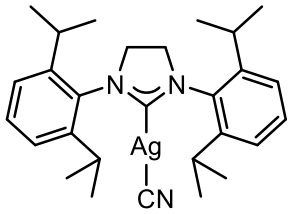

The general procedure was followed with [(SIPr)AgCl] (55.5 mg, 0.10 mmol) and KCN (6.8 mg, 0.10 mmol), in 2 mL of degassed MeOH giving 43.6 mg (83%) as an off-white solid. **^{1}H NMR (400 MHz, $CDCl_3$):** δ 7.42 (t, *J* = 7.78 Hz, 2H), 7.24 (d, *J* = 7.81 Hz, 4H), 4.06 (s, 4H), 3.06 – 2.97 (m, 4H), 1.34 (d, *J* = 6.91 Hz, 12H), 1.30 (d, *J* = 6.85 Hz, 12H) ppm. **^{13}C{^{1}H} NMR (101 MHz, $CDCl_3$):** δ 209.3 (d, *J* = 14.16 Hz), 146.7, 130.2, 124.8, 29.0, 25.5, 24.1 ppm.

Chapter 5

Conclusions and Future Work

In Chapter 2, the synthesis of a variety of Cu^{I}-NHC complexes using triethylamine as a base was presented. This method offers several advantages, including mild reaction conditions, short reaction times, and compatibility with air, which makes it both scalable and accessible for broader applications. Notably, the unsaturated NHC precursors generally performed better than the saturated ones, likely due to a decrease in acidity. We found that the smaller ligands, IMes and SIMes, produced multiple products with CuI. The bulkier ligands, IPr and SIPr, did not exhibit the same results.

Future work involves investigations on expanding the substrate scope of the NHC precursors that can be coordinated to Cu^{I} precursors using this weak base method. Our group is further interested in applying this methodology towards the coordination of NHC precursors to different transition metals. Preliminary investigations of expanding the scope of NHC precursors metallated using this method is underway.

In Chapter 3, the synthesis of the sterically modular and electron-rich 2,6-*bis*(alkoxyphenyl) substituted NHCs and their coordination to copper, silver, and palladium was presented. Attempts to metallate these ligands to Cu^{I} precursors using the weak base method developed in Chapter 2 was low yielding, likely due to the decreased acidity of the NHC precursors. This was mitigated by the use of a strong base, NaHMDS, yielding [Cu(RO-NHC)X] (X = Cl, Br, I) type complexes. The different steric parameters were observed using X-ray crystallography of CuCl complexes **3-34** to **3-36**. Metallation to palladium was achieved using two different methods, silver transmetallation and the free carbene route. However, the silver

transmetallation method was low yielding due to the presence of multiple products. The free carbene route effectively mitigated the low yield issue obtaining high yields of [(RO-NHC)Pd(allyl)Cl] type complexes. The direct impact of the steric parameters was demonstrated using SMR of aryl chlorides using well-defined [(RO-NHC)Pd(allyl)Cl] precatalysts. The more sterically bulky ligands provided higher conversions, showcasing the importance of steric control in ligand design.

Future work will delve into further optimizations in the usage of these NHC ligands in catalysis. Preliminary investigations towards the synthesis of their unsaturated counterparts are underway. Additionally, our group is interested in synthesizing several new ligands pushing the steric boundaries that this methodology can achieve. Applications of these new ligands will then be further studied in catalysis.

In Chapter 4, explores a more economical and practical alternatives to measuring electronic properties of NHC ligands, utilizing Cu^{I} and Ag^{I} NHC complexes bound to cyanide. The synthesis and characterization of these complexes revealed several challenges, particularly with sterically demanding ligands such as X-IPr* derivatives, likely due to complex reaction pathways and potential formation of macromolecular structures. The shift to a different method synthesizing Ag(I) complexes provided some success with the smaller ligands, showing clear trends in electron-donating abilities, as indicated by IR spectroscopy. Yet, even with these successes, the structural identity of the synthesized complexes remains ambiguous, and the inability to consistently form complexes with larger ligands points to the limitations of this method.

Future work involves the optimization of the synthetic method to achieve [Ag(X-IPr*)CN] complexes using the homogeneous TMSCN as an alternative to KCN. Our group is further

interested in the isolation of single crystals suitable for X-ray crystallography of these AgCN complexes to eliminate structure ambiguities.

References

(1) Yorimitsu, H.; Kotora, M.; Patil, N. T. Special Issue: Recent Advances in Transition-Metal Catalysis. *Chem. Rec.* **2021**, *21* (12), 3335–3337. https://doi.org/10.1002/tcr.202100305.

(2) Hartwig, J. F. *Organotransition Metal Chemistry: From Bonding to Catalysis*; University Science Books, 2010.

(3) *Green Catalysis*; Anastas, P. T., Crabtree, R. H., Eds.; Wiley-VCH, 2009; Vol. 1.

(4) Lundgren, R. J.; Stradiotto, M. Addressing Challenges in Palladium-Catalyzed Cross-Coupling Reactions Through Ligand Design. *Chem. – Eur. J.* **2012**, *18* (32), 9758–9769. https://doi.org/10.1002/chem.201201195.

(5) Sigman, M. S.; Werner, E. W. Imparting Catalyst Control upon Classical Palladium-Catalyzed Alkenyl C–H Bond Functionalization Reactions. *Acc. Chem. Res.* **2012**, *45* (6), 874–884. https://doi.org/10.1021/ar200236v.

(6) Marion, N.; Díez-González, S.; Nolan, S. P. N-Heterocyclic Carbenes as Organocatalysts. *Angew. Chem. Int. Ed.* **2007**, *46* (17), 2988–3000. https://doi.org/10.1002/anie.200603380.

(7) Andrus, M. B.; Song, C. Palladium−Imidazolium Carbene Catalyzed Aryl, Vinyl, and Alkyl Suzuki−Miyaura Cross Coupling. *Org. Lett.* **2001**, *3* (23), 3761–3764. https://doi.org/10.1021/ol016724c.

(8) Hahn, F. E. Substrate Recognition and Regioselective Catalysis with Complexes Bearing NR,NH-NHC Ligands. *ChemCatChem* **2013**, *5* (2), 419–430. https://doi.org/10.1002/cctc.201200567.

(9) Fanourakis, A.; Docherty, P. J.; Chuentragool, P.; Phipps, R. J. Recent Developments in Enantioselective Transition Metal Catalysis Featuring Attractive Noncovalent Interactions between Ligand and Substrate. *ACS Catal.* **2020**, *10* (18), 10672–10714. https://doi.org/10.1021/acscatal.0c02957.

(10) Gillespie, J. A.; Zuidema, E.; van Leeuwen, P. W. N. M.; Kamer, P. C. J. Phosphorus Ligand Effects in Homogeneous Catalysis and Rational Catalyst Design. In *Phosphorus(III) Ligands in Homogeneous Catalysis: Design and Synthesis*; John Wiley & Sons, Ltd, 2012; pp 1–26. https://doi.org/10.1002/9781118299715.ch1.

(11) *Phosphorus(III) Ligands in Homogeneous Catalysis: Design and Synthesis*; Kamer, P. C. J., van Leeuwen, P. W. N. M., Eds.; John Wiley & Sons, Ltd: West Sussex, United Kingdom, 2012.

(12) Rajmane, A.; Kumbhar, A. Polydentate P, N-Based Ligands for Palladium-Catalyzed Cross-Coupling Reactions. *Mol. Catal.* **2022**, *532*, 112699. https://doi.org/10.1016/j.mcat.2022.112699.

(13) Martin, R.; Buchwald, S. L. Palladium-Catalyzed Suzuki−Miyaura Cross-Coupling Reactions Employing Dialkylbiaryl Phosphine Ligands. *Acc. Chem. Res.* **2008**, *41* (11), 1461–1473. https://doi.org/10.1021/ar800036s.

(14) Li, H.; Johansson Seechurn, C. C. C.; Colacot, T. J. Development of Preformed Pd Catalysts for Cross-Coupling Reactions, Beyond the 2010 Nobel Prize. *ACS Catal.* **2012**, *2* (6), 1147–1164. https://doi.org/10.1021/cs300082f.

(15) Herrmann, W. A.; Köcher, C. N-Heterocyclic Carbenes. *Angew. Chem. Int. Ed. Engl.* **1997**, *36* (20), 2162–2187. https://doi.org/10.1002/anie.199721621.

(16) Hahn, F. E.; Jahnke, M. C. Heterocyclic Carbenes: Synthesis and Coordination Chemistry. *Angew. Chem. Int. Ed.* **2008**, *47* (17), 3122–3172. https://doi.org/10.1002/anie.200703883.

(17) Igau, Alain.; Grutzmacher, Hansjorg.; Baceiredo, Antoine.; Bertrand, Guy. Analogous .Alpha.,.Alpha.'-Bis-Carbenoid, Triply Bonded Species: Synthesis of a Stable .Lambda.3-Phosphino Carbene-.Lambda.5-Phosphaacetylene. *J. Am. Chem. Soc.* **1988**, *110* (19), 6463–6466. https://doi.org/10.1021/ja00227a028.
(18) Arduengo, A. J.; Harlow, R. L.; Kline, M. A Stable Crystalline Carbene. *J. Am. Chem. Soc.* **1991**, *113* (1), 361–363. https://doi.org/10.1021/ja00001a054.
(19) Hopkinson, M. N.; Richter, C.; Schedler, M.; Glorius, F. An Overview of N-Heterocyclic Carbenes. *Nature* **2014**, *510* (7506), 485–496. https://doi.org/10.1038/nature13384.
(20) Housecroft, C. E.; Sharpe, A. G. *Inorganic Chemistry*; Pearson, 2012.
(21) Nielsen, D. J.; Cavell, K. J. Pd-NHC Complexes as Catalysts in Telomerization and Aryl Amination Reactions. In *N-Heterocyclic Carbenes in Synthesis*; Nolan, S. P., Ed.; Wiley-VCH: Weinheim, Germany, 2006; pp 73–102.
(22) Fortman, G. C.; Nolan, S. P. N-Heterocyclic Carbene (NHC) Ligands and Palladium in Homogeneous Cross-Coupling Catalysis: A Perfect Union. *Chem. Soc. Rev.* **2011**, *40* (10), 5151. https://doi.org/10.1039/c1cs15088j.
(23) Murphy, L. J.; Robertson, K. N.; Masuda, J. D.; Clyburne, J. A. C. NHC Complexes of Main Group Elements: Novel Structures, Reactivity, and Catalytic Behavior. In *N-Heterocyclic Carbenes: Effective Tools for Organometallic Synthesis*; Nolan, S. P., Ed.; Wiley-VCH: Weinheim, Germany, 2014; pp 427–497.
(24) Díez-González, S.; Marion, N.; Nolan, S. P. N-Heterocyclic Carbenes in Late Transition Metal Catalysis. *Chem. Rev.* **2009**, *109* (8), 3612–3676. https://doi.org/10.1021/cr900074m.
(25) Rogers, M. M.; Stahl, S. S. N-Heterocyclic Carbenes as Ligands for High Oxidation State Metal Complexes and Oxidation Catalysis. In *N-Heterocyclic Carbenes in Transition Metal Catalysis*; Glorius, F., Ed.; Springer-Verlag: New York; Vol. 21, pp 21–46.
(26) Kantchev, E. A. B.; O'Brien, C. J.; Organ, M. G. Palladium Complexes of N-Heterocyclic Carbenes as Catalysts for Cross-Coupling Reactions—A Synthetic Chemist's Perspective. *Angew. Chem. Int. Ed.* **2007**, *46* (16), 2768–2813. https://doi.org/10.1002/anie.200601663.
(27) Huynh, H. V. Electronic Properties of N-Heterocyclic Carbenes and Their Experimental Determination. *Chem. Rev.* **2018**, *118* (19), 9457–9492. https://doi.org/10.1021/acs.chemrev.8b00067.
(28) Dröge, T.; Glorius, F. The Measure of All Rings—N-Heterocyclic Carbenes. *Angew. Chem. Int. Ed.* **2010**, *49* (39), 6940–6952. https://doi.org/10.1002/anie.201001865.
(29) Arduengo, A. J. III.; Goerlich, J. R.; Marshall, W. J. A Stable Diaminocarbene. *J. Am. Chem. Soc.* **1995**, *117* (44), 11027–11028. https://doi.org/10.1021/ja00149a034.
(30) Magill, A. M.; Yates, B. F. An Assessment of Theoretical Protocols for Calculation of the pKa Values of the Prototype Imidazolium Cation. *Aust. J. Chem.* **2004**, *57* (12), 1205–1210. https://doi.org/10.1071/CH04159.
(31) Magill, A. M.; Cavell, K. J.; Yates, B. F. Basicity of Nucleophilic Carbenes in Aqueous and Nonaqueous SolventsTheoretical Predictions. *J. Am. Chem. Soc.* **2004**, *126* (28), 8717–8724. https://doi.org/10.1021/ja038973x.
(32) O'Brien, C. J.; Kantchev, E. A. B.; Valente, C.; Hadei, N.; Chass, G. A.; Lough, A.; Hopkinson, A. C.; Organ, M. G. Easily Prepared Air- and Moisture-Stable Pd–NHC (NHC=N-Heterocyclic Carbene) Complexes: A Reliable, User-Friendly, Highly Active Palladium Precatalyst for the Suzuki–Miyaura Reaction. *Chem. – Eur. J.* **2006**, *12* (18), 4743–4748. https://doi.org/10.1002/chem.200600251.

(33) Poyatos, M.; Mas-Marzá, E.; Mata, J. A.; Sanaú, M.; Peris, E. Synthesis, Reactivity, Crystal Structures and Catalytic Activity of New Chelating Bisimidazolium-Carbene Complexes of Rh. *Eur. J. Inorg. Chem.* **2003**, *2003* (6), 1215–1221. https://doi.org/10.1002/ejic.200390157.
(34) Raynal, M.; Cazin, C. S. J.; Vallée, C.; Olivier-Bourbigou, H.; Braunstein, P. An Unprecedented, Figure-of-Eight, Dinuclear Iridium(I) Dicarbene and New Iridium(III) 'Pincer' Complexes. *Chem. Commun.* **2008**, No. 34, 3983–3985. https://doi.org/10.1039/B808806C.
(35) Krüger, A.; Neels, A.; Albrecht, M. Rhodium-Mediated Activation of an Alkane-Type C–H Bond. *Chem. Commun.* **2009**, *46* (2), 315–317. https://doi.org/10.1039/B918660C.
(36) Lin, I. J. B.; Vasam, C. S. Preparation and Application of N-Heterocyclic Carbene Complexes of Ag(I). *Coord. Chem. Rev.* **2007**, *251* (5–6), 642–670. https://doi.org/10.1016/j.ccr.2006.09.004.
(37) Wang, H. M. J.; Lin, I. J. B. Facile Synthesis of Silver(I)−Carbene Complexes. Useful Carbene Transfer Agents. *Organometallics* **1998**, *17* (5), 972–975. https://doi.org/10.1021/om9709704.
(38) Huynh, H. V. The Organometallic Chemistry of N-Heterocyclic Carbenes; John Wiley & Sons, Ltd, 2017; pp 330–334. https://doi.org/10.1002/9781118698785.index.
(39) Scarborough, C. C.; Popp, B. V.; Guzei, I. A.; Stahl, S. S. Development of 7-Membered N-Heterocyclic Carbene Ligands for Transition Metals. *J. Organomet. Chem.* **2005**, *690* (24), 6143–6155. https://doi.org/10.1016/j.jorganchem.2005.08.022.
(40) Tulloch, A. A. D.; Danopoulos, A. A.; Winston, S.; Kleinhenz, S.; Eastham, G. N-Functionalised Heterocyclic Carbene Complexes of Silver. *J. Chem. Soc. Dalton Trans.* **2000**, No. 24, 4499–4506. https://doi.org/10.1039/B007504N.
(41) Xu, G.; Gilbertson, S. R. Development of Building Blocks for the Synthesis of N-Heterocyclic Carbene Ligands. *Org. Lett.* **2005**, *7* (21), 4605–4608. https://doi.org/10.1021/ol0516521.
(42) Van Veldhuizen, J. J.; Garber, S. B.; Kingsbury, J. S.; Hoveyda, A. H. A Recyclable Chiral Ru Catalyst for Enantioselective Olefin Metathesis. Efficient Catalytic Asymmetric Ring-Opening/Cross Metathesis in Air. *J. Am. Chem. Soc.* **2002**, *124* (18), 4954–4955. https://doi.org/10.1021/ja020259c.
(43) Strohmeier, W.; Müller, F.-J. Klassifizierung phosphorhaltiger Liganden in Metallcarbonyl-Derivaten nach der π-Acceptorstärke. *Chem. Ber.* **1967**, *100* (9), 2812–2821. https://doi.org/10.1002/cber.19671000907.
(44) Bouquet, G.; Loutellier, A.; Bigorgne, M. Étude Spectroscopique Des Vibrations M-C ET M-C-O DU Nickel Carbonyle ET DE SES Dérivés. *J. Mol. Struct.* **1968**, *1* (3), 211–237. https://doi.org/10.1016/0022-2860(68)87005-X.
(45) Tolman, C. A. Steric Effects of Phosphorus Ligands in Organometallic Chemistry and Homogeneous Catalysis. *Chem. Rev.* **1977**, *77* (3), 313–348. https://doi.org/10.1021/cr60307a002.
(46) Dorta, R.; Stevens, E. D.; Scott, N. M.; Costabile, C.; Cavallo, L.; Hoff, C. D.; Nolan, S. P. Steric and Electronic Properties of N-Heterocyclic Carbenes (NHC): A Detailed Study on Their Interaction with Ni(CO)4. *J. Am. Chem. Soc.* **2005**, *127* (8), 2485–2495. https://doi.org/10.1021/ja0438821.
(47) Huynh, H. V.; Han, Y.; Jothibasu, R.; Yang, J. A. 13C NMR Spectroscopic Determination of Ligand Donor Strengths Using N-Heterocyclic Carbene Complexes of Palladium(II). *Organometallics* **2009**, *28* (18), 5395–5404. https://doi.org/10.1021/om900667d.

(48) Lever, A. B. P. Electrochemical Parametrization of Metal Complex Redox Potentials, Using the Ruthenium(III)/Ruthenium(II) Couple to Generate a Ligand Electrochemical Series. *Inorg. Chem.* **1990**, *29* (6), 1271–1285. https://doi.org/10.1021/ic00331a030.
(49) Lever, A. B. P. Electrochemical Parametrization of Rhenium Redox Couples. *Inorg. Chem.* **1991**, *30* (9), 1980–1985. https://doi.org/10.1021/ic00009a008.
(50) Fielder, S. S.; Osborne, M. C.; Lever, A. B. P.; Pietro, W. J. First-Principles Interpretation of Ligand Electrochemical (EL(L)) Parameters. Factorization of the .Sigma. and .Pi. Donor and .Pi. Acceptor Capabilities of Ligands. *J. Am. Chem. Soc.* **1995**, *117* (26), 6990–6993. https://doi.org/10.1021/ja00131a022.
(51) Perrin, L.; Clot, E.; Eisenstein, O.; Loch, J.; Crabtree, R. H. Computed Ligand Electronic Parameters from Quantum Chemistry and Their Relation to Tolman Parameters, Lever Parameters, and Hammett Constants. *Inorg. Chem.* **2001**, *40* (23), 5806–5811. https://doi.org/10.1021/ic0105258.
(52) Arduengo, A. J.; Krafczyk, R.; Schmutzler, R.; Craig, H. A.; Goerlich, J. R.; Marshall, W. J.; Unverzagt, M. Imidazolylidenes, Imidazolinylidenes and Imidazolidines. *Tetrahedron* **1999**, *55* (51), 14523–14534. https://doi.org/10.1016/S0040-4020(99)00927-8.
(53) Gómez-Suárez, A.; Nelson, D. J.; Nolan, S. P. Quantifying and Understanding the Steric Properties of N-Heterocyclic Carbenes. *Chem. Commun.* **2017**, *53* (18), 2650–2660. https://doi.org/10.1039/C7CC00255F.
(54) Falivene, L.; Credendino, R.; Poater, A.; Petta, A.; Serra, L.; Oliva, R.; Scarano, V.; Cavallo, L. SambVca 2. A Web Tool for Analyzing Catalytic Pockets with Topographic Steric Maps. *Organometallics* **2016**, *35* (13), 2286–2293. https://doi.org/10.1021/acs.organomet.6b00371.
(55) Cavallo, L.; Correa, A.; Costabile, C.; Jacobsen, H. Steric and Electronic Effects in the Bonding of N-Heterocyclic Ligands to Transition Metals. *J. Organomet. Chem.* **2005**, *690* (24–25), 5407–5413. https://doi.org/10.1016/j.jorganchem.2005.07.012.
(56) Cremer, D.; Kraka, E. Generalization of the Tolman Electronic Parameter: The Metal–Ligand Electronic Parameter and the Intrinsic Strength of the Metal–Ligand Bond. *Dalton Trans.* **2017**, *46* (26), 8323–8338. https://doi.org/10.1039/C7DT00178A.
(57) Poater, A.; Cosenza, B.; Correa, A.; Giudice, S.; Ragone, F.; Scarano, V.; Cavallo, L. SambVca: A Web Application for the Calculation of the Buried Volume of N-Heterocyclic Carbene Ligands. *Eur. J. Inorg. Chem.* **2009**, *2009* (13), 1759–1766. https://doi.org/10.1002/ejic.200801160.
(58) Huang, J.; Schanz, H.-J.; Stevens, E. D.; Nolan, S. P. Stereoelectronic Effects Characterizing Nucleophilic Carbene Ligands Bound to the Cp*RuCl (Cp* = η^5-C_5Me_5) Moiety: A Structural and Thermochemical Investigation. *Organometallics* **1999**, *18* (12), 2370–2375. https://doi.org/10.1021/om9900541.
(59) Herrmann, W. A.; Elison, M.; Fischer, J.; Köcher, C.; Artus, G. R. J. Metal Complexes of N-Heterocyclic Carbenes—A New Structural Principle for Catalysts in Homogeneous Catalysis. *Angew. Chem. Int. Ed. Engl.* **1995**, *34* (21), 2371–2374. https://doi.org/10.1002/anie.199523711.
(60) A. Herrmann, W.; Reisinger, C.-P.; Spiegler, M. Chelating N-Heterocyclic Carbene Ligands in Palladium-Catalyzed Heck-Type Reactions. *J. Organomet. Chem.* **1998**, *557* (1), 93–96. https://doi.org/10.1016/S0022-328X(97)00736-5.
(61) Maluenda, I.; Navarro, O. Recent Developments in the Suzuki-Miyaura Reaction: 2010–2014. *Molecules* **2015**, *20* (5), 7528–7557. https://doi.org/10.3390/molecules20057528.

(62) Gstöttmayr, C. W. K.; Böhm, V. P. W.; Herdtweck, E.; Grosche, M.; Herrmann, W. A. A Defined N-Heterocyclic Carbene Complex for the Palladium-Catalyzed Suzuki Cross-Coupling of Aryl Chlorides at Ambient Temperatures. *Angew. Chem. Int. Ed.* **2002**, *41* (8), 1363–1365. https://doi.org/10.1002/1521-3773(20020415)41:8<1363::AID-ANIE1363>3.0.CO;2-G.

(63) Organ, M. G.; Çalimsiz, S.; Sayah, M.; Hoi, K. H.; Lough, A. J. Pd-PEPPSI-IPent: An Active, Sterically Demanding Cross-Coupling Catalyst and Its Application in the Synthesis of Tetra-*Ortho* -Substituted Biaryls. *Angew. Chem. Int. Ed.* **2009**, *48* (13), 2383–2387. https://doi.org/10.1002/anie.200805661.

(64) Manzini, S.; Urbina Blanco, C. A.; Slawin, A. M. Z.; Nolan, S. P. Effect of Ligand Bulk in Ruthenium-Catalyzed Olefin Metathesis: IPr* vs IPr. *Organometallics* **2012**, *31* (18), 6514–6517. https://doi.org/10.1021/om300719t.

(65) Carroll, T. G.; Ryan, D. E.; Erickson, J. D.; Bullock, R. M.; Tran, B. L. Isolation of a Cu–H Monomer Enabled by Remote Steric Substitution of a *N* -Heterocyclic Carbene Ligand: Stoichiometric Insertion and Catalytic Hydroboration of Internal Alkenes. *J. Am. Chem. Soc.* **2022**, *144* (30), 13865–13873. https://doi.org/10.1021/jacs.2c05376.

(66) Patrick, E. A.; Bowden, M. E.; Erickson, J. D.; Bullock, R. M.; Tran, B. L. Single-Crystal to Single-Crystal Transformations: Stepwise CO_2 Insertions into Bridging Hydrides of $[(NHC)CuH]_2$ Complexes. *Angew. Chem. Int. Ed.* **2023**, *62* (30), e202304648. https://doi.org/10.1002/anie.202304648.

(67) Speelman, A. L.; Tran, B. L.; Erickson, J. D.; Vasiliu, M.; Dixon, D. A.; Bullock, R. M. Accelerating the Insertion Reactions of (NHC)Cu–H *via* Remote Ligand Functionalization. *Chem. Sci.* **2021**, *12* (34), 11495–11505. https://doi.org/10.1039/D1SC01911B.

(68) Tran, B. L.; Neisen, B. D.; Speelman, A. L.; Gunasekara, T.; Wiedner, E. S.; Bullock, R. M. Mechanistic Studies on the Insertion of Carbonyl Substrates into Cu-H: Different Rate-Limiting Steps as a Function of Electrophilicity. *Angew. Chem. Int. Ed.* **2020**, *59* (22), 8645–8653. https://doi.org/10.1002/anie.201916406.

(69) Chartoire, A.; Lesieur, M.; Falivene, L.; Slawin, A. M. Z.; Cavallo, L.; Cazin, C. S. J.; Nolan, S. P. [Pd(IPr*)(Cinnamyl)Cl]: An Efficient Pre-Catalyst for the Preparation of Tetra-Ortho-Substituted Biaryls by Suzuki–Miyaura Cross-Coupling. *Chem. – Eur. J.* **2012**, *18* (15), 4517–4521. https://doi.org/10.1002/chem.201104009.

(70) Wu, L.; Drinkel, E.; Gaggia, F.; Capolicchio, S.; Linden, A.; Falivene, L.; Cavallo, L.; Dorta, R. Room-Temperature Synthesis of Tetra-Ortho-Substituted Biaryls by NHC-Catalyzed Suzuki–Miyaura Couplings. *Chem. – Eur. J.* **2011**, *17* (46), 12886–12890. https://doi.org/10.1002/chem.201102442.

(71) Meiries, S.; Speck, K.; Cordes, D. B.; Slawin, A. M. Z.; Nolan, S. P. [Pd(IPr* ^{OMe})(Acac)Cl]: Tuning the N-Heterocyclic Carbene in Catalytic C–N Bond Formation. *Organometallics* **2013**, *32* (1), 330–339. https://doi.org/10.1021/om3011867.

(72) Martin, A. R.; Nelson, D. J.; Meiries, S.; Slawin, A. M. Z.; Nolan, S. P. Efficient C–N and C–S Bond Formation Using the Highly Active [Ni(Allyl)Cl(IPr*OMe)] Precatalyst. *Eur. J. Org. Chem.* **2014**, *2014* (15), 3127–3131. https://doi.org/10.1002/ejoc.201402022.

(73) Tian, X.; Lin, J.; Zou, S.; Lv, J.; Huang, Q.; Zhu, J.; Huang, S.; Wang, Q. [Pd(IPr*R)(Acac)Cl]: Efficient Bulky Pd-NHC Catalyst for Buchwald-Hartwig C-N Cross-Coupling Reaction. *J. Organomet. Chem.* **2018**, *861*, 125–130. https://doi.org/10.1016/j.jorganchem.2018.02.035.

(74) Bastug, G.; Nolan, S. P. [Pd(IPr*OMe)(Cin)Cl] (Cin = Cinnamyl): A Versatile Catalyst for C–N and C–C Bond Formation. *Organometallics* **2014**, *33* (5), 1253–1258. https://doi.org/10.1021/om500026s.
(75) De Frémont, P.; Marion, N.; Nolan, S. P. Carbenes: Synthesis, Properties, and Organometallic Chemistry. *Coord. Chem. Rev.* **2009**, *253* (7–8), 862–892. https://doi.org/10.1016/j.ccr.2008.05.018.
(76) Herrmann, W. A. N-Heterocyclic Carbenes: A New Concept in Organometallic Catalysis. *Angew. Chem. Int. Ed.* **2002**, *41* (8), 1290–1309. https://doi.org/10.1002/1521-3773(20020415)41:8<1290::AID-ANIE1290>3.0.CO;2-Y.
(77) Lazreg, F.; Nahra, F.; Cazin, C. S. J. Copper–NHC Complexes in Catalysis. *Coord. Chem. Rev.* **2015**, *293–294*, 48–79. https://doi.org/10.1016/j.ccr.2014.12.019.
(78) Kaicharla, T.; Zimmermann, B. M.; Oestreich, M.; Teichert, J. F. Using Alcohols as Simple H_2 -Equivalents for Copper-Catalysed Transfer Semihydrogenations of Alkynes. *Chem. Commun.* **2019**, *55* (89), 13410–13413. https://doi.org/10.1039/C9CC06637C.
(79) Pape, F.; Thiel, N. O.; Teichert, J. F. *Z* -Selective Copper(I)-Catalyzed Alkyne Semihydrogenation with Tethered Cu–Alkoxide Complexes. *Chem. – Eur. J.* **2015**, *21* (45), 15934–15938. https://doi.org/10.1002/chem.201501739.
(80) Wakamatsu, T.; Nagao, K.; Ohmiya, H.; Sawamura, M. Copper-Catalyzed Semihydrogenation of Internal Alkynes with Molecular Hydrogen. *Organometallics* **2016**, *35* (10), 1354–1357. https://doi.org/10.1021/acs.organomet.6b00126.
(81) Kaur, H.; Zinn, F. K.; Stevens, E. D.; Nolan, S. P. (NHC)Cu ^{I} (NHC = N-Heterocyclic Carbene) Complexes as Efficient Catalysts for the Reduction of Carbonyl Compounds. *Organometallics* **2004**, *23* (5), 1157–1160. https://doi.org/10.1021/om034285a.
(82) Díez-González, S.; Escudero-Adán, E. C.; Benet-Buchholz, J.; Stevens, E. D.; Slawin, A. M. Z.; Nolan, S. P. [(NHC)CuX] Complexes: Synthesis, Characterization and Catalytic Activities in Reduction Reactions and Click Chemistry. On the Advantage of Using Well-Defined Catalytic Systems. *Dalton Trans.* **2010**, *39* (32), 7595. https://doi.org/10.1039/c0dt00218f.
(83) Martin, D.; Kehrli, S.; d'Augustin, M.; Clavier, H.; Mauduit, M.; Alexakis, A. Copper-Catalyzed Asymmetric Conjugate Addition of Grignard Reagents to Trisubstituted Enones. Construction of All-Carbon Quaternary Chiral Centers. *J. Am. Chem. Soc.* **2006**, *128* (26), 8416–8417. https://doi.org/10.1021/ja0629920.
(84) Shi, C.-Y.; Pan, Z.-Z.; Tian, P.; Yin, L. Copper(I)-Catalyzed Asymmetric 1,6-Conjugate Allylation. *Nat. Commun.* **2020**, *11* (1), 5480. https://doi.org/10.1038/s41467-020-19293-9.
(85) Corberán, R.; Mszar, N. W.; Hoveyda, A. H. NHC-Cu-Catalyzed Enantioselective Hydroboration of Acyclic and Exocyclic 1,1-Disubstituted Aryl Alkenes. *Angew. Chem. Int. Ed.* **2011**, *50* (31), 7079–7082. https://doi.org/10.1002/anie.201102398.
(86) Park, J. K.; Ondrusek, B. A.; McQuade, D. T. Regioselective Catalytic Hydroboration of Propargylic Species Using Cu(I)-NHC Complexes. *Org. Lett.* **2012**, *14* (18), 4790–4793. https://doi.org/10.1021/ol302086v.
(87) Bonet, A.; Lillo, V.; Ramírez, J.; Díaz-Requejo, M. M.; Fernández, E. The Selective Catalytic Formation of β-Boryl Aldehydes through a Base-Free Approach. *Org. Biomol. Chem.* **2009**, *7* (8), 1533. https://doi.org/10.1039/b901767d.
(88) Lillo, V.; Fructos, M. R.; Ramírez, J.; Braga, A. A. C.; Maseras, F.; Díaz-Requejo, M. M.; Pérez, P. J.; Fernández, E. A Valuable, Inexpensive Cu (I) N-Heterocyclic Carbene Catalyst

for the Selective Diboration of Styrene. *Chem. – Eur. J.* **2007**, *13* (9), 2614–2621. https://doi.org/10.1002/chem.200601146.
(89) Mikhaylov, V. N.; Pavlov, A. O.; Ogorodnov, Y. V.; Spiridonova, D. V.; Sorokoumov, V. N.; Balova, I. A. N-Propargylation and Copper(I)-Catalyzed Azide-Alkyne Cycloaddition as a Convenient Strategy for Directed Post-Synthetic Modification of 4-Oxo-1,4-Dihydrocinnoline Derivatives. *Chem. Heterocycl. Compd.* **2020**, *56* (7), 915–922. https://doi.org/10.1007/s10593-020-02750-0.
(90) Díaz Velázquez, H.; Ruiz García, Y.; Vandichel, M.; Madder, A.; Verpoort, F. Water-Soluble NHC-Cu Catalysts: Applications in Click Chemistry, Bioconjugation and Mechanistic Analysis. *Org Biomol Chem* **2014**, *12* (46), 9350–9356. https://doi.org/10.1039/C4OB01350F.
(91) Sebest, F.; Dunsford, J. J.; Adams, M.; Pivot, J.; Newman, P. D.; Díez-González, S. Ring-Expanded N-Heterocyclic Carbenes for Copper-Mediated Azide–Alkyne Click Cycloaddition Reactions. *ChemCatChem* **2018**, *10* (9), 2041–2045. https://doi.org/10.1002/cctc.201701992.
(92) Díez-González, S.; Correa, A.; Cavallo, L.; Nolan, S. P. (NHC)Copper(I)-Catalyzed [3+2] Cycloaddition of Azides and Mono- or Disubstituted Alkynes. *Chem. – Eur. J.* **2006**, *12* (29), 7558–7564. https://doi.org/10.1002/chem.200600961.
(93) Zhang, L.; Hou, Z. N-Heterocyclic Carbene (NHC)–Copper-Catalysed Transformations of Carbon Dioxide. *Chem. Sci.* **2013**, *4* (9), 3395. https://doi.org/10.1039/c3sc51070k.
(94) Boogaerts, I. I. F.; Fortman, G. C.; Furst, M. R. L.; Cazin, C. S. J.; Nolan, S. P. Carboxylation of N-H/C-H Bonds Using N-Heterocyclic Carbene Copper(I) Complexes. *Angew. Chem. Int. Ed.* **2010**, *49* (46), 8674–8677. https://doi.org/10.1002/anie.201004153.
(95) Nahra, F.; Gómez-Herrera, A.; Cazin, C. S. J. Copper(I)–NHC Complexes as NHC Transfer Agents. *Dalton Trans* **2017**, *46* (3), 628–631. https://doi.org/10.1039/C6DT03687B.
(96) Venkatachalam, G.; Heckenroth, M.; Neels, A.; Albrecht, M. Synthesis, Structural Diversity, and Ligand-Transfer Potential of (Carbene)Copper(I) Complexes. *Helv. Chim. Acta* **2009**, *92* (6), 1034–1045. https://doi.org/10.1002/hlca.200800406.
(97) Kuehn, L.; Eichhorn, A. F.; Marder, T. B.; Radius, U. Copper(I) Complexes of N-Alkyl-Substituted N-Heterocyclic Carbenes. *J. Organomet. Chem.* **2019**, *881*, 25–33. https://doi.org/10.1016/j.jorganchem.2018.11.032.
(98) Deutsch, C.; Lipshutz, B. H.; Krause, N. (NHC)CuH-Catalyzed Entry to Allenes via Propargylic Carbonate SN2′-Reductions. *Org. Lett.* **2009**, *11* (21), 5010–5012. https://doi.org/10.1021/ol901868m.
(99) Mszar, N. W.; Haeffner, F.; Hoveyda, A. H. NHC–Cu-Catalyzed Addition of Propargylboron Reagents to Phosphinoylimines. Enantioselective Synthesis of Trimethylsilyl-Substituted Homoallenylamides and Application to the Synthesis of S-(−)-Cyclooroidin. *J. Am. Chem. Soc.* **2014**, *136* (9), 3362–3365. https://doi.org/10.1021/ja500373s.
(100) Shi, Y.; Gao, Q.; Xu, S. NHC-Copper-Catalyzed Asymmetric Dearomative Silylation of Indoles. *J. Org. Chem.* **2018**, *83* (23), 14758–14767. https://doi.org/10.1021/acs.joc.8b02308.
(101) Chun, J.; Lee, H. S.; Jung, I. G.; Lee, S. W.; Kim, H. J.; Son, S. U. Cu $_2$ O: A Versatile Reagent for Base-Free Direct Synthesis of NHC-Copper Complexes and Decoration of 3D-MOF with Coordinatively Unsaturated NHC-Copper Species. *Organometallics* **2010**, *29* (7), 1518–1521. https://doi.org/10.1021/om900768w.

(102) Gibard, C.; Ibrahim, H.; Gautier, A.; Cisnetti, F. Simplified Preparation of Copper(I) NHCs Using Aqueous Ammonia. *Organometallics* **2013**, *32* (15), 4279–4283. https://doi.org/10.1021/om400440b.
(103) Santoro, O.; Collado, A.; Slawin, A. M. Z.; Nolan, S. P.; Cazin, C. S. J. A General Synthetic Route to [Cu(X)(NHC)] (NHC = N-Heterocyclic Carbene, X = Cl, Br, I) Complexes. *Chem. Commun.* **2013**, *49* (89), 10483. https://doi.org/10.1039/c3cc45488f.
(104) Collado, A.; Gómez-Suárez, A.; Martin, A. R.; Slawin, A. M. Z.; Nolan, S. P. Straightforward Synthesis of [Au(NHC)X] (NHC = N-Heterocyclic Carbene, X = Cl, Br, I) Complexes. *Chem. Commun.* **2013**, *49* (49), 5541. https://doi.org/10.1039/c3cc43076f.
(105) Simoens, A.; Scattolin, T.; Cauwenbergh, T.; Pisanò, G.; Cazin, C. S. J.; Stevens, C. V.; Nolan, S. P. Continuous Flow Synthesis of Metal–NHC Complexes. *Chem. – Eur. J.* **2021**, *27* (18), 5653–5657. https://doi.org/10.1002/chem.202100190.
(106) Pisanò, G.; Cazin, C. S. J. Mechanochemical Synthesis of Cu(I)-N-Heterocyclic Carbene Complexes. *Green Chem.* **2020**, *22* (16), 5253–5256. https://doi.org/10.1039/D0GC01923B.
(107) Tzouras, N. V.; Nahra, F.; Falivene, L.; Cavallo, L.; Saab, M.; Van Hecke, K.; Collado, A.; Collett, C. J.; Smith, A. D.; Cazin, C. S. J.; Nolan, S. P. A Mechanistically and Operationally Simple Route to Metal–N-Heterocyclic Carbene (NHC) Complexes. *Chem. – Eur. J.* **2020**, *26* (20), 4515–4519. https://doi.org/10.1002/chem.202000564.
(108) Giziroglu, E.; Donnadieu, B.; Bertrand, G. Synthesis and Characterization of a Pyrazolium Bearing N-Heterocyclic Carbene–Palladium(II) Complex. *J. Organomet. Chem.* **2013**, *724*, 251–254. https://doi.org/10.1016/j.jorganchem.2012.11.021.
(109) Korukçu, M. Ç.; Coşkun, N. Synthesis and Catalytic Activities of 1-Alkoxycarbonyl- and 1-Carbamoylmethyl-5-Phenyl-3-Aryl-3H-Imidazol-1-Yliden-Pd(II) Complexes. *J. Organomet. Chem.* **2017**, *832*, 47–56. https://doi.org/10.1016/j.jorganchem.2017.01.010.
(110) Gutiérrez-Blanco, A.; Peris, E.; Poyatos, M. Pyrene-Connected Tetraimidazolylidene Complexes of Iridium and Rhodium. Structural Features and Catalytic Applications. *Organometallics* **2018**, *37* (21), 4070–4076. https://doi.org/10.1021/acs.organomet.8b00633.
(111) Viciano, M.; Poyatos, M.; Sanaú, M.; Peris, E.; Rossin, A.; Ujaque, G.; Lledós, A. C−H Oxidative Addition of Bisimidazolium Salts to Iridium and Rhodium Complexes, and N-Heterocyclic Carbene Generation. A Combined Experimental and Theoretical Study. *Organometallics* **2006**, *25* (5), 1120–1134. https://doi.org/10.1021/om051004l.
(112) Chianese, A. R.; Mo, A.; Lampland, N. L.; Swartz, R. L.; Bremer, P. T. Iridium Complexes of CCC-Pincer N-Heterocyclic Carbene Ligands: Synthesis and Catalytic C−H Functionalization. *Organometallics* **2010**, *29* (13), 3019–3026. https://doi.org/10.1021/om100302g.
(113) Raynal, M.; Pattacini, R.; Cazin, C. S. J.; Vallée, C.; Olivier-Bourbigou, H.; Braunstein, P. Reaction Intermediates in the Synthesis of New Hydrido, N-Heterocyclic Dicarbene Iridium(III) Pincer Complexes. *Organometallics* **2009**, *28* (14), 4028–4047. https://doi.org/10.1021/om900226c.
(114) Berthon-Gelloz, G.; Siegler, M. A.; Spek, A. L.; Tinant, B.; Reek, J. N. H.; Markó, I. E. IPr* an Easily Accessible Highly Hindered N-Heterocyclic Carbene. *Dalton Trans* **2010**, *39* (6), 1444–1446. https://doi.org/10.1039/B921894G.
(115) Yoo, W.; Nguyen, T. V. Q.; Kobayashi, S. Synthesis of Isocoumarins through Three-Component Couplings of Arynes, Terminal Alkynes, and Carbon Dioxide Catalyzed by an NHC–Copper Complex. *Angew. Chem. Int. Ed.* **2014**, *53* (38), 10213–10217. https://doi.org/10.1002/anie.201404692.

(116) Bantreil, X.; Nolan, S. P. Synthesis of N-Heterocyclic Carbene Ligands and Derived Ruthenium Olefin Metathesis Catalysts. *Nat. Protoc.* **2011**, *6* (1), 69–77. https://doi.org/10.1038/nprot.2010.177.
(117) Trnka, T. M.; Morgan, J. P.; Sanford, M. S.; Wilhelm, T. E.; Scholl, M.; Choi, T.-L.; Ding, S.; Day, M. W.; Grubbs, R. H. Synthesis and Activity of Ruthenium Alkylidene Complexes Coordinated with Phosphine and N-Heterocyclic Carbene Ligands. *J. Am. Chem. Soc.* **2003**, *125* (9), 2546–2558. https://doi.org/10.1021/ja021146w.
(118) Huang, J.; Nolan, S. P. Efficient Cross-Coupling of Aryl Chlorides with Aryl Grignard Reagents (Kumada Reaction) Mediated by a Palladium/Imidazolium Chloride System. *J. Am. Chem. Soc.* **1999**, *121* (42), 9889–9890. https://doi.org/10.1021/ja991703n.
(119) Brick, K. J.; Keske, E. C. Palladium N-Heterocyclic Carbene Complexes in Cross-Coupling Reactions: Ligand and Catalyst Development. M.Sc. Thesis, Trent University, Peterborough, ON, 2023.
(120) Vougioukalakis, G. C.; Grubbs, R. H. Ruthenium-Based Heterocyclic Carbene-Coordinated Olefin Metathesis Catalysts. *Chem. Rev.* **2010**, *110* (3), 1746–1787. https://doi.org/10.1021/cr9002424.
(121) Egbert, J. D.; Cazin, C. S. J.; Nolan, S. P. Copper N-Heterocyclic Carbene Complexes in Catalysis. *Catal. Sci. Technol.* **2013**, *3* (4), 912. https://doi.org/10.1039/c2cy20816d.
(122) Leuthäußer, S.; Schwarz, D.; Plenio, H. Tuning the Electronic Properties of N-Heterocyclic Carbenes. *Chem. - Eur. J.* **2007**, *13* (25), 7195–7203. https://doi.org/10.1002/chem.200700228.
(123) Hoi, K. H.; Coggan, J. A.; Organ, M. G. Pd-PEPPSI-IPent^{Cl}: An Effective Catalyst for the Preparation of Triarylamines. *Chem. - Eur. J.* **2013**, *19* (3), 843–845. https://doi.org/10.1002/chem.201203379.
(124) Zhang, Y.; Lavigne, G.; César, V. Buchwald–Hartwig Amination of (Hetero)Aryl Tosylates Using a Well-Defined N-Heterocyclic Carbene/Palladium(II) Precatalyst. *J. Org. Chem.* **2015**, *80* (15), 7666–7673. https://doi.org/10.1021/acs.joc.5b01272.
(125) Carter, J. D.; Schrodi, Y. Olefin Metathesis Catalyst Supported by a Hemilabile NHC Ligand Bearing Polyether Arms: Structure, Activity, and Decomposition. *Organometallics* **2020**, *39* (3), 378–382. https://doi.org/10.1021/acs.organomet.9b00832.
(126) Schedler, M.; Fröhlich, R.; Daniliuc, C.-G.; Glorius, F. 2,6-Dimethoxyphenyl-Substituted N-Heterocyclic Carbenes (NHCs): A Family of Highly Electron-Rich Organocatalysts. *Eur. J. Org. Chem.* **2012**, *2012* (22), 4164–4171. https://doi.org/10.1002/ejoc.201200408.
(127) Winkelmann, O.; Näther, C.; Lüning, U. Synthesis, Structure and Catalytic Activity of a Bimacrocylic NHC Palladium Allyl Complex. *J. Organomet. Chem.* **2008**, *693* (16), 2784–2788. https://doi.org/10.1016/j.jorganchem.2008.05.034.
(128) Meiries, S.; Le Duc, G.; Chartoire, A.; Collado, A.; Speck, K.; Arachchige, K. S. A.; Slawin, A. M. Z.; Nolan, S. P. Large yet Flexible N-Heterocyclic Carbene Ligands for Palladium Catalysis. *Chem. – Eur. J.* **2013**, *19* (51), 17358–17368. https://doi.org/10.1002/chem.201302471.
(129) Collado, A.; Balogh, J.; Meiries, S.; Slawin, A. M. Z.; Falivene, L.; Cavallo, L.; Nolan, S. P. Steric and Electronic Parameters of a Bulky yet Flexible N-Heterocyclic Carbene: 1,3-Bis(2,6-Bis(1-Ethylpropyl)Phenyl)Imidazol-2-Ylidene (IPent). *Organometallics* **2013**, *32* (11), 3249–3252. https://doi.org/10.1021/om400168b.

(130) Arduengo, A. J.; Dias, H. V. R.; Calabrese, J. C.; Davidson, F. Homoleptic Carbene-Silver(I) and Carbene-Copper(I) Complexes. *Organometallics* **1993**, *12* (9), 3405–3409. https://doi.org/10.1021/om00033a009.
(131) Lim, M. Q.; Keske, E. C. Convenient Preparation of Copper(I) *N* -Heterocyclic Carbene Complexes under Mild Conditions. *Can. J. Chem.* **2023**, *101* (7), 434–439. https://doi.org/10.1139/cjc-2022-0229.
(132) Cox, N.; Dang, H.; Whittaker, A. M.; Lalic, G. NHC–Copper Hydrides as Chemoselective Reducing Agents: Catalytic Reduction of Alkynes, Alkyl Triflates, and Alkyl Halides. *Tetrahedron* **2014**, *70* (27–28), 4219–4231. https://doi.org/10.1016/j.tet.2014.04.004.
(133) Campeau, L.-C.; Hazari, N. Cross-Coupling and Related Reactions: Connecting Past Success to the Development of New Reactions for the Future. *Organometallics* **2019**, *38* (1), 3–35. https://doi.org/10.1021/acs.organomet.8b00720.
(134) Biffis, A.; Centomo, P.; Del Zotto, A.; Zecca, M. Pd Metal Catalysts for Cross-Couplings and Related Reactions in the 21st Century: A Critical Review. *Chem. Rev.* **2018**, *118* (4), 2249–2295. https://doi.org/10.1021/acs.chemrev.7b00443.
(135) Froese, R. D. J.; Lombardi, C.; Pompeo, M.; Rucker, R. P.; Organ, M. G. Designing Pd–N-Heterocyclic Carbene Complexes for High Reactivity and Selectivity for Cross-Coupling Applications. *Acc. Chem. Res.* **2017**, *50* (9), 2244–2253. https://doi.org/10.1021/acs.accounts.7b00249.
(136) Winkelmann, O.; Näther, C.; Lüning, U. Concave Imidazolinium Salts as Precursors to Concave N-Heterocyclic Carbenes. *Eur. J. Org. Chem.* **2007**, *2007* (6), 981–987. https://doi.org/10.1002/ejoc.200600843.
(137) Brick, K. J.; Lim, M. Q.; Keske, E. C. [(NHC)Pd(Allyl)Cl] Precatalysts in The Hiyama Reaction of Aryl Chlorides with Aryl Trimethoxysilanes: A Study in Side Reactions. *Organometallics* **2023**, *42* (22), 3192–3198. https://doi.org/10.1021/acs.organomet.3c00312.
(138) See Experimental for More Information.
(139) Díez-González, S.; Kaur, H.; Zinn, F. K.; Stevens, E. D.; Nolan, S. P. A Simple and Efficient Copper-Catalyzed Procedure for the Hydrosilylation of Hindered and Functionalized Ketones. *J. Org. Chem.* **2005**, *70* (12), 4784–4796. https://doi.org/10.1021/jo050397v.
(140) Zhao, Q.; Meng, G.; Li, G.; Flach, C.; Mendelsohn, R.; Lalancette, R.; Szostak, R.; Szostak, M. IPr# – Highly Hindered, Broadly Applicable N-Heterocyclic Carbenes. *Chem. Sci.* **2021**, *12* (31), 10583–10589. https://doi.org/10.1039/D1SC02619D.
(141) Marion, N.; De Frémont, P.; Puijk, I. M.; Ecarnot, E. C.; Amoroso, D.; Bell, A.; Nolan, S. P. N-Heterocyclic Carbene–Palladium Complexes [(NHC)Pd(Acac)Cl]: Improved Synthesis and Catalytic Activity in Large-Scale Cross-Coupling Reactions. *Adv. Synth. Catal.* **2007**, *349* (14–15), 2380–2384. https://doi.org/10.1002/adsc.200700195.
(142) Lin, I. J. B.; Vasam, C. S. Silver(I) N-Heterocyclic Carbenes. *Comments Inorg. Chem.* **2004**, *25* (3–4), 75–129. https://doi.org/10.1080/02603590490883652.
(143) Heath, R.; Müller-Bunz, H.; Albrecht, M. Silver(I) NHC Mediated C–C Bond Activation of Alkyl Nitriles and Catalytic Efficiency in Oxazoline Synthesis. *Chem. Commun.* **2015**, *51* (41), 8699–8701. https://doi.org/10.1039/C5CC02558C.
(144) De Frémont, P.; Scott, N. M.; Stevens, E. D.; Ramnial, T.; Lightbody, O. C.; Macdonald, C. L. B.; Clyburne, J. A. C.; Abernethy, C. D.; Nolan, S. P. Synthesis of Well-Defined *N* -Heterocyclic Carbene Silver(I) Complexes. *Organometallics* **2005**, *24* (26), 6301–6309. https://doi.org/10.1021/om050735i.

(145) Keske, E. C.; Zenkina, O. V.; Wang, R.; Crudden, C. M. Synthesis and Structure of Silver and Rhodium 1,2,3-Triazol-5-Ylidene Mesoionic Carbene Complexes. *Organometallics* **2012**, *31* (1), 456–461. https://doi.org/10.1021/om201104f.
(146) See Appendix for More Information.
(147) Izquierdo, F.; Corpet, M.; Nolan, S. P. The Suzuki–Miyaura Reaction Performed Using a Palladium–N-Heterocyclic Carbene Catalyst and a Weak Inorganic Base. *Eur. J. Org. Chem.* **2015**, *2015* (9), 1920–1924. https://doi.org/10.1002/ejoc.201500043.
(148) Herrmann, W. A.; Schütz, J.; Frey, G. D.; Herdtweck, E. N-Heterocyclic Carbenes: Synthesis, Structures, and Electronic Ligand Properties,. *Organometallics* **2006**, *25* (10), 2437–2448. https://doi.org/10.1021/om0600801.
(149) Teng, Q.; Huynh, H. V. A Unified Ligand Electronic Parameter Based on 13C NMR Spectroscopy of N-Heterocyclic Carbene Complexes. *Dalton Trans.* **2017**, *46* (3), 614–627. https://doi.org/10.1039/C6DT04222H.
(150) Elie, M.; Mahoro, G. U.; Duverger, E.; Renaud, J.-L.; Daniellou, R.; Gaillard, S. Cytotoxicity of Cationic NHC Copper(I) Complexes Coordinated to 2,2'-Bis-Pyridyl Ligands. *J. Organomet. Chem.* **2019**, *893*, 21–31. https://doi.org/10.1016/j.jorganchem.2019.04.003.
(151) McIndoe, J. S.; Vikse, K. L. Assigning the ESI Mass Spectra of Organometallic and Coordination Compounds. *J. Mass Spectrom.* **2019**, *54* (5), 466–479. https://doi.org/10.1002/jms.4359.
(152) Fortman, G. C.; Slawin, A. M. Z.; Nolan, S. P. A Versatile Cuprous Synthon: [Cu(IPr)(OH)] (IPr = 1,3 Bis(Diisopropylphenyl)Imidazol-2-Ylidene). *Organometallics* **2010**, *29* (17), 3966–3972. https://doi.org/10.1021/om100733n.
(153) Refer to Chapter 3.
(154) Lin, Y.-Y.; Lai, S.-W.; Che, C.-M.; Fu; Zhou, Z.-Y.; Zhu, N. Structural Variations and Spectroscopic Properties of Luminescent Mono- and Multinuclear Silver(I) and Copper(I) Complexes Bearing Phosphine and Cyanide Ligands. *Inorg. Chem.* **2005**, *44* (5), 1511–1524. https://doi.org/10.1021/ic048876k.
(155) Herberhold, M.; Milius, W.; Akkus, N. The Molecular Structure of the 1:1 Adduct of Silver Cyanide with Tri(1-Cyclohepta-2,4,6-Trienyl)Phosphane, Ag(CN)[P(C7H7)3]. *Z. Für Anorg. Allg. Chem.* **2006**, *632* (1), 97–100. https://doi.org/10.1002/zaac.200500327.
(156) Macrae, C. F.; Sovago, I.; Cottrell, S. J.; Galek, P. T. A.; McCabe, P.; Pidcock, E.; Platings, M.; Shields, G. P.; Stevens, J. S.; Towler, M.; Wood, P. A. Mercury 4.0: From Visualization to Analysis, Design and Prediction. *J. Appl. Crystallogr.* **2020**, *53* (1), 226–235. https://doi.org/10.1107/S1600576719014092.

Appendix A: Representative NMR Spectra

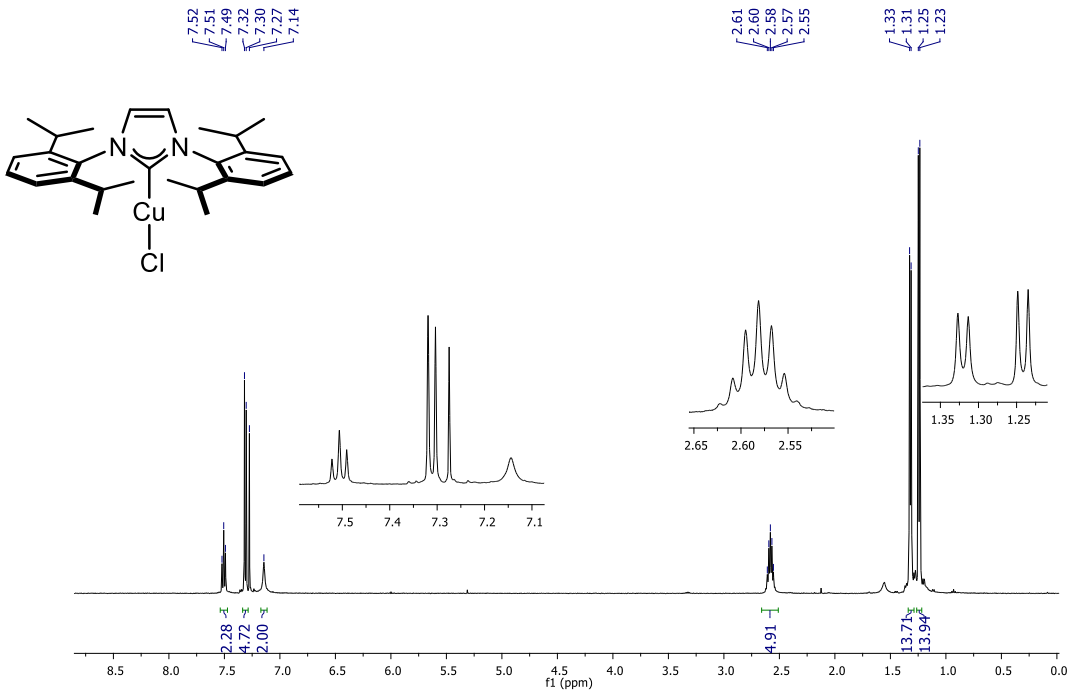

Figure A1: ^{1}H NMR spectrum of 2-1 in $CDCl_3$ at 500 MHz

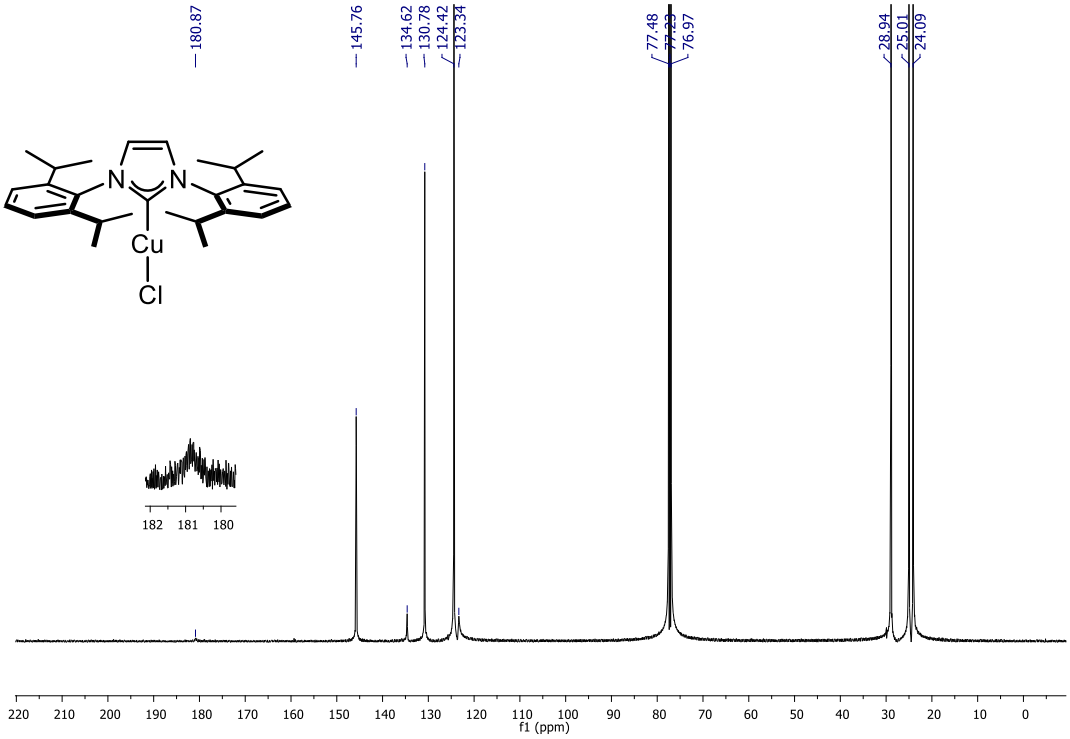

Figure A2: $^{13}C\{^{1}H\}$ NMR spectrum of 2-1 in $CDCl_3$ at 126 MHz

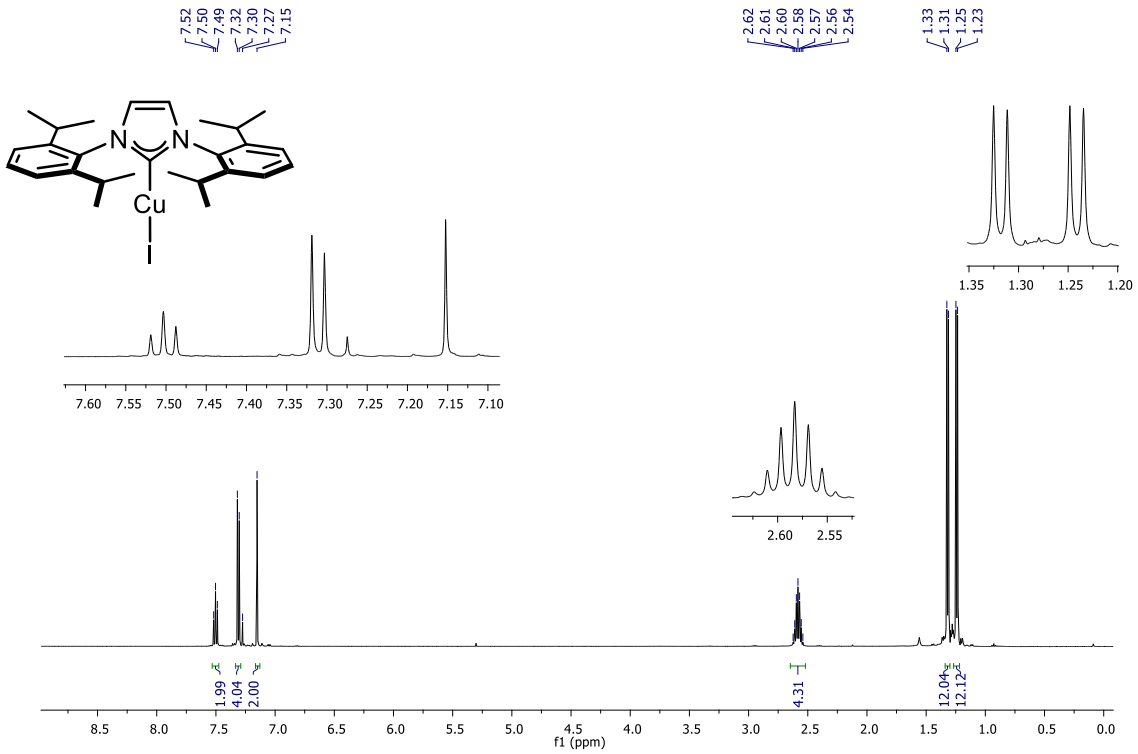

Figure A3: ^{1}H NMR spectrum of 2-2 in $CDCl_3$ at 500 MHz

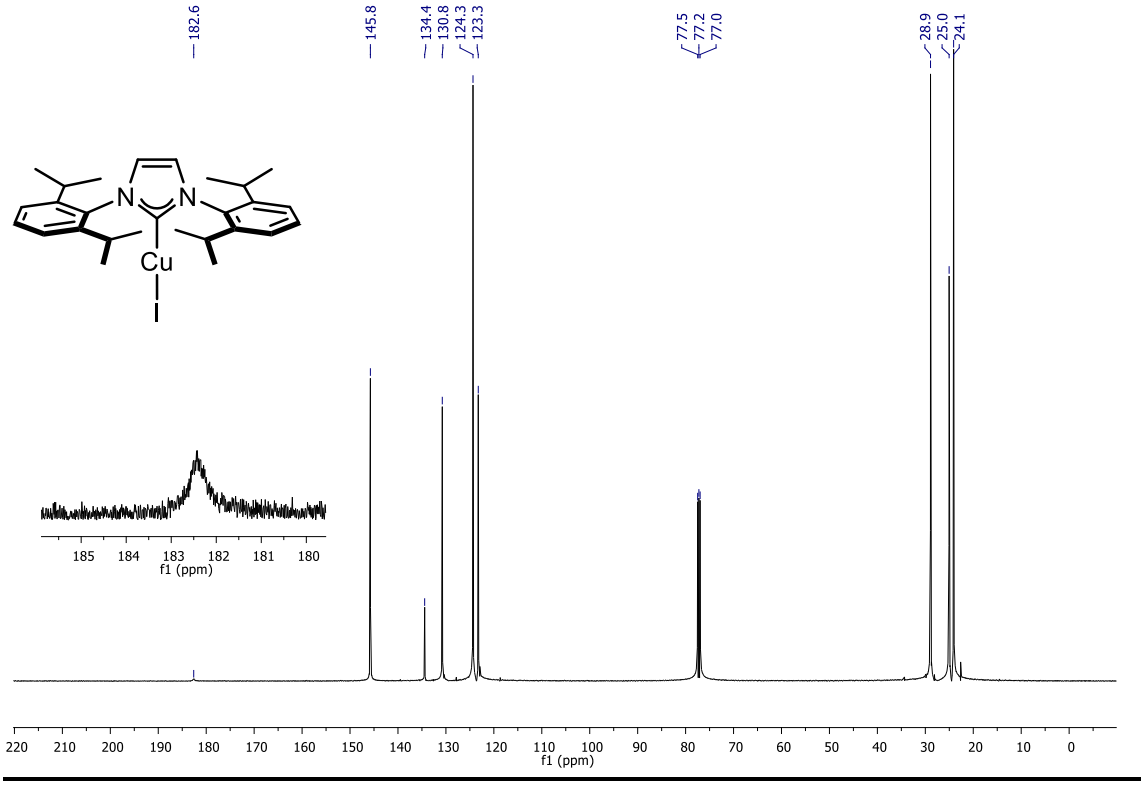

Figure A4: $^{13}C\{^{1}H\}$ NMR spectrum of 2-2 in $CDCl_3$ at 126 MHz

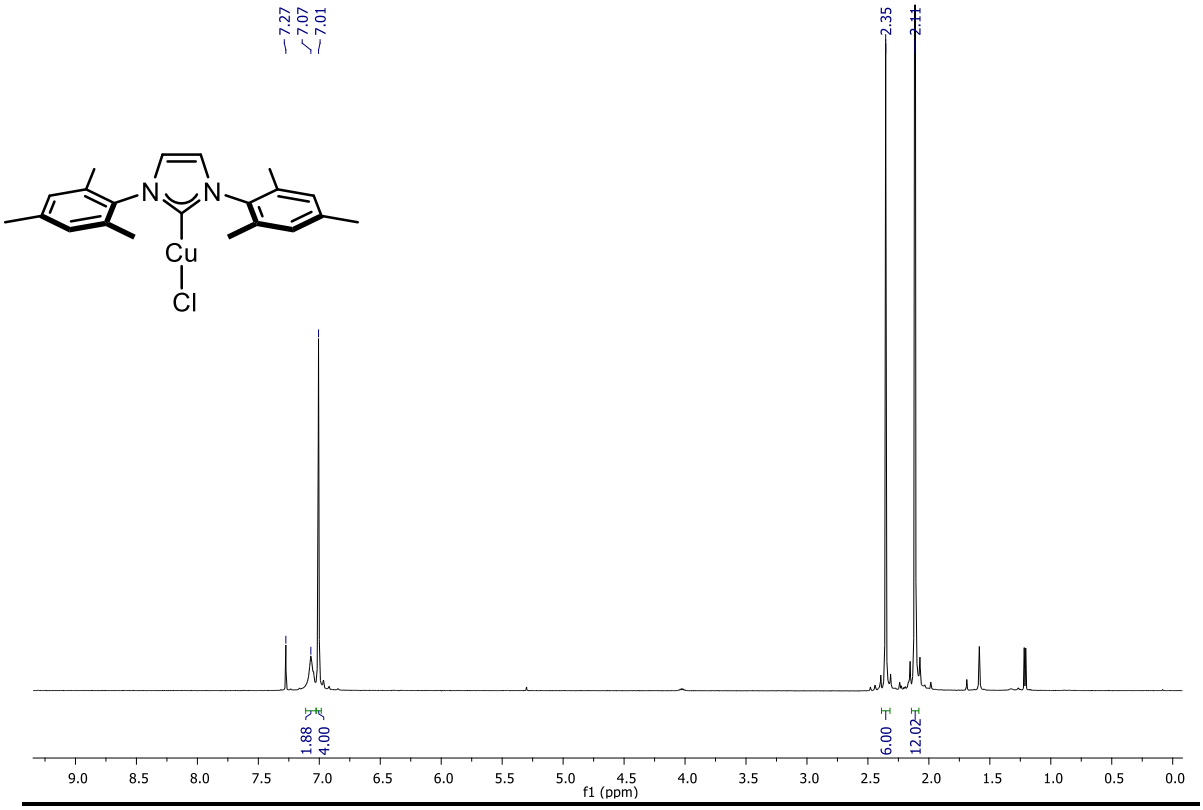

Figure A5: ^{1}H NMR spectrum of 2-3 in $CDCl_3$ at 500 MHz

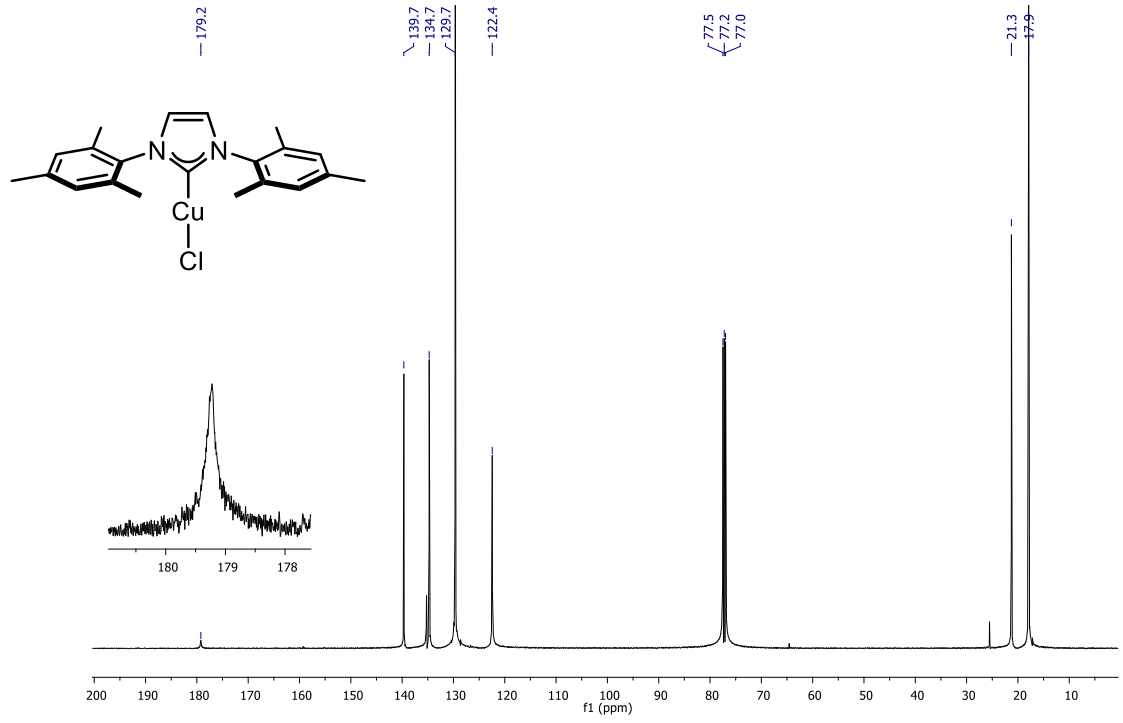

Figure A6: ^{13}C{^{1}H} NMR spectrum of 2-3 in $CDCl_3$ at 126 MHz

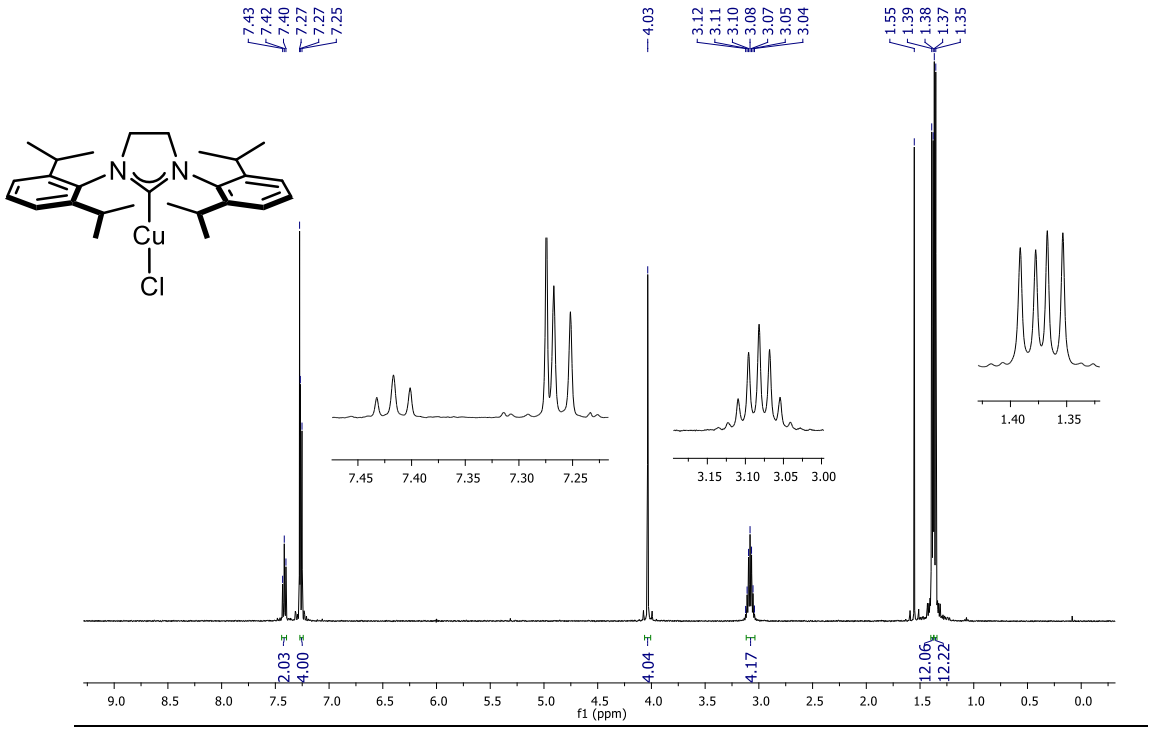

Figure A7: ^{1}H NMR spectrum of 2-4 in $CDCl_3$ at 500 MHz

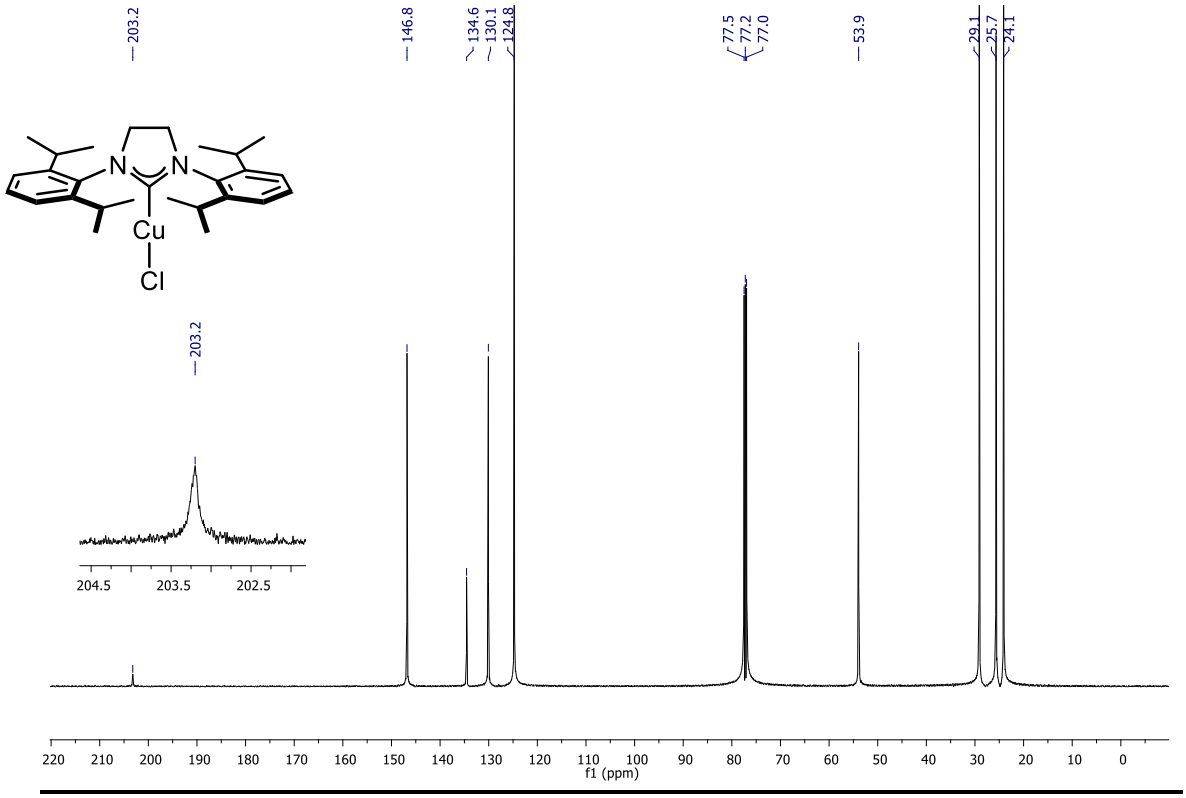

Figure A8: ^{13}C{^{1}H} NMR spectrum of 2-4 in $CDCl_3$ at 126 MHz

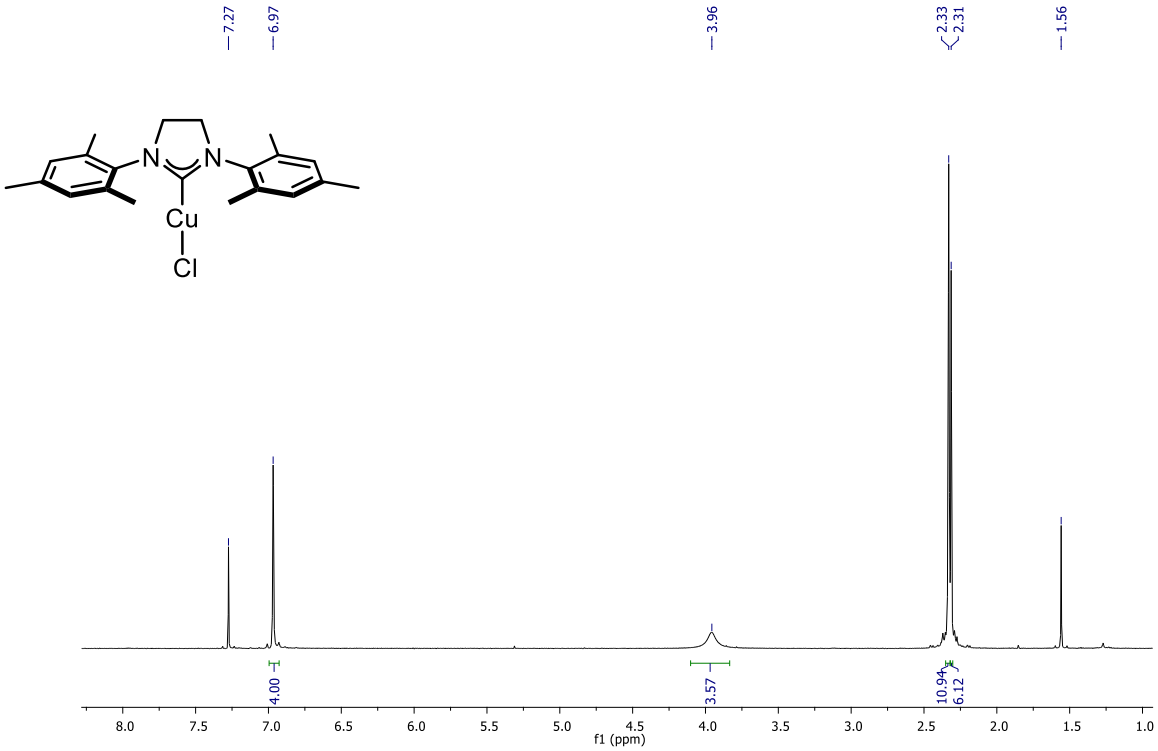

Figure A9: ^{1}H NMR spectrum of 2-5 in $CDCl_3$ at 500 MHz

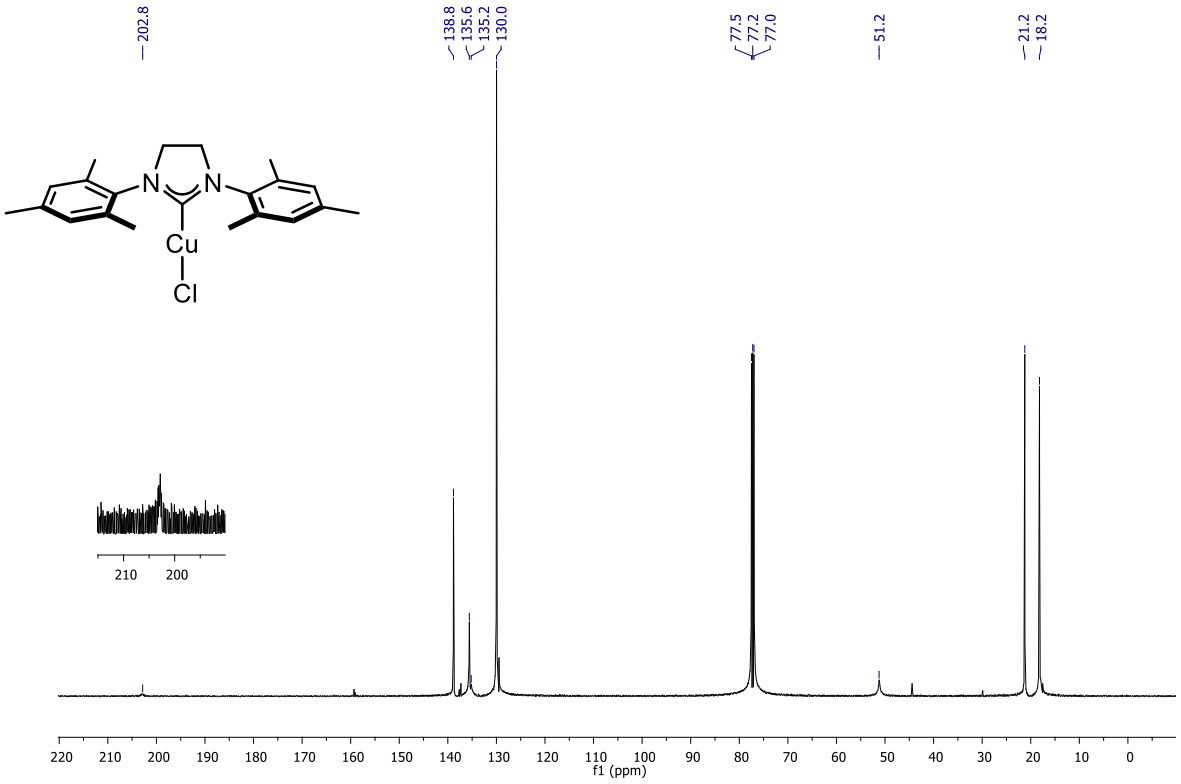

Figure A10: $^{13}C\{^{1}H\}$ NMR spectrum of 2-5 in $CDCl_3$ at 126 MHz

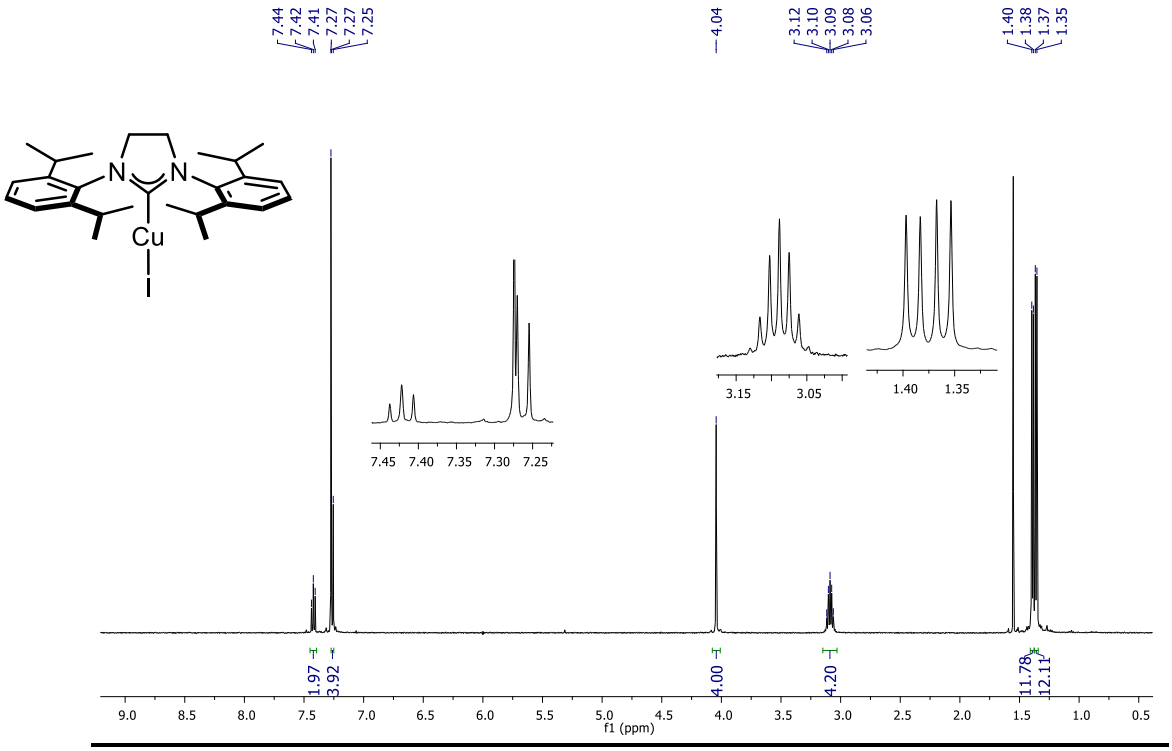

Figure A11: ^{1}H NMR spectrum of 2-6 in $CDCl_3$ at 500 MHz

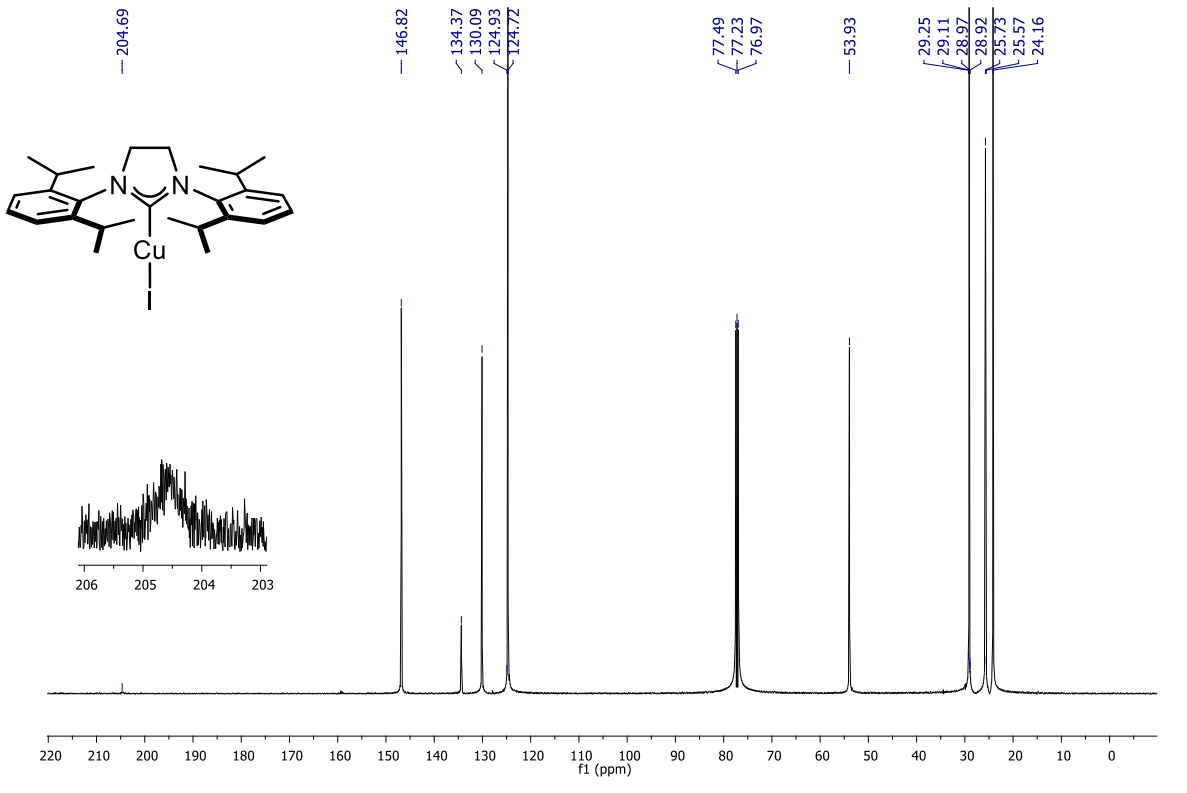

Figure A12: $^{13}C\{^{1}H\}$ NMR spectrum of 2-6 in $CDCl_3$ at 126 MHz

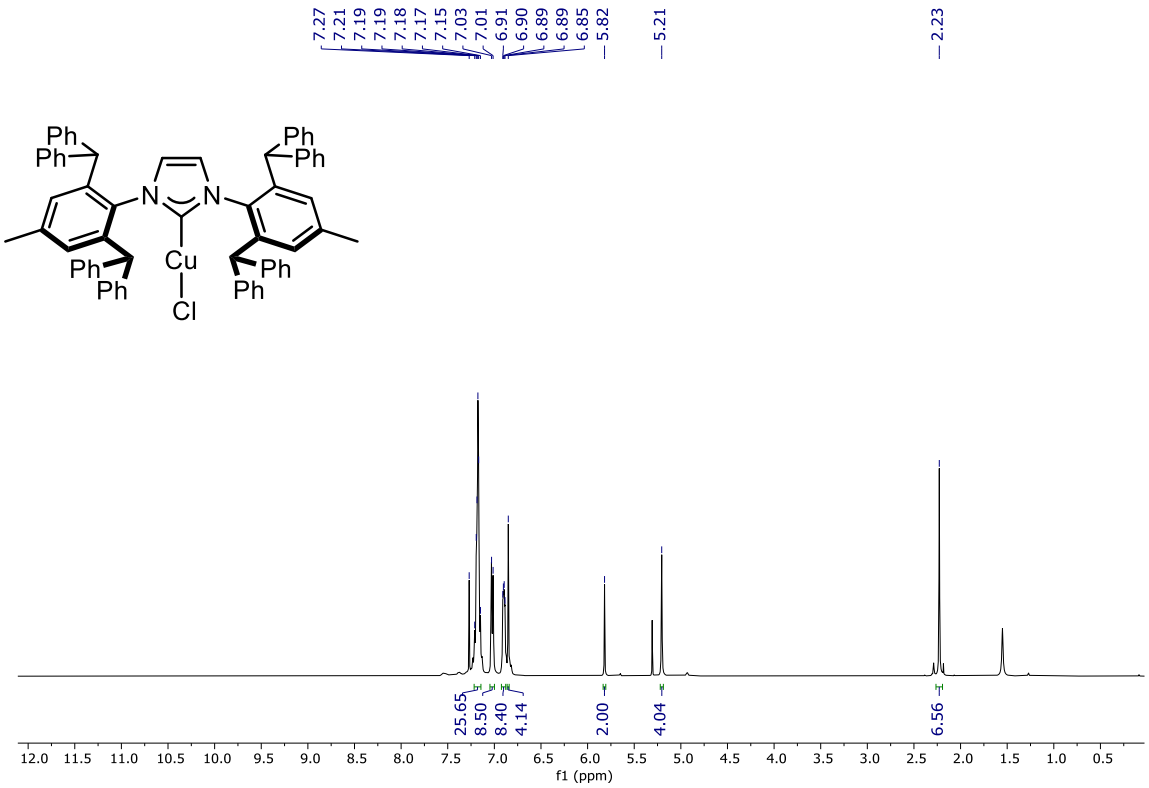

Figure A13: ^{1}H NMR spectrum of 2-11 in $CDCl_3$ at 400 MHz

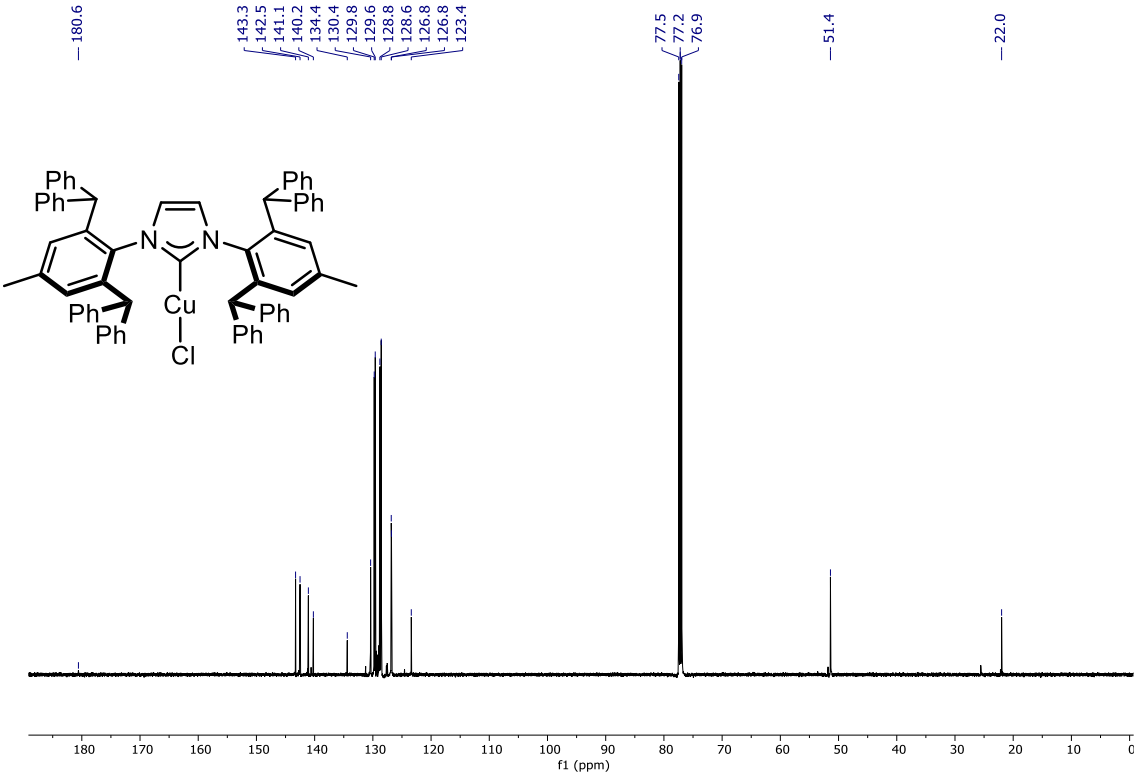

Figure A14: $^{13}C\{^{1}H\}$ NMR spectrum of 2-11 in $CDCl_3$ at 126 MHz

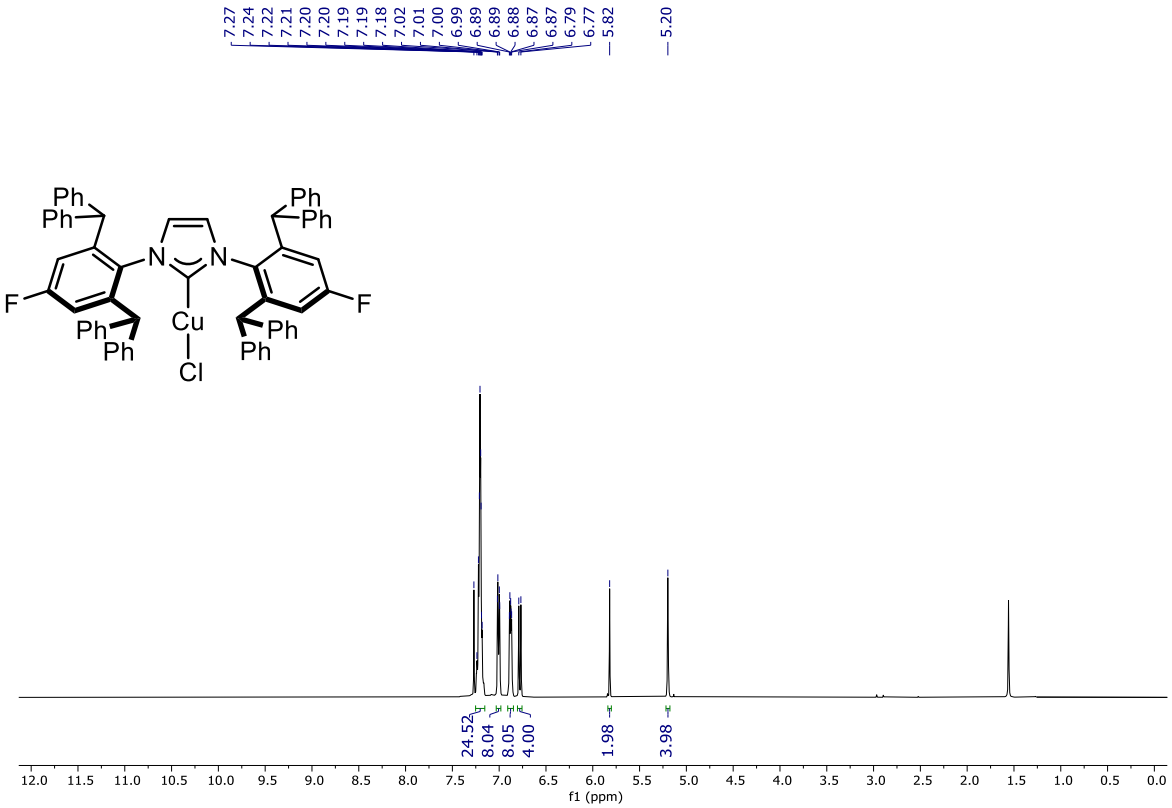

Figure A15: ^{1}H NMR spectrum of 2-12 in $CDCl_3$ at 400 MHz

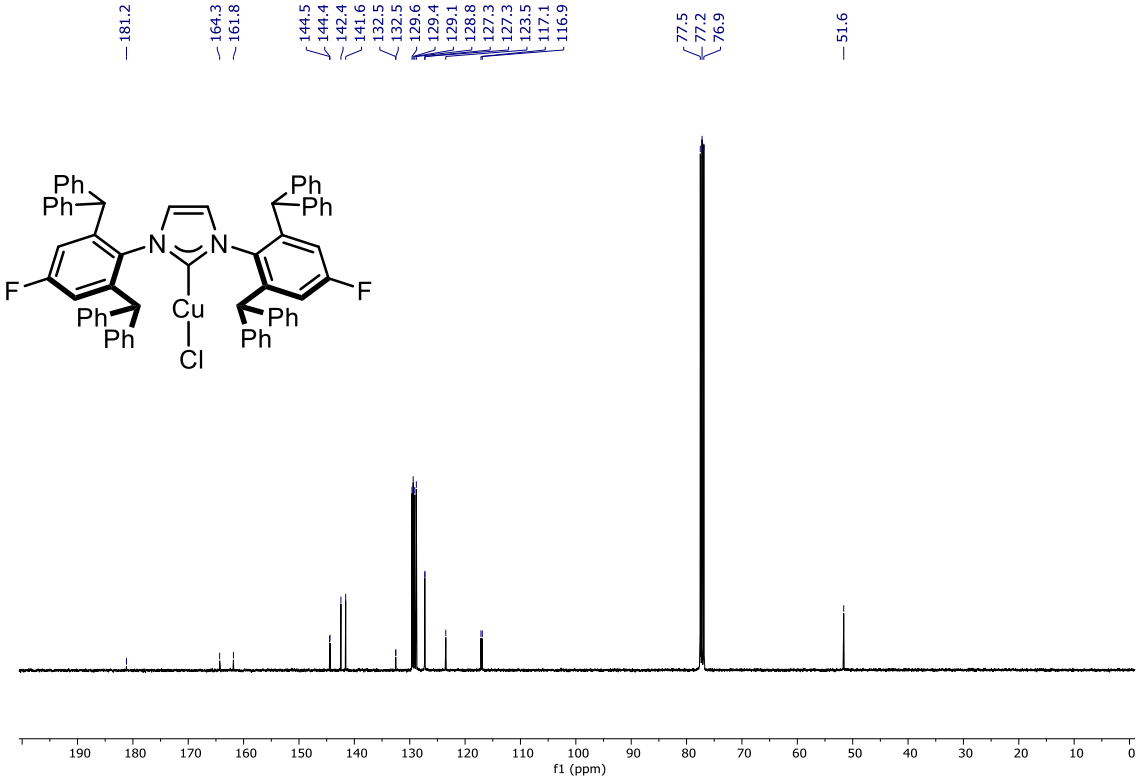

Figure A16: $^{13}C\{^{1}H\}$ NMR spectrum of 2-12 in $CDCl_3$ at 101 MHz

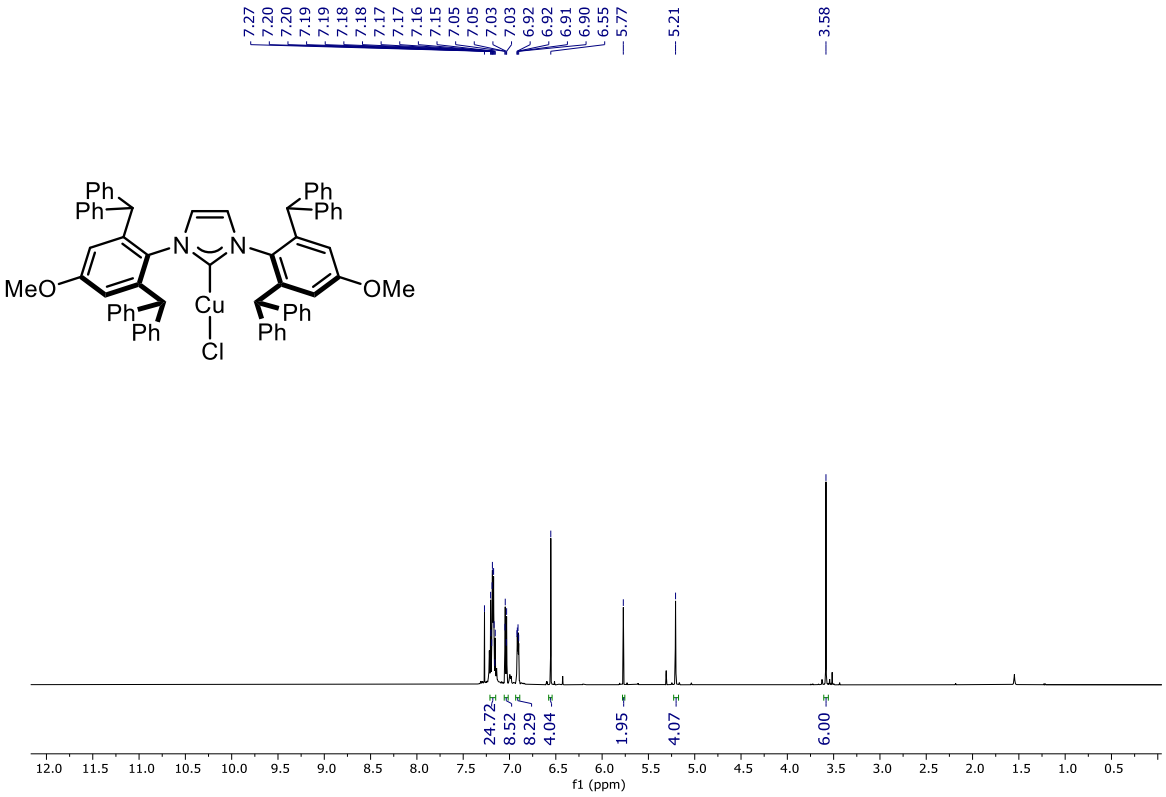

Figure A17: ^{1}H NMR spectrum of 2-13 in $CDCl_3$ at 500 MHz

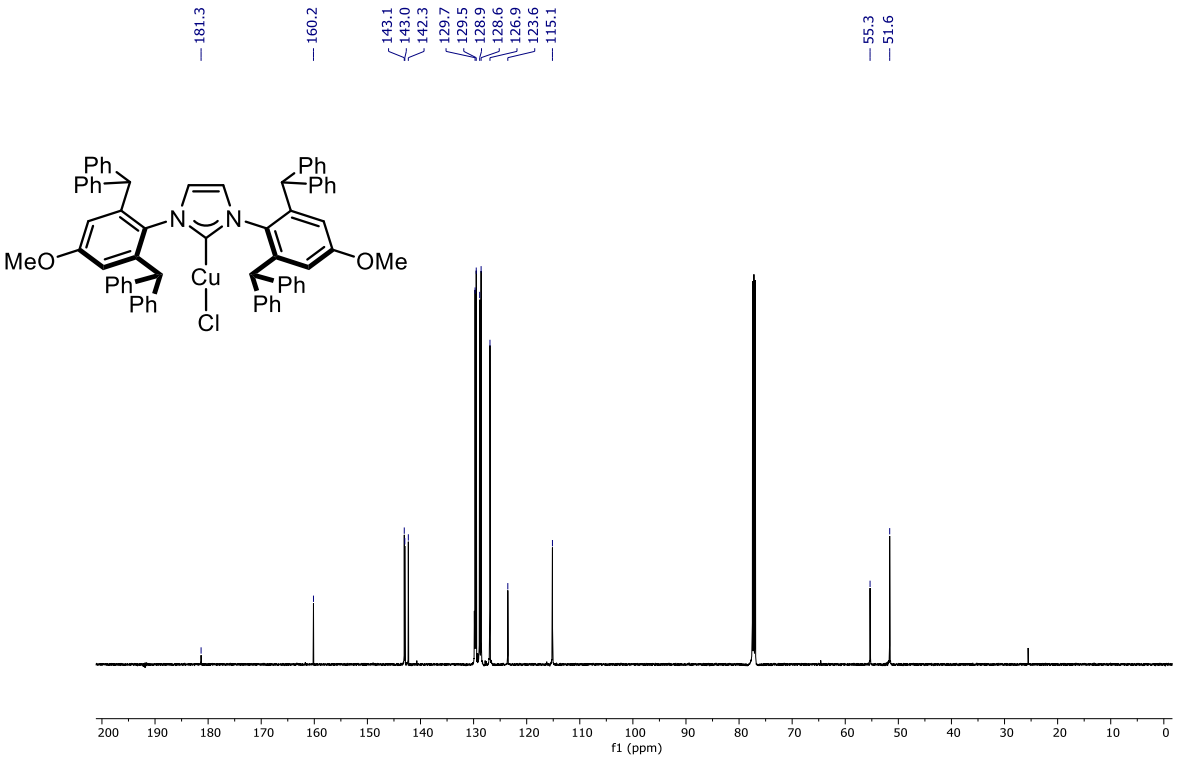

Figure A18: $^{13}C\{^{1}H\}$ NMR spectrum of 2-13 in $CDCl_3$ at 126 MHz

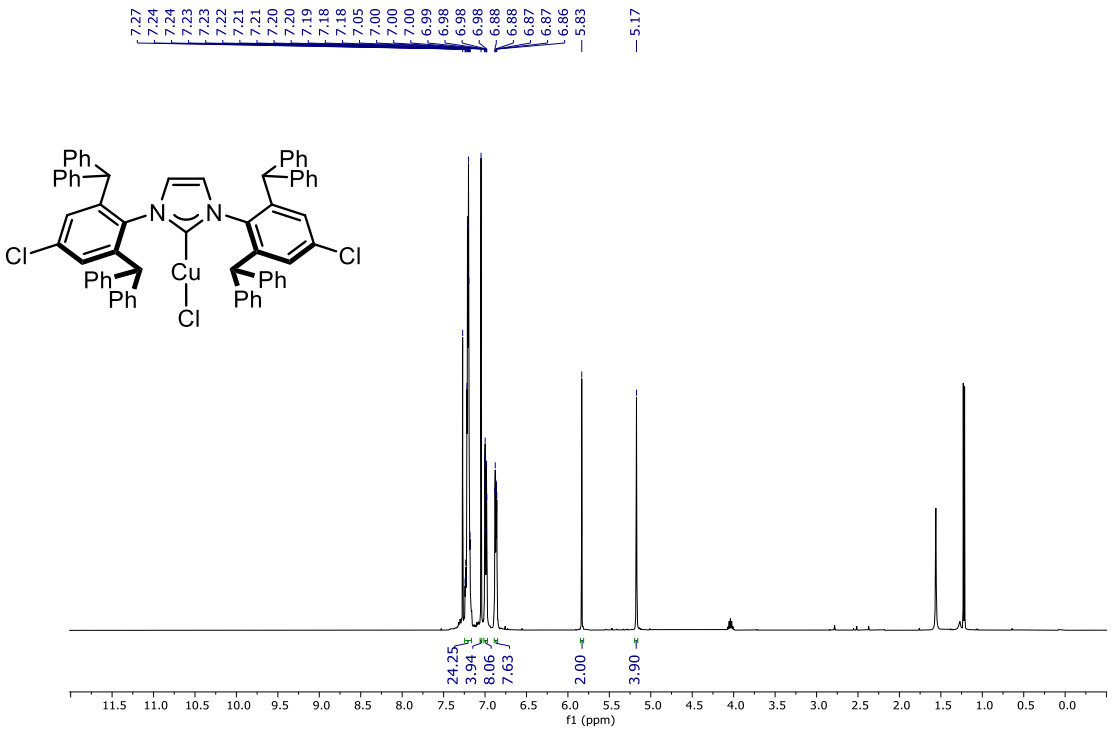

Figure A19: ^{1}H NMR spectrum of 2-14 in $CDCl_3$ at 400 MHz

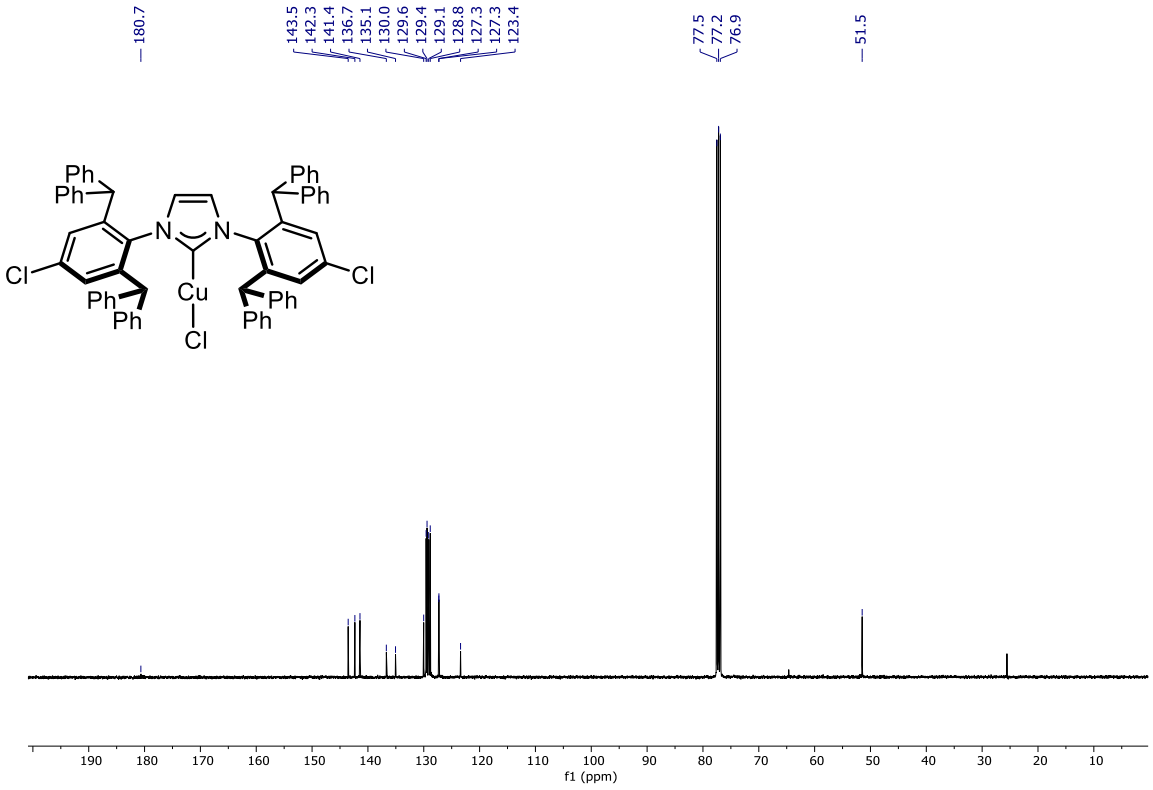

Figure A20: $^{13}C\{^{1}H\}$ NMR spectrum of 2-14 in $CDCl_3$ at 101 MHz

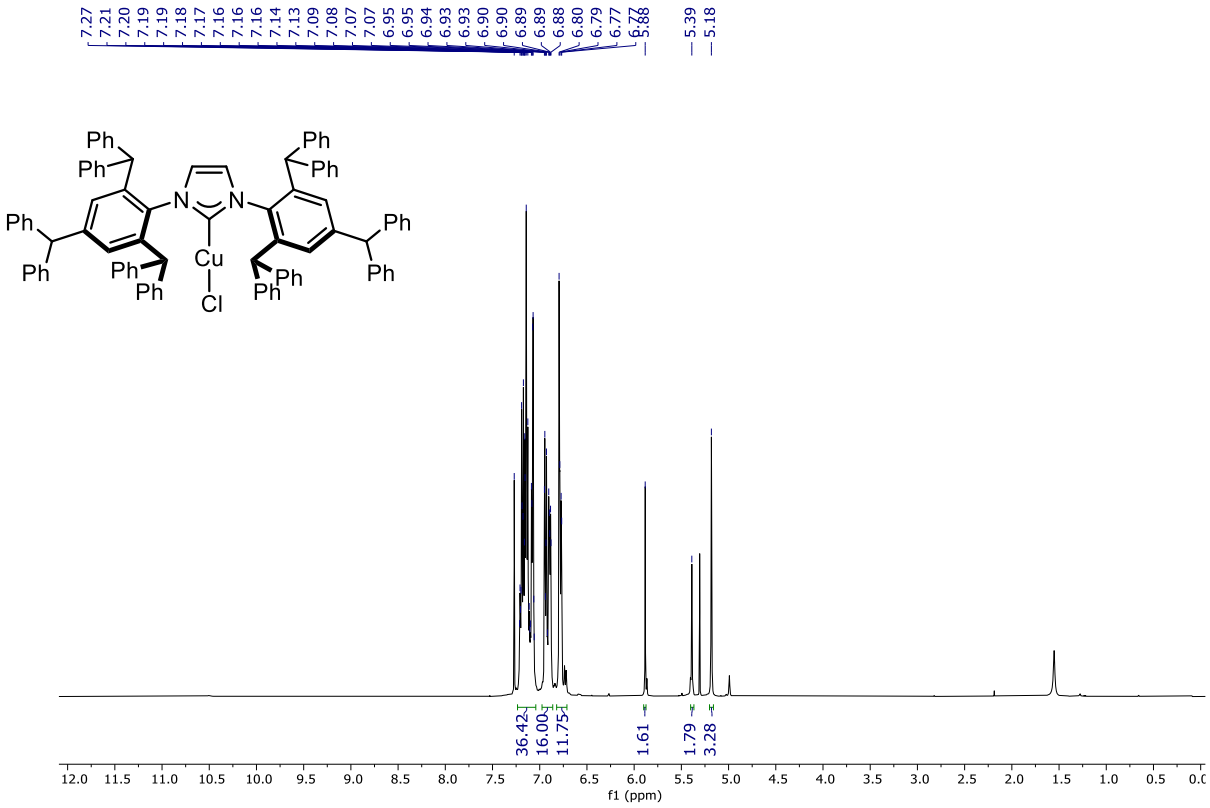

Figure A21: ^{1}H NMR spectrum of 2-15 in $CDCl_3$ at 400 MHz

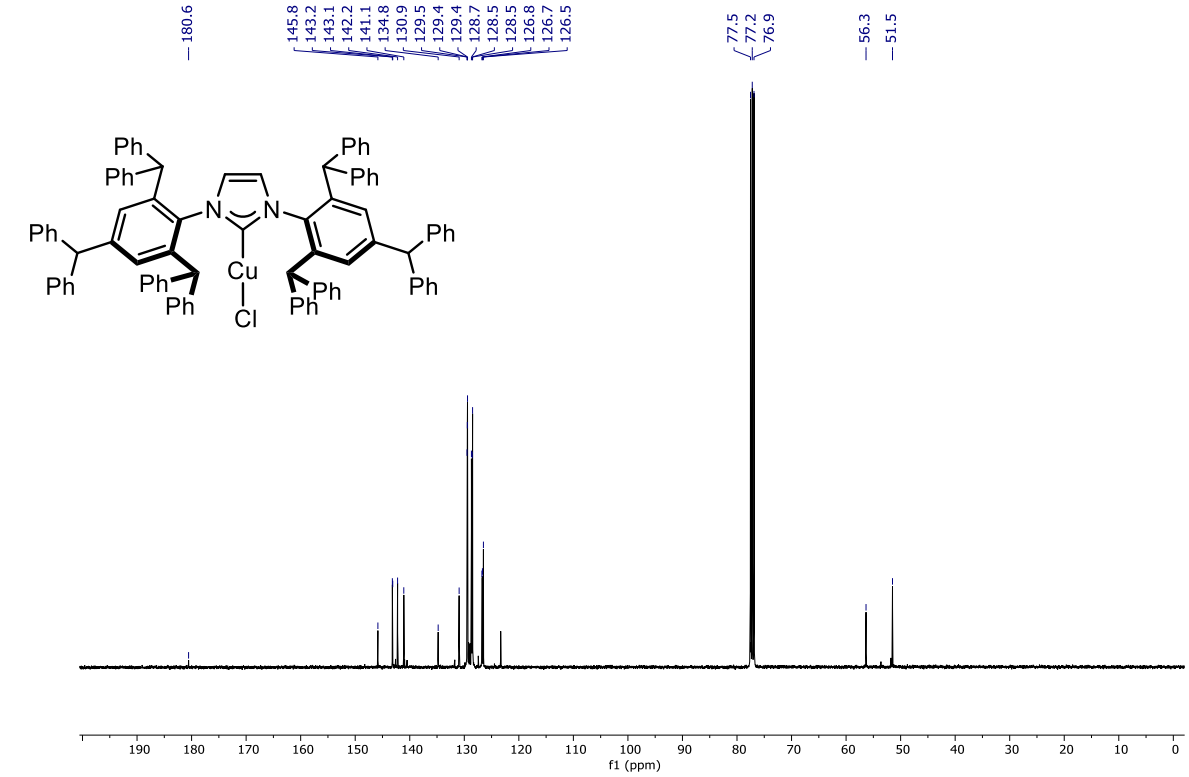

Figure A22: $^{13}C\{^{1}H\}$ NMR spectrum of 2-15 in $CDCl_3$ at 101 MHz

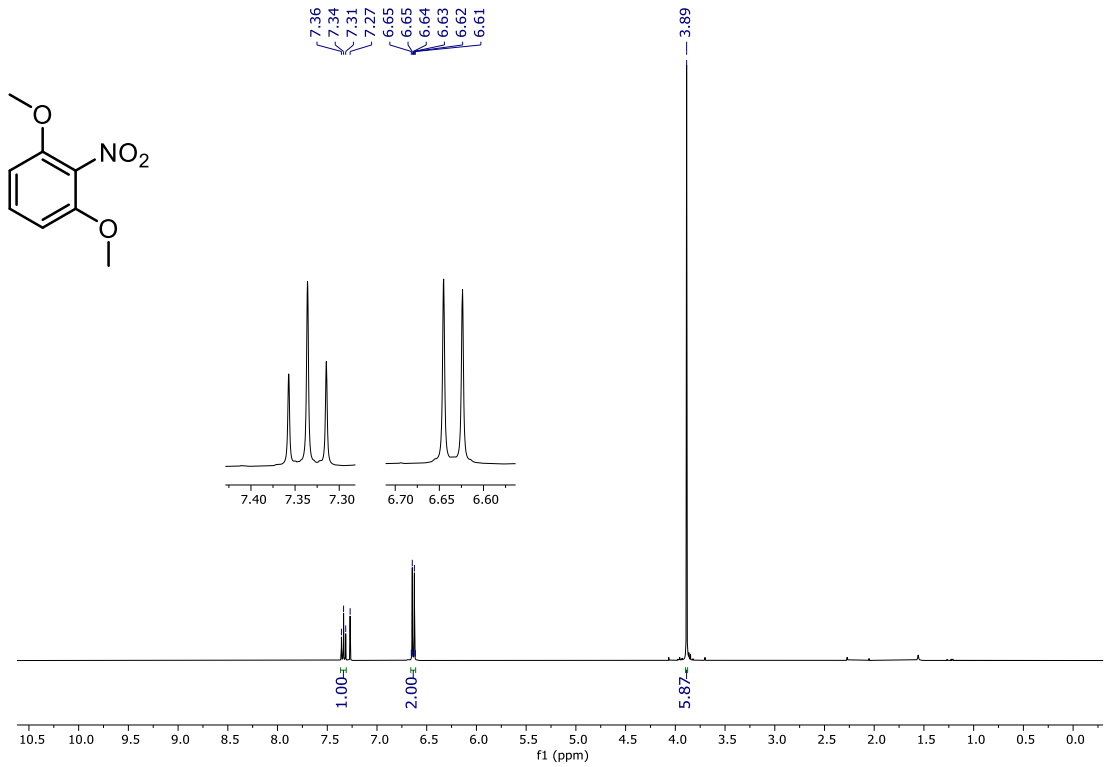

Figure A23: ^{1}H NMR spectrum of 3-1 in $CDCl_3$ at 400 MHz

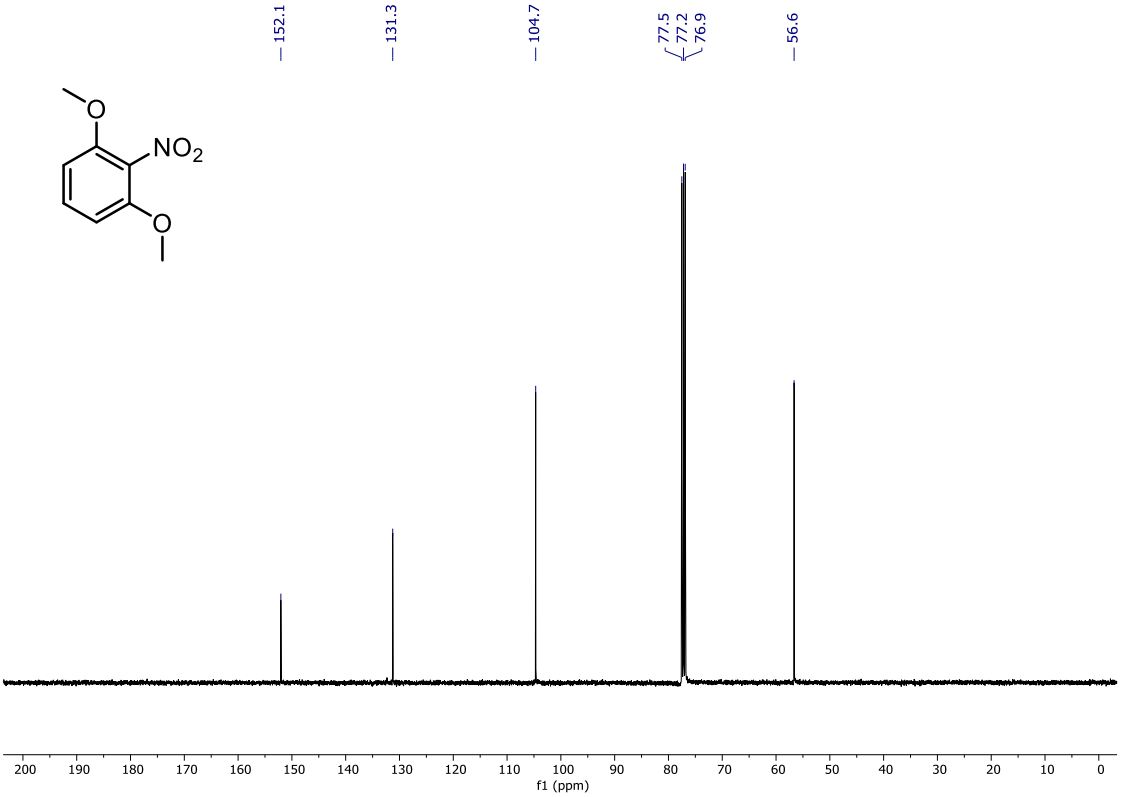

Figure A24: $^{13}C\{^{1}H\}$ NMR spectrum of 3-1 in $CDCl_3$ at 101 MHz

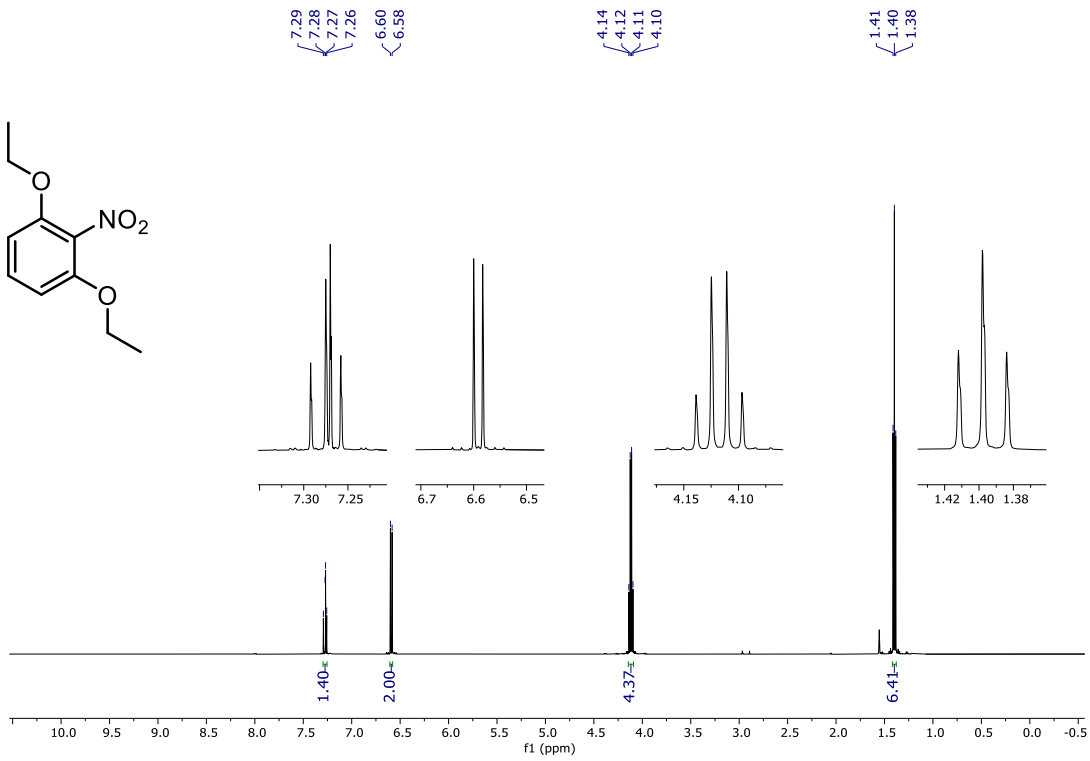

Figure A25: ^{1}H NMR spectrum of 3-2 in $CDCl_3$ at 500 MHz

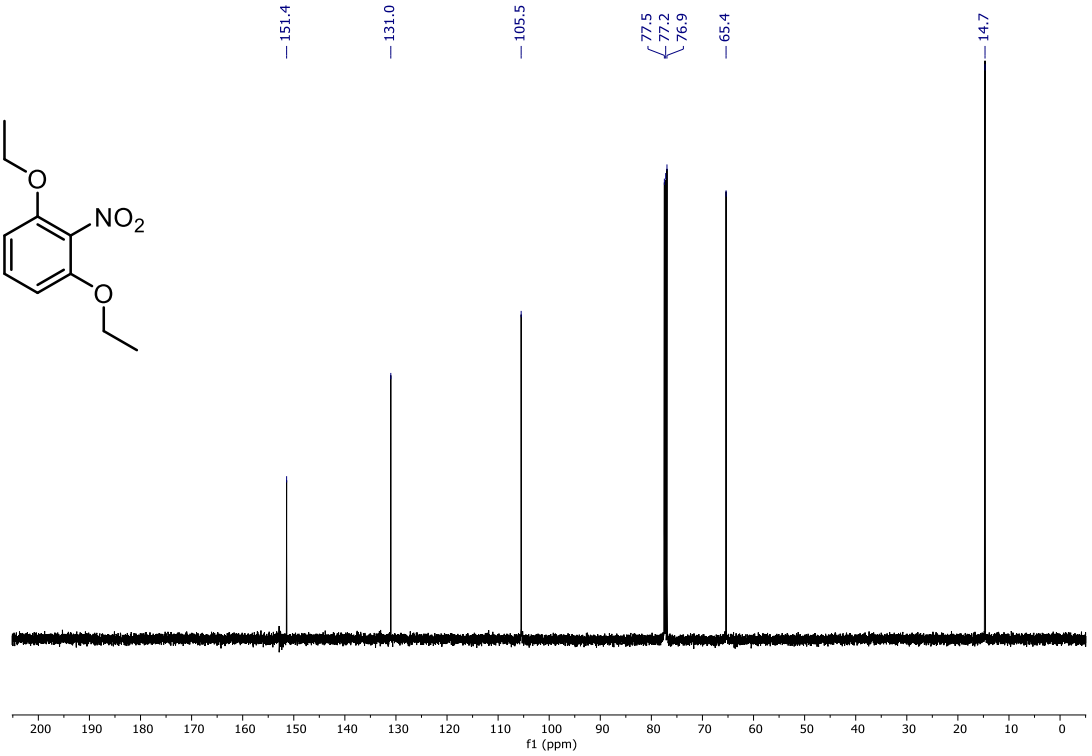

Figure A26: $^{13}C\{^{1}H\}$ NMR spectrum of 3-2 in $CDCl_3$ at 126 MHz

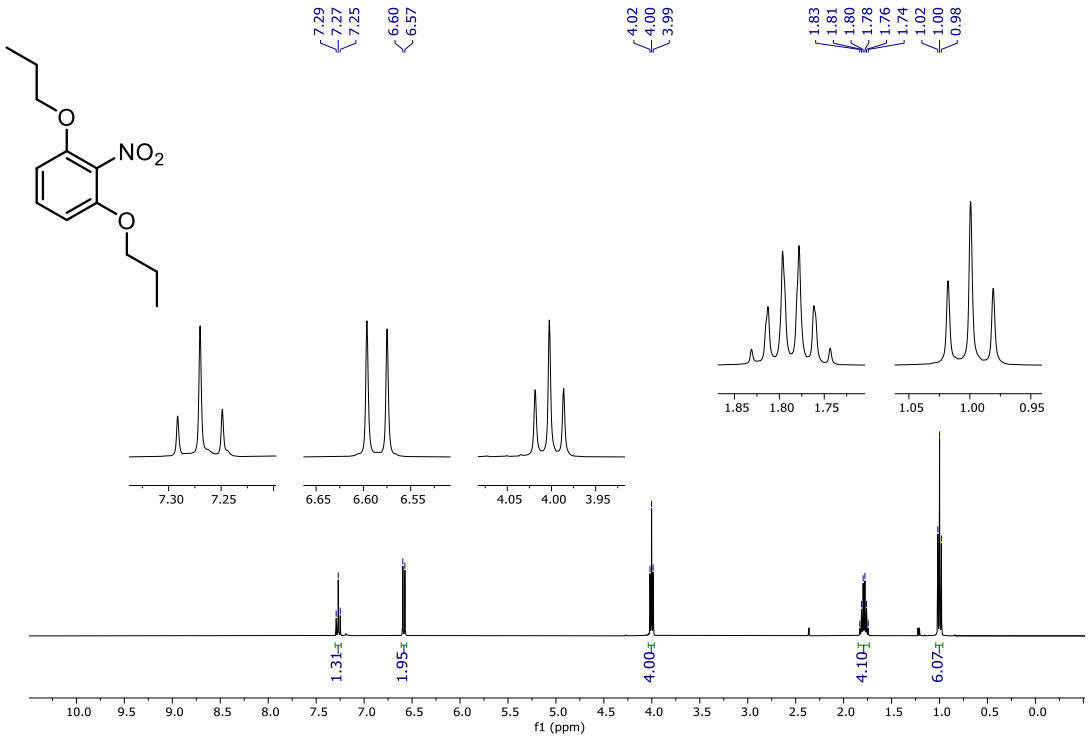

Figure A27: ^{1}H NMR spectrum of 3-3 in $CDCl_3$ at 400 MHz

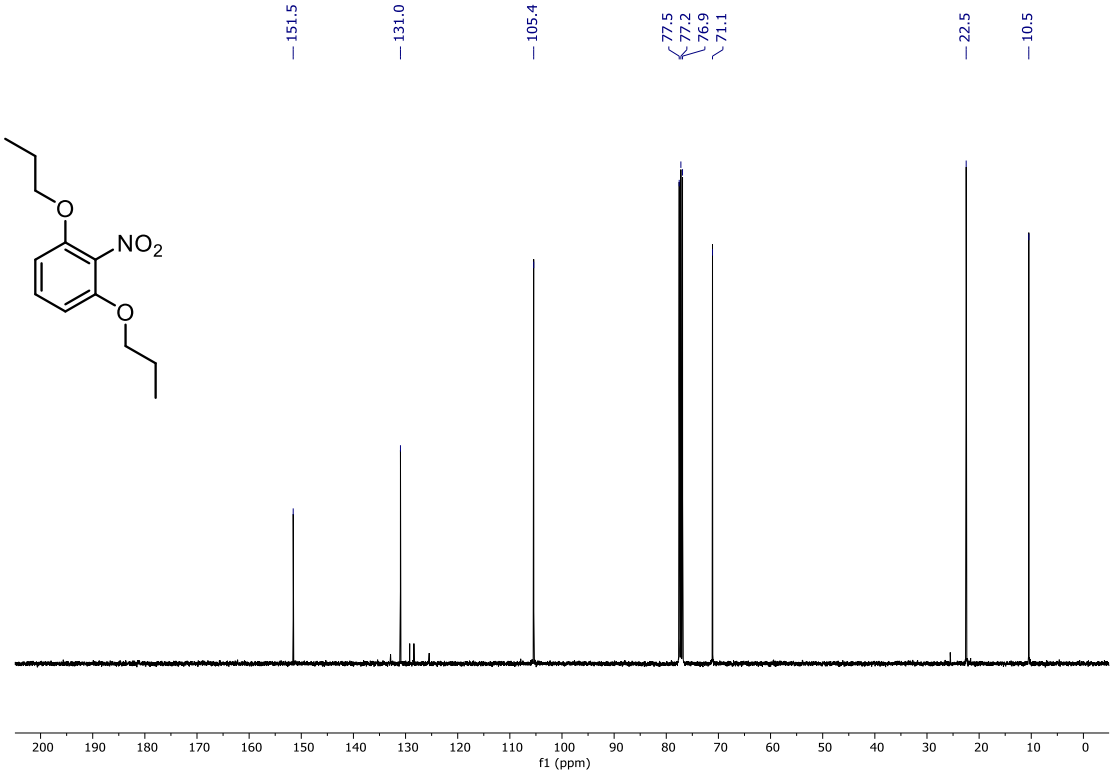

Figure A28: $^{13}C\{^{1}H\}$ NMR spectrum of 3-3 in $CDCl_3$ at 101 MHz

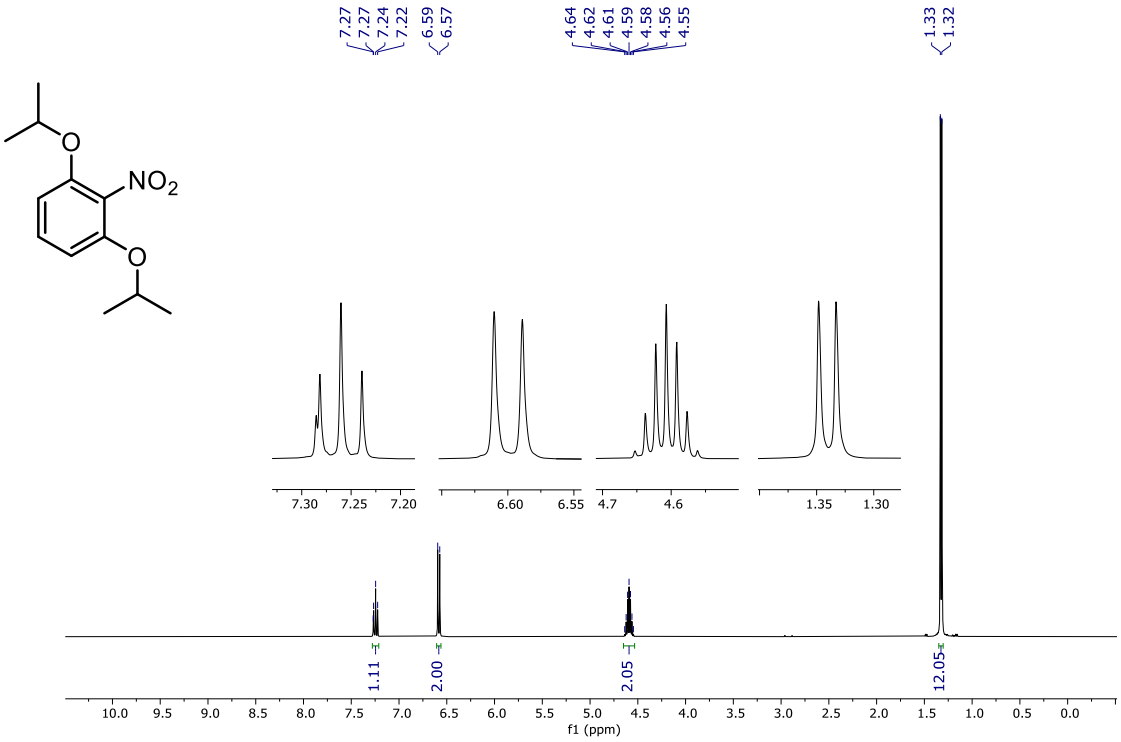

Figure A29: ^{1}H NMR spectrum of 3-4 in $CDCl_3$ at 400 MHz

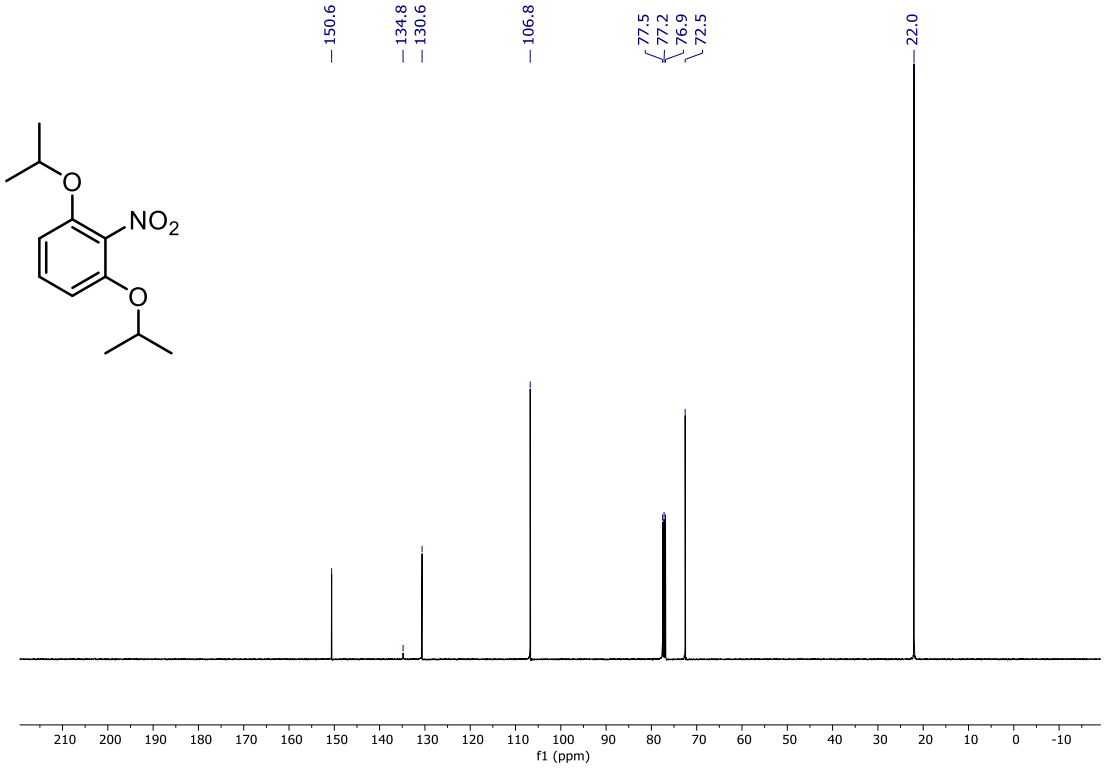

Figure A30: $^{13}C\{^{1}H\}$ NMR spectrum of 3-4 in $CDCl_3$ at 101 MHz

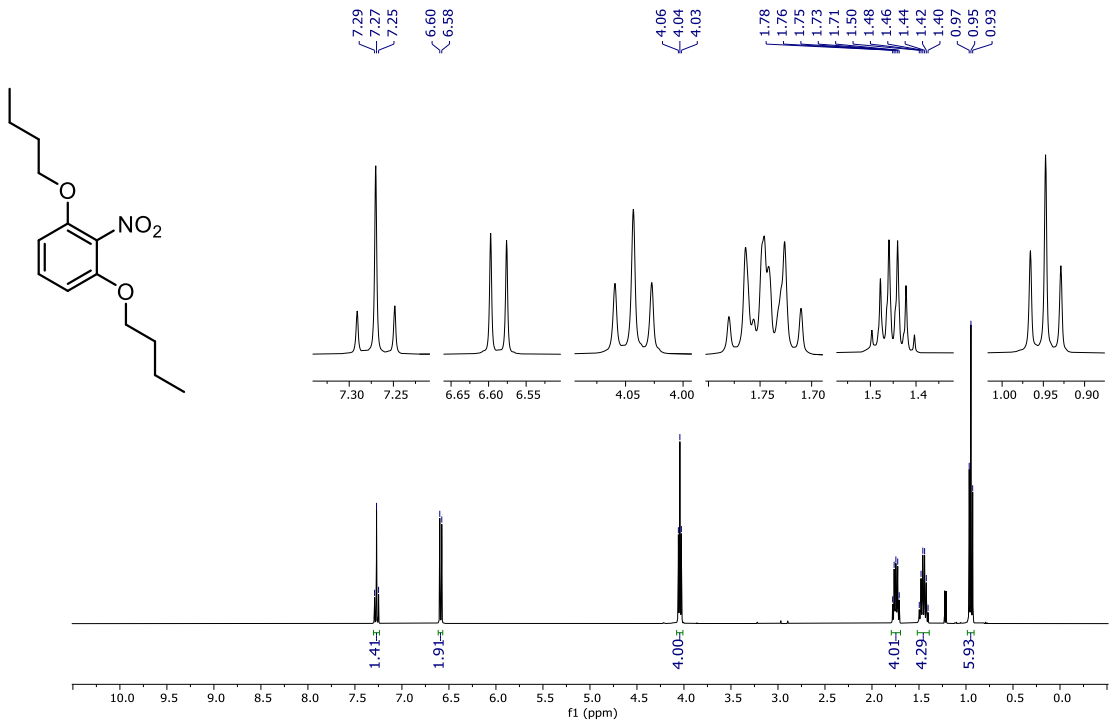

Figure A31: ^{1}H NMR spectrum of 3-5 in $CDCl_3$ at 400 MHz

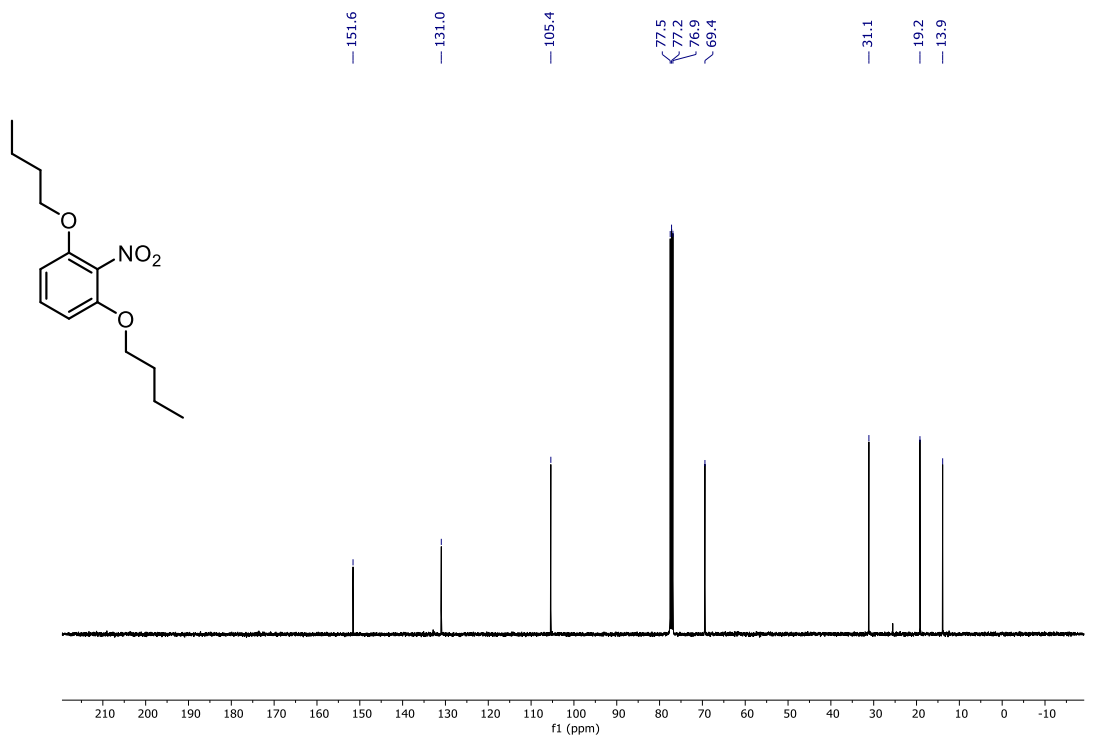

Figure A32: $^{13}C\{^{1}H\}$ NMR spectrum of 3-5 in $CDCl_3$ at 101 MHz

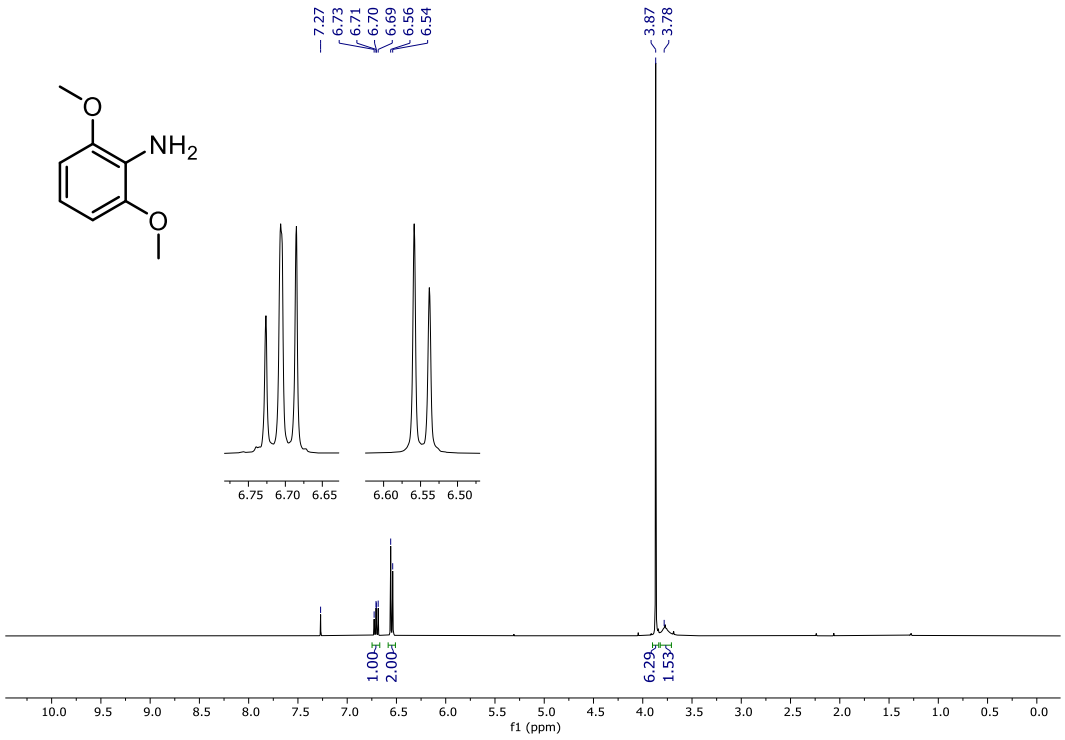

Figure A33: ^{1}H NMR spectrum of 3-6 in $CDCl_3$ at 400 MHz

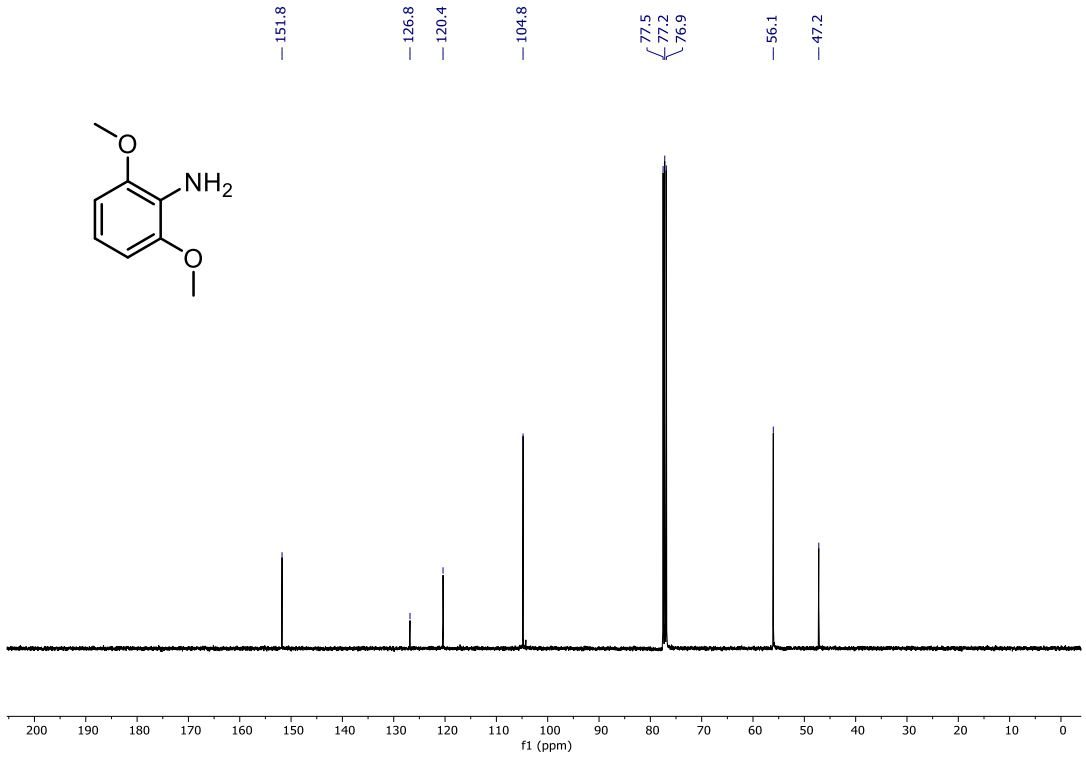

Figure A34: $^{13}C\{^{1}H\}$ NMR spectrum of 3-6 in $CDCl_3$ at 101 MHz

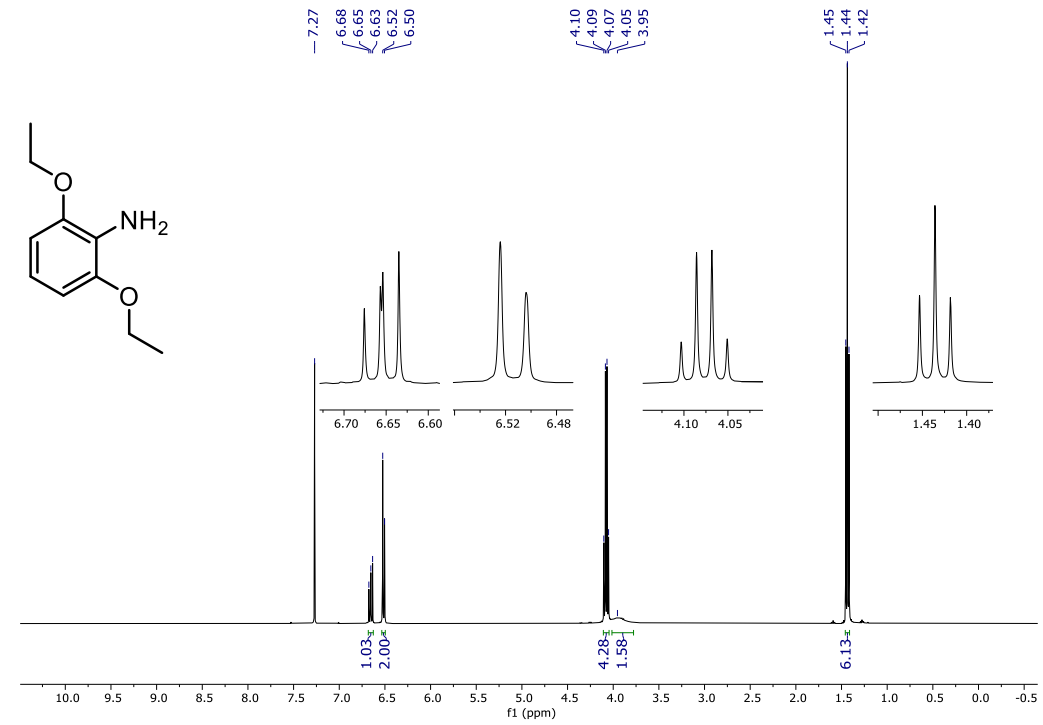

Figure A35: ^{1}H NMR spectrum of 3-7 in $CDCl_3$ at 400 MHz

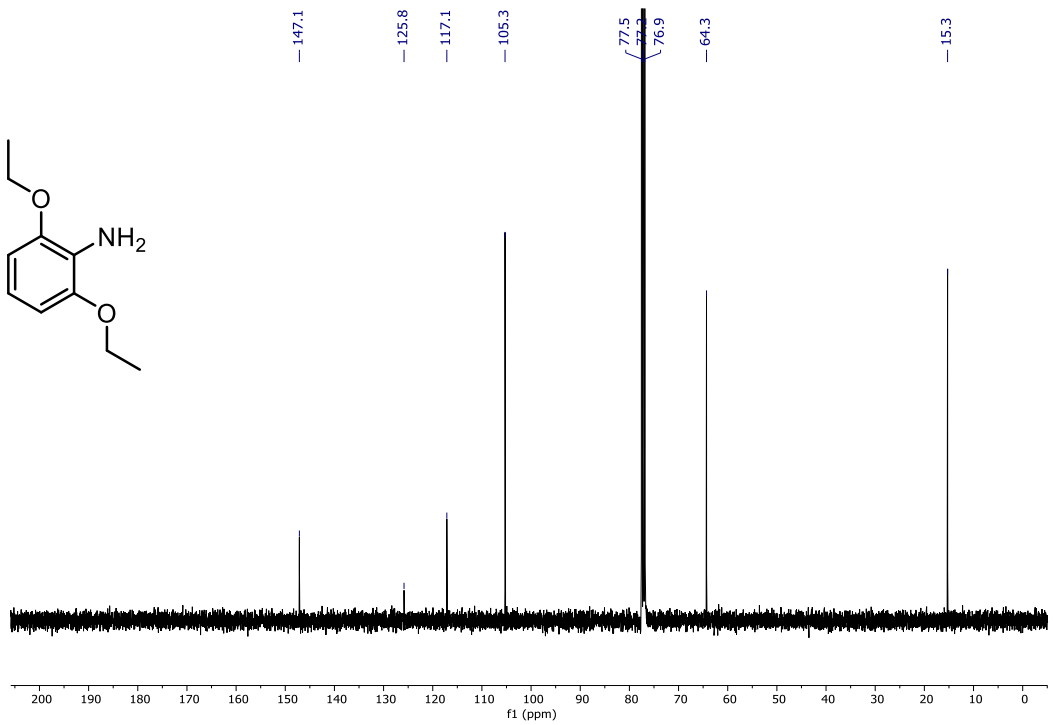

Figure A36: $^{13}C\{^{1}H\}$ NMR spectrum of 3-7 in $CDCl_3$ at 101 MHz

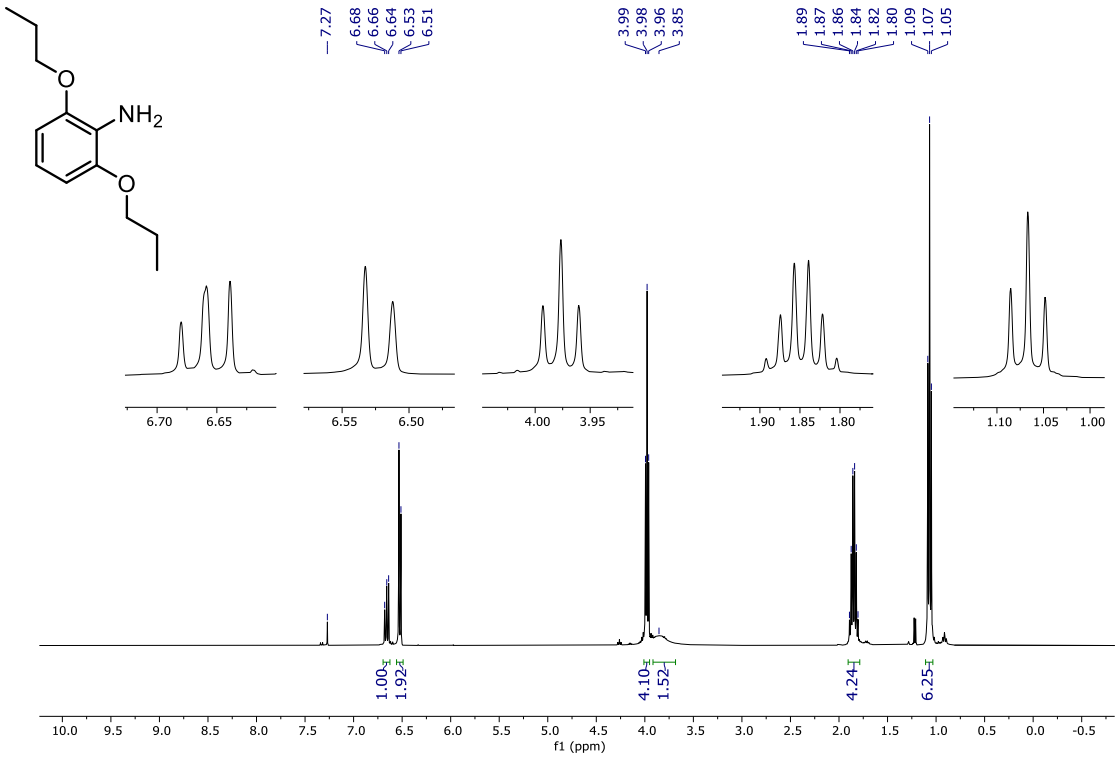

Figure A37: ^{1}H NMR spectrum of 3-8 in $CDCl_3$ at 400 MHz

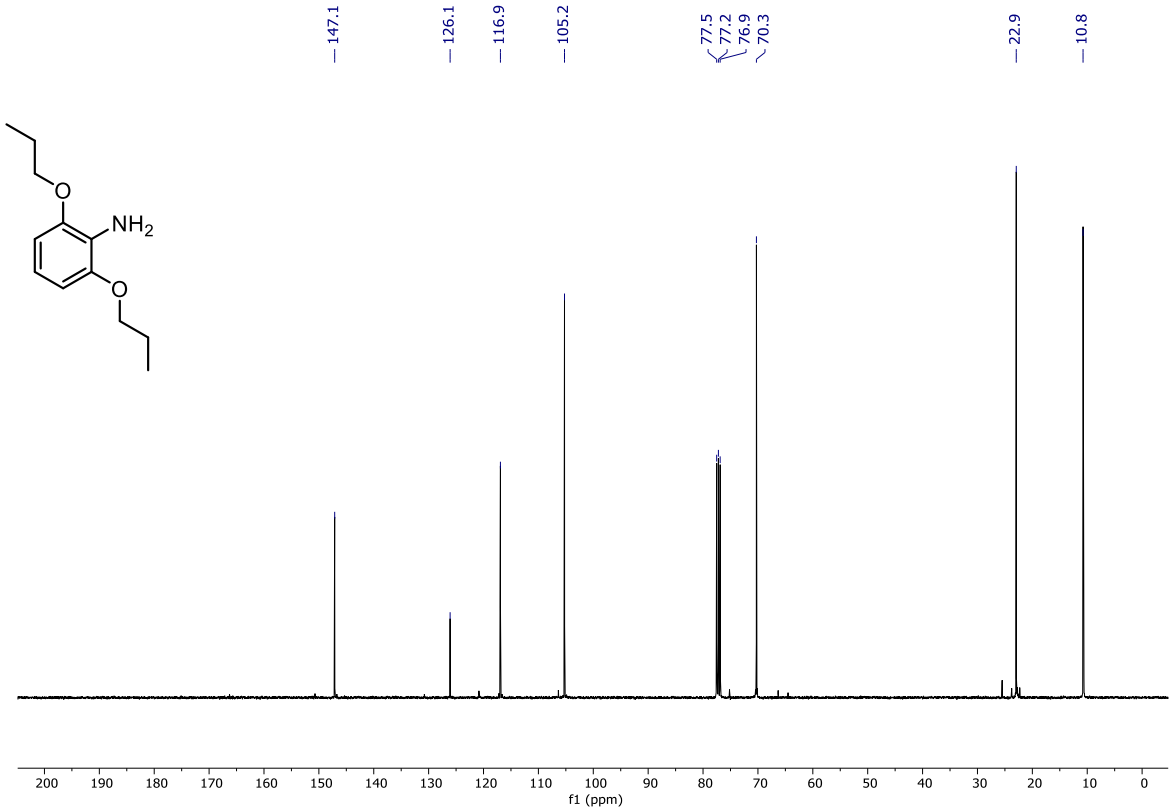

Figure A38: $^{13}C\{^{1}H\}$ NMR spectrum of 3-8 in $CDCl_3$ at 101 MHz

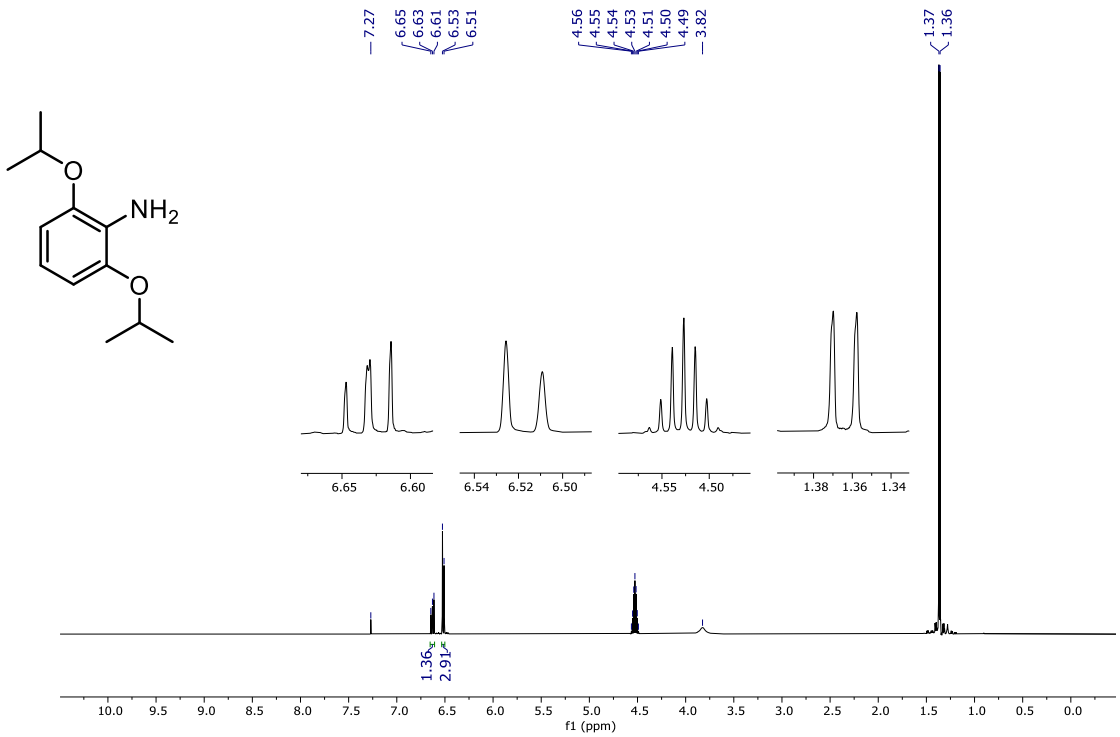

Figure A39: ^{1}H NMR spectrum of 3-9 in $CDCl_3$ at 500 MHz

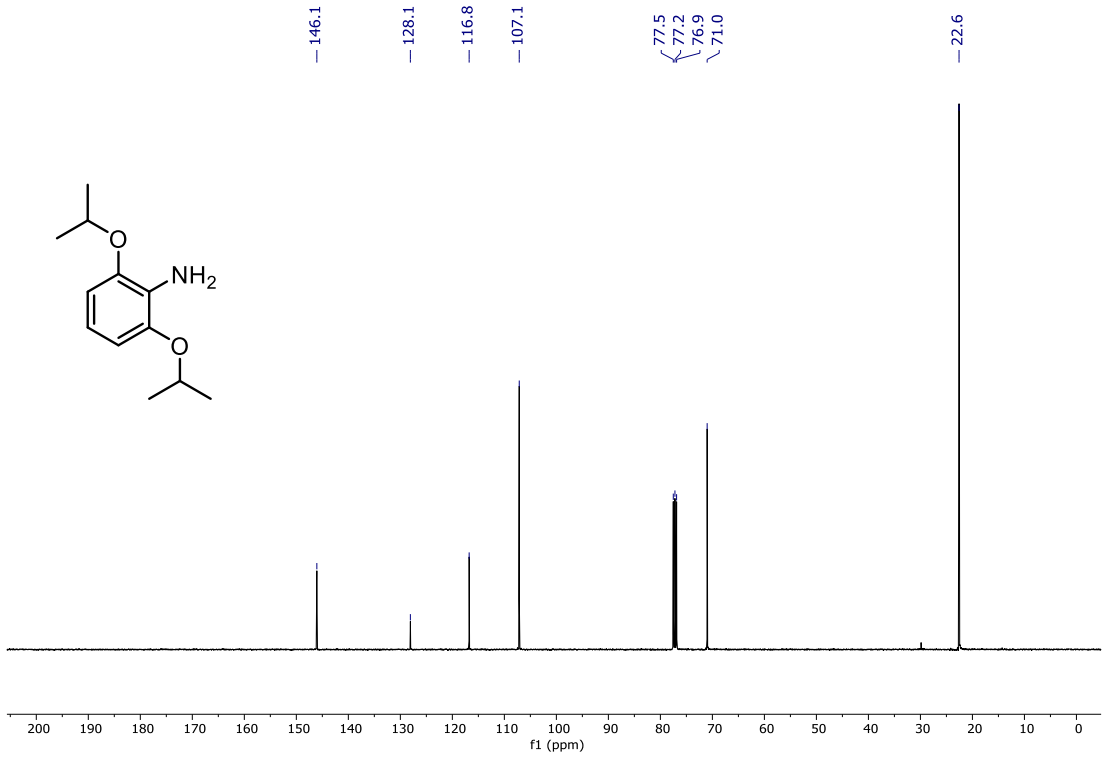

Figure A40: $^{13}C\{^{1}H\}$ NMR spectrum of 3-9 in $CDCl_3$ at 101 MHz

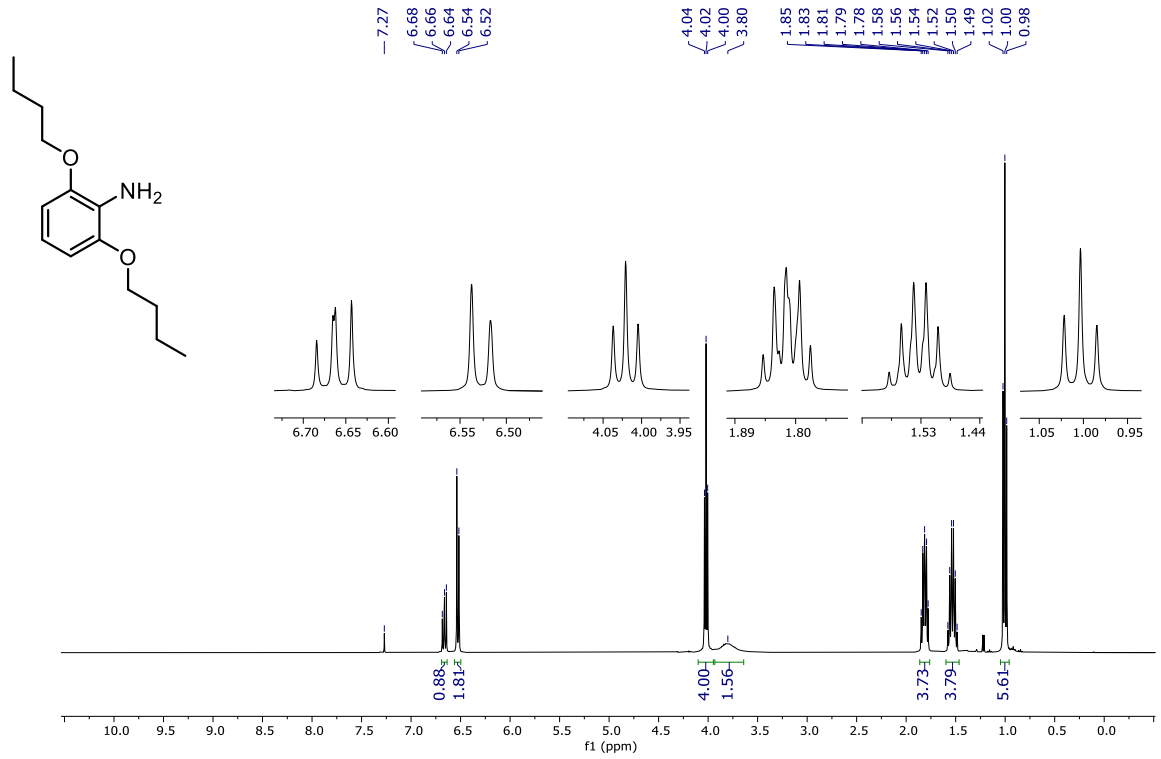

Figure A41: ^{1}H NMR spectrum of 3-10 in $CDCl_3$ at 400 MHz

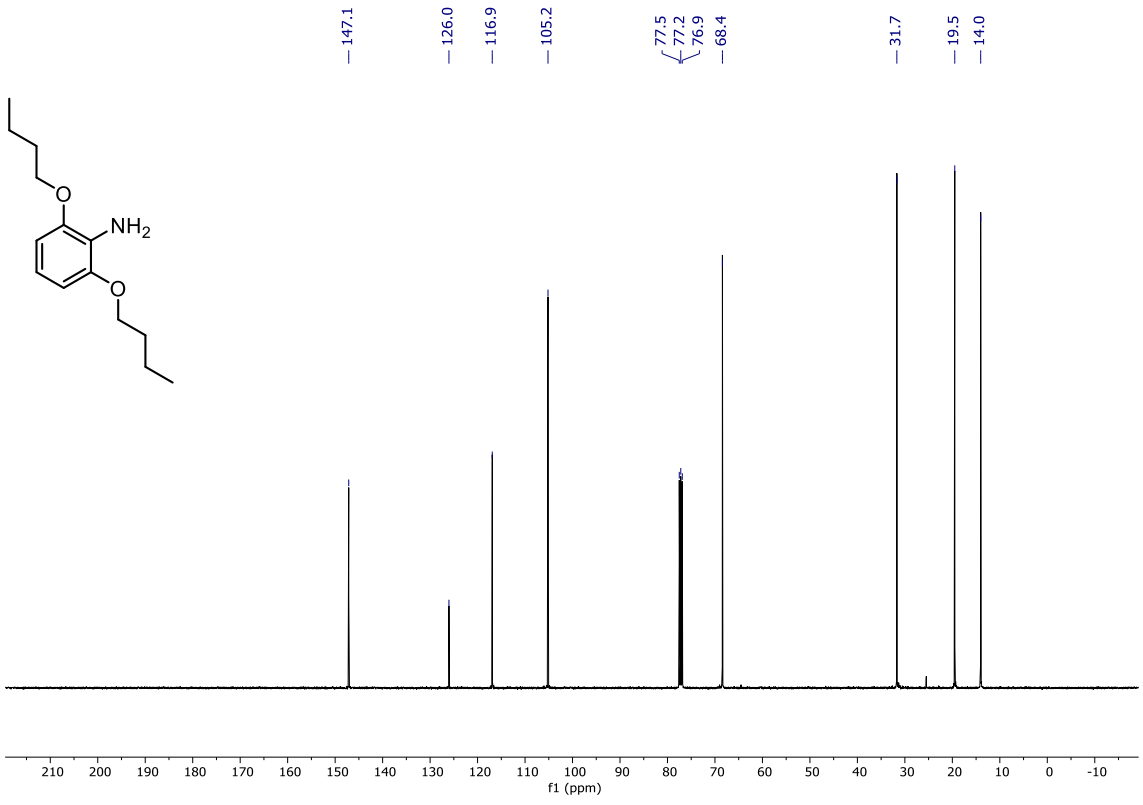

Figure A42: $^{13}C\{^{1}H\}$ NMR spectrum of 3-10 in $CDCl_3$ at 101 MHz

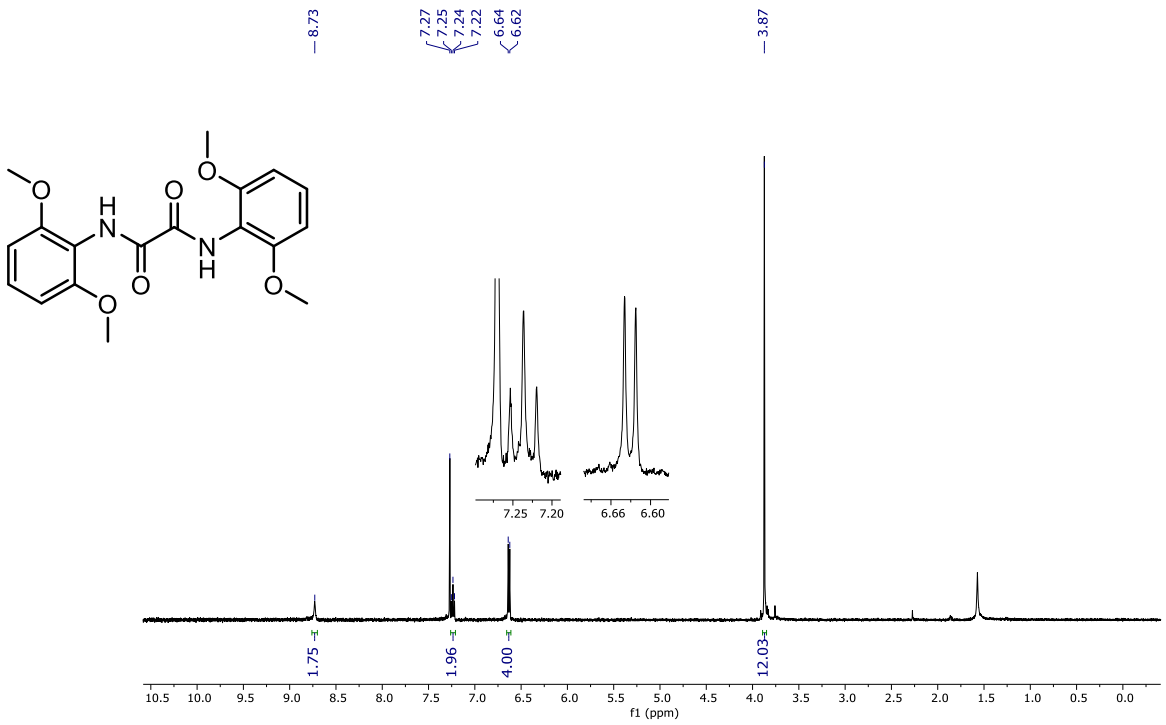

Figure A43: ^{1}H NMR spectrum of 3-11 in $CDCl_3$ at 500 MHz

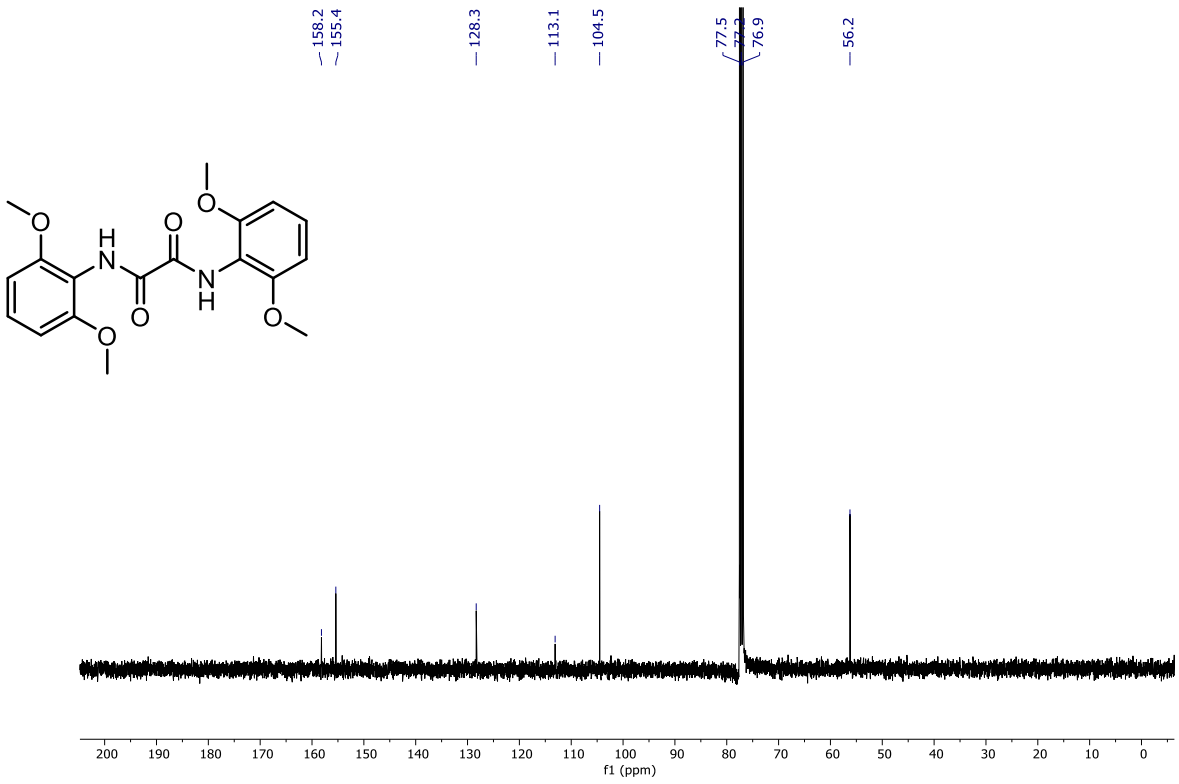

Figure A44: $^{13}C\{^{1}H\}$ NMR spectrum of 3-11 in $CDCl_3$ at 101 MHz

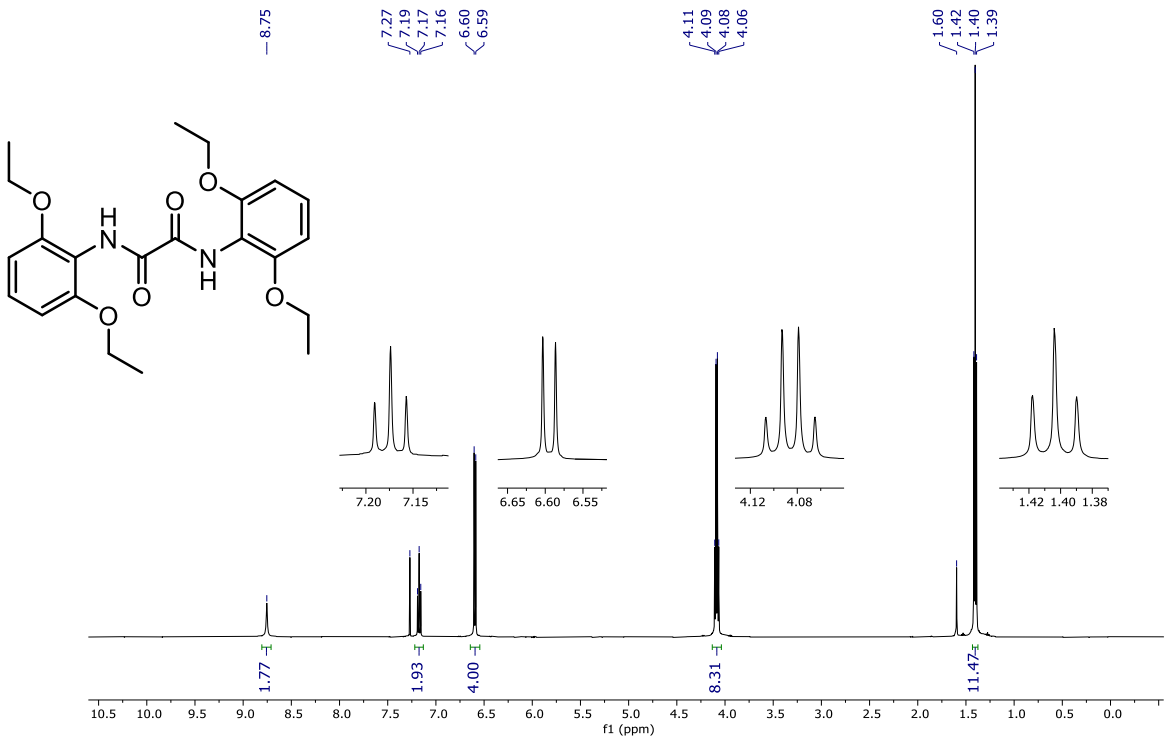

Figure A45: ^{1}H NMR spectrum of 3-12 in $CDCl_3$ at 500 MHz

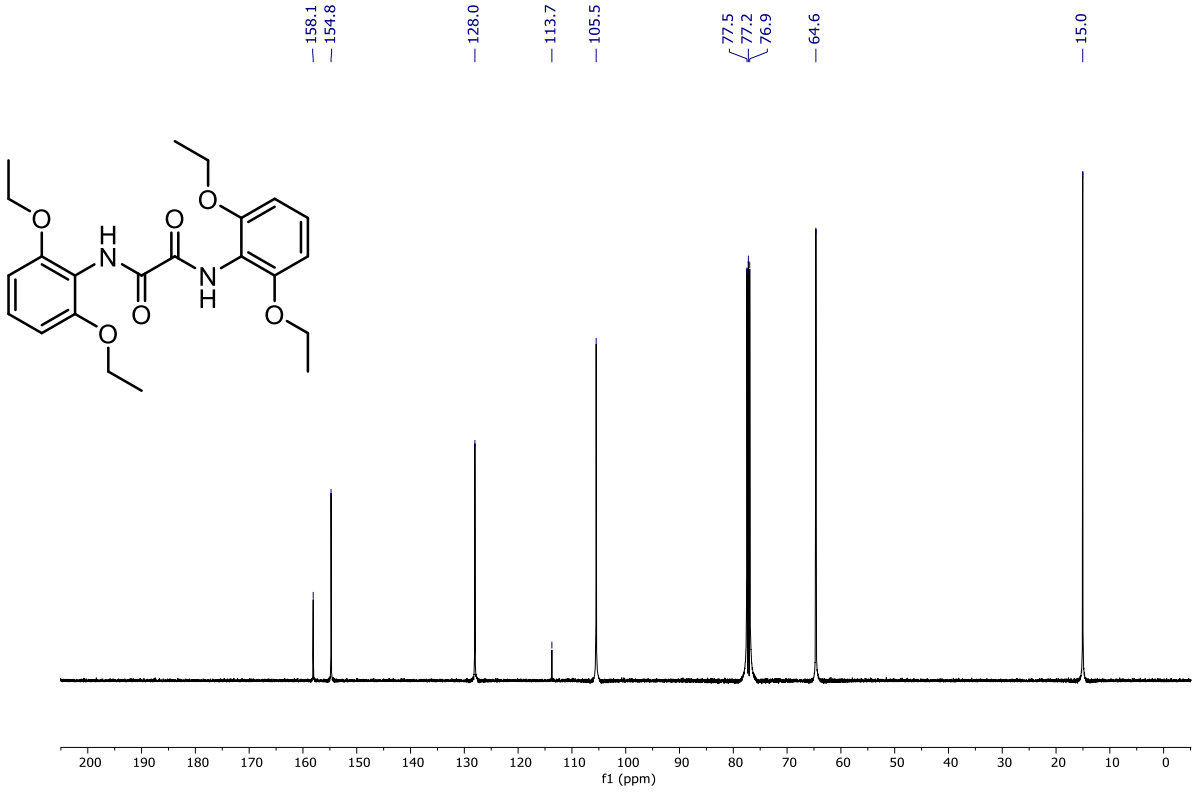

Figure A46: $^{13}C\{^{1}H\}$ NMR spectrum of 3-12 in $CDCl_3$ at 126 MHz

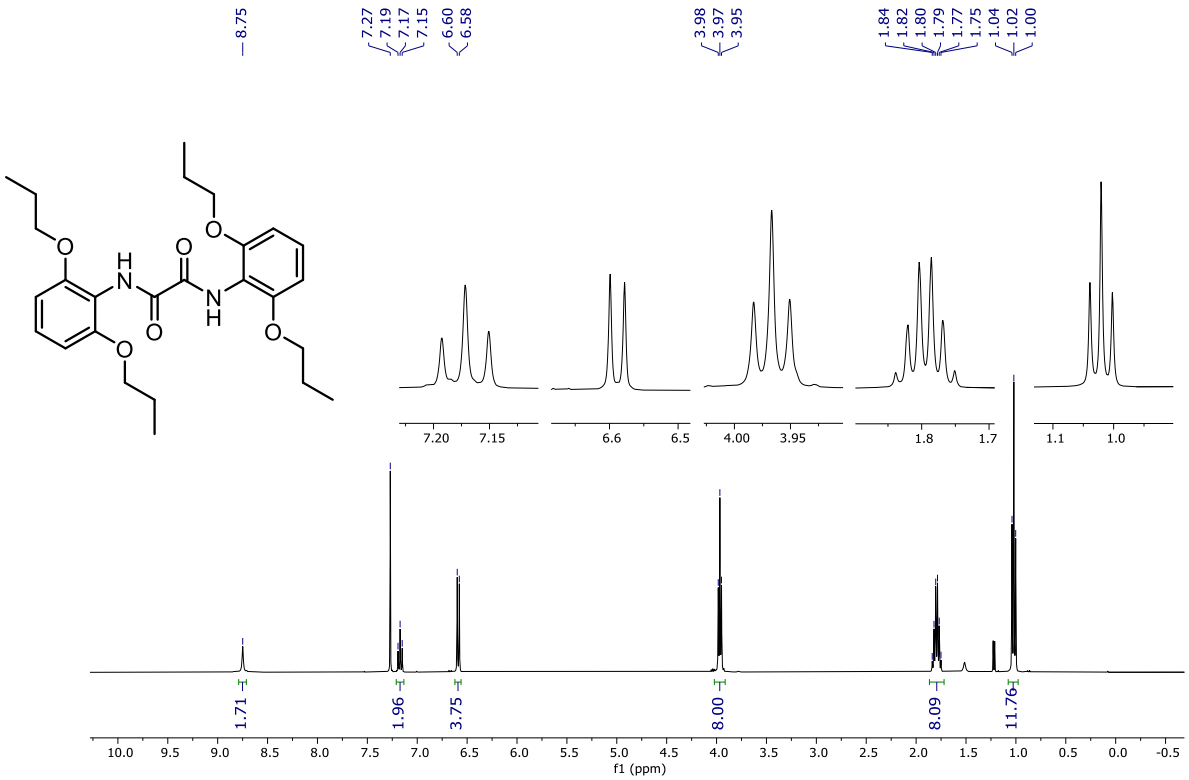

Figure A47: ^{1}H NMR spectrum of 3-13 in $CDCl_3$ at 400 MHz

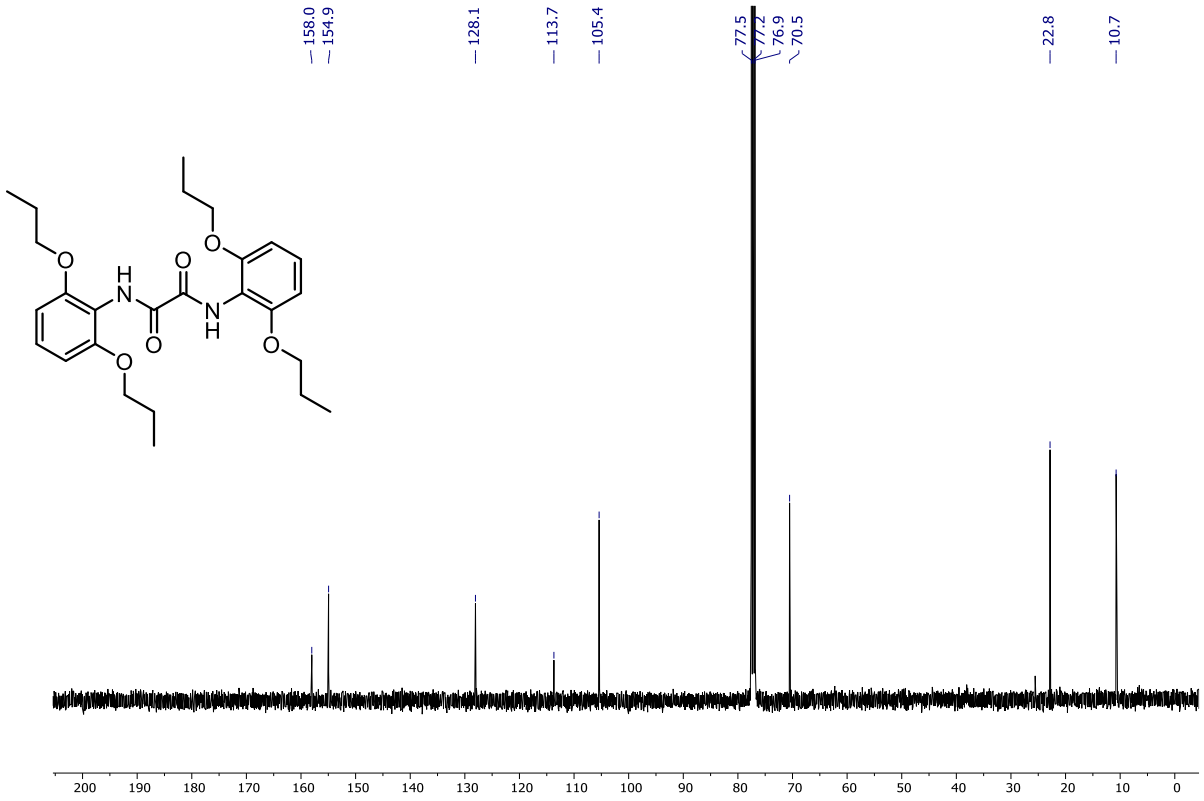

Figure A48: $^{13}C\{^{1}H\}$ NMR spectrum of 3-13 in $CDCl_3$ at 101 MHz

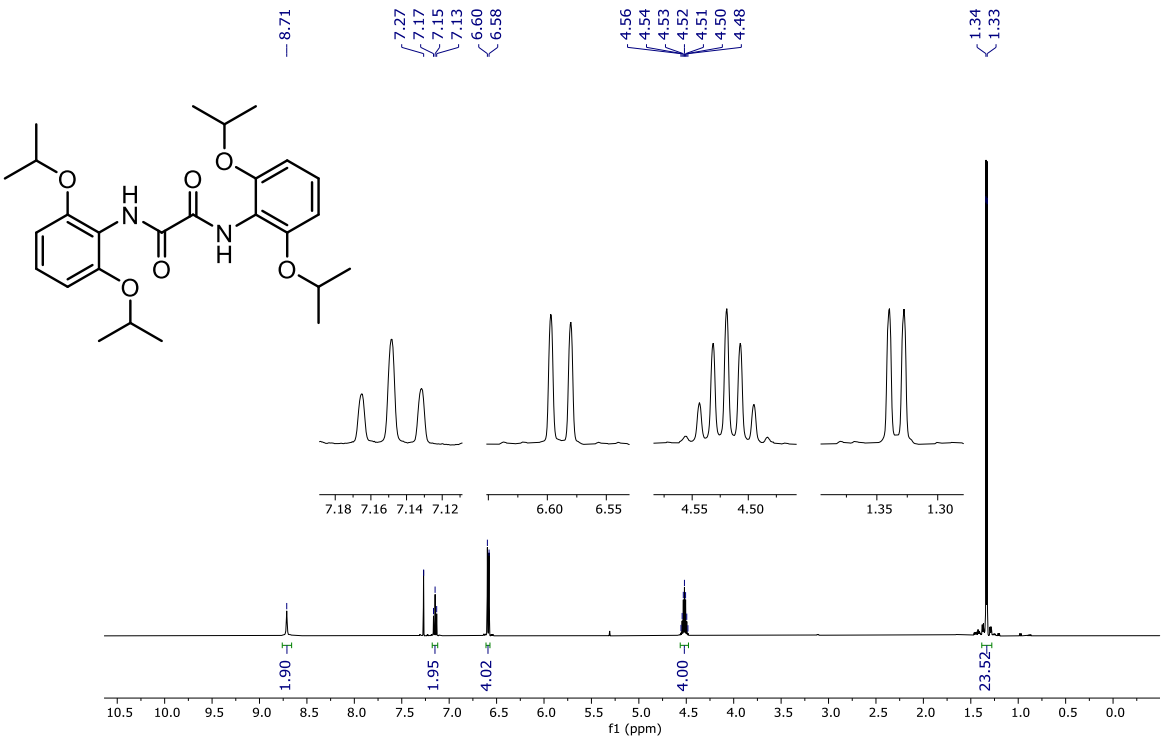

Figure A49: ^{1}H NMR spectrum of 3-14 in $CDCl_3$ at 500 MHz

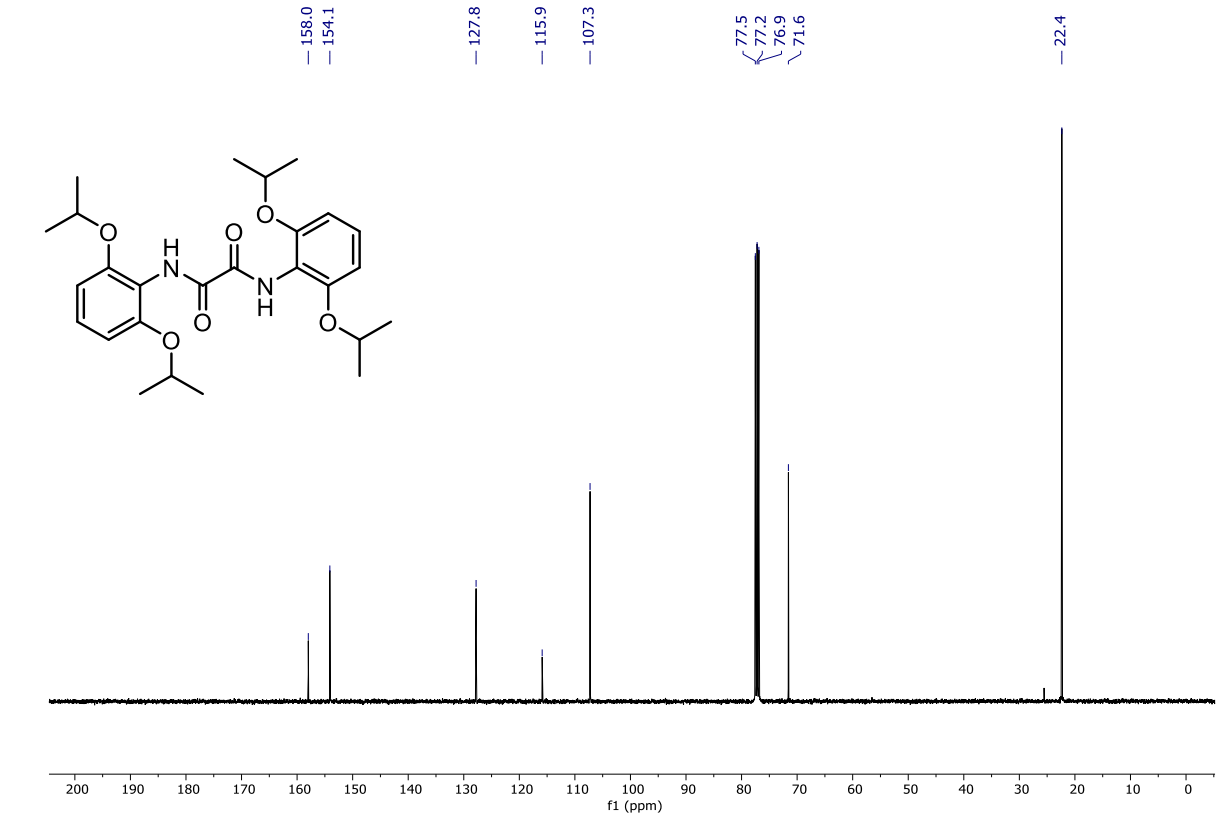

Figure A50: $^{13}C\{^{1}H\}$ NMR spectrum of 3-14 in $CDCl_3$ at 101 MHz

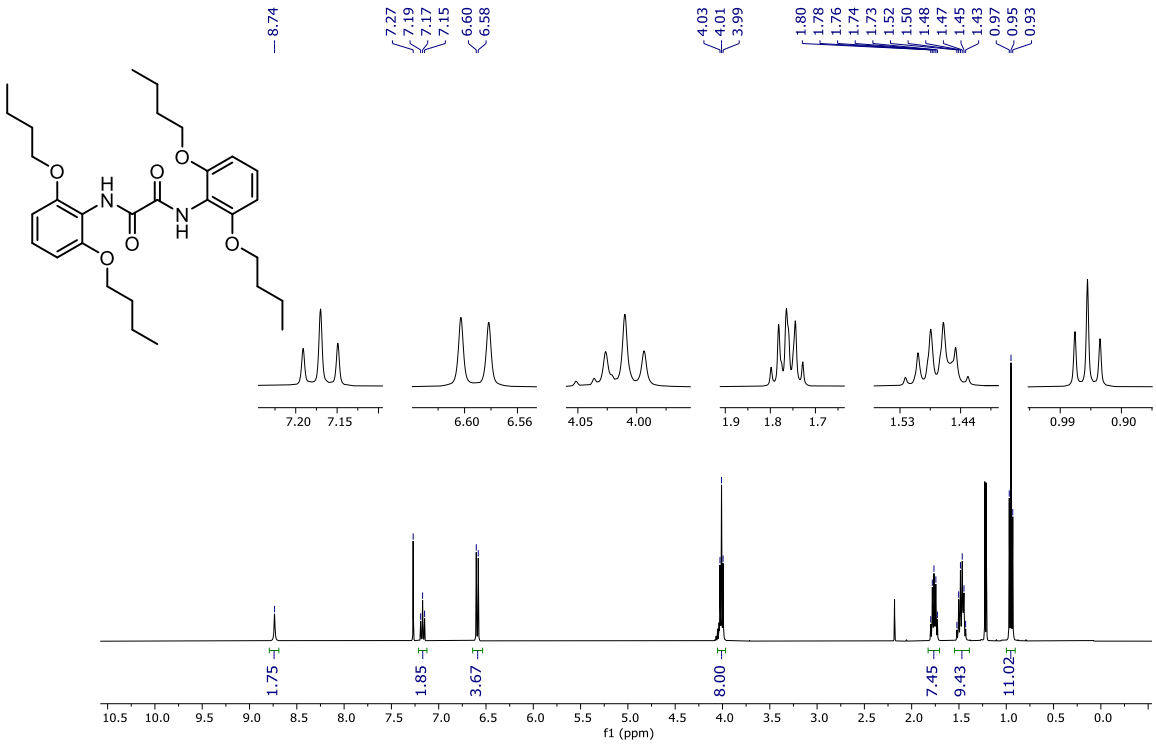

Figure A 51: ^{1}H NMR spectrum of 3-15 in $CDCl_3$ at 400 MHz

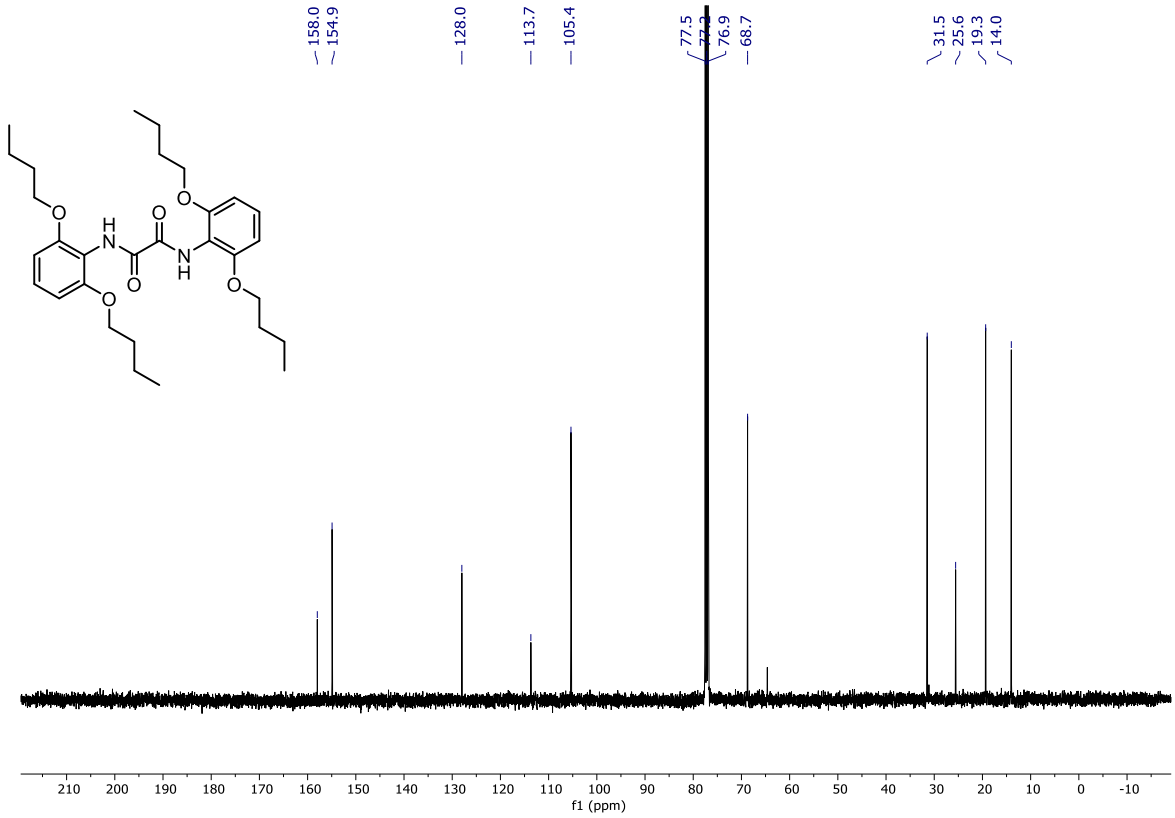

Figure A52: $^{13}C\{^{1}H\}$ NMR spectrum of 3-15 in $CDCl_3$ at 101 MHz

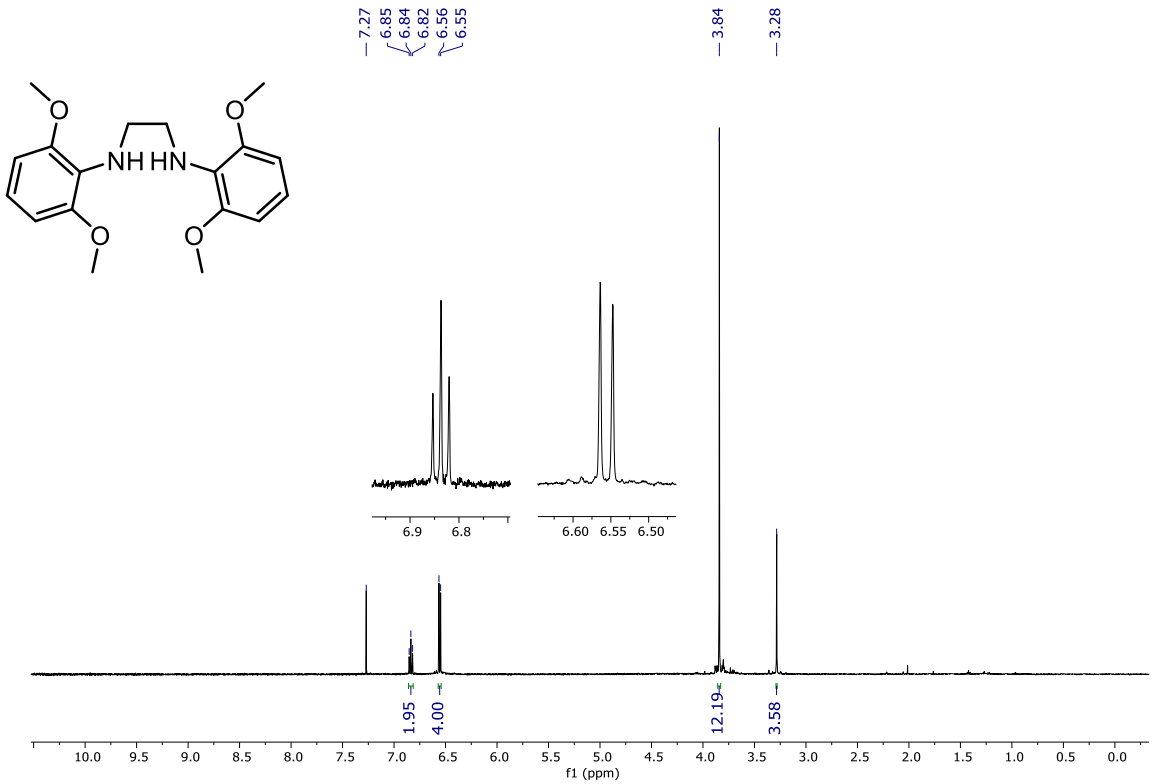

Figure A53: ^{1}H NMR spectrum of 3-16 in $CDCl_3$ at 500 MHz

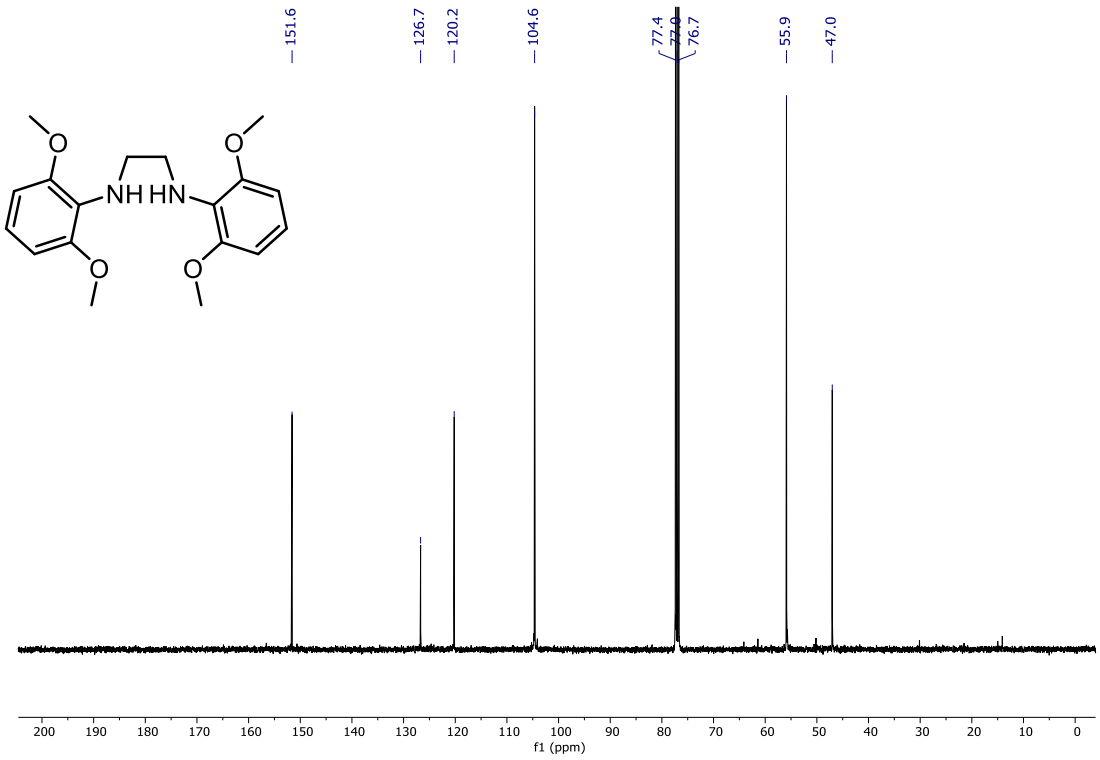

Figure A54: $^{13}C\{^{1}H\}$ NMR spectrum of 3-16 in $CDCl_3$ at 101 MHz

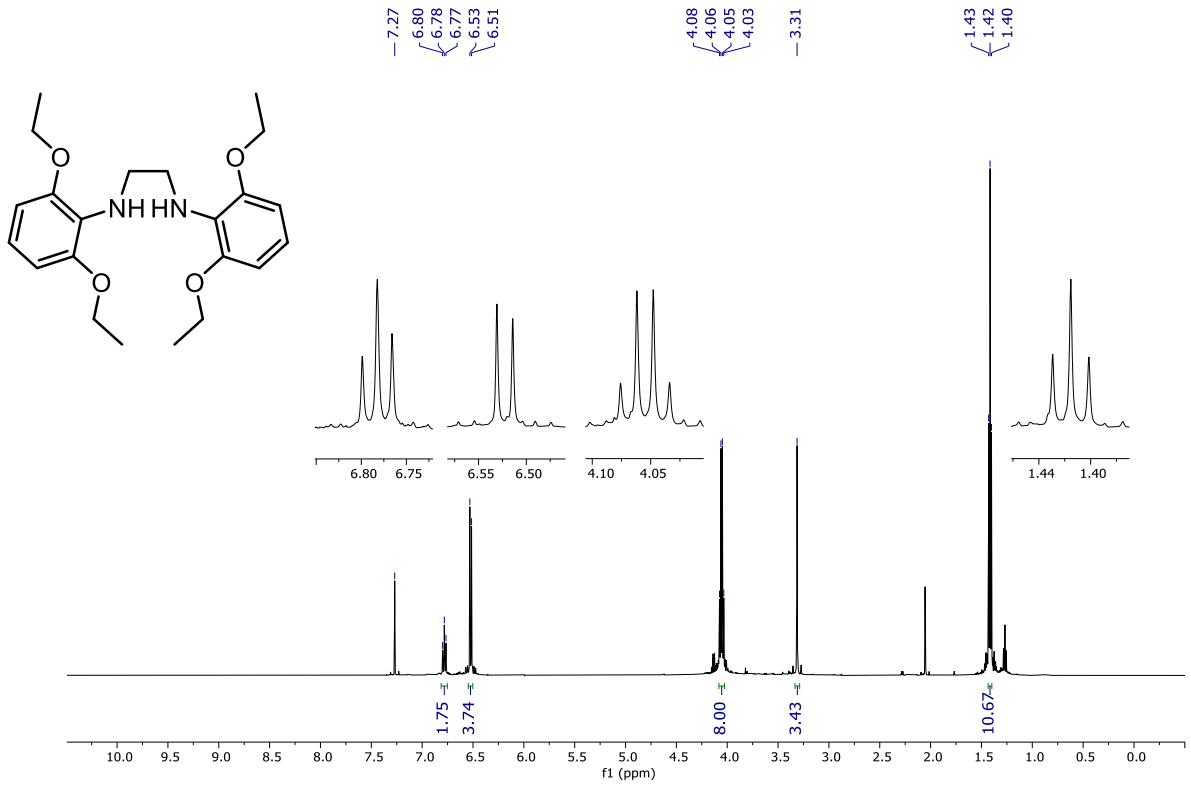

Figure A55: ^{1}H NMR spectrum of 3-17 in $CDCl_3$ at 500 MHz

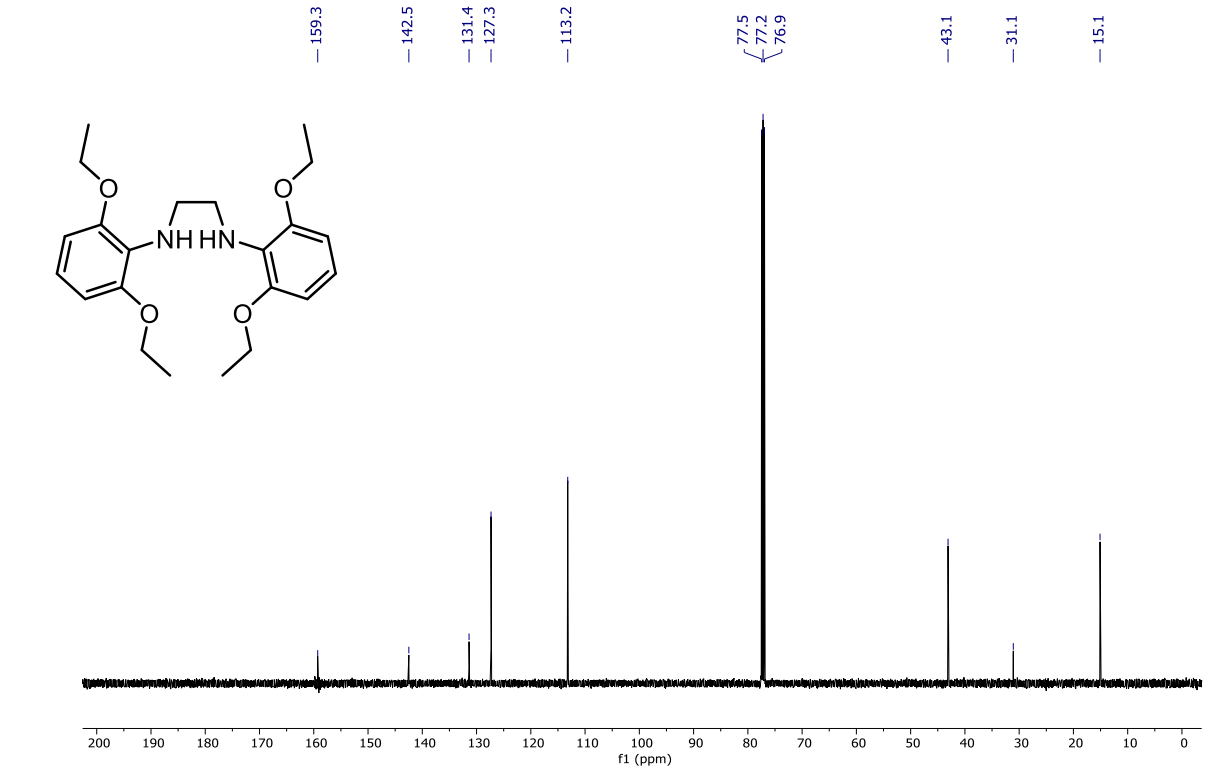

Figure A56: $^{13}C\{^{1}H\}$ NMR spectrum of 3-17 in $CDCl_3$ at 126 MHz

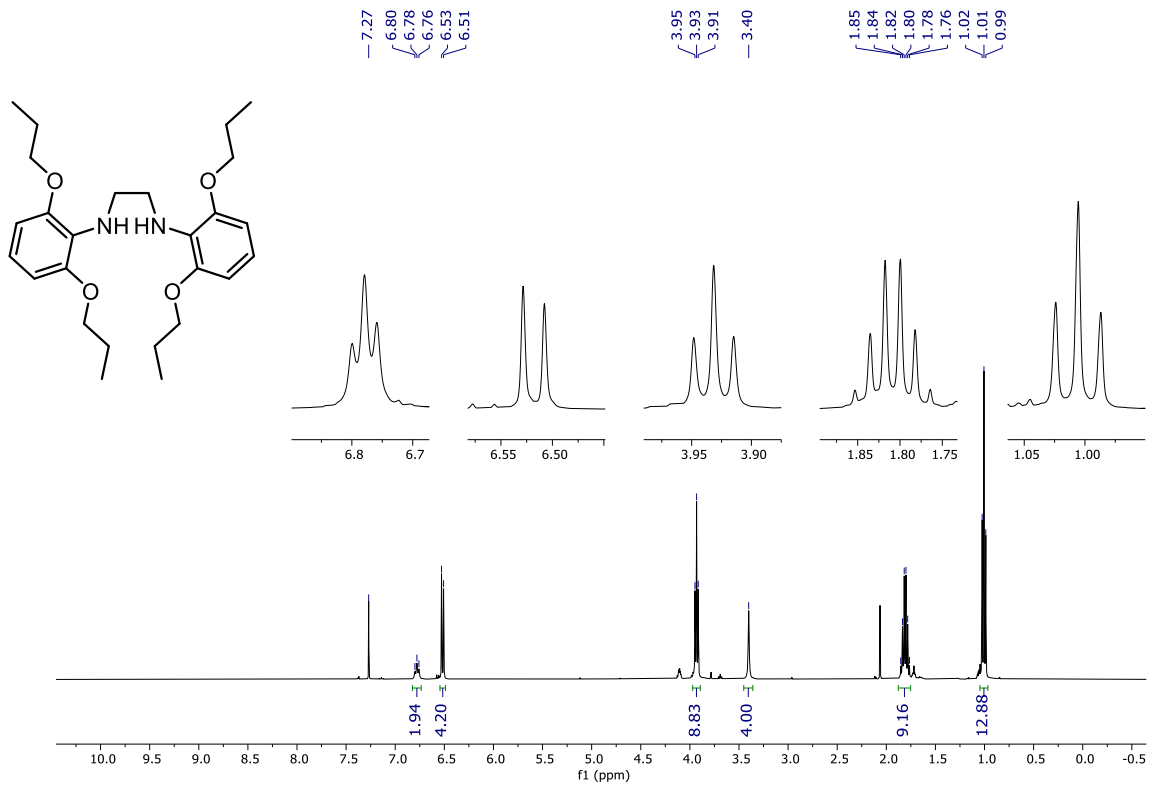

Figure A57: ^{1}H NMR spectrum of 3-18 in $CDCl_3$ at 400 MHz

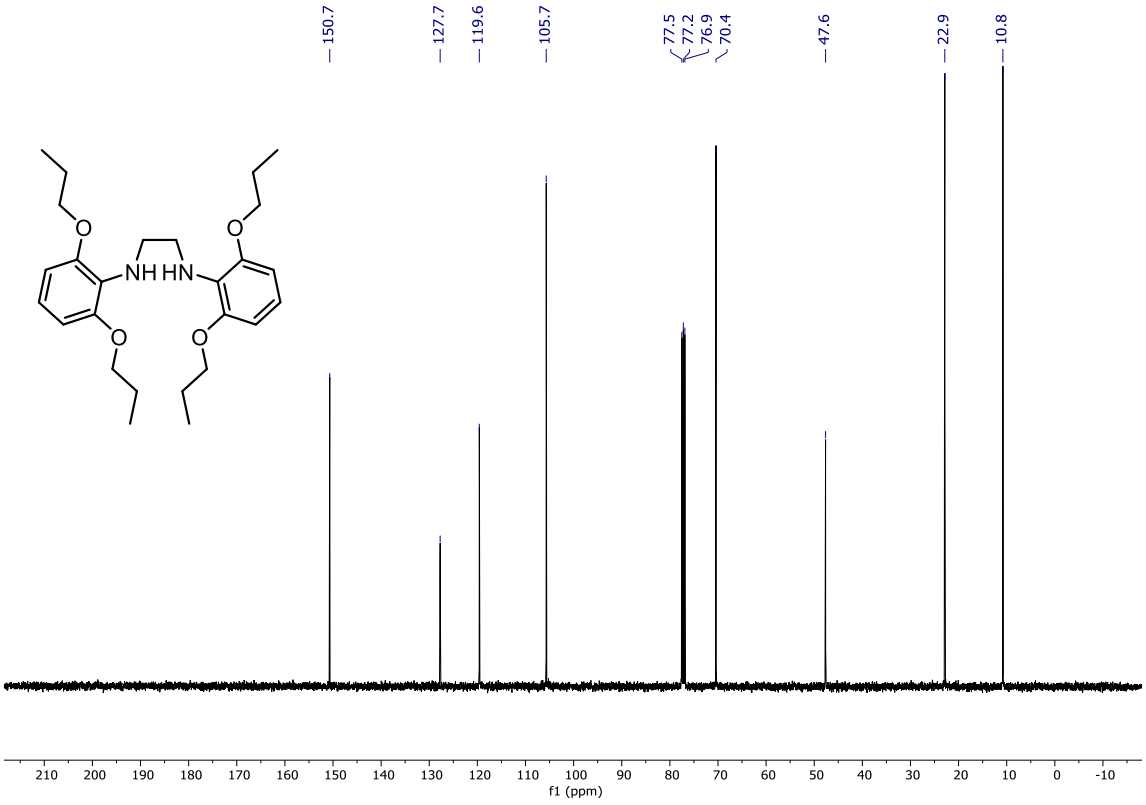

Figure A58: $^{13}C\{^{1}H\}$ NMR spectrum of 3-18 in $CDCl_3$ at 101 MHz

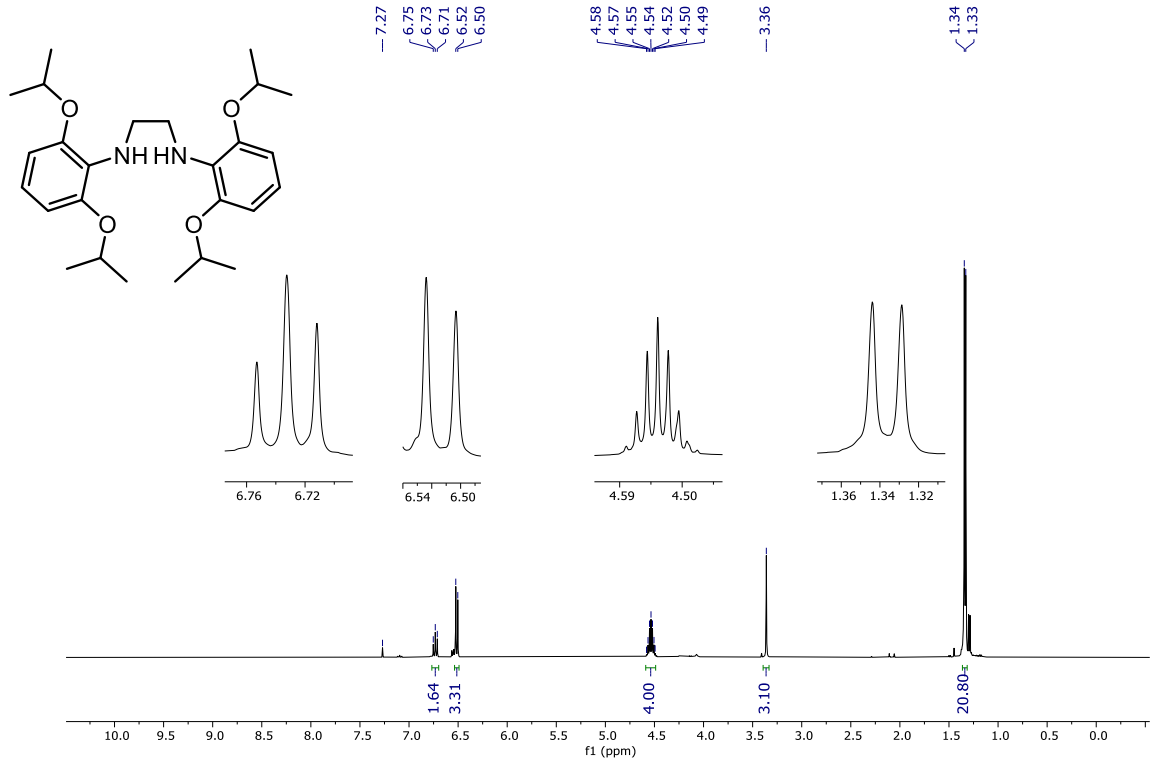

Figure A59: ^{1}H NMR spectrum of 3-19 in $CDCl_3$ at 400 MHz

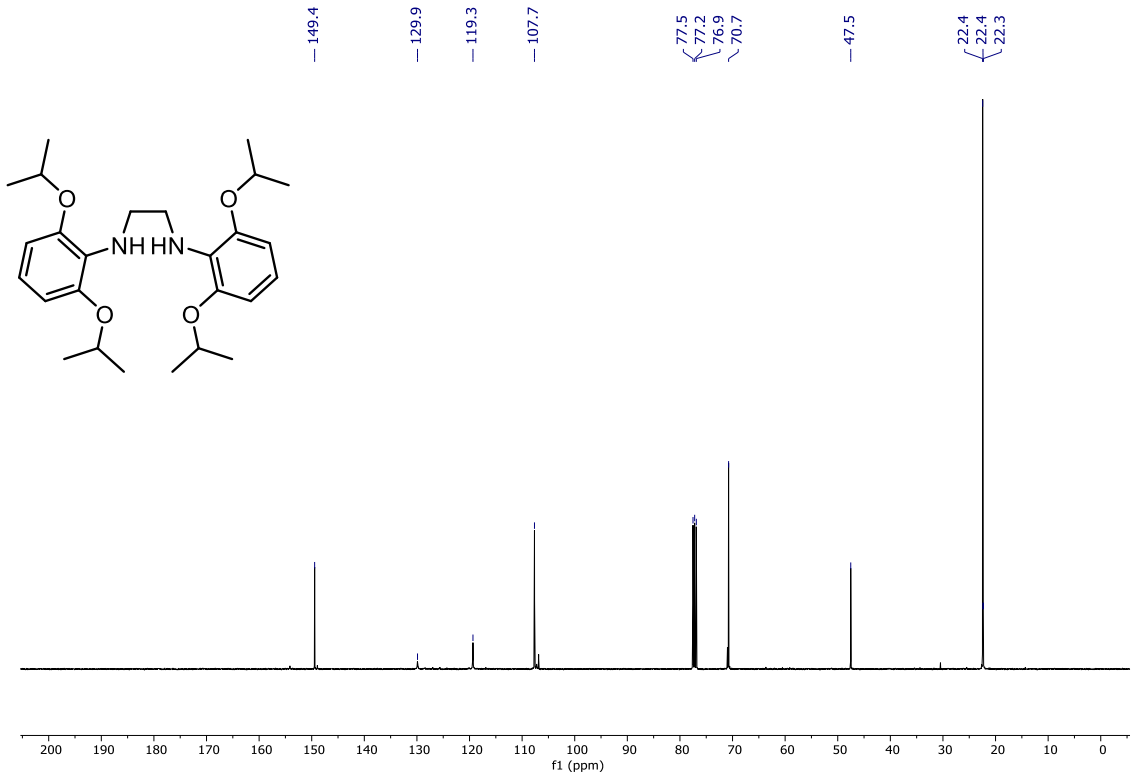

Figure A60: $^{13}C\{^{1}H\}$ NMR spectrum of 3-19 in $CDCl_3$ at 101 MHz

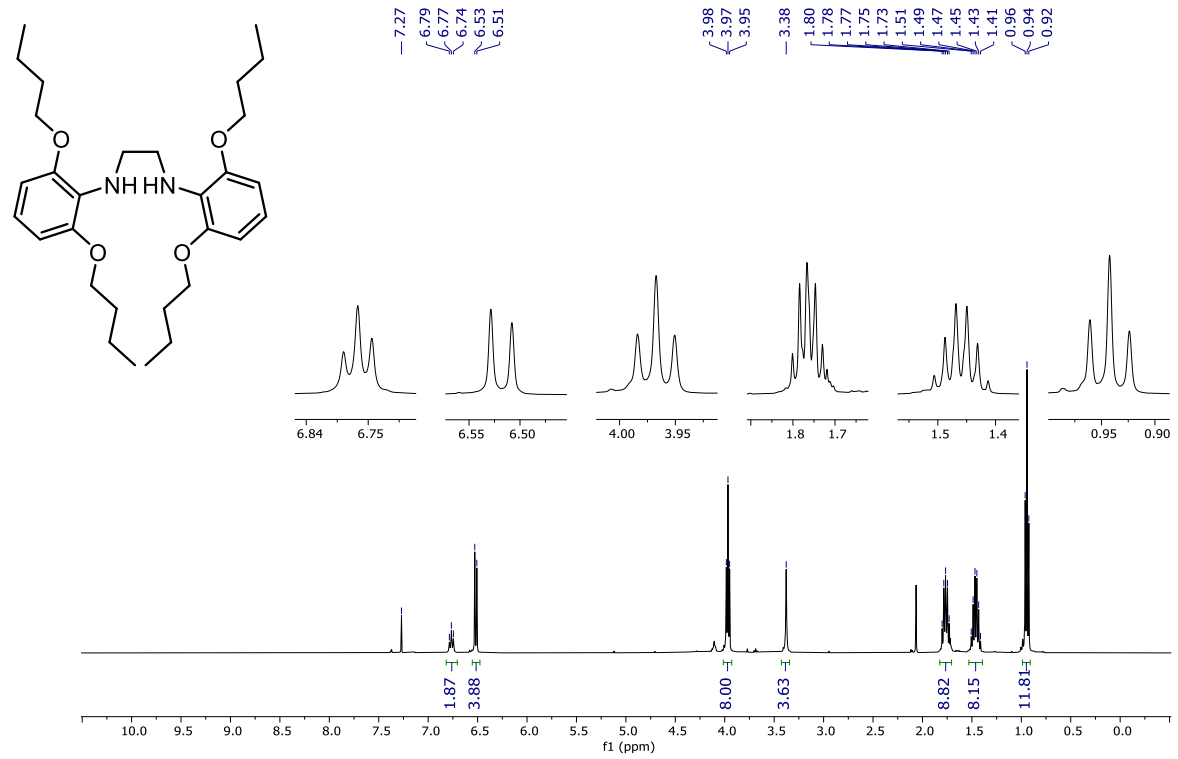

Figure A61: ^{1}H NMR spectrum of 3-20 in $CDCl_3$ at 400 MHz

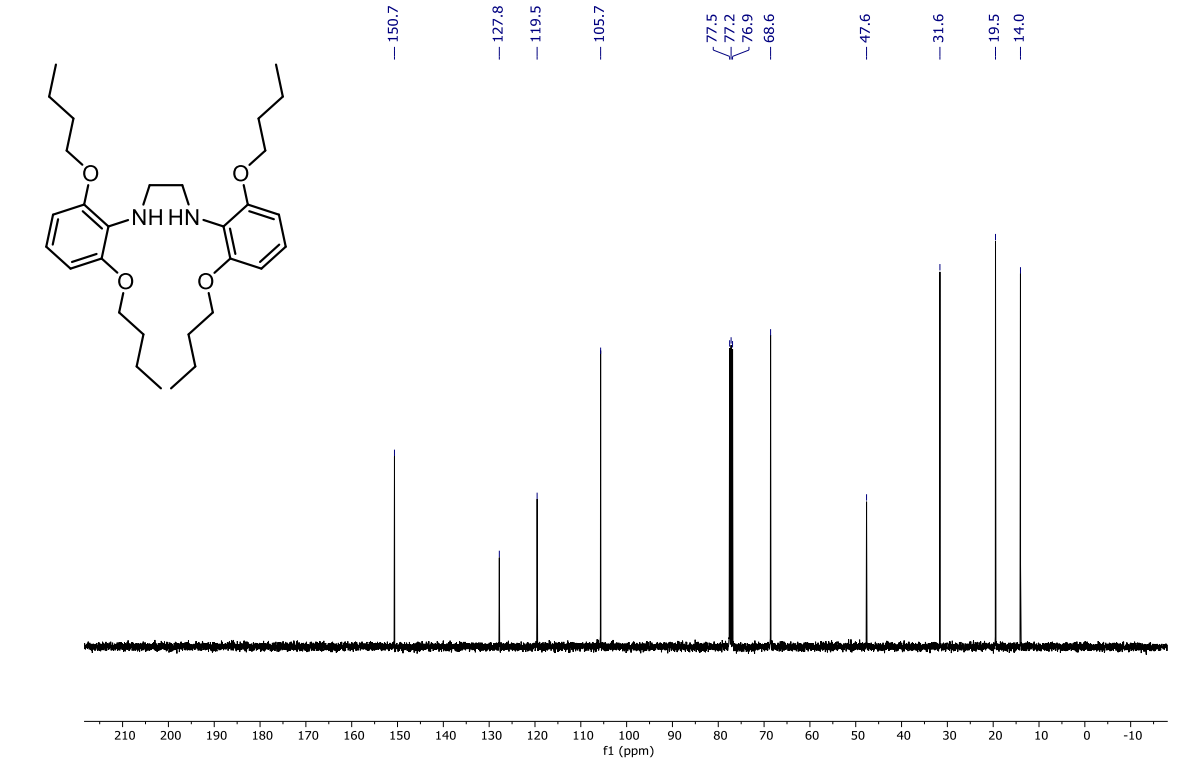

Figure A62: $^{13}C\{^{1}H\}$ NMR spectrum of 3-20 in $CDCl_3$ at 101 MHz

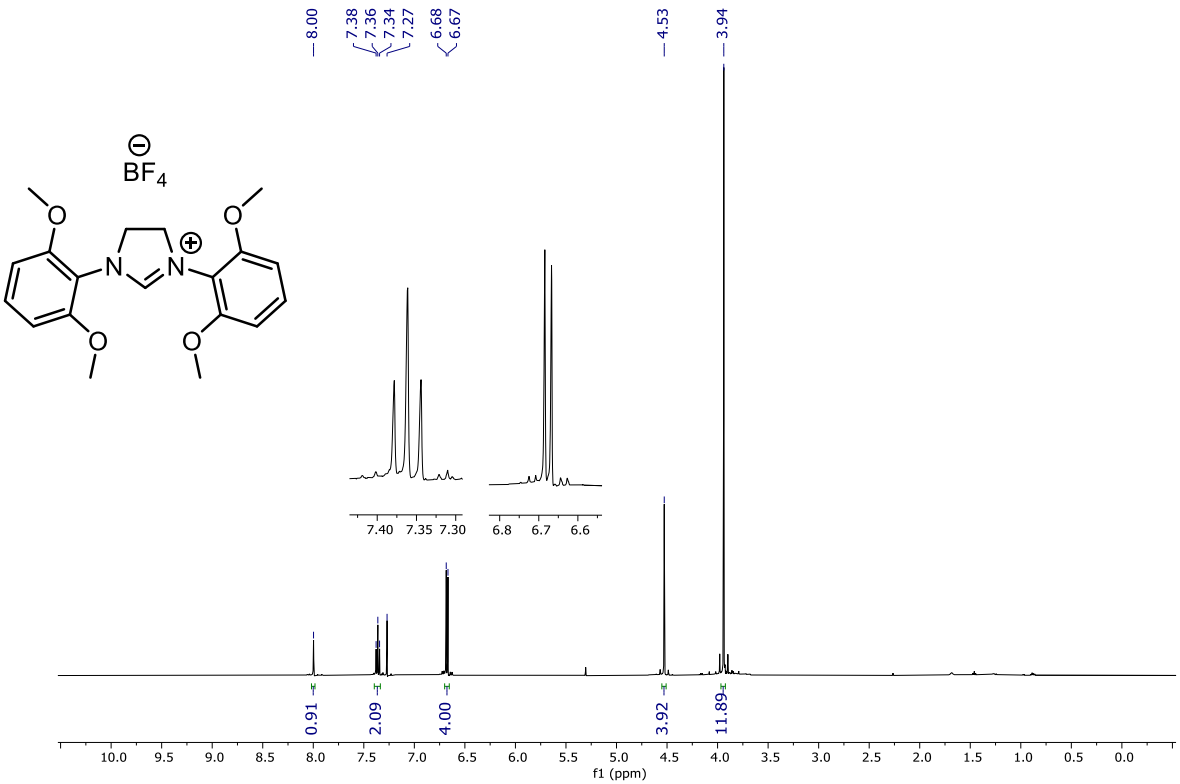

Figure A63: ^{1}H NMR spectrum of 3-23 in $CDCl_3$ at 500 MHz

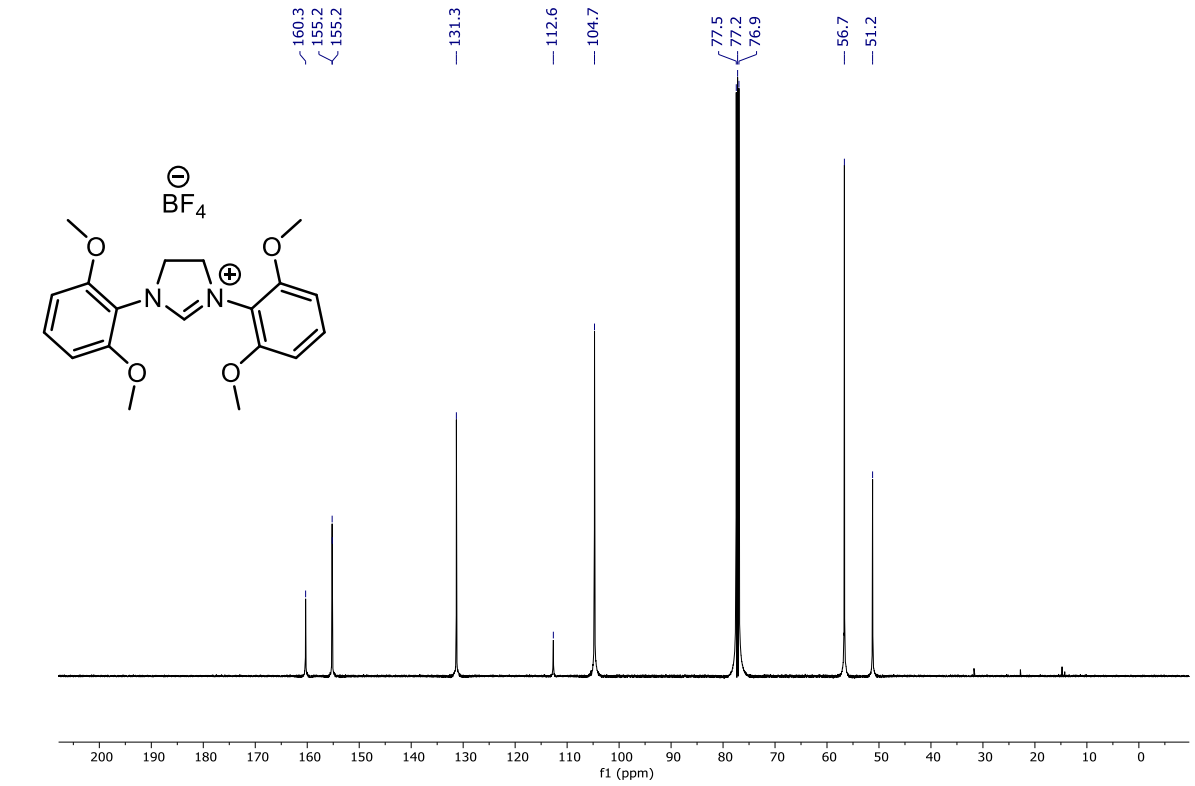

Figure A64: $^{13}C\{^{1}H\}$ NMR spectrum of 3-23 in $CDCl_3$ at 126 MHz

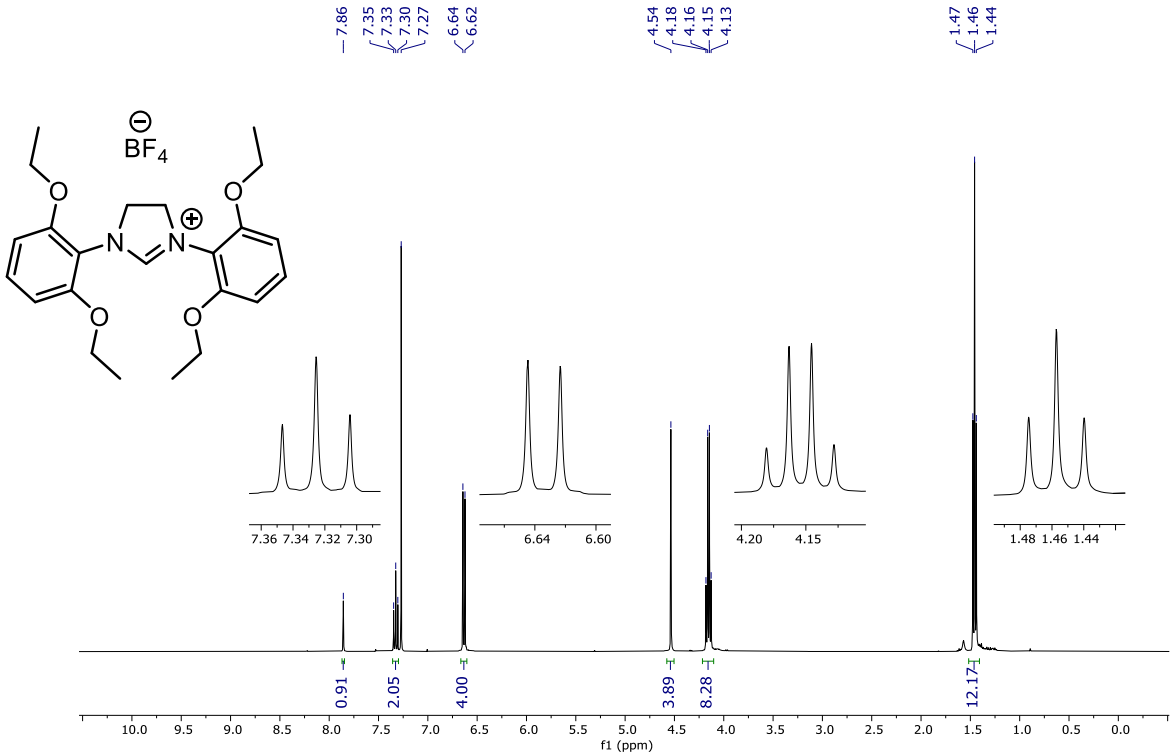

Figure A65: ^{1}H NMR spectrum of 3-24 in $CDCl_3$ at 400 MHz

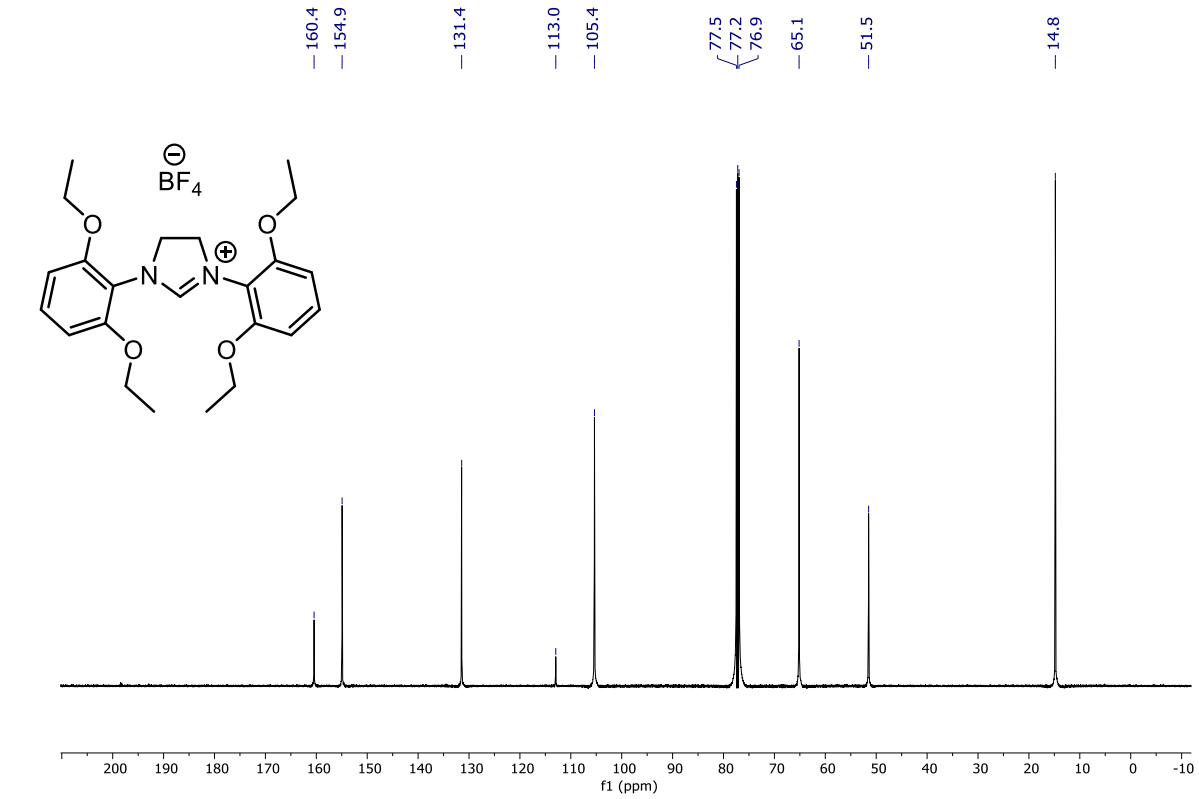

Figure A66: $^{13}C\{^{1}H\}$ NMR spectrum of 3-24 in $CDCl_3$ at 126 MHz

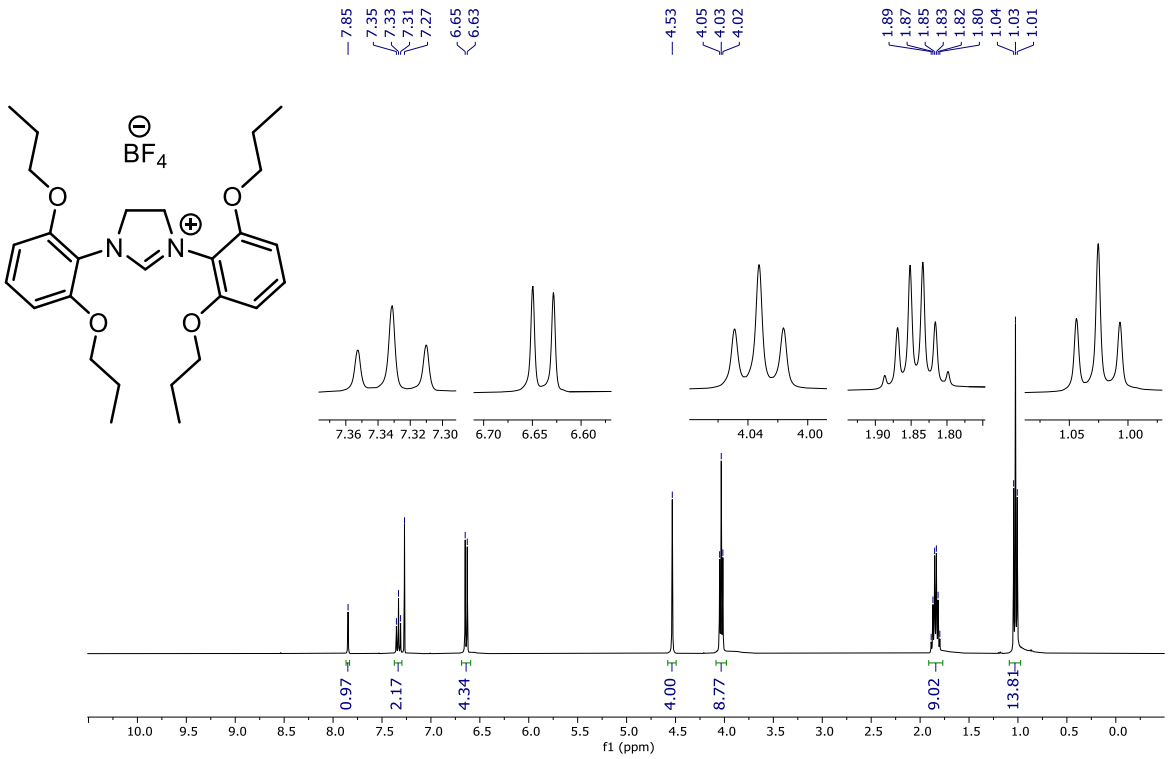

Figure A67: ^{1}H NMR spectrum of 3-25 in $CDCl_3$ at 400 MHz

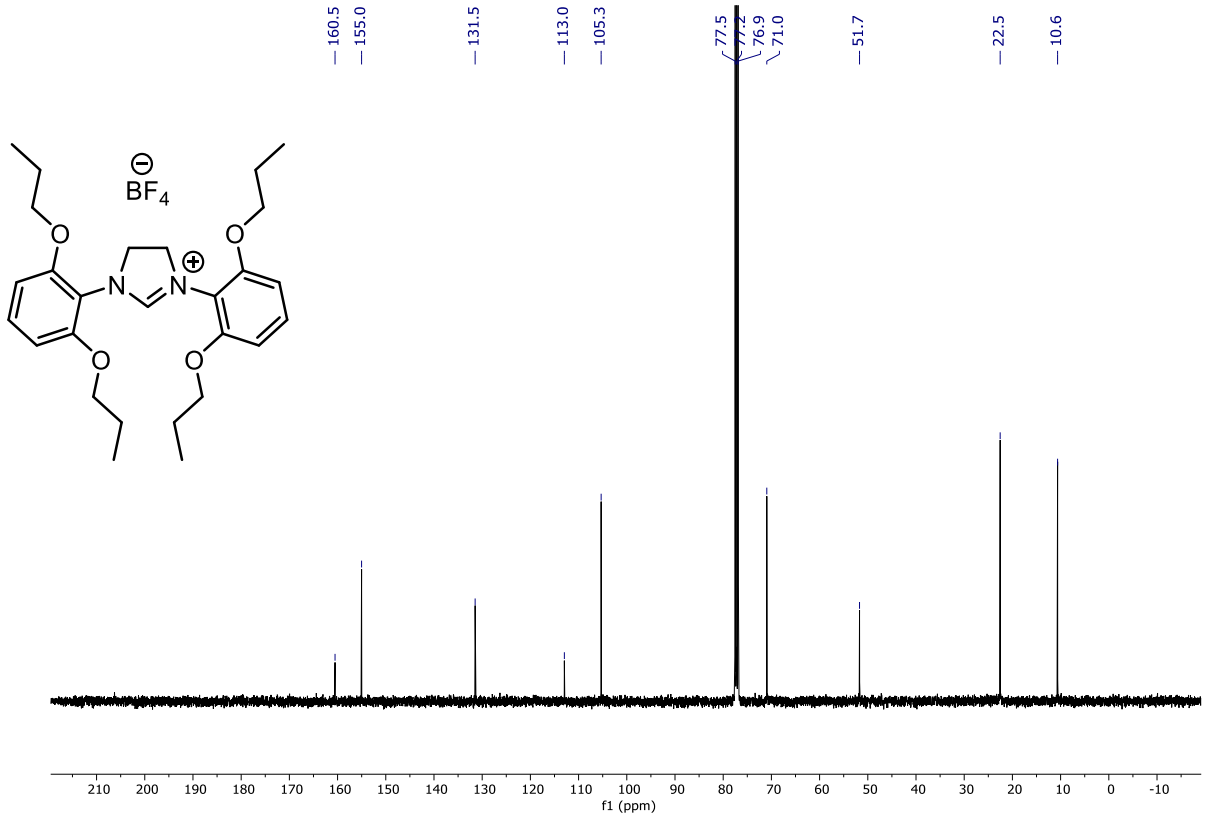

Figure A68: $^{13}C\{^{1}H\}$ NMR spectrum of 3-25 in $CDCl_3$ at 101 MHz

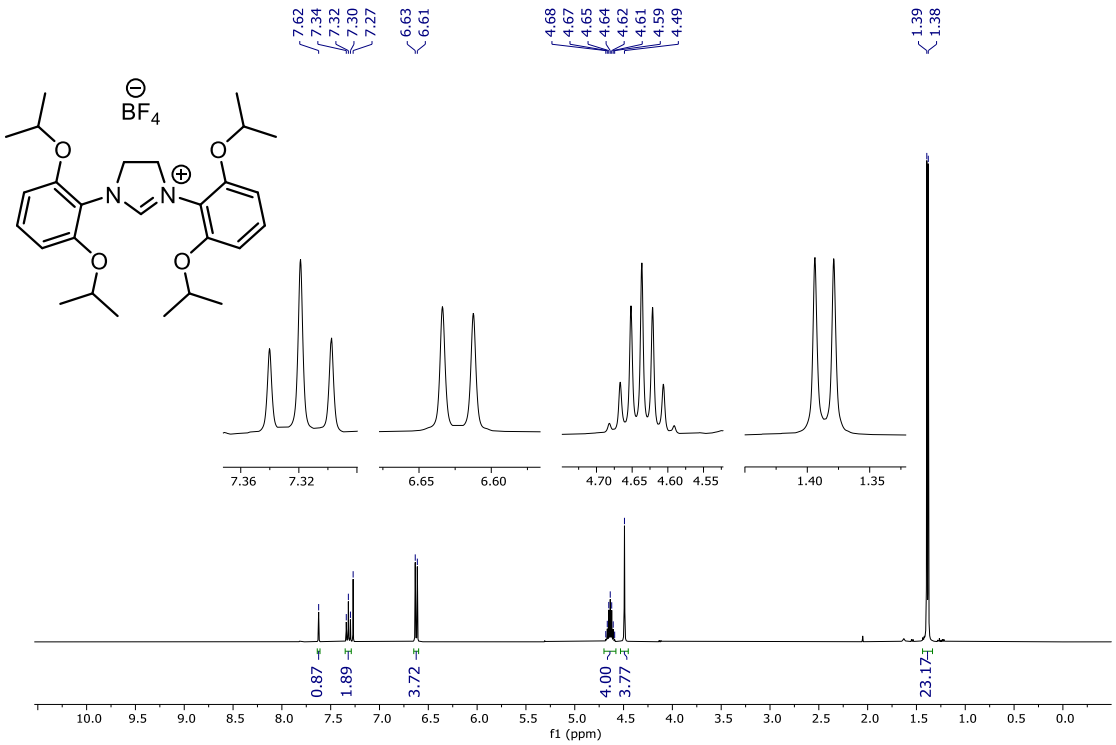

Figure A69: ^{1}H NMR spectrum of 3-26 in $CDCl_3$ at 400 MHz

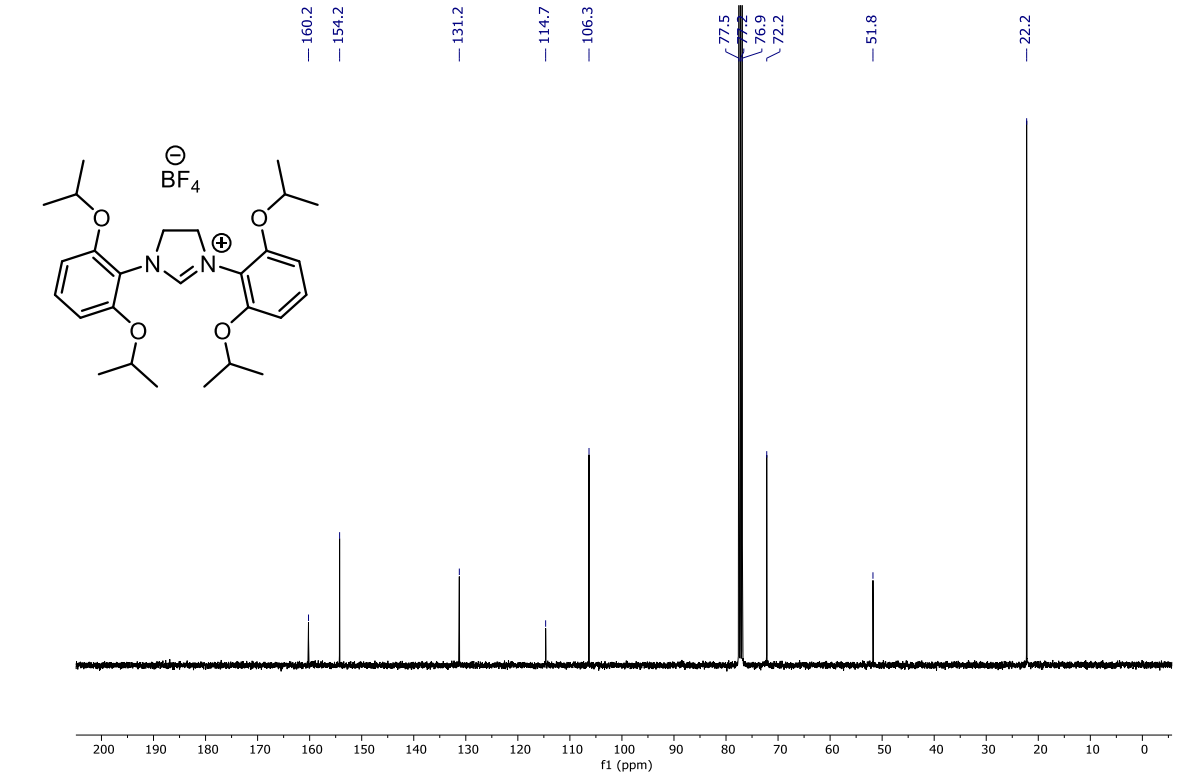

Figure A70: $^{13}C\{^{1}H\}$ NMR spectrum of 3-26 in $CDCl_3$ at 101 MHz

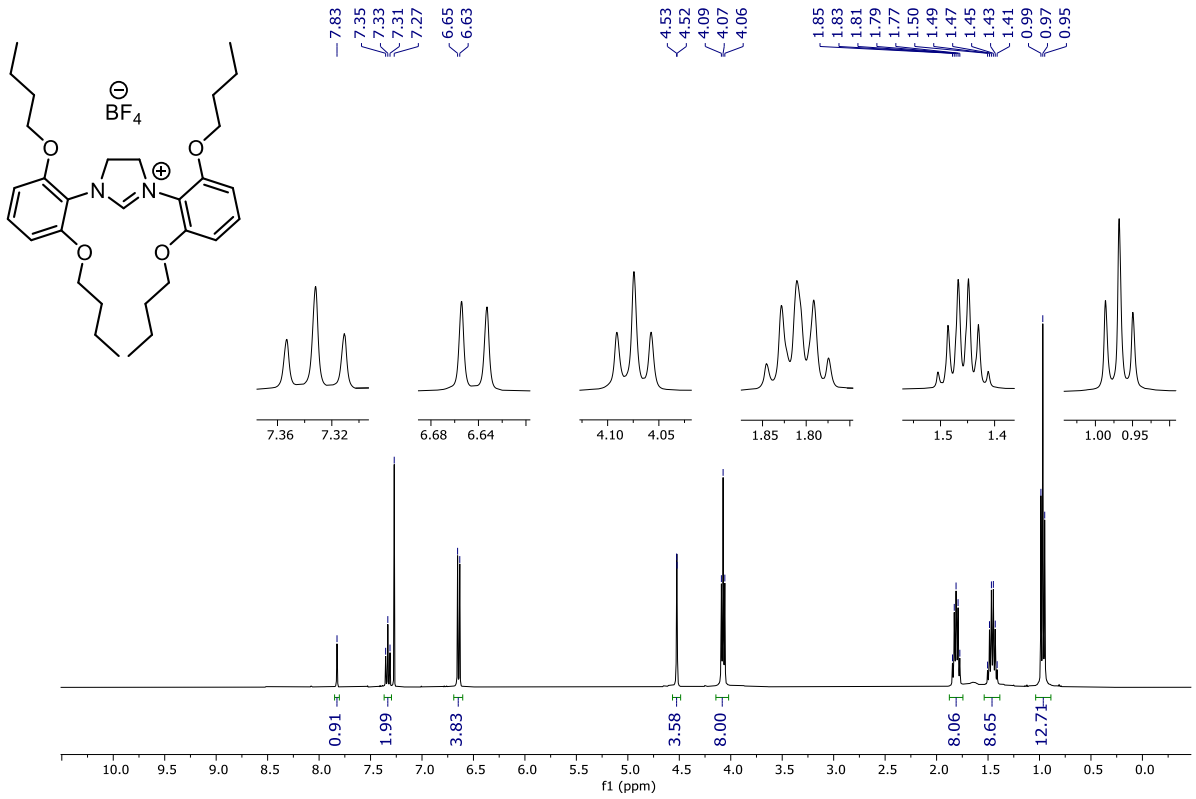

Figure A71: ^{1}H NMR spectrum of 3-27 in $CDCl_3$ at 400 MHz

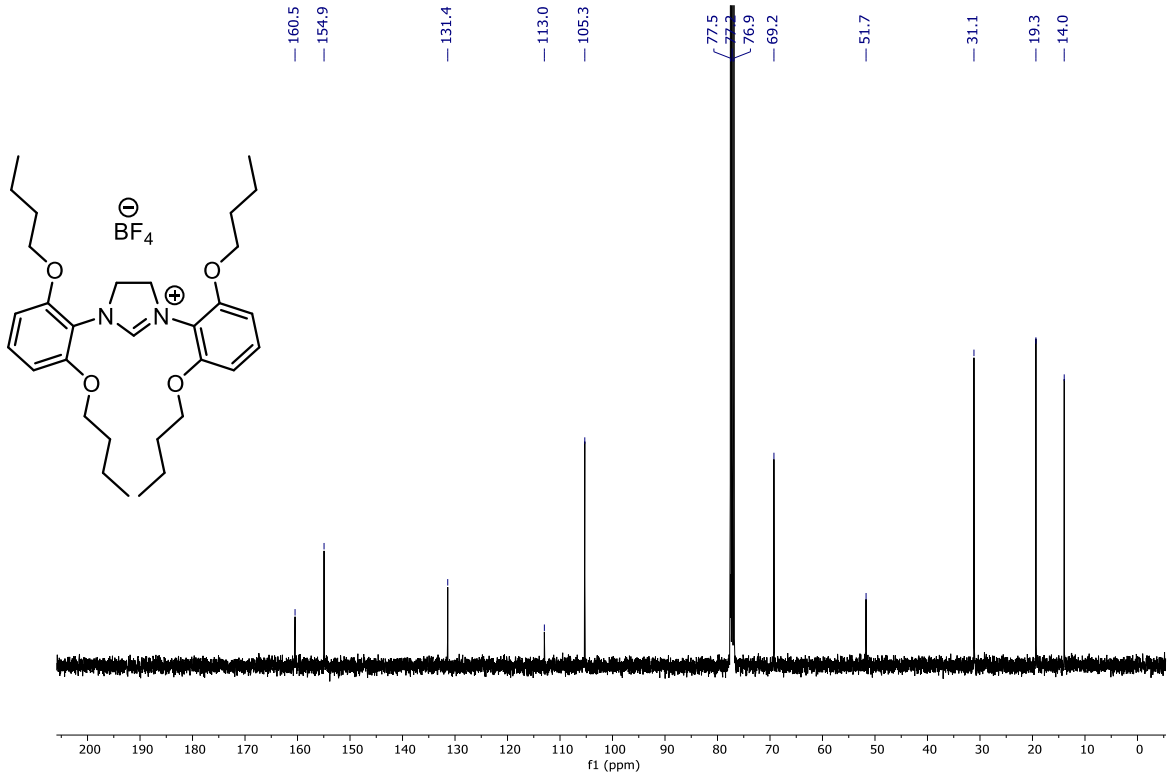

Figure A72: $^{13}C\{^{1}H\}$ NMR spectrum of 3-27 in $CDCl_3$ at 101 MHz

Figure A73: ^{1}H NMR spectrum of 3-28 in $CDCl_3$ at 400 MHz

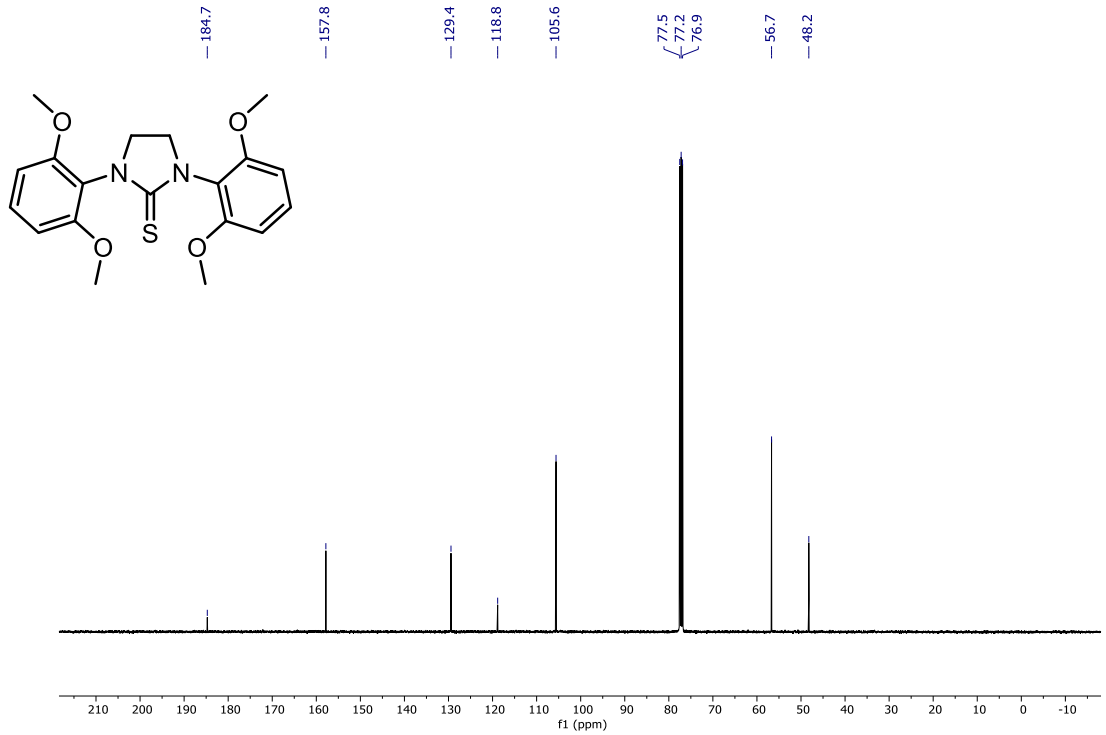

Figure A74: $^{13}C\{^{1}H\}$ NMR spectrum of 3-28 in $CDCl_3$ at 101 MHz

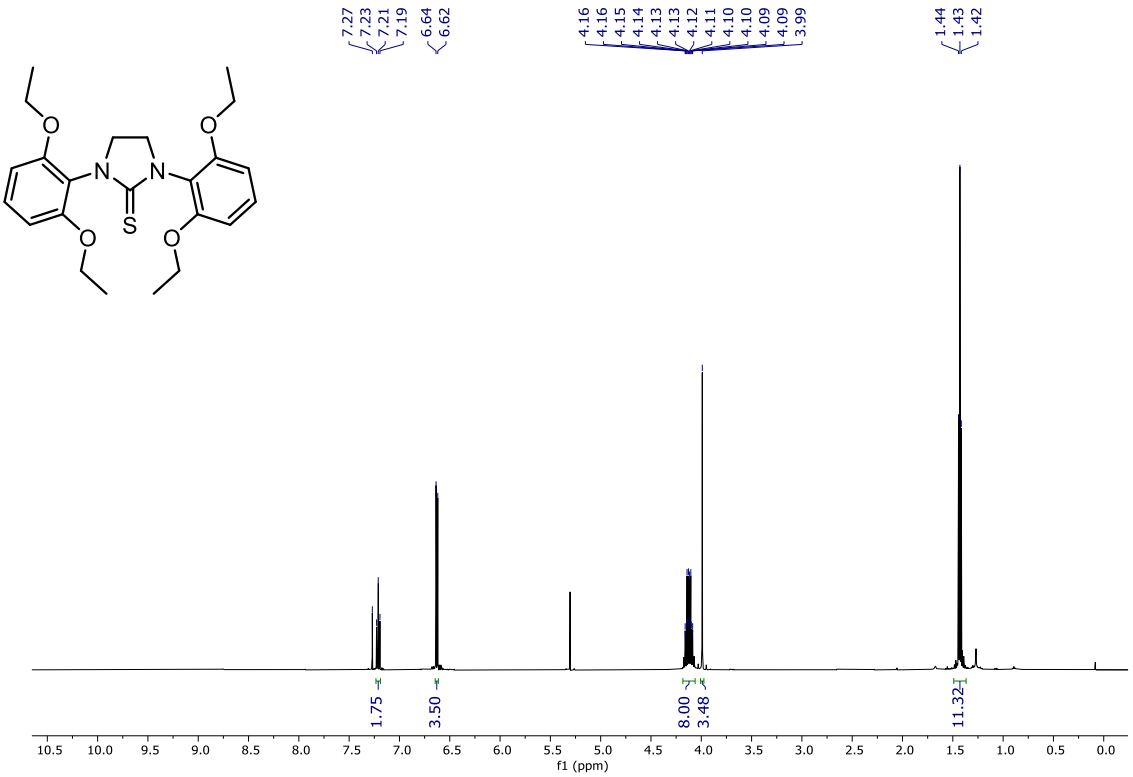

Figure A75: ^{1}H NMR spectrum of 3-29 in $CDCl_3$ at 500 MHz

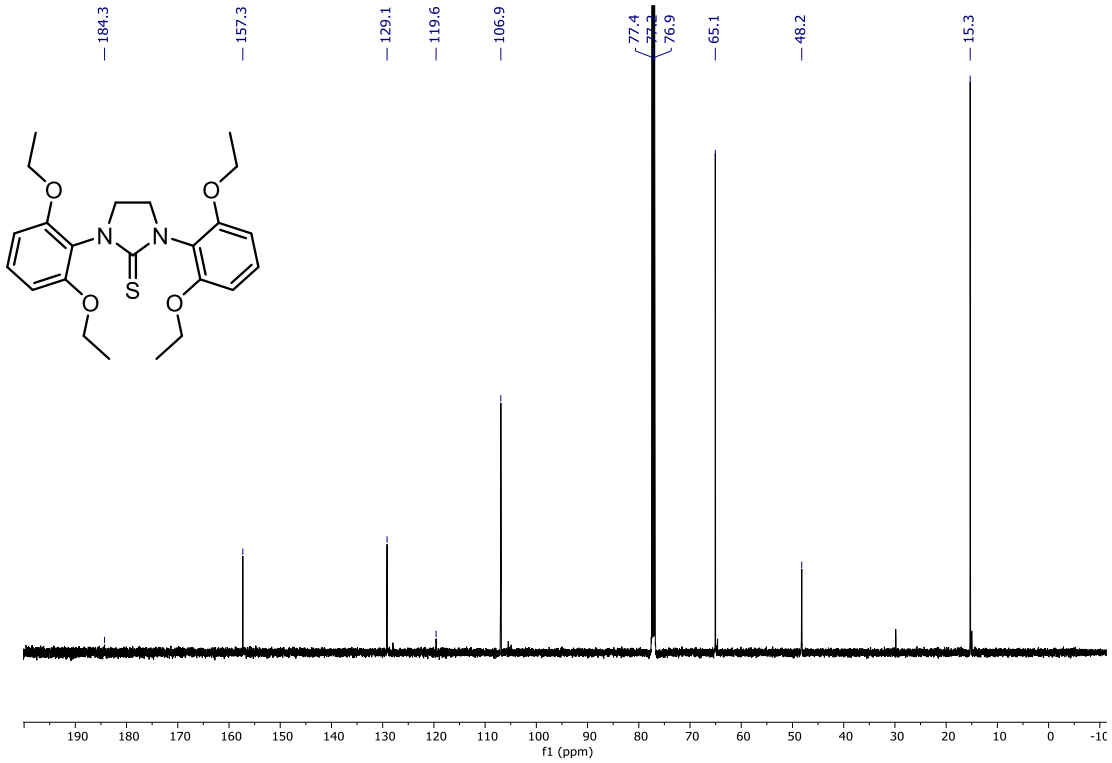

Figure A76: $^{13}C\{^{1}H\}$ NMR spectrum of 3-29 in $CDCl_3$ at 126 MHz

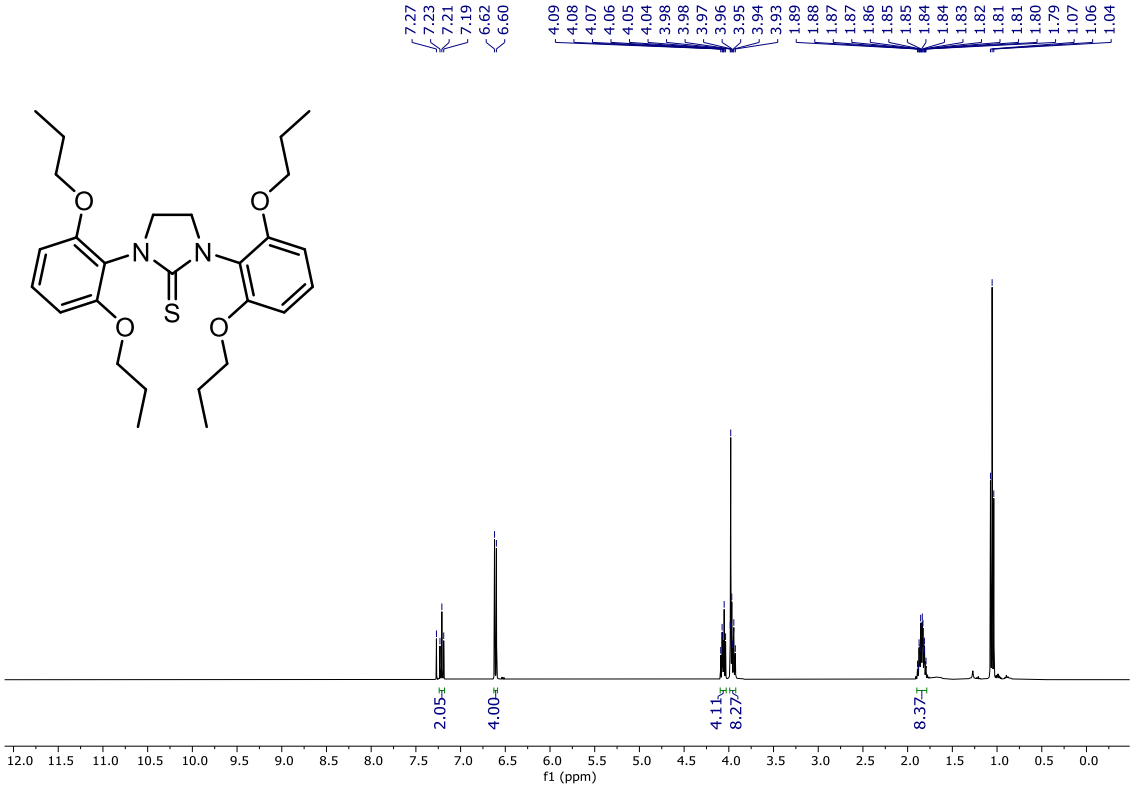

Figure A77: ^{1}H NMR spectrum of 3-30 in $CDCl_3$ at 400 MHz

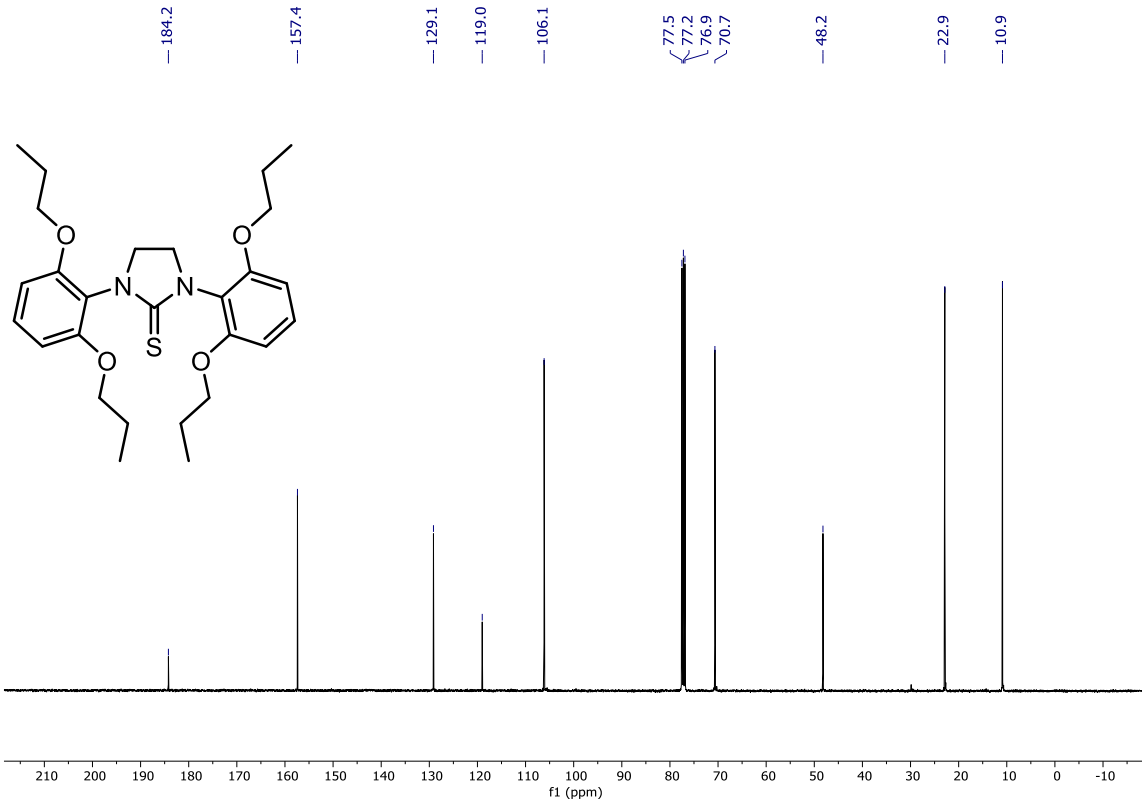

Figure A 78: $^{13}C\{^{1}H\}$ NMR spectrum of 3-30 in $CDCl_3$ at 101 MHz

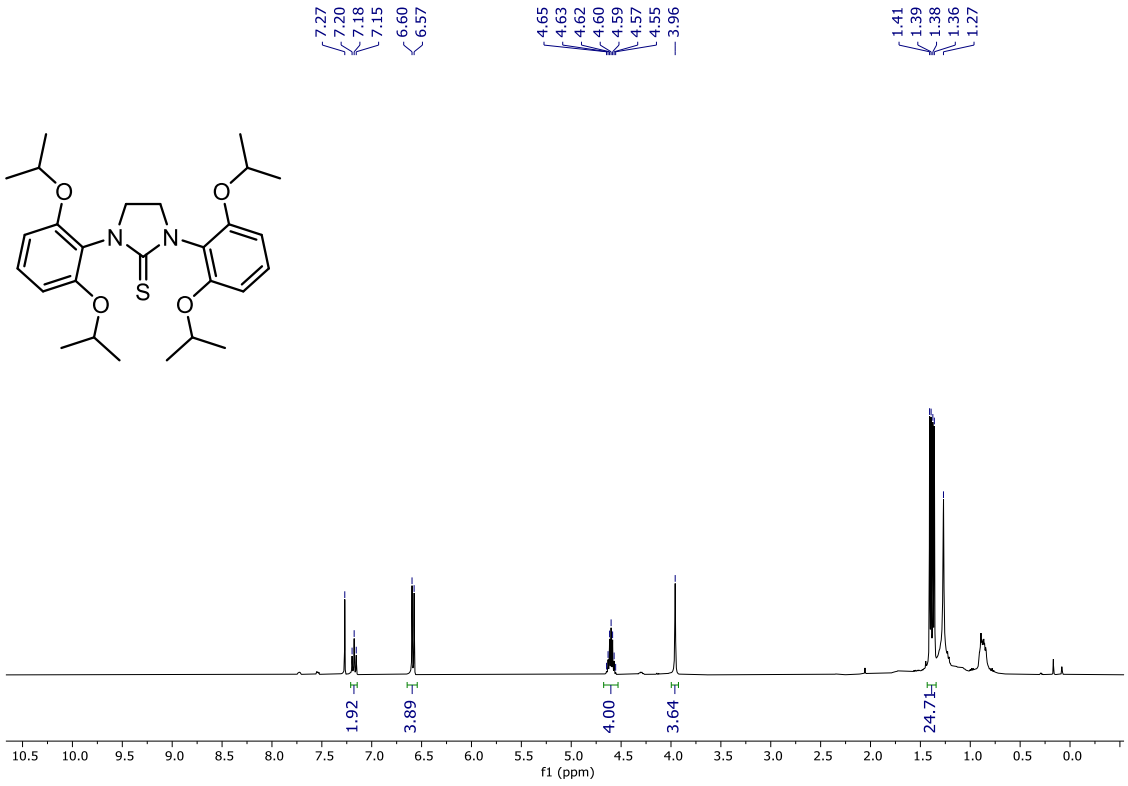

Figure A79: ^{1}H NMR spectrum of 3-31 in $CDCl_3$ at 400 MHz

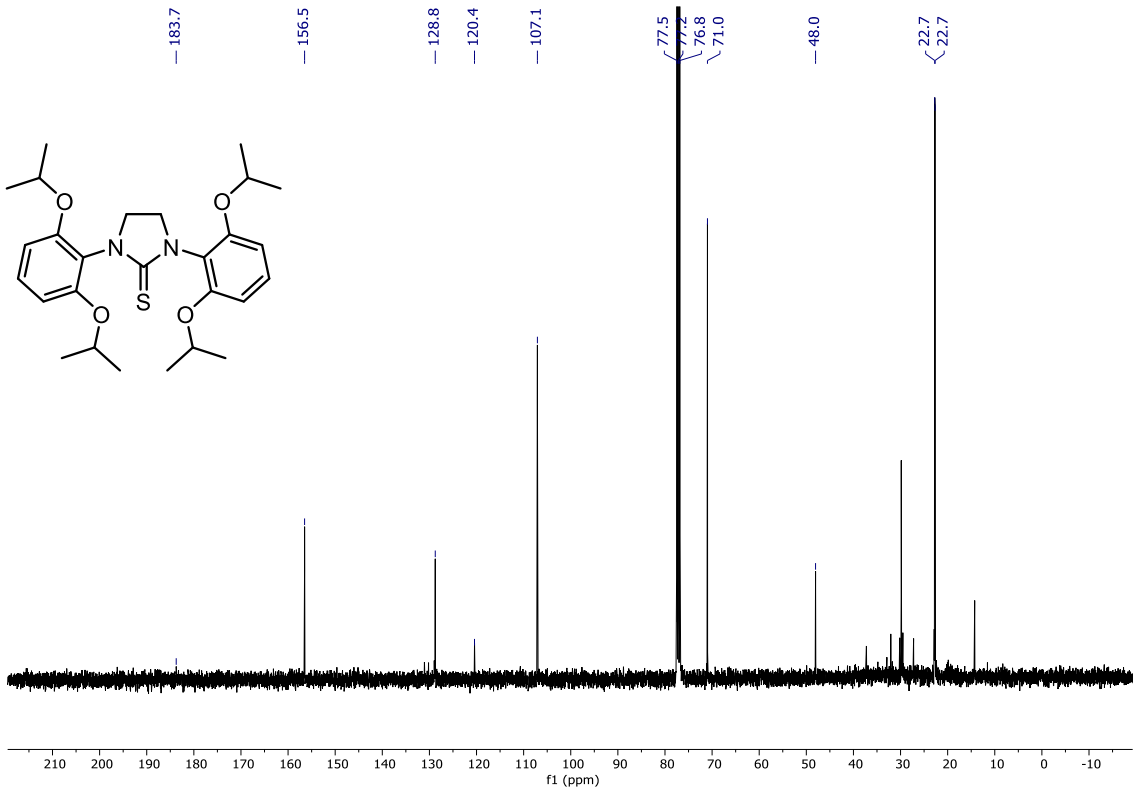

Figure A80: $^{13}C\{^{1}H\}$ NMR spectrum of 3-31 in $CDCl_3$ at 101 MHz

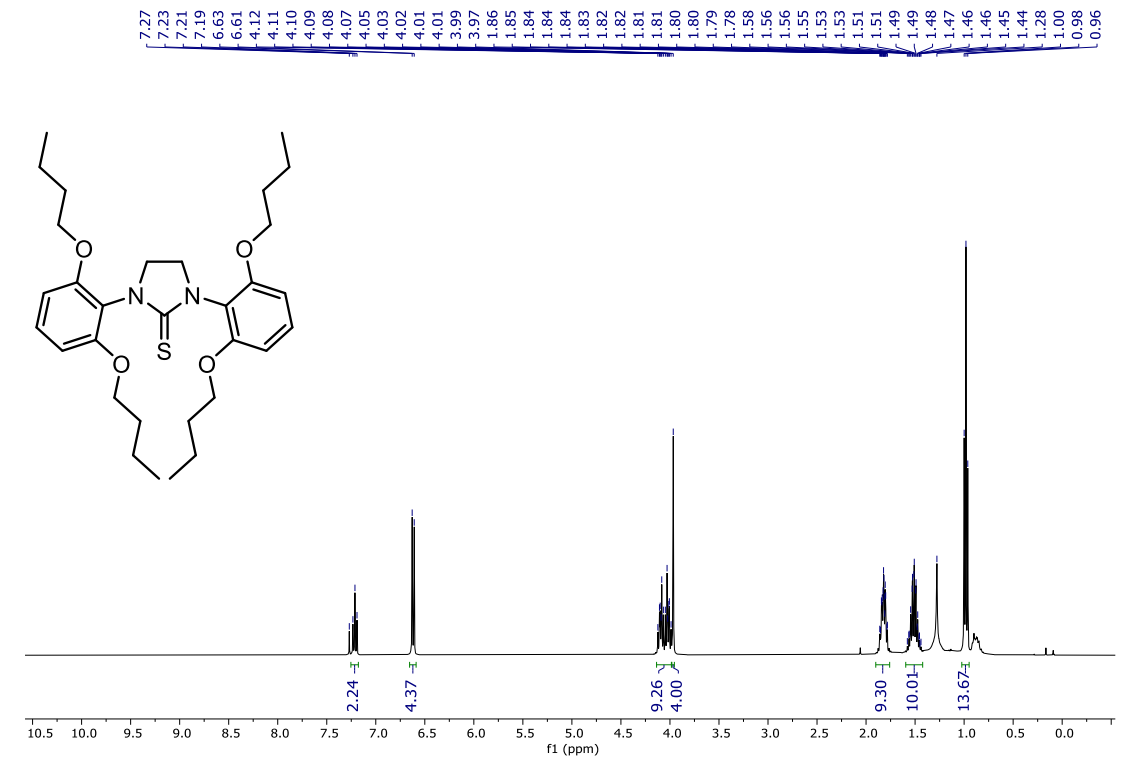

Figure A81: ^{1}H NMR spectrum of 3-32 in $CDCl_3$ at 400 MHz

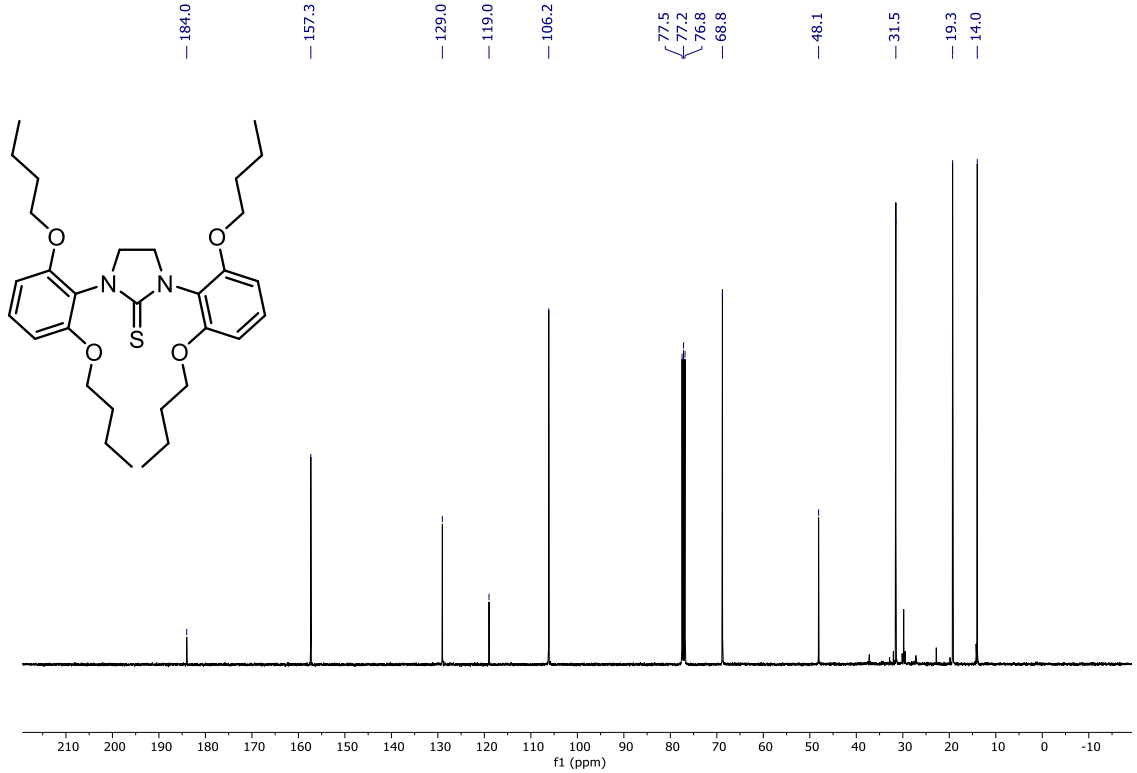

Figure A82: $^{13}C\{^{1}H\}$ NMR spectrum of 3-32 in $CDCl_3$ at 101 MHz

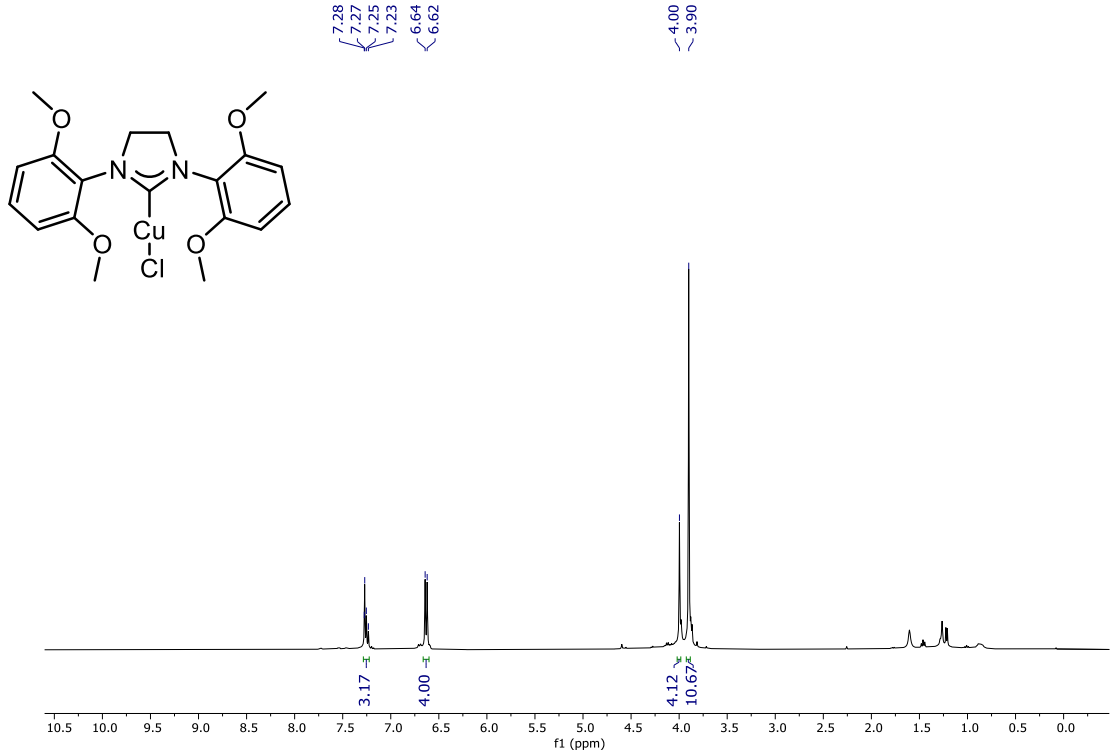

Figure A83: ^{1}H NMR spectrum of 3-33 in $CDCl_3$ at 400 MHz

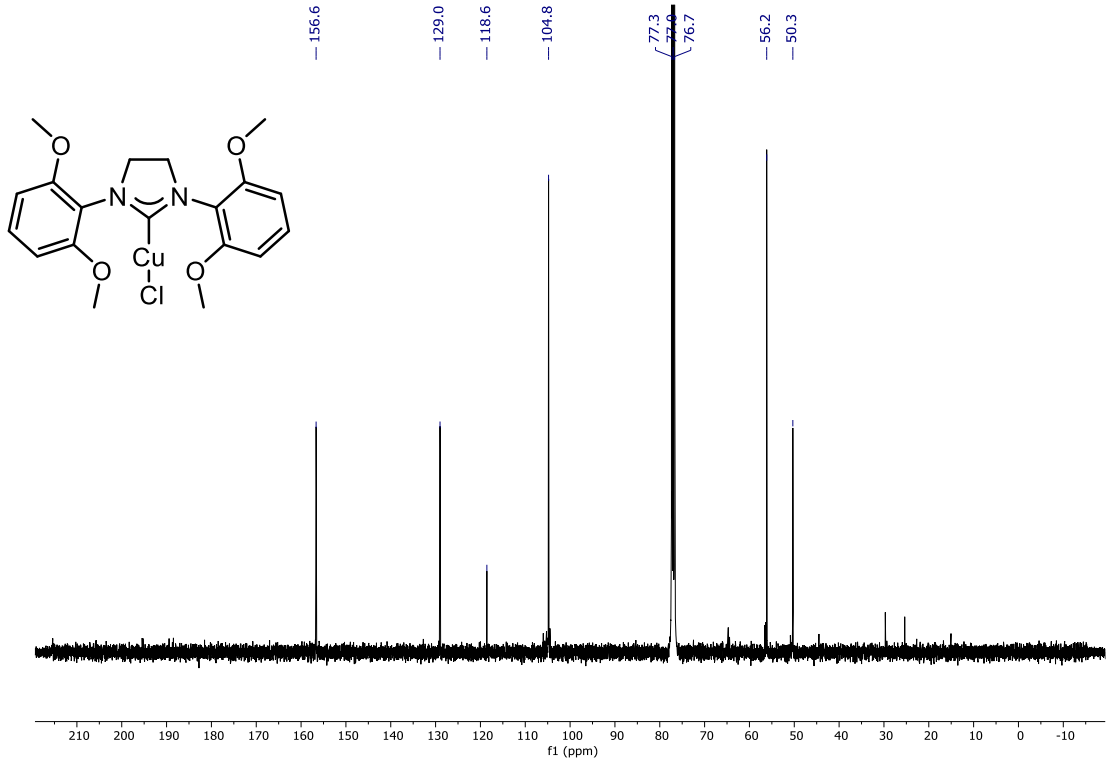

Figure A84: ^{13}C{^{1}H} NMR spectrum of 3-33 in $CDCl_3$ at 101 MHz

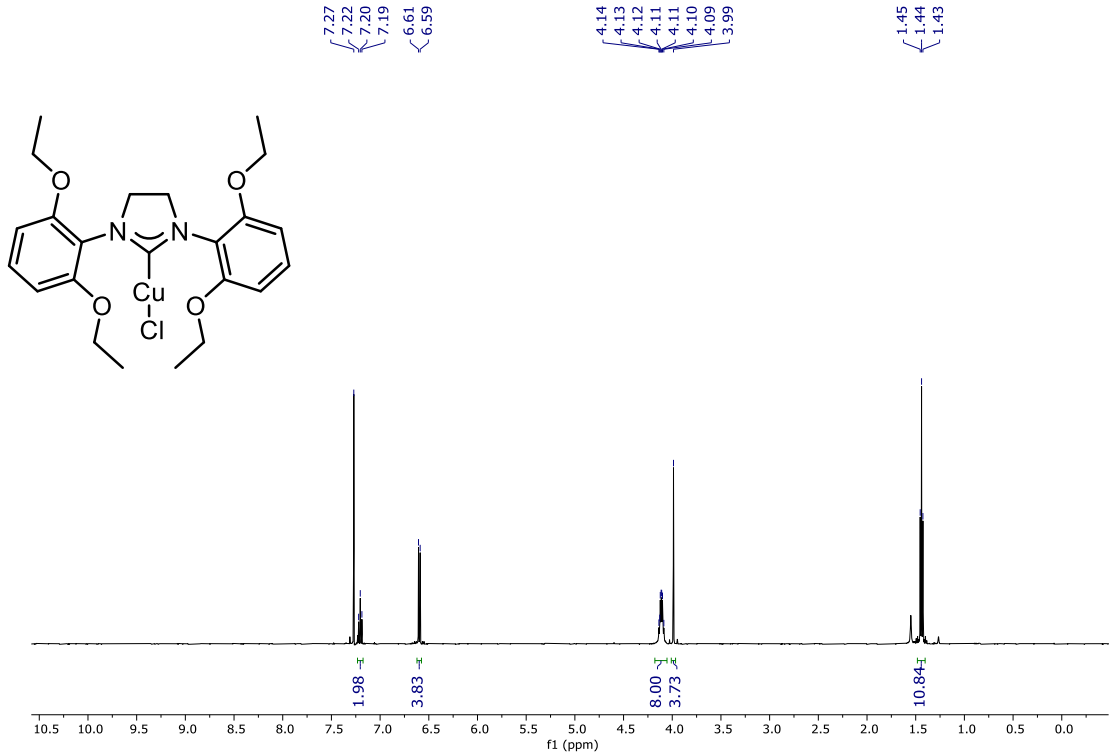

Figure A85: ^{1}H NMR spectrum of 3-34 in $CDCl_3$ at 500 MHz

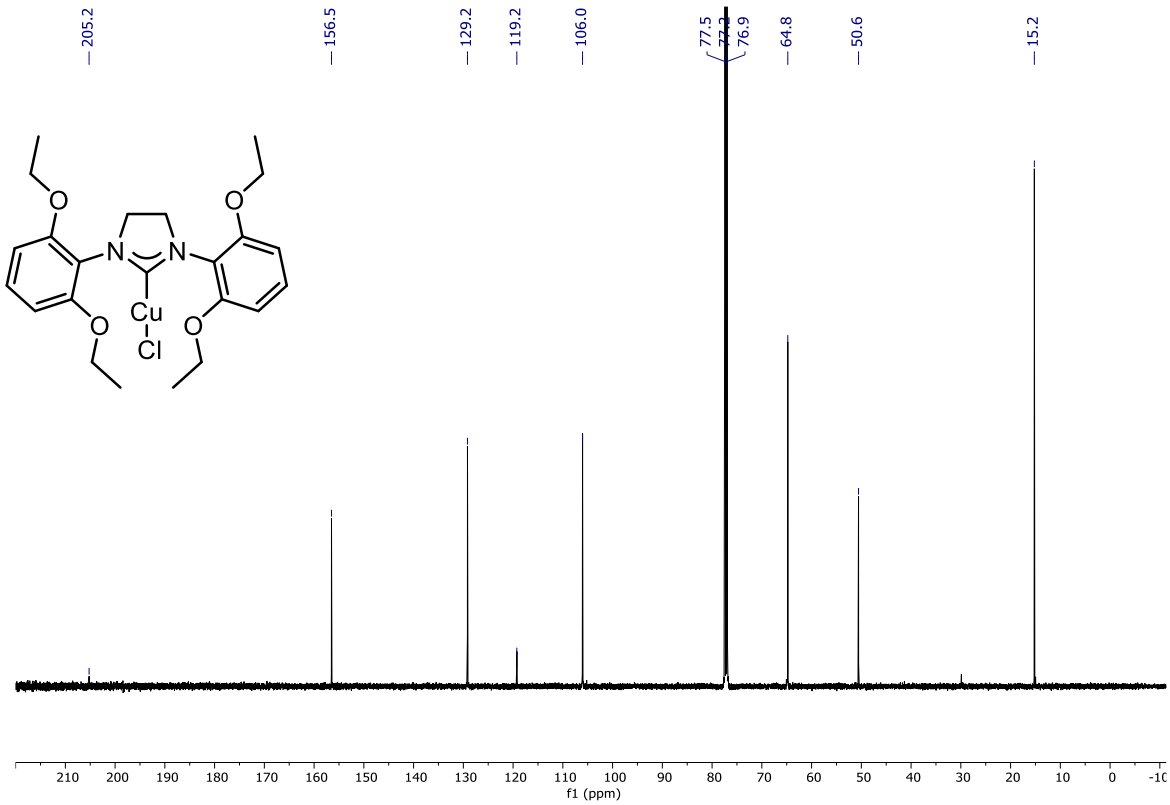

Figure A86: $^{13}C\{^{1}H\}$ NMR spectrum of 3-34 in $CDCl_3$ at 126 MHz

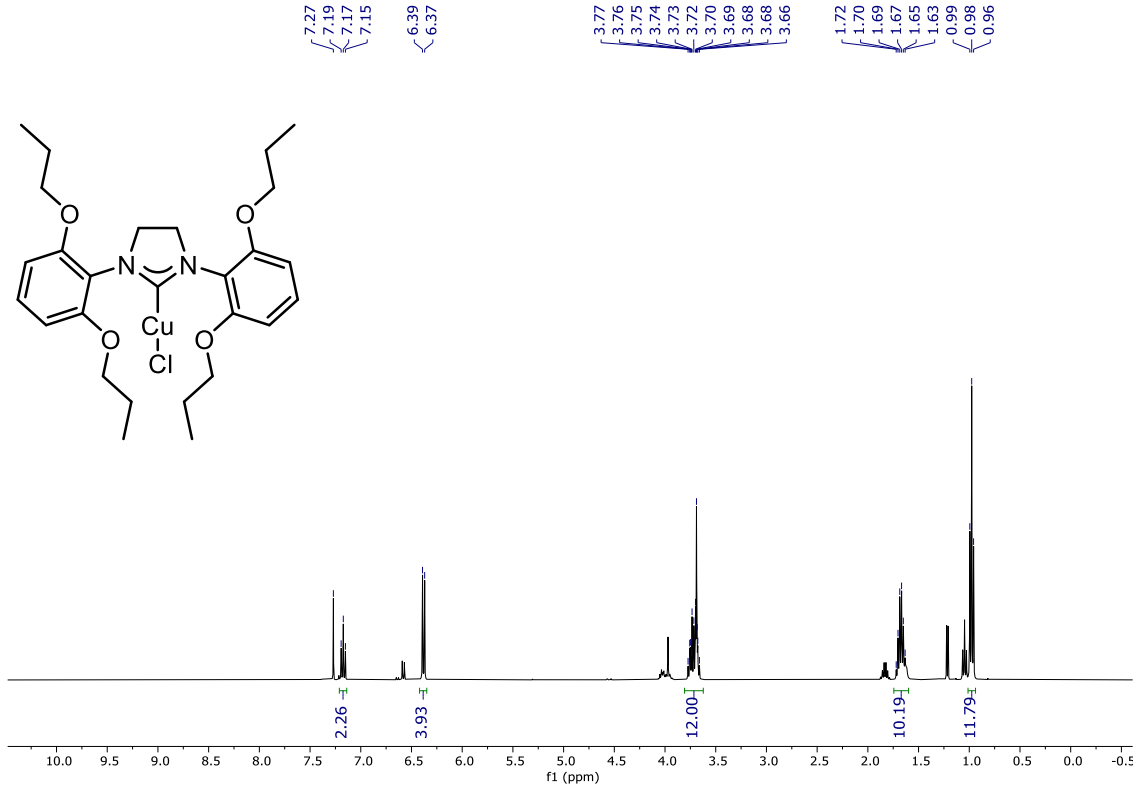

Figure A87: ^{1}H NMR spectrum of 3-35 in $CDCl_3$ at 400 MHz

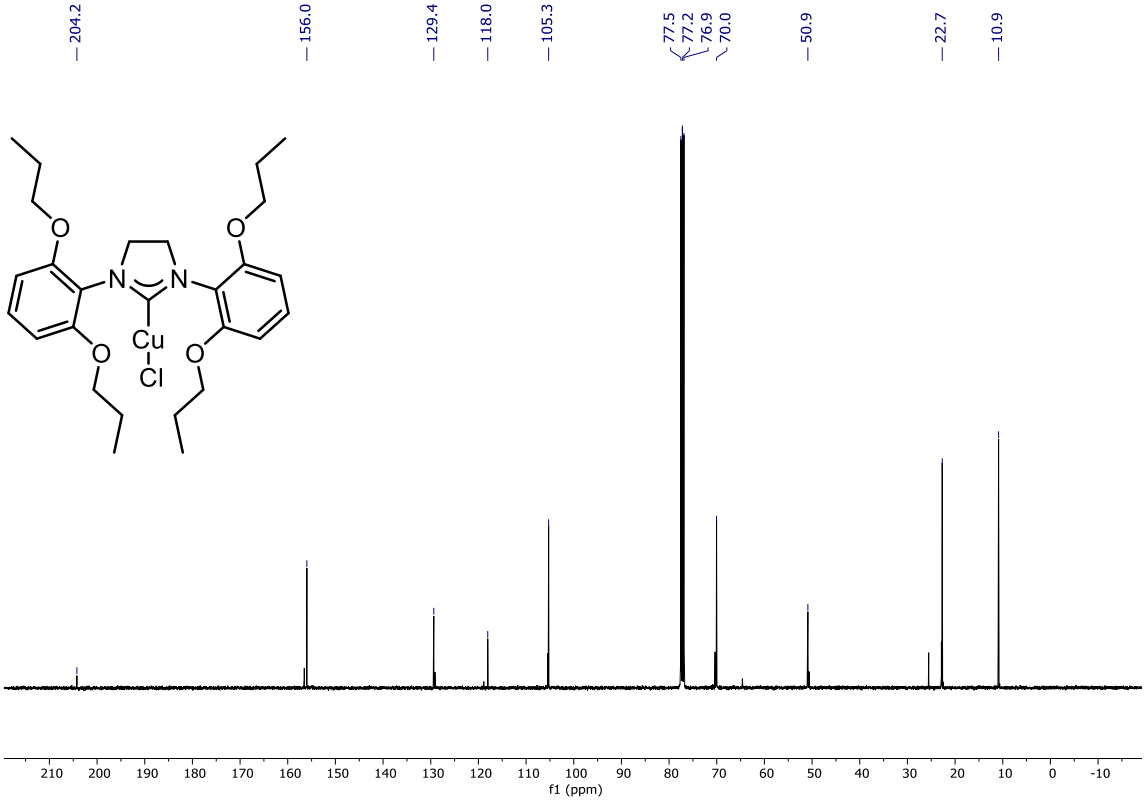

Figure A88: $^{13}C\{^{1}H\}$ NMR spectrum of 3-35 in $CDCl_3$ at 101 MHz

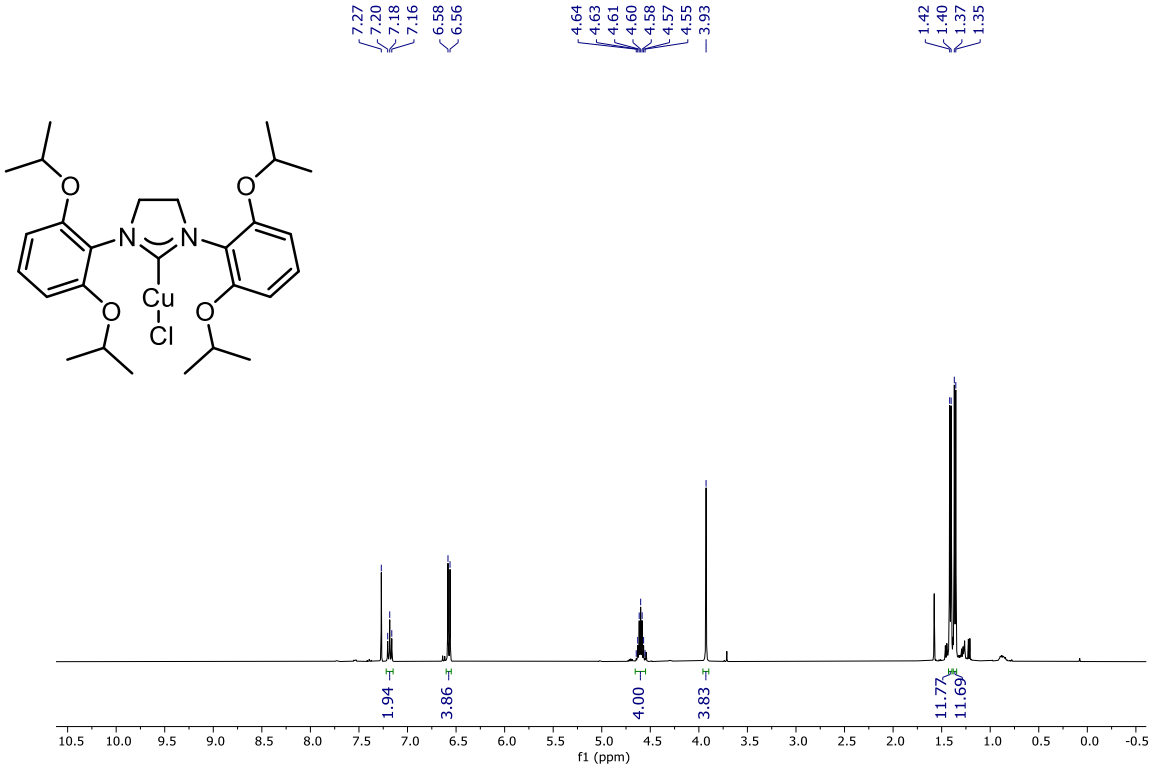

Figure A89: ^{1}H NMR spectrum of 3-36 in $CDCl_3$ at 400 MHz

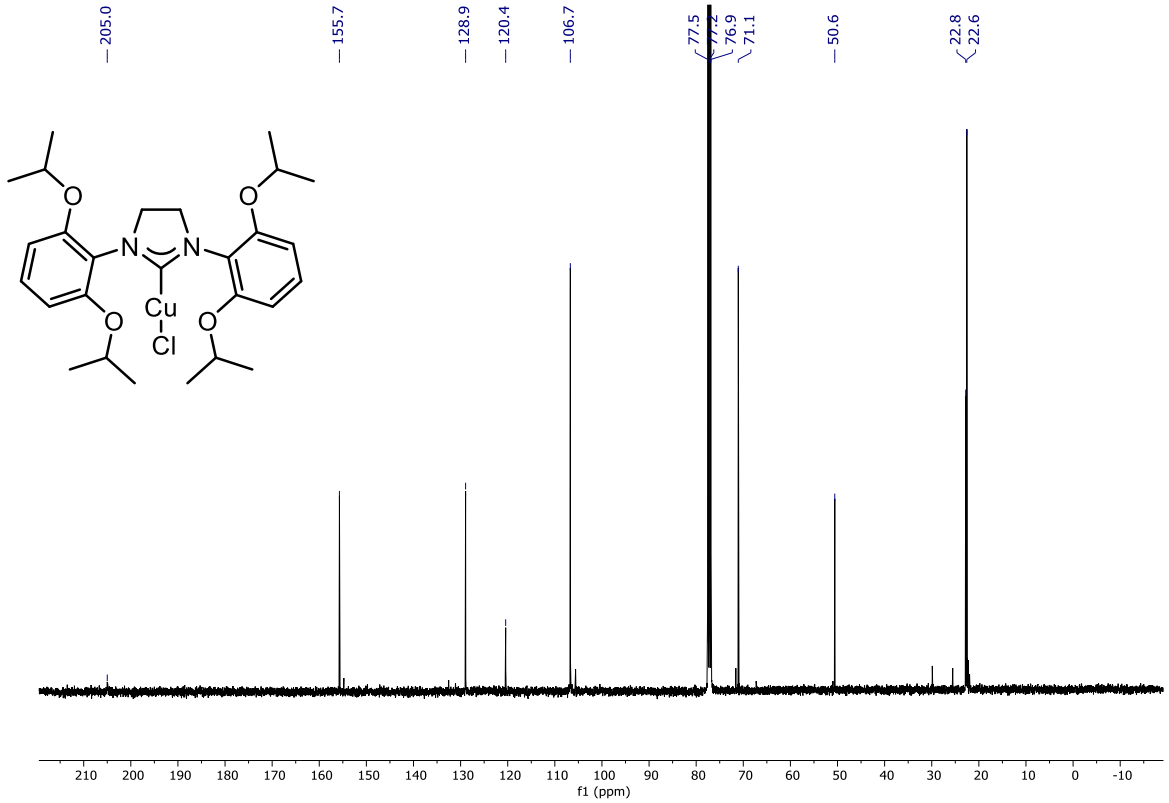

Figure A90: $^{13}C\{^{1}H\}$ NMR spectrum of 3-36 in $CDCl_3$ at 101 MHz

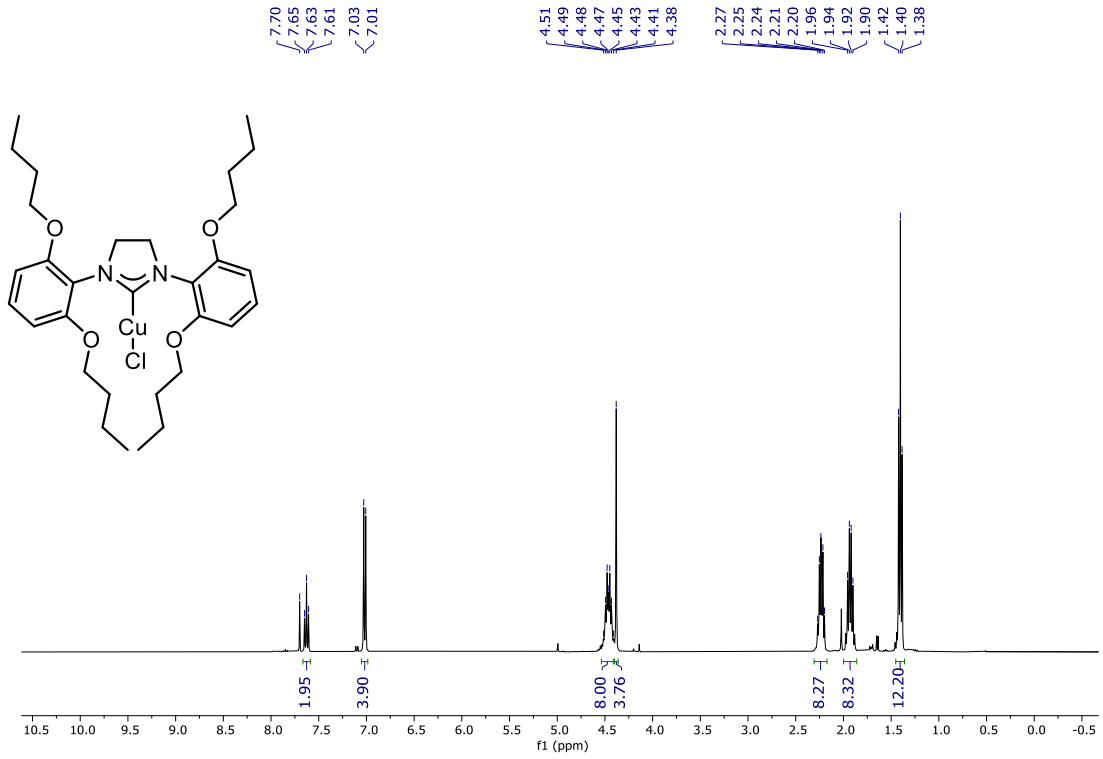

Figure A91: ^{1}H NMR spectrum of 3-37 in $CDCl_3$ at 400 MHz

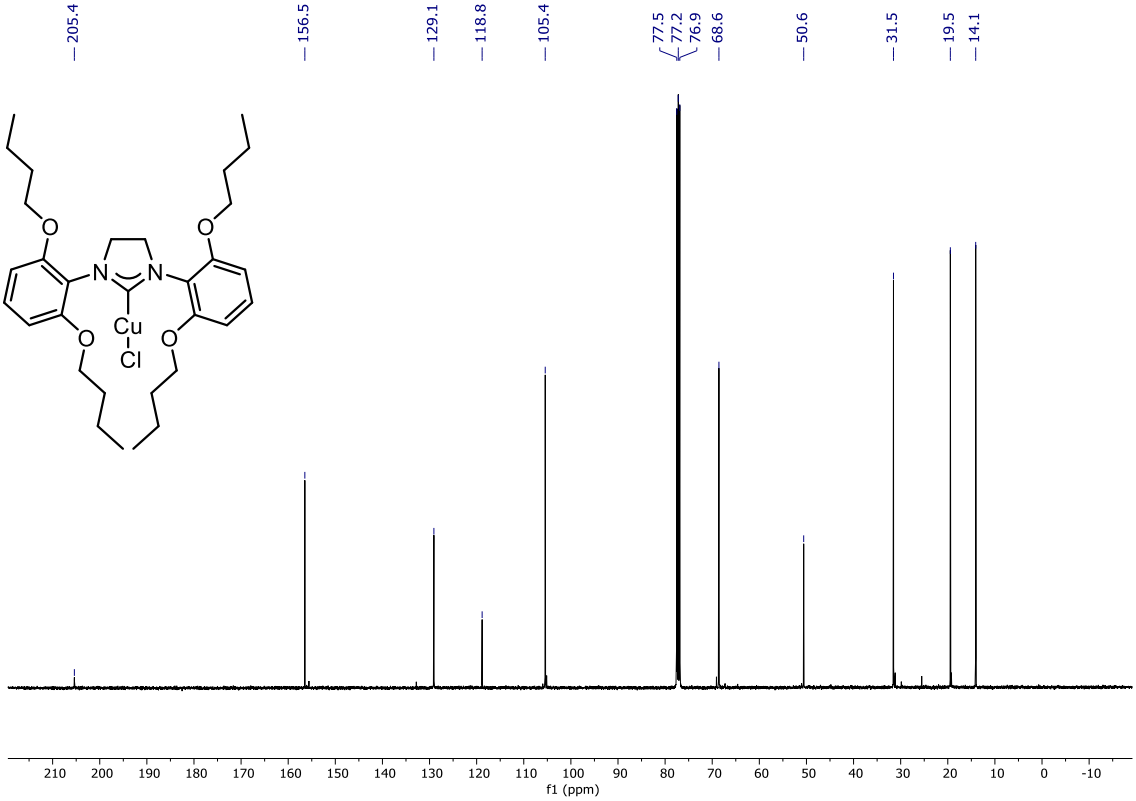

Figure A92: $^{13}C\{^{1}H\}$ NMR spectrum of 3-37 in $CDCl_3$ at 101 MHz

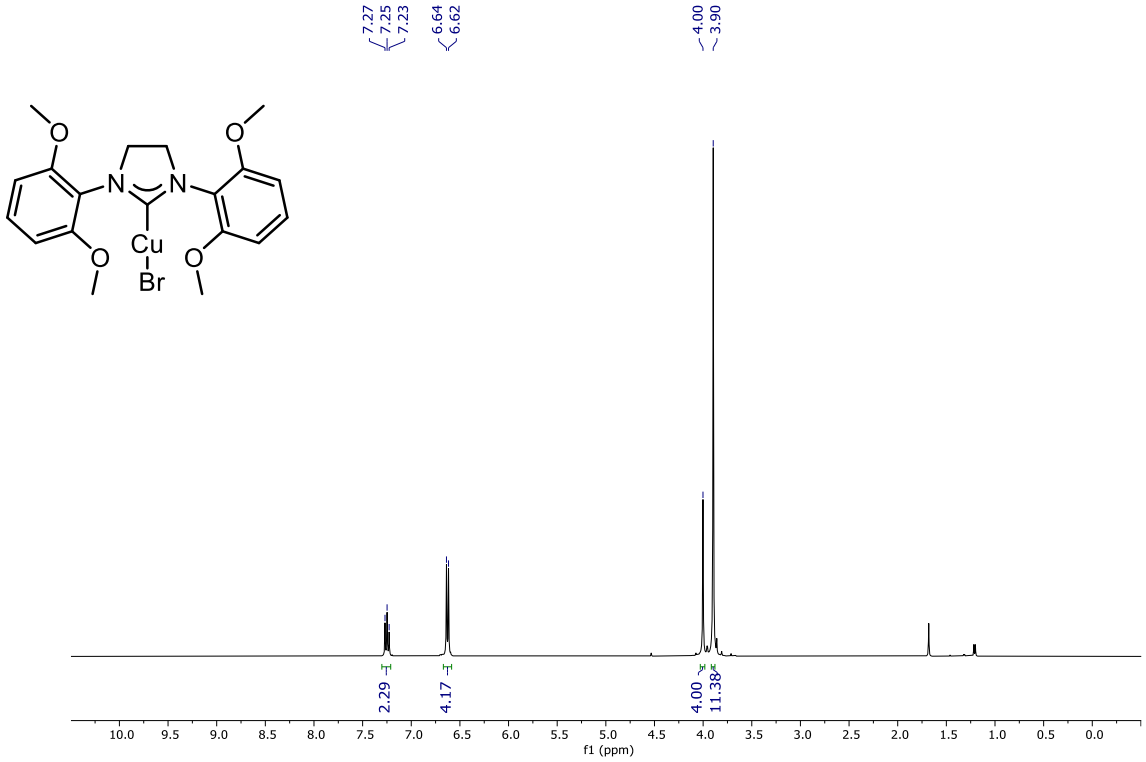

Figure A93: ^{1}H NMR spectrum of 3-38 in $CDCl_3$ at 400 MHz

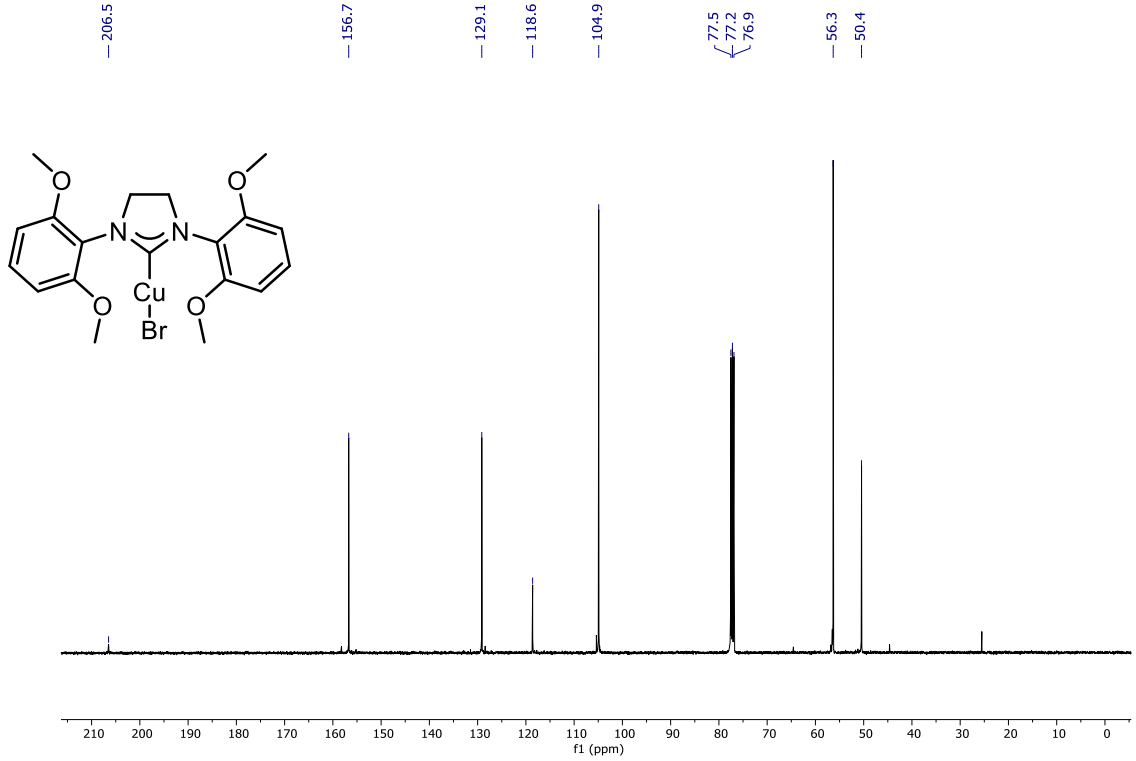

Figure A94: $^{13}C\{^{1}H\}$ NMR spectrum of 3-38 in $CDCl_3$ at 101 MHz

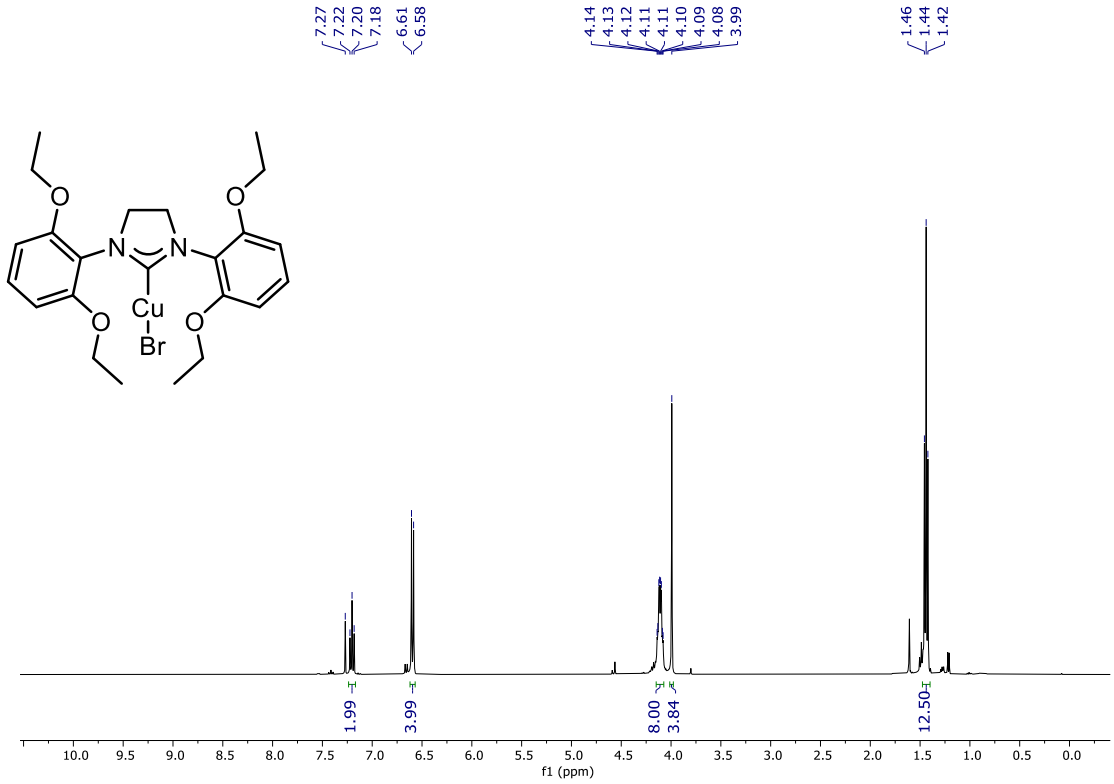

Figure A95: ^{1}H NMR spectrum of 3-39 in $CDCl_3$ at 400 MHz

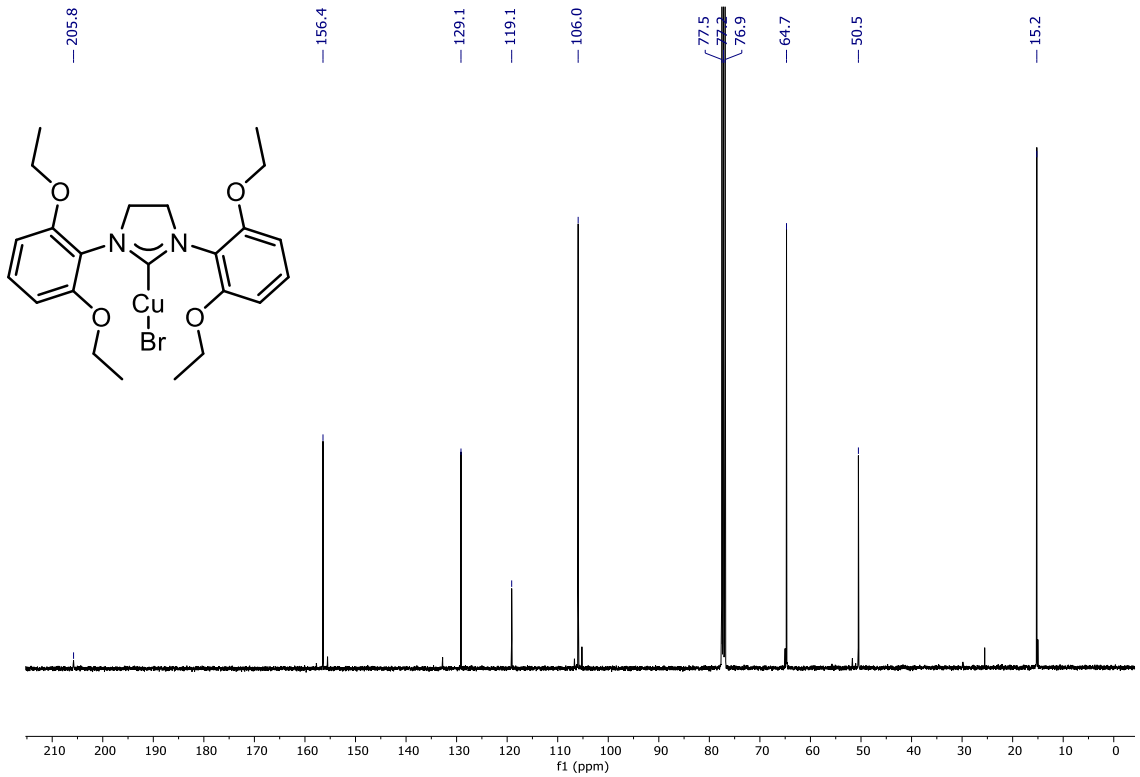

Figure A96: $^{13}C\{^{1}H\}$ NMR spectrum of 3-39 in $CDCl_3$ at 101 MHz

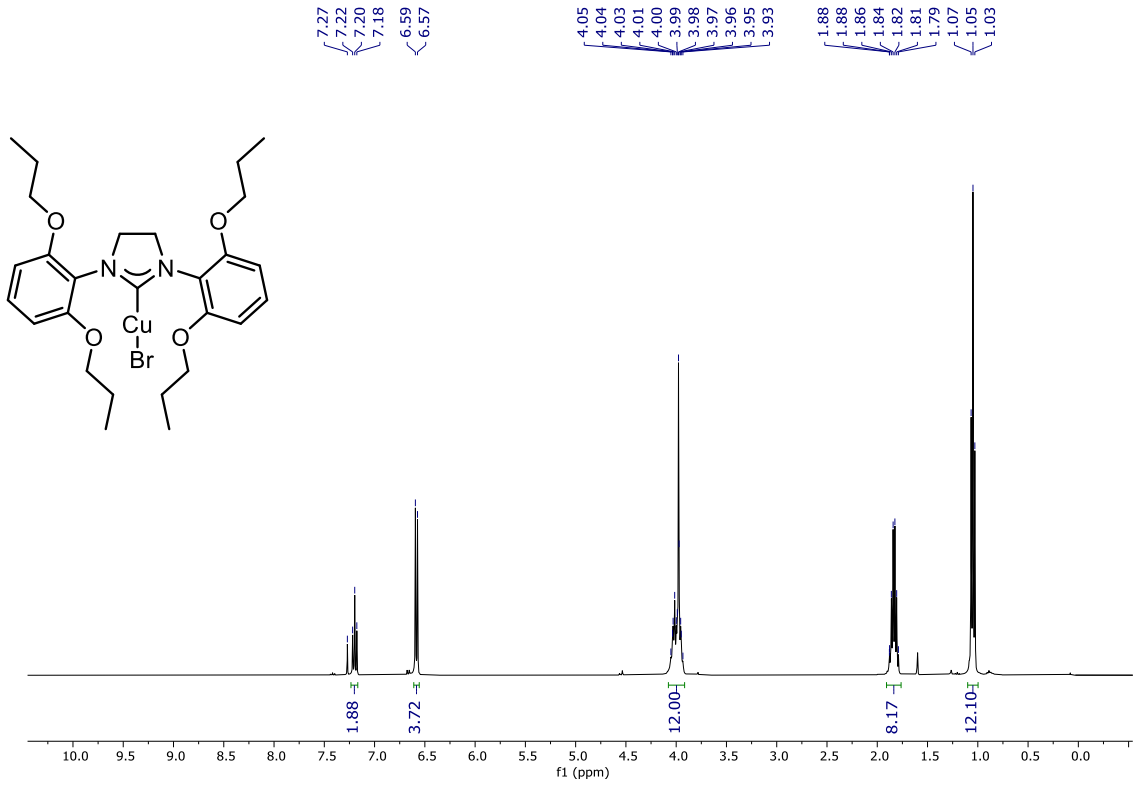

Figure A97: ^{1}H NMR spectrum of 3-40 in $CDCl_3$ at 400 MHz

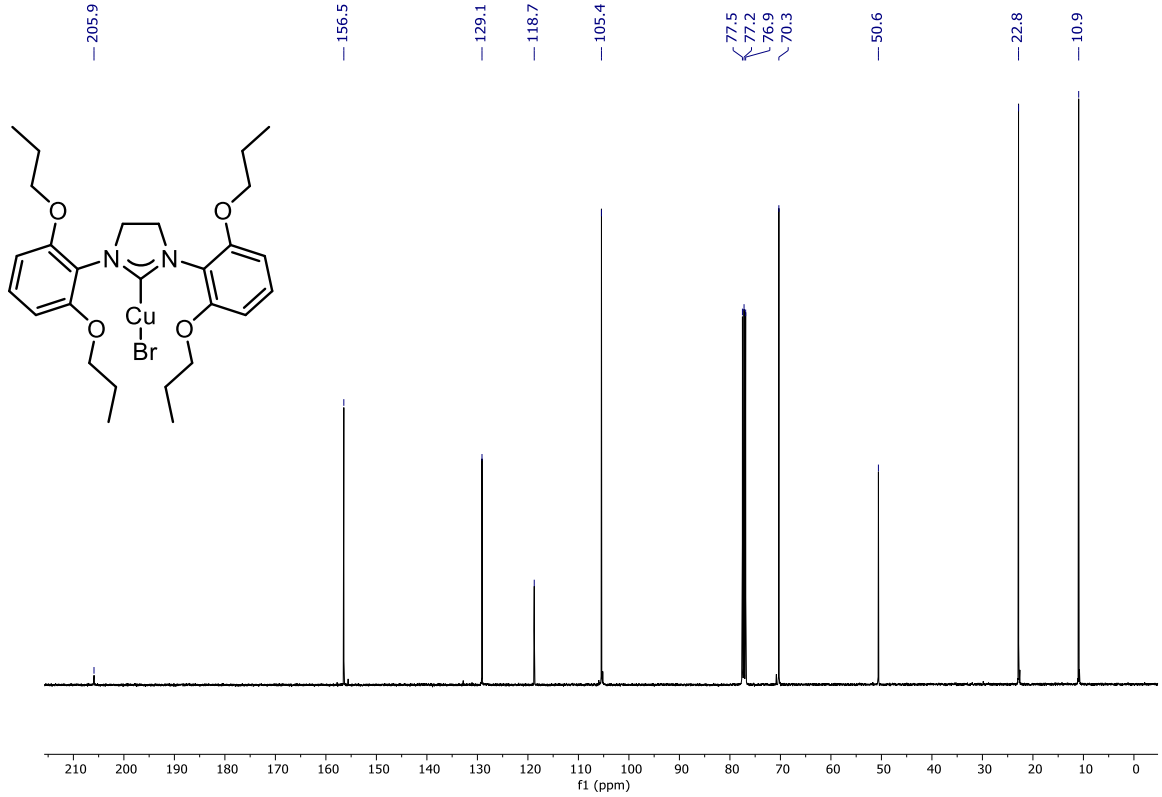

Figure A98: $^{13}C\{^{1}H\}$ NMR spectrum of 3-40 in $CDCl_3$ at 101 MHz

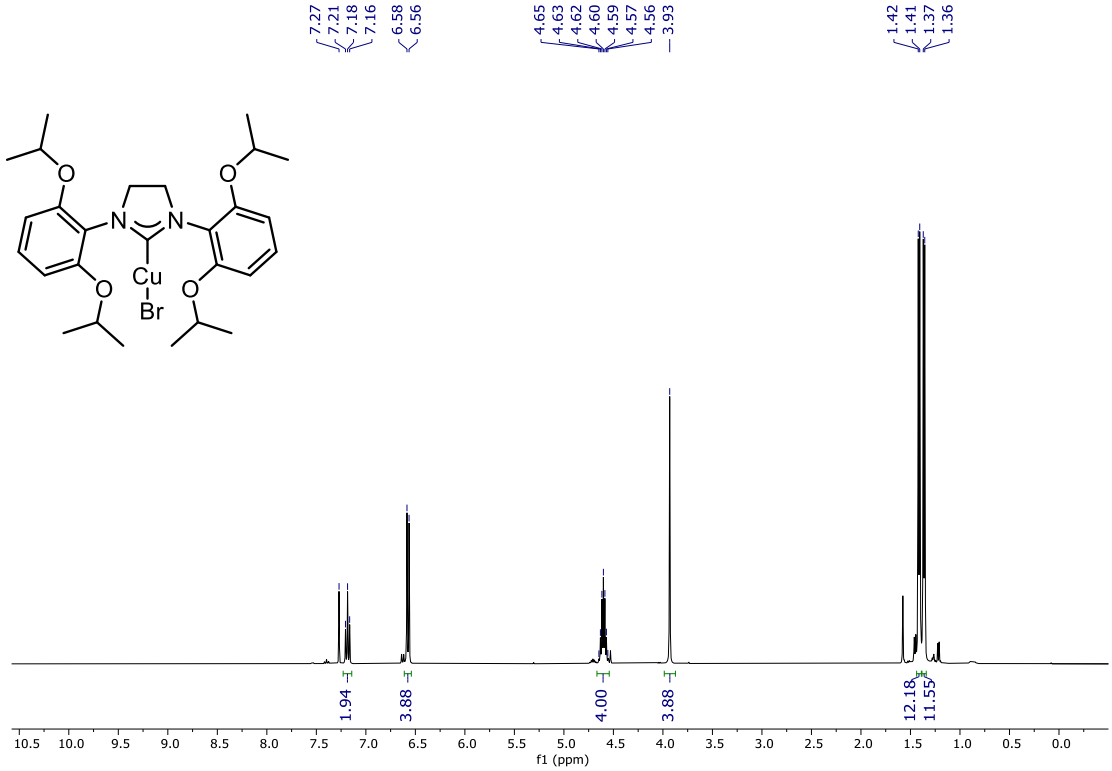

Figure A99: ^{1}H NMR spectrum of 3-41 in $CDCl_3$ at 400 MHz

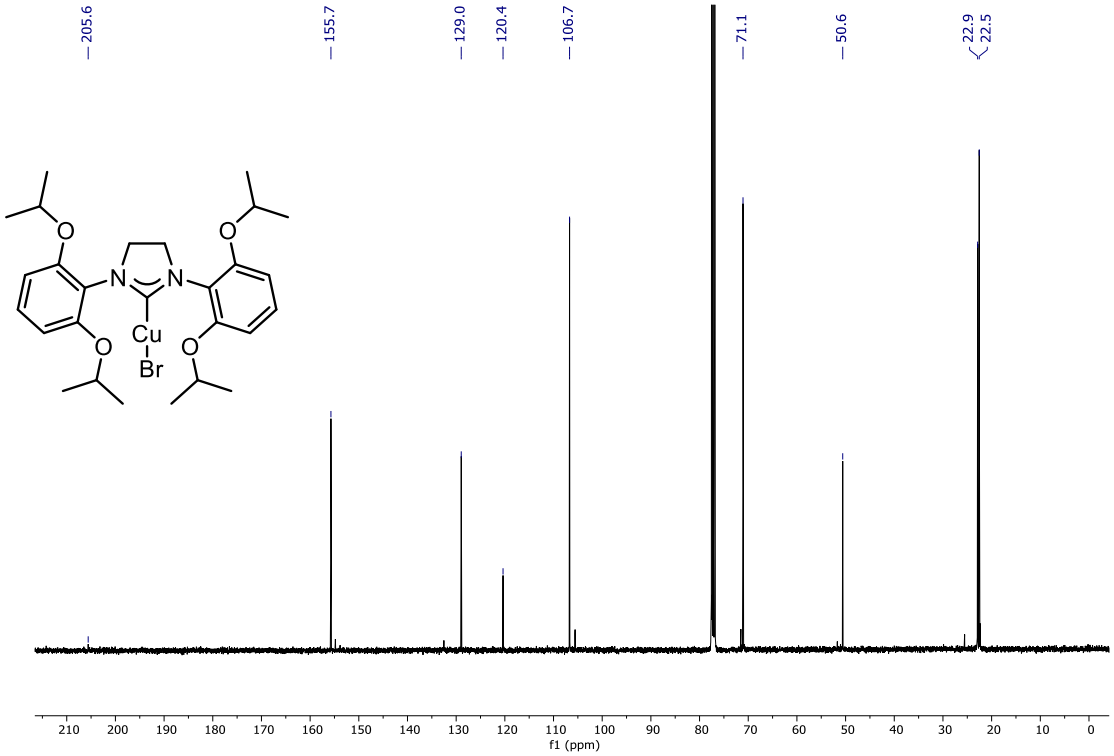

Figure A100: $^{13}C\{^{1}H\}$ NMR spectrum of 3-41 in $CDCl_3$ at 101 MHz

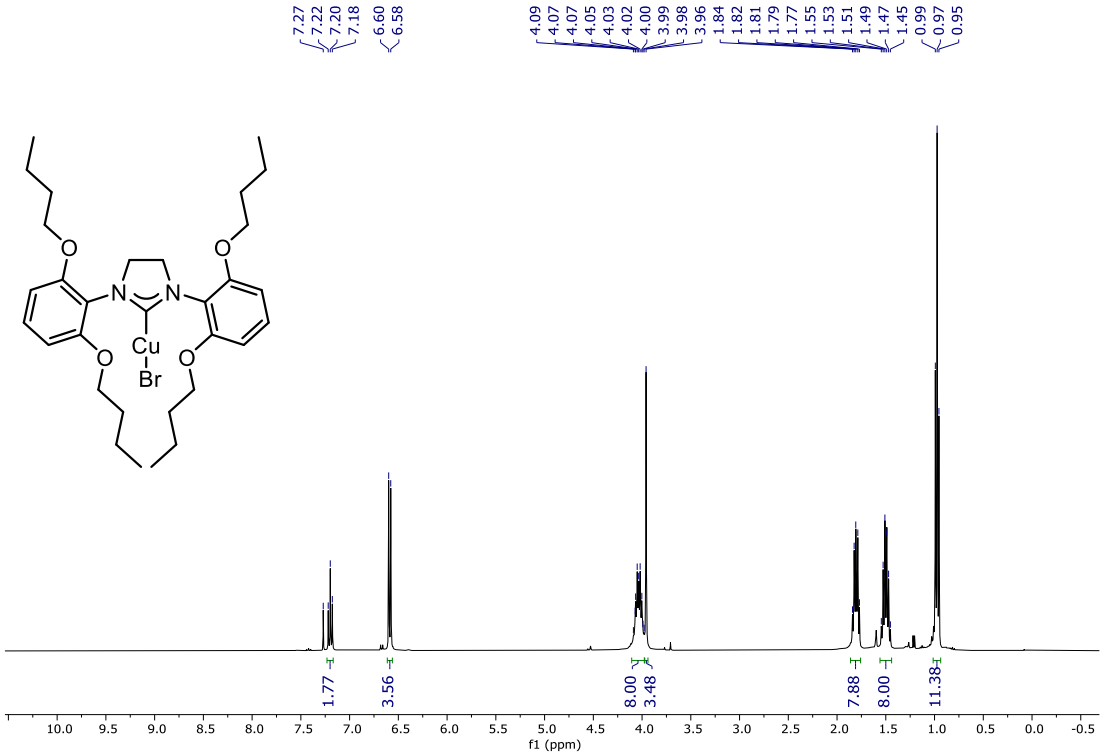

Figure A101: ^{1}H NMR spectrum of 3-42 in $CDCl_3$ at 400 MHz

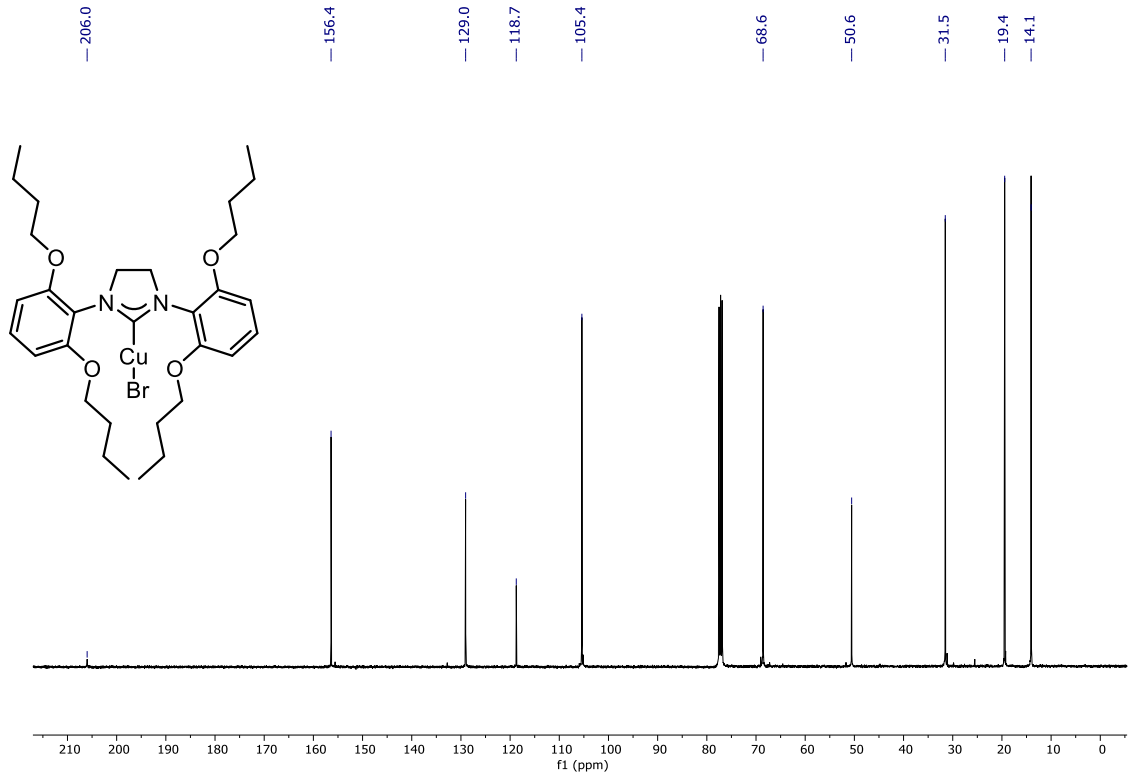

Figure A102: $^{13}C\{^{1}H\}$ NMR spectrum of 3-42 in $CDCl_3$ at 101 MHz

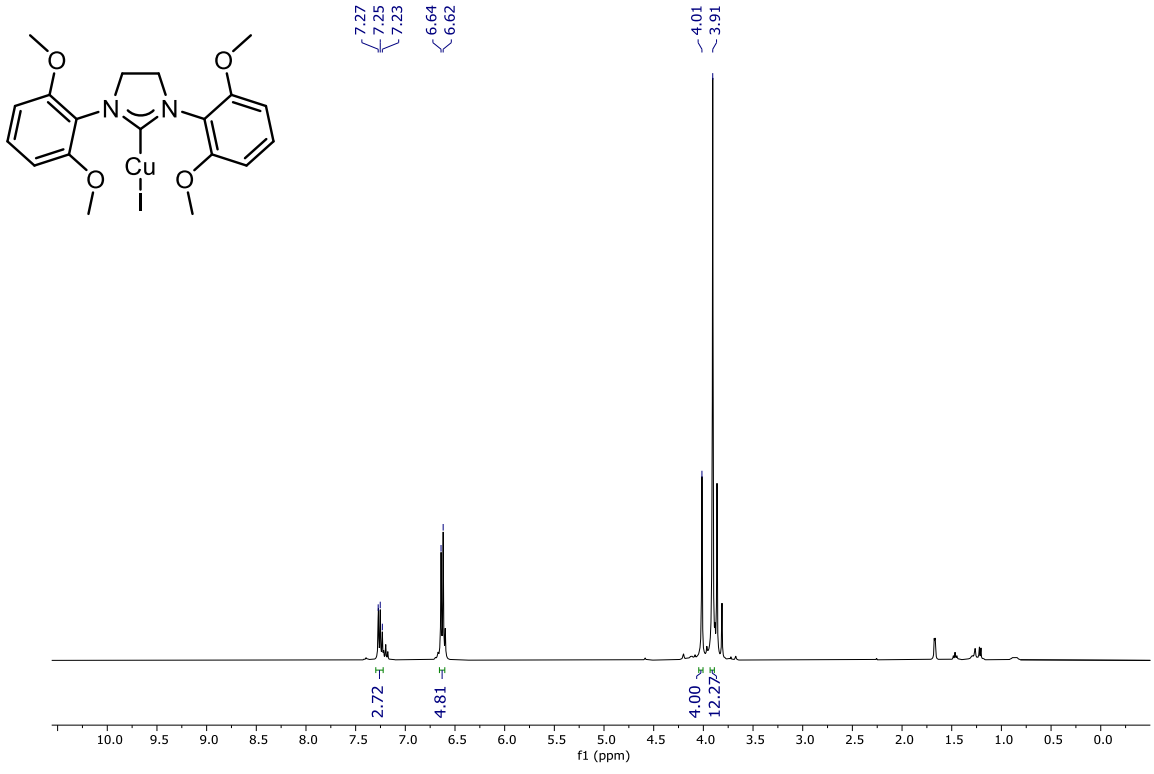

Figure A103: ^{1}H NMR spectrum of 3-43 in $CDCl_3$ at 400 MHz

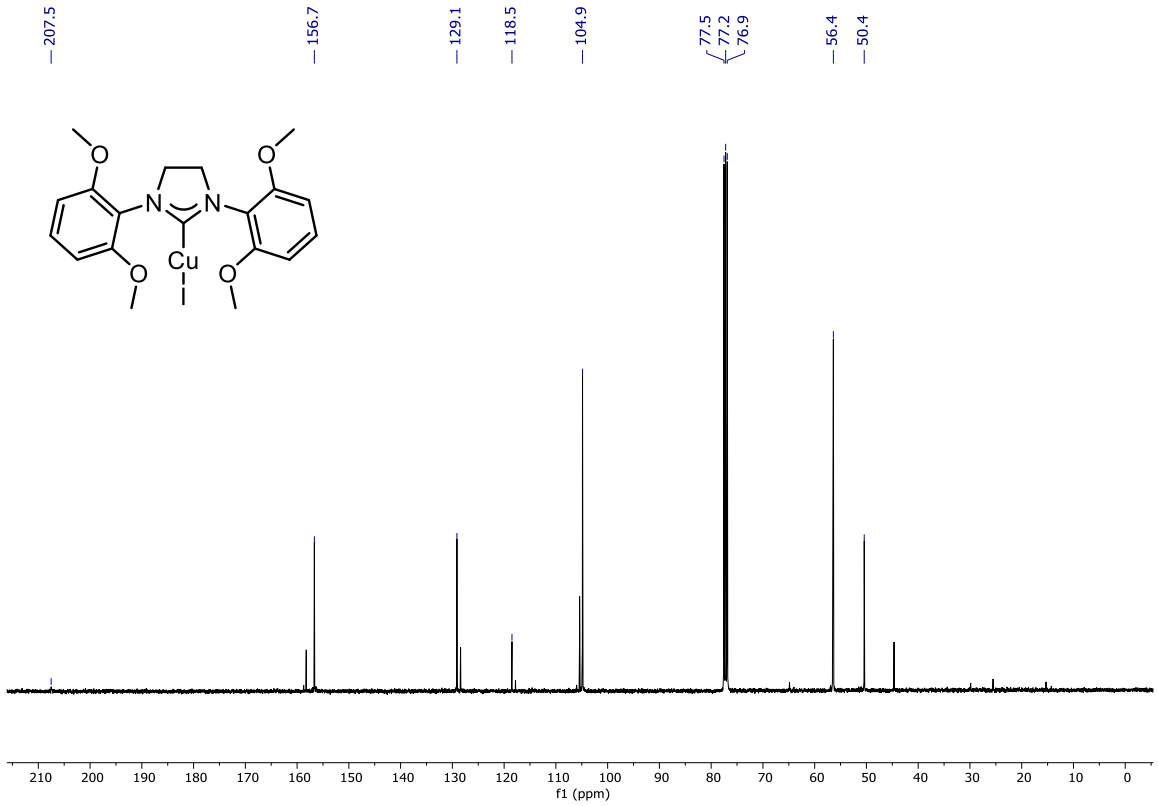

Figure A104: $^{13}C\{^{1}H\}$ NMR spectrum of 3-43 in $CDCl_3$ at 101 MHz

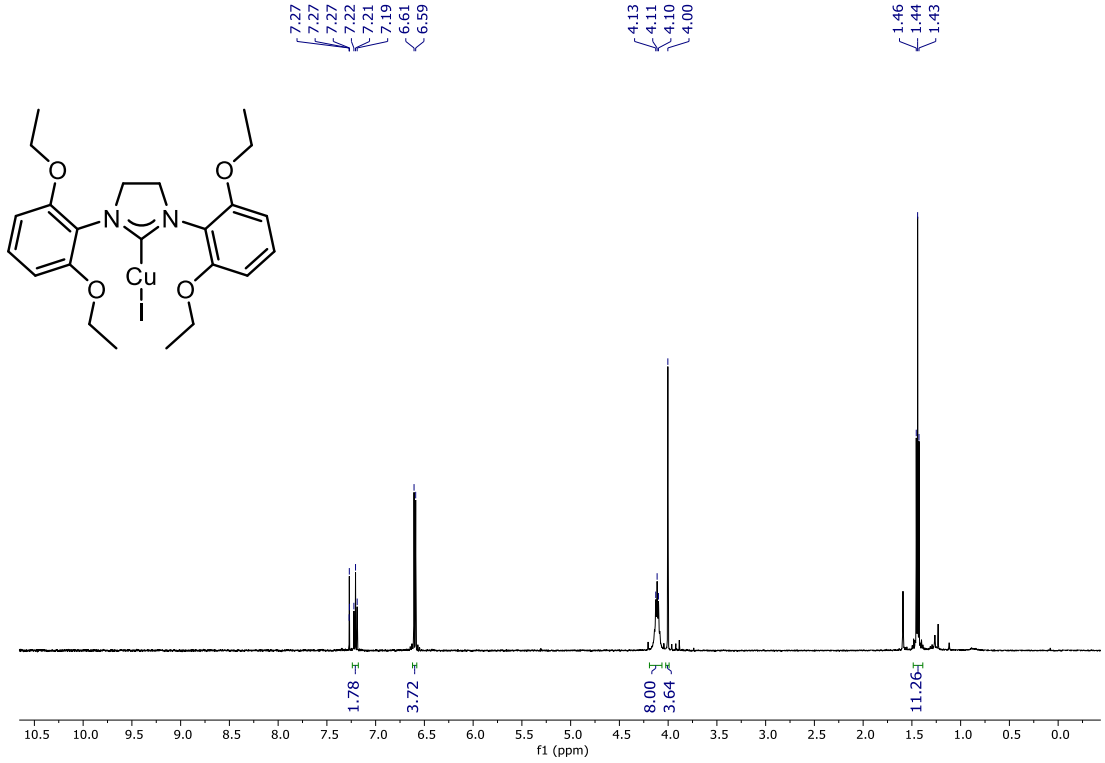

Figure A105: ^{1}H NMR spectrum of 3-44 in $CDCl_3$ at 500 MHz

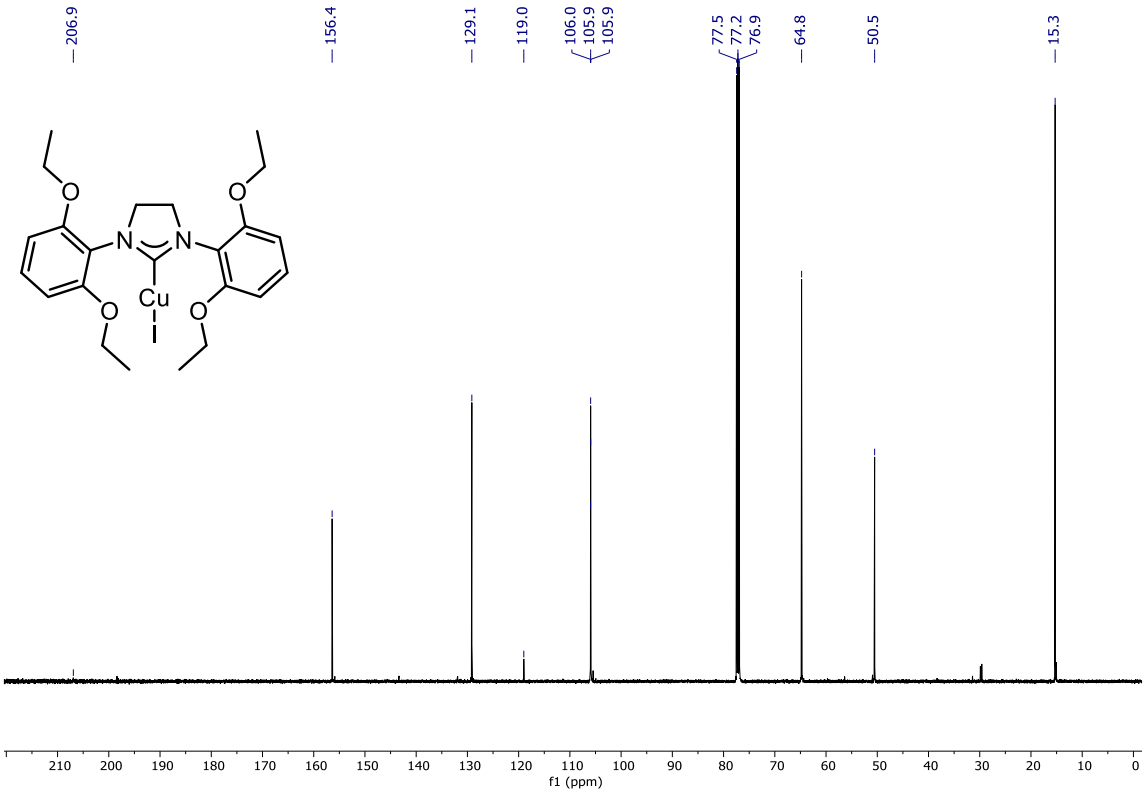

Figure A106: $^{13}C\{^{1}H\}$ NMR spectrum of 3-44 in $CDCl_3$ at 126 MHz

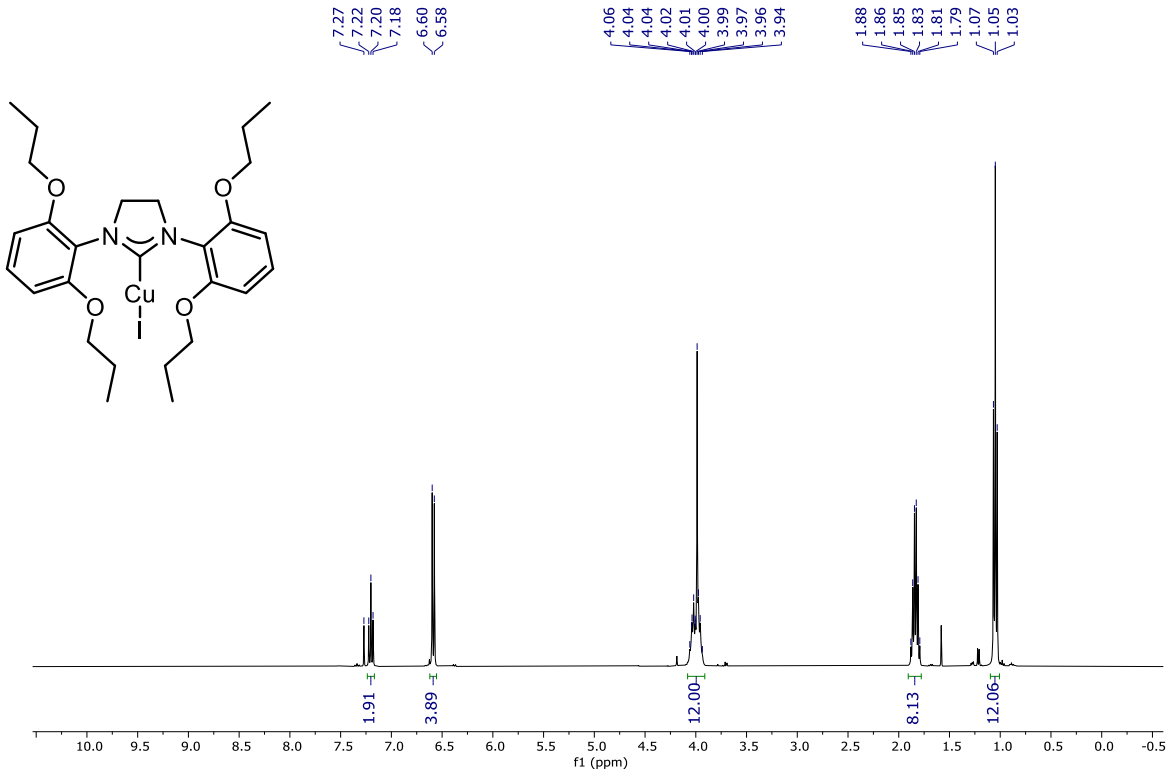

Figure A107: ^{1}H NMR spectrum of 3-45 in $CDCl_3$ at 400 MHz

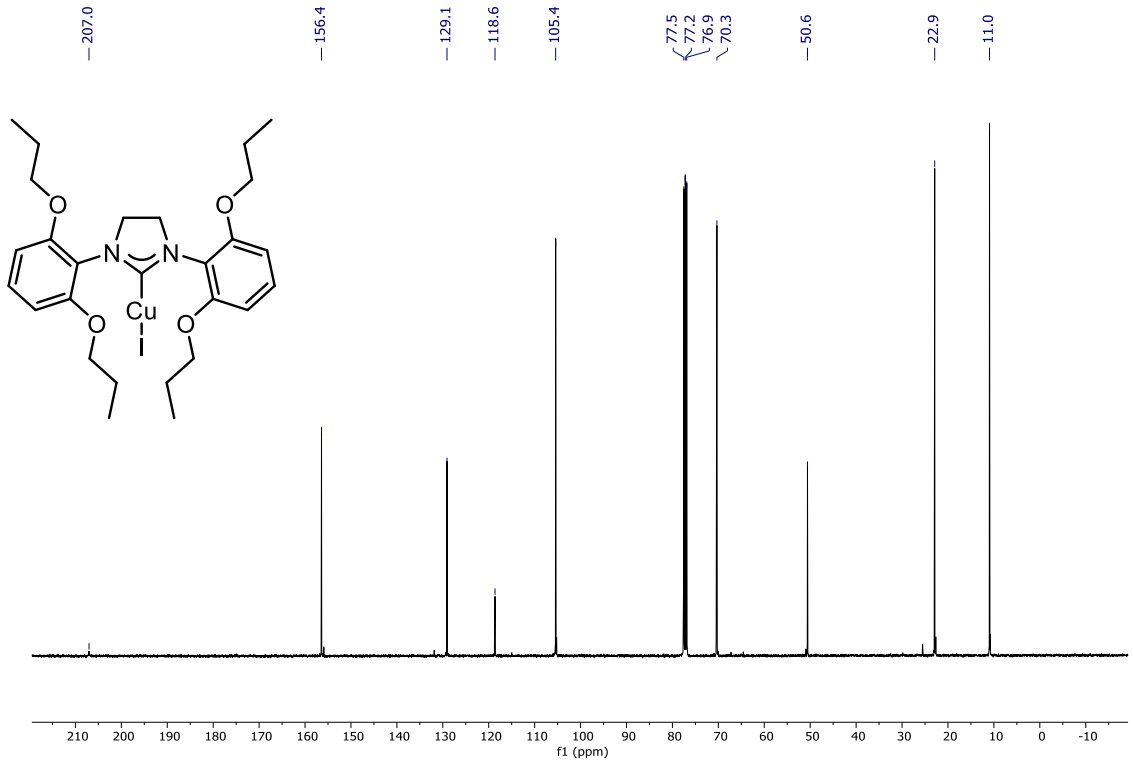

Figure A108: $^{13}C\{^{1}H\}$ NMR spectrum of 3-45 in $CDCl_3$ at 101 MHz

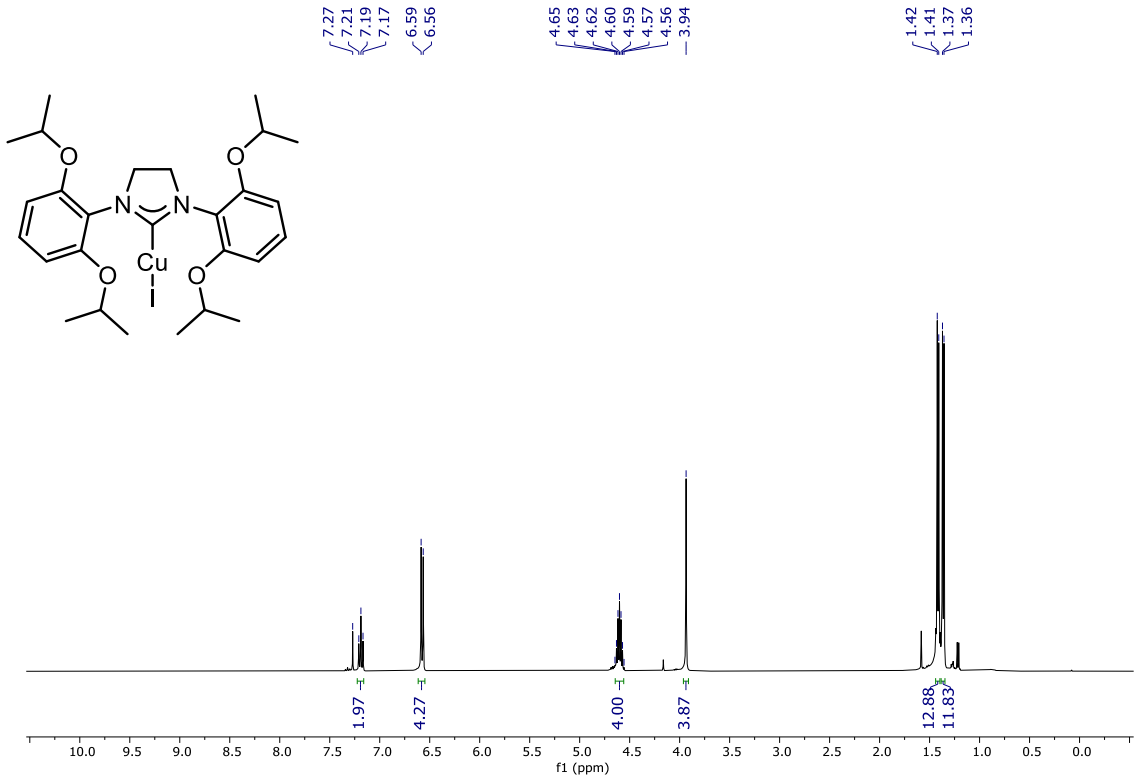

Figure A109: ^{1}H NMR spectrum of 3-46 in $CDCl_3$ at 400 MHz

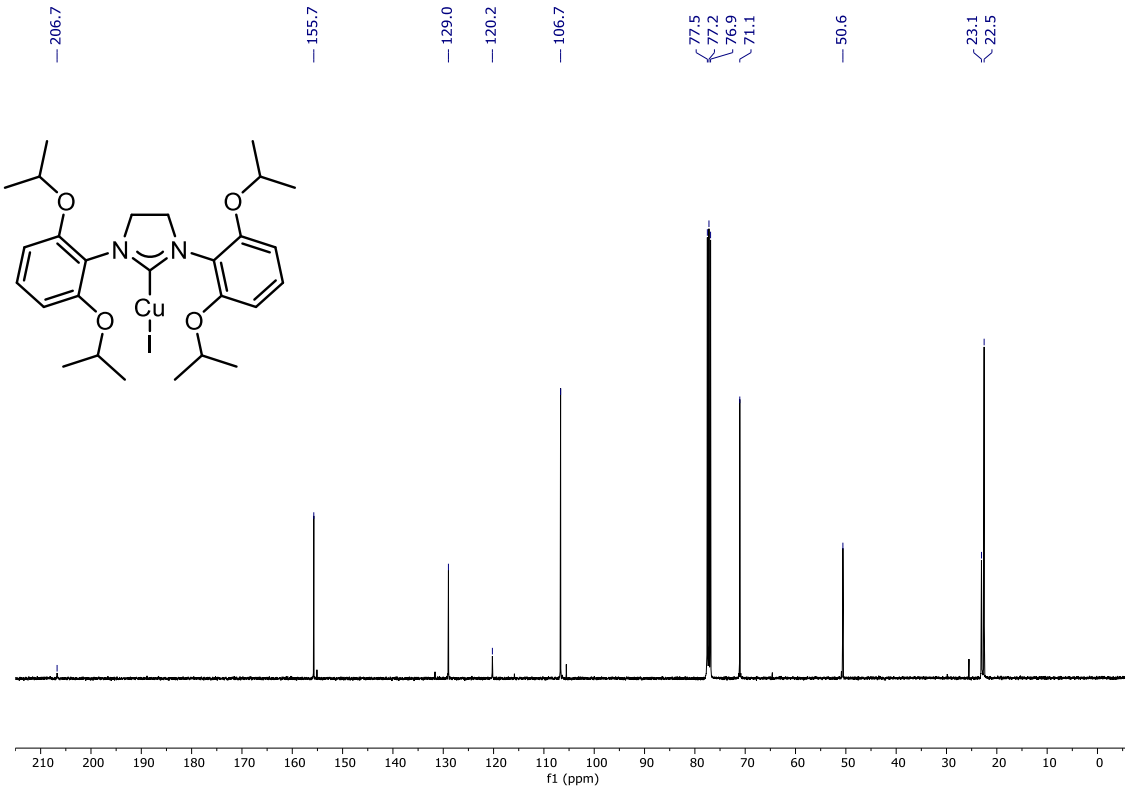

Figure A110: $^{13}C\{^{1}H\}$ NMR spectrum of 3-46 in $CDCl_3$ at 101 MHz

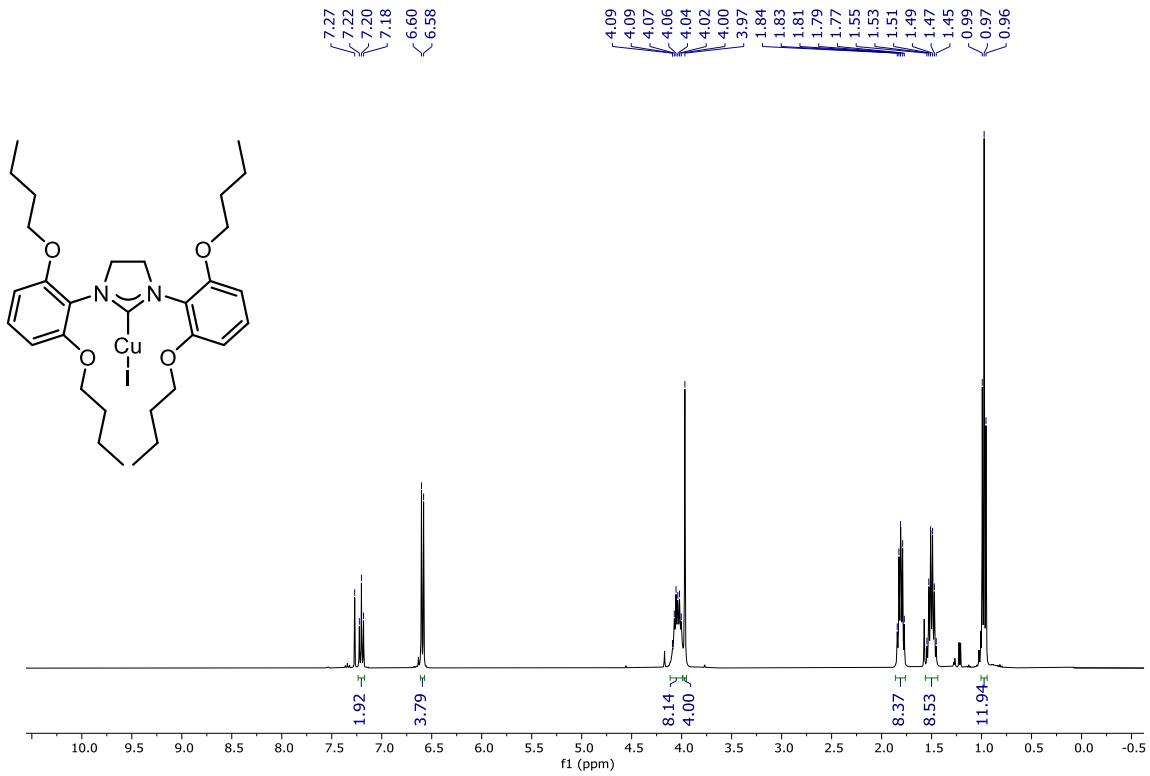

Figure A111: ^{1}H NMR spectrum of 3-47 in $CDCl_3$ at 400 MHz

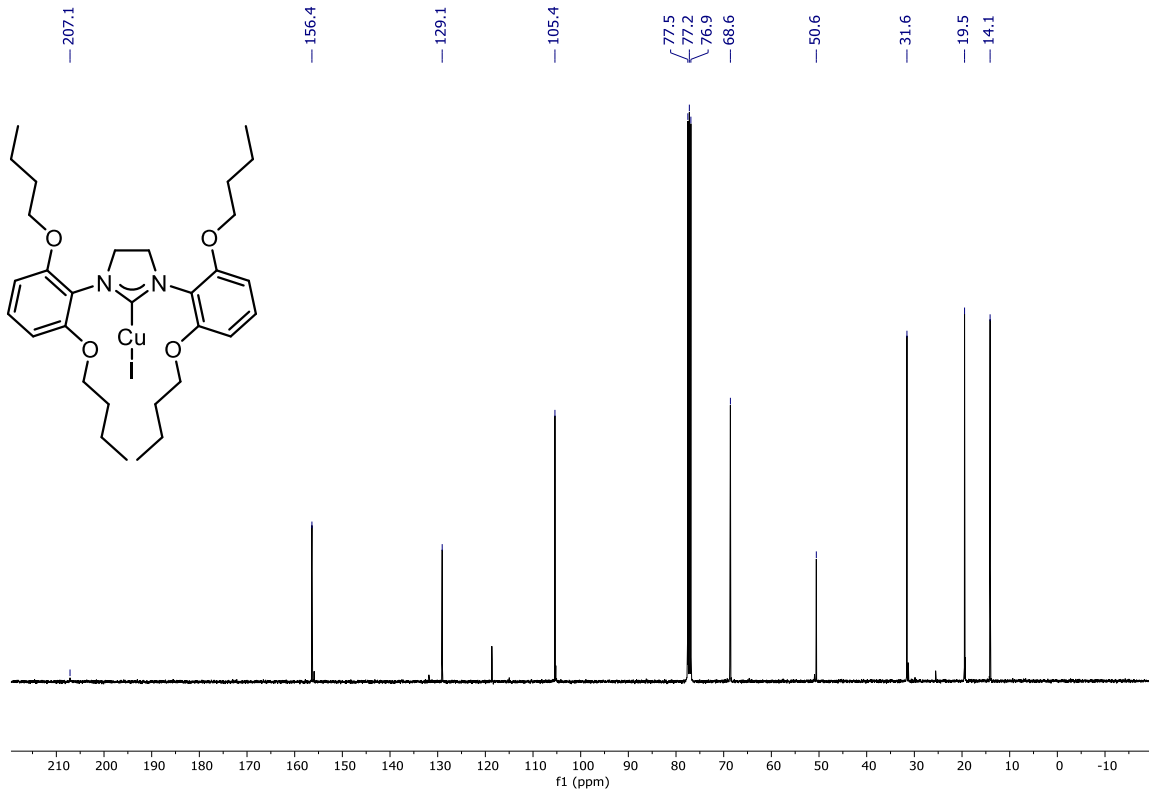

Figure A112: $^{13}C\{^{1}H\}$ NMR spectrum of 3-47 in $CDCl_3$ at 101 MHz

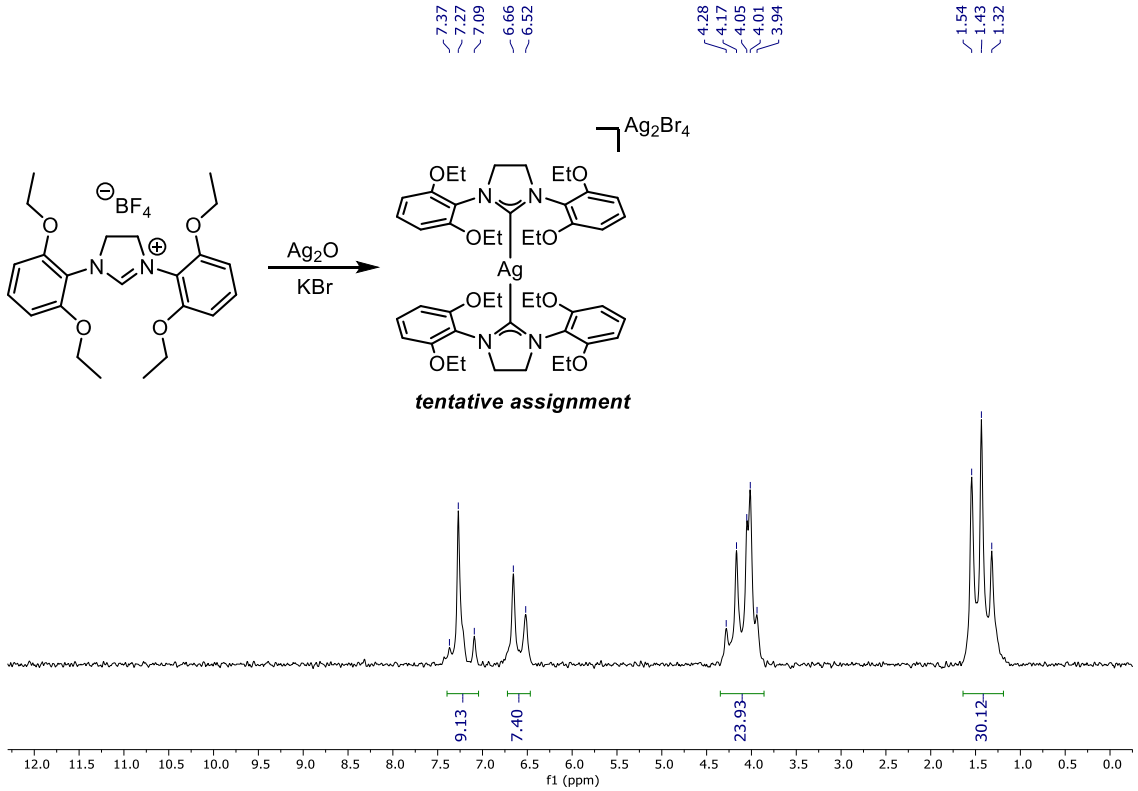

Figure A113: ^{1}H NMR spectrum of Ag intermediate (3-49) in $CDCl_3$ at 60 MHz

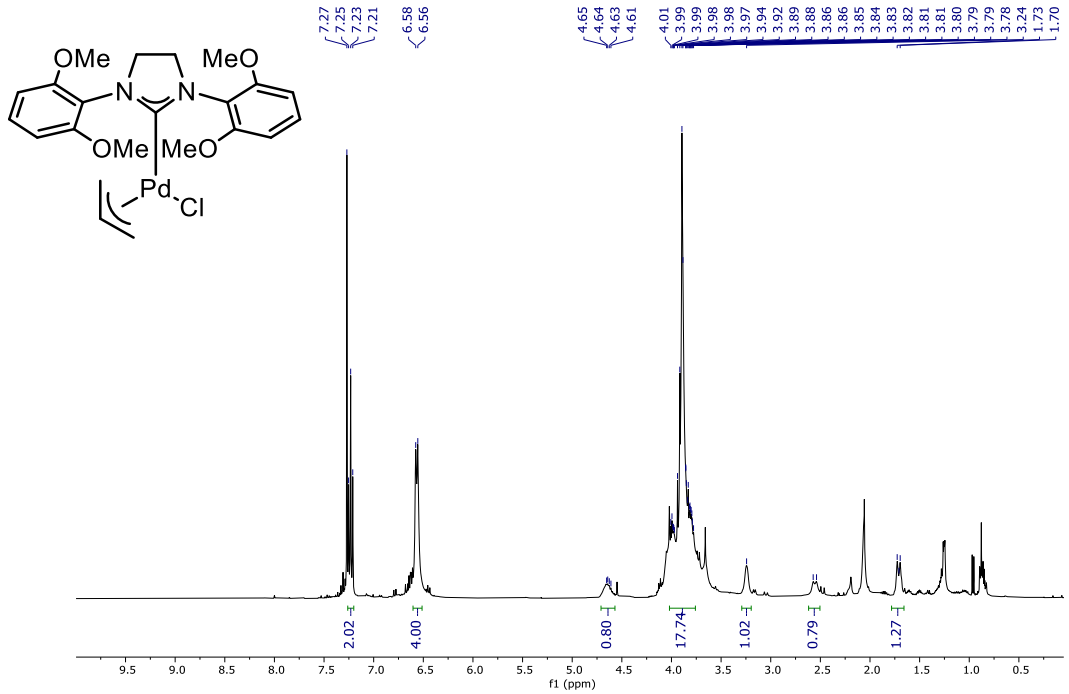

Figure A114: ^{1}H NMR spectrum of 3-51 at 400 MHz in $CDCl_3$ *(Despite our best efforts, minor impurities were caused by decomposition even when stored under a glovebox.)*

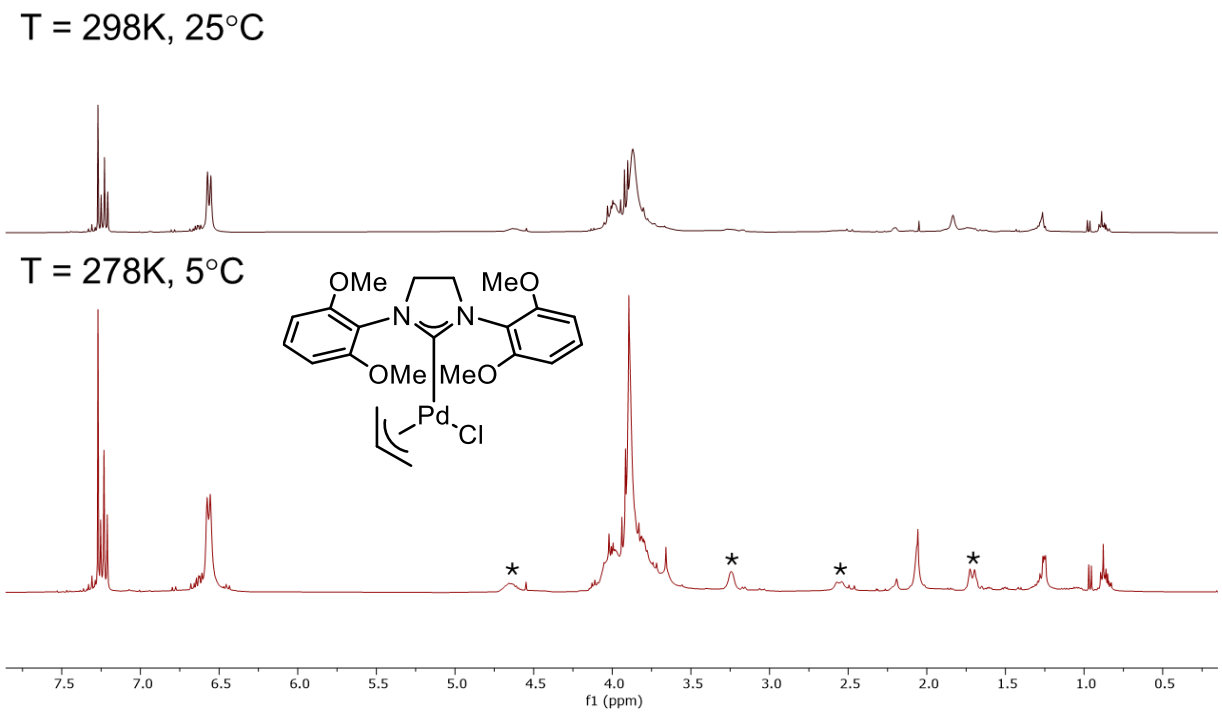

Figure A115: VT-^{1}H NMR spectrum of 3-51 in $CDCl_3$ at 400 MHz *(*denotes allyl peaks)*

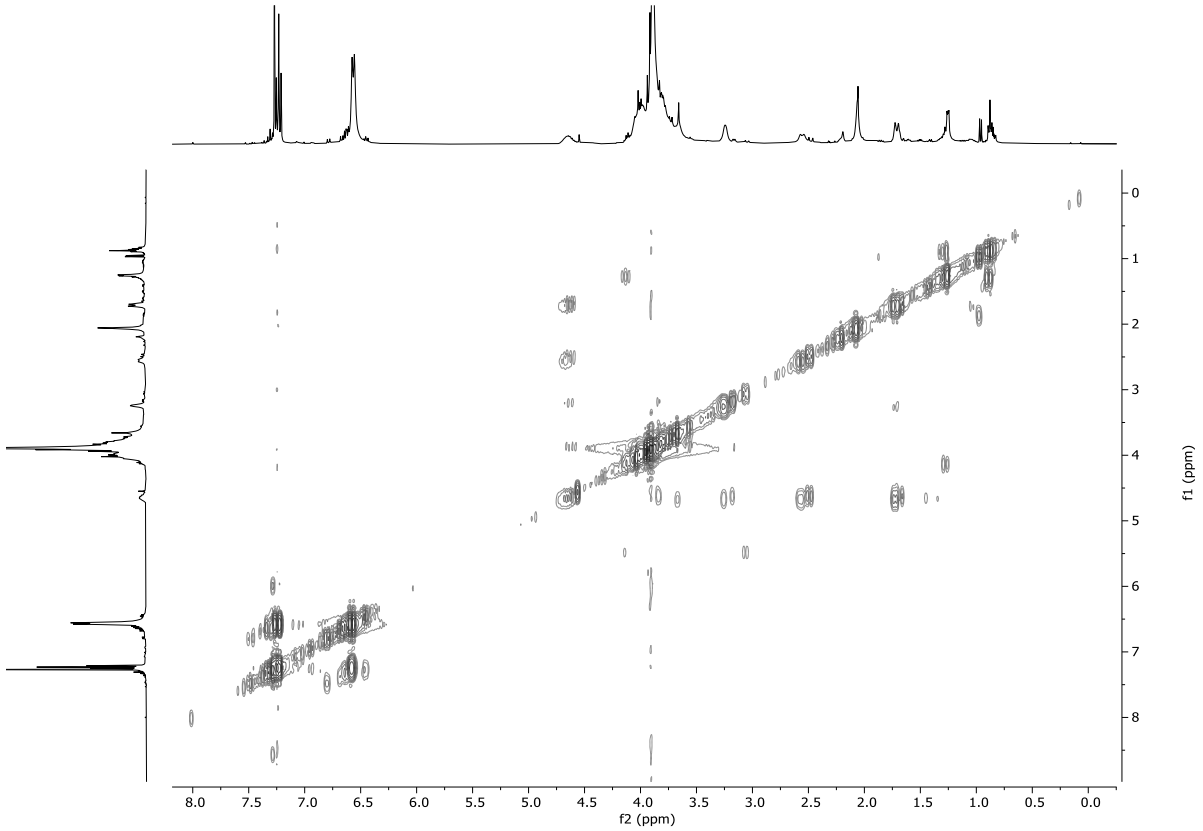

Figure A116: ^{1}H, ^{1}H-COSY NMR (400 MHz) spectrum of 3-51 in $CDCl_3$ at 278 K (5°C)

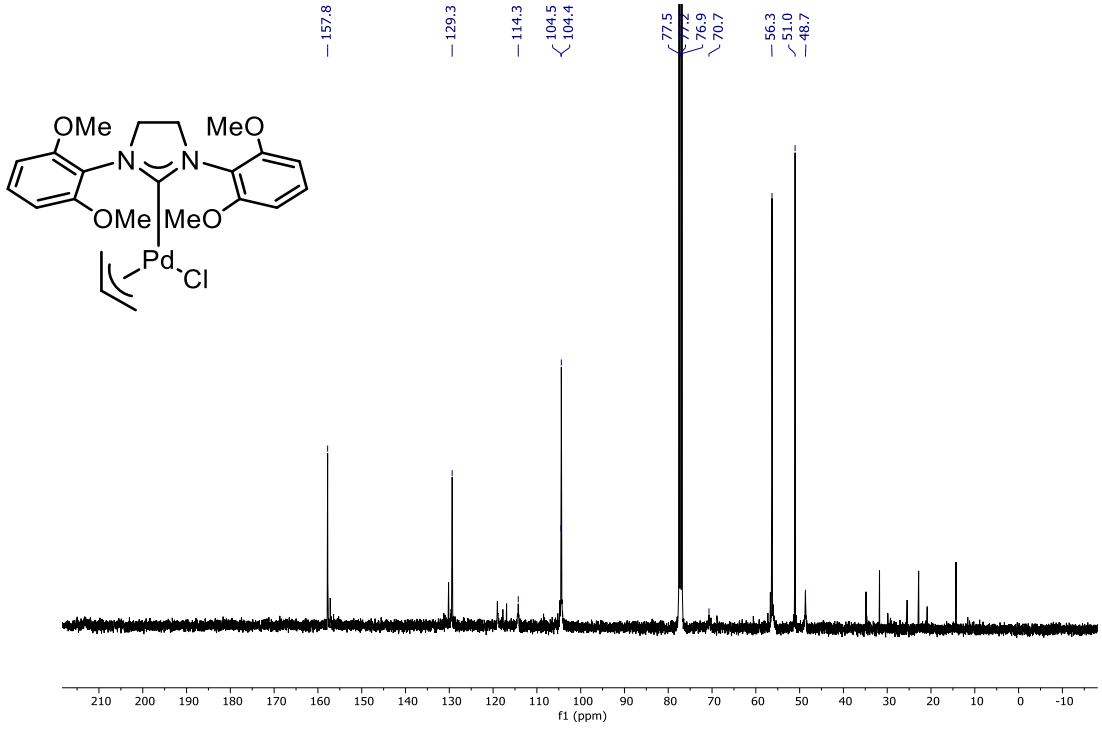

Figure A 117: ^{13}C{^{1}H} NMR spectrum of 3-51 in $CDCl_3$ at 101 MHz *(Despite our best efforts, minor impurities were caused by decomposition even when stored under a glovebox.)*

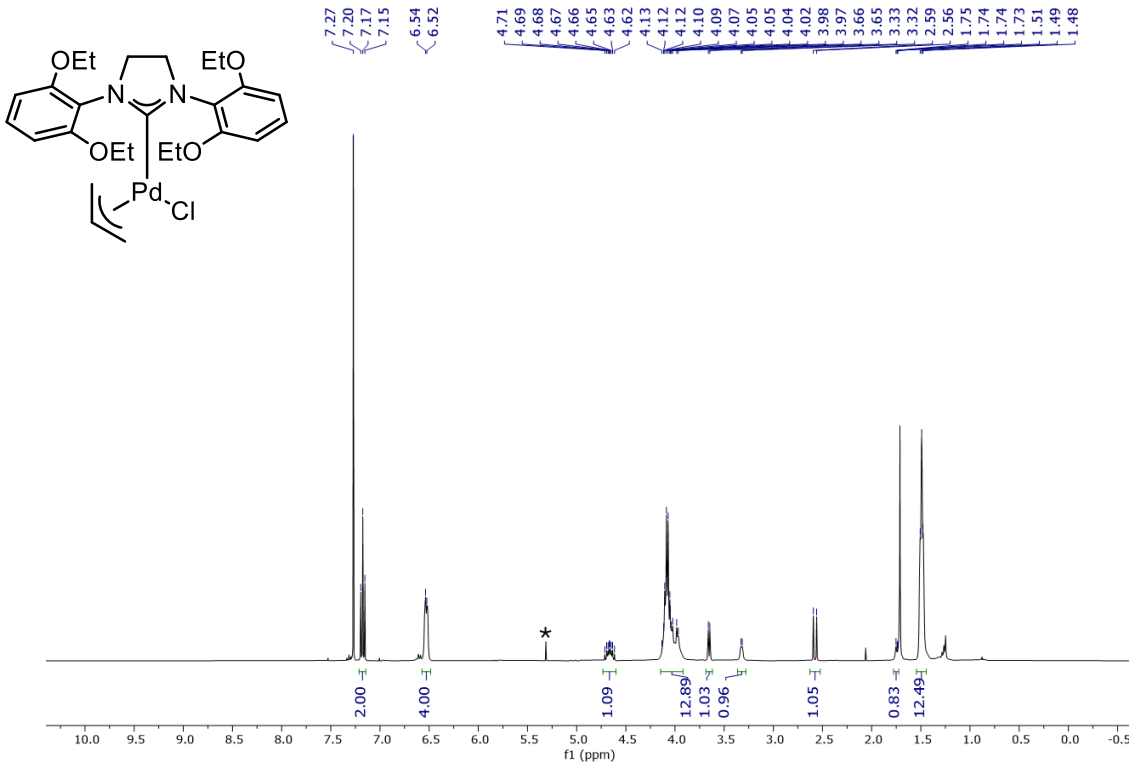

Figure A118: ^{1}H NMR spectrum of 3-52 in $CDCl_3$ at 400 MHz *(*denotes residual CH_2Cl_2)*

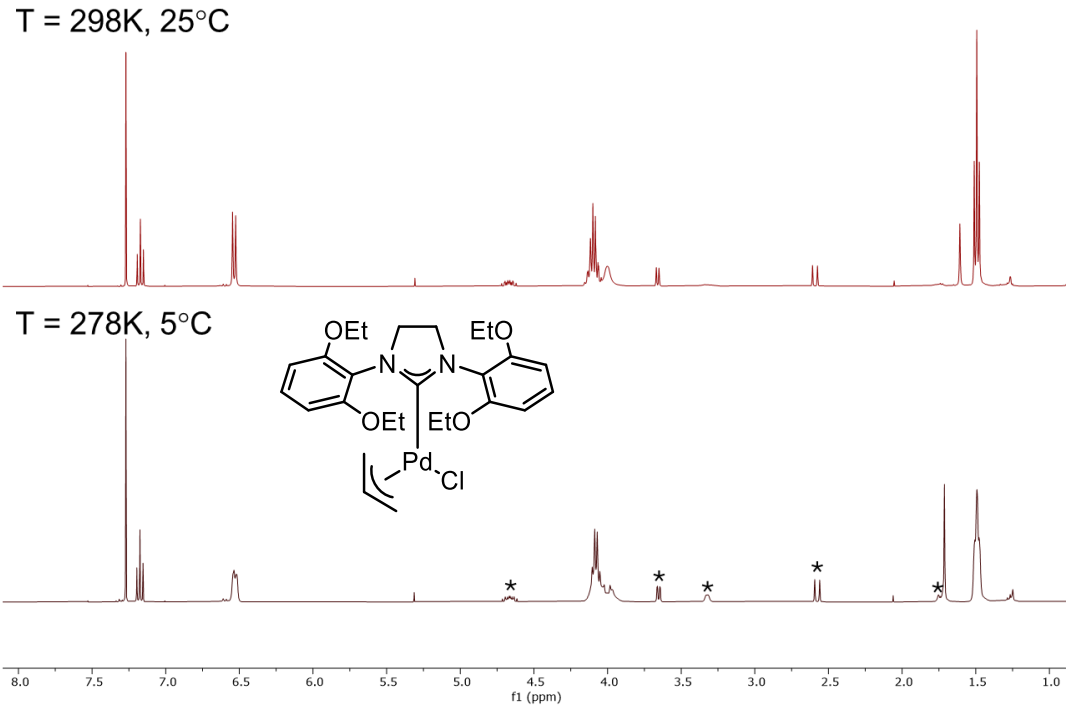

Figure A119: VT-^{1}H NMR spectrum of 3-52 in $CDCl_3$ at 400 MHz *(*denotes allyl peaks)*

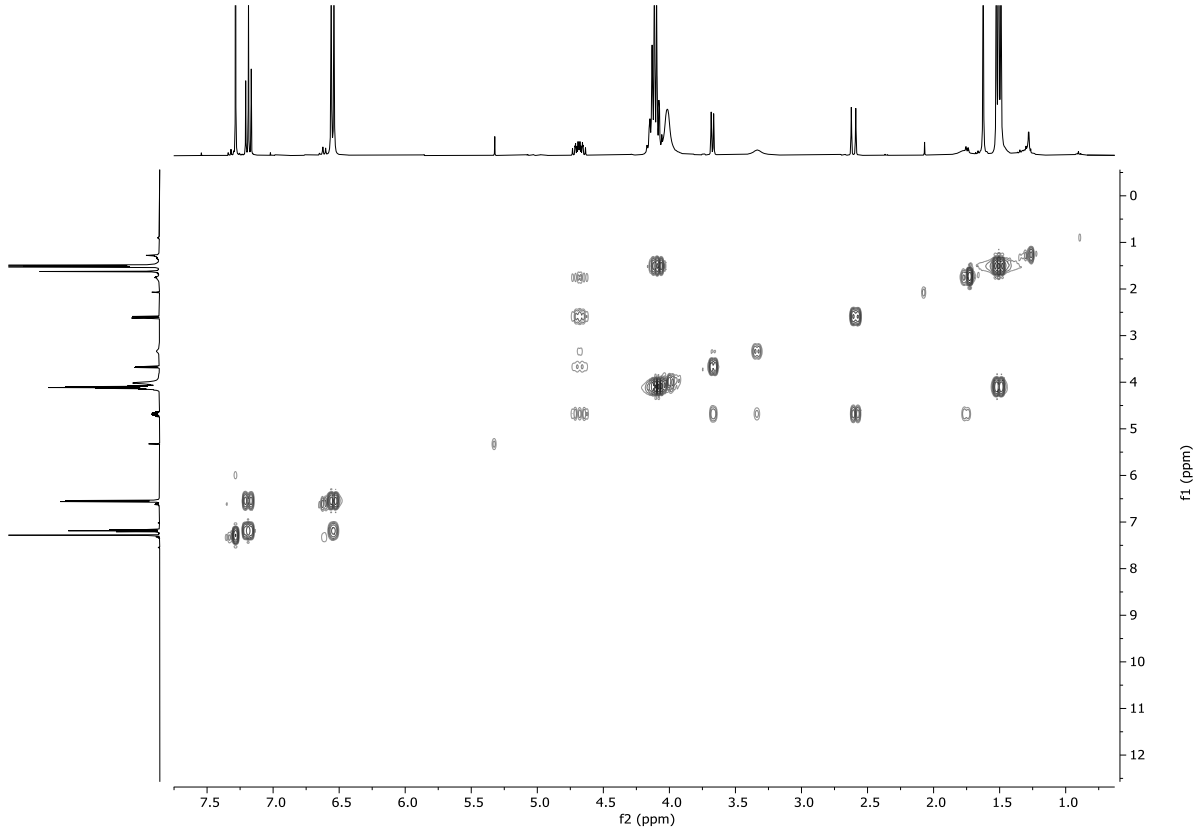

Figure A120: ^{1}H, ^{1}H-COSY NMR (400 MHz) spectrum of 3-52 in $CDCl_3$ at 278 K (5°C)

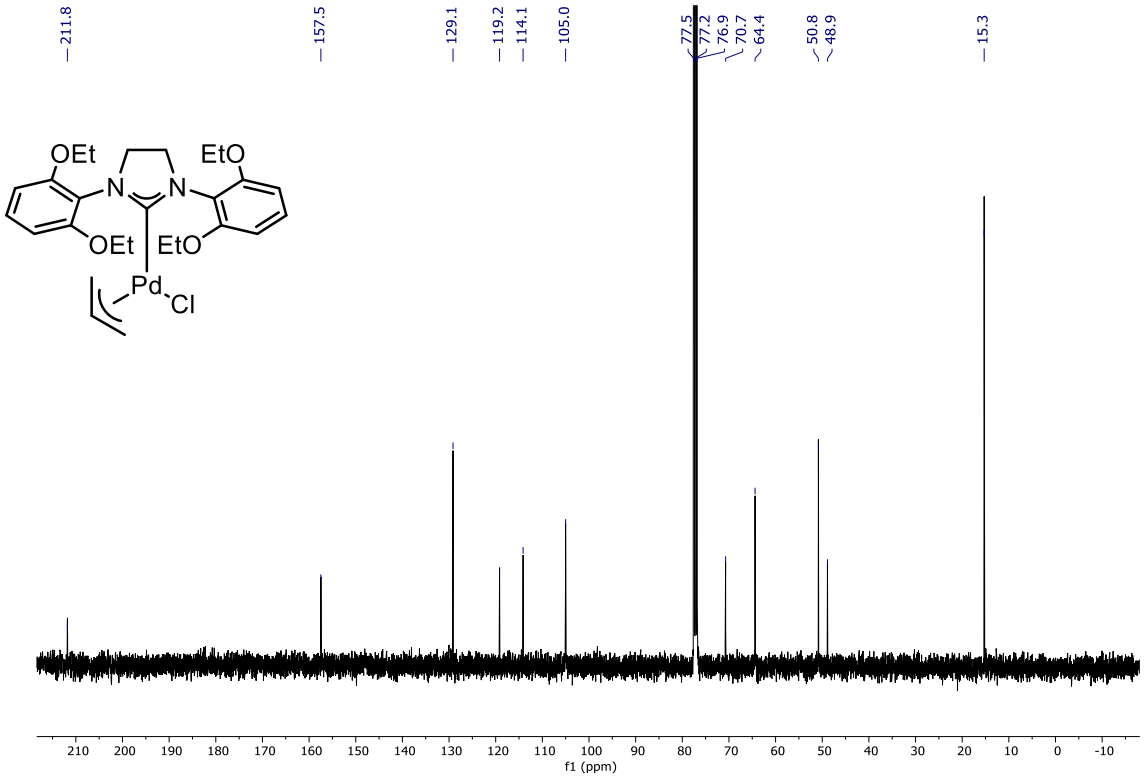

Figure A121: $^{13}C\{^{1}H\}$ NMR spectrum of 3-52 in $CDCl_3$ at 101 MHz

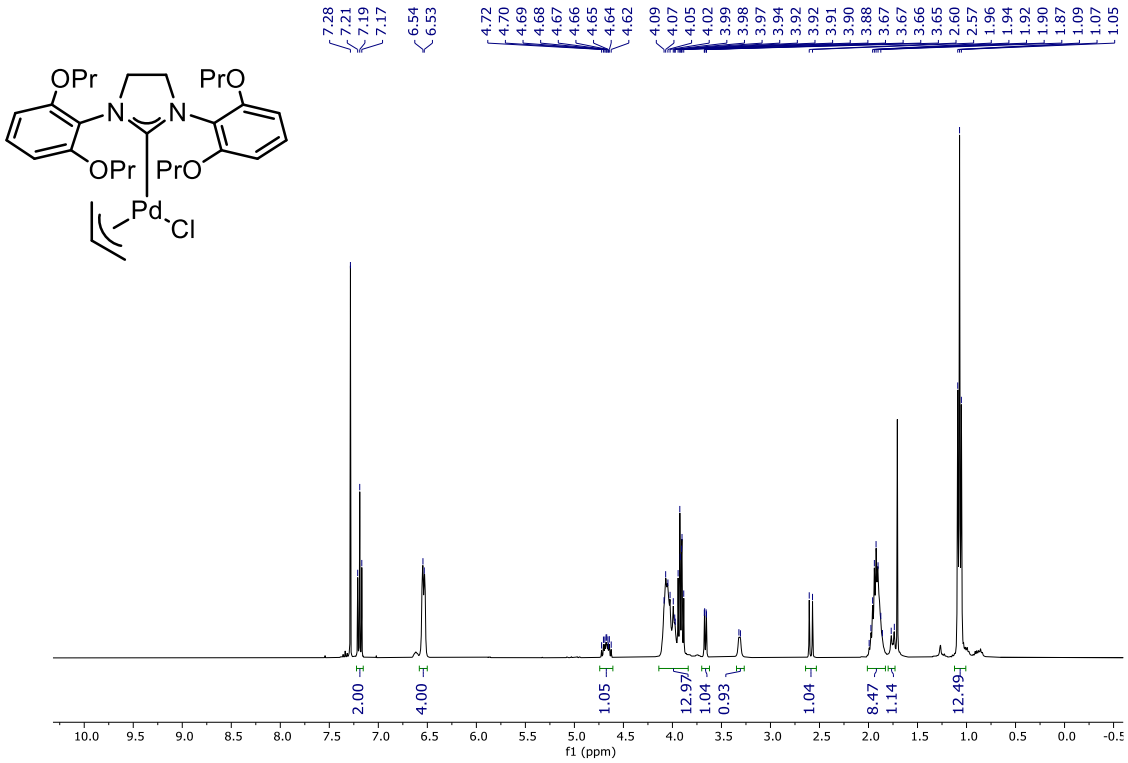

Figure A122: ^{1}H NMR spectrum of 3-53 in $CDCl_3$ at 400 MHz

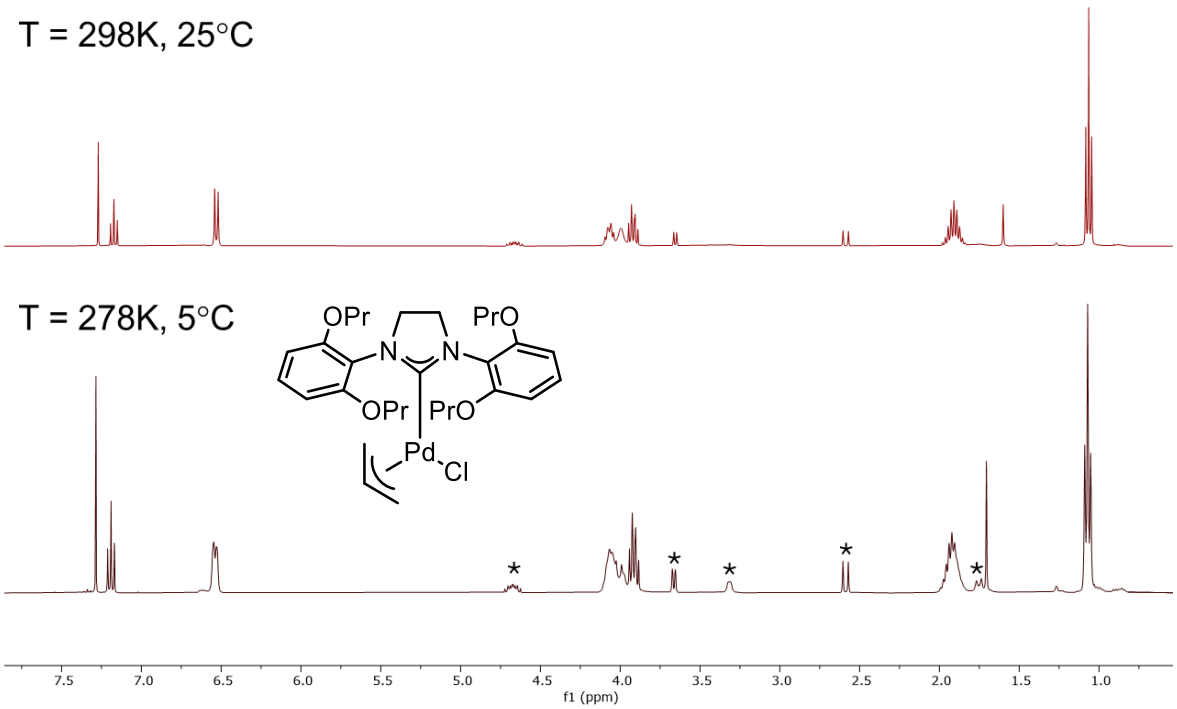

Figure A123: VT-^{1}H NMR spectrum of 3-53 in $CDCl_3$ at 400 MHz *(*denotes allyl peaks)*

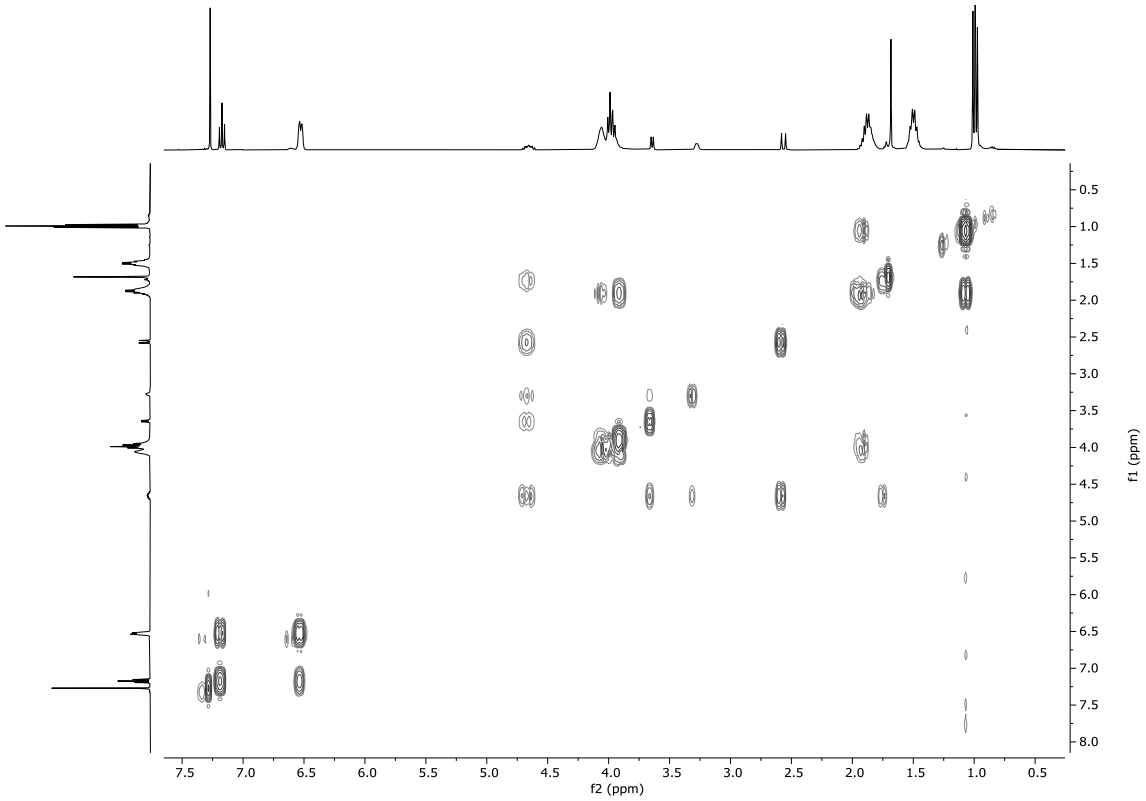

Figure A124: ^{1}H, ^{1}H-COSY NMR (400 MHz) spectrum of 3-53 in $CDCl_3$ at 278 K (5°C)

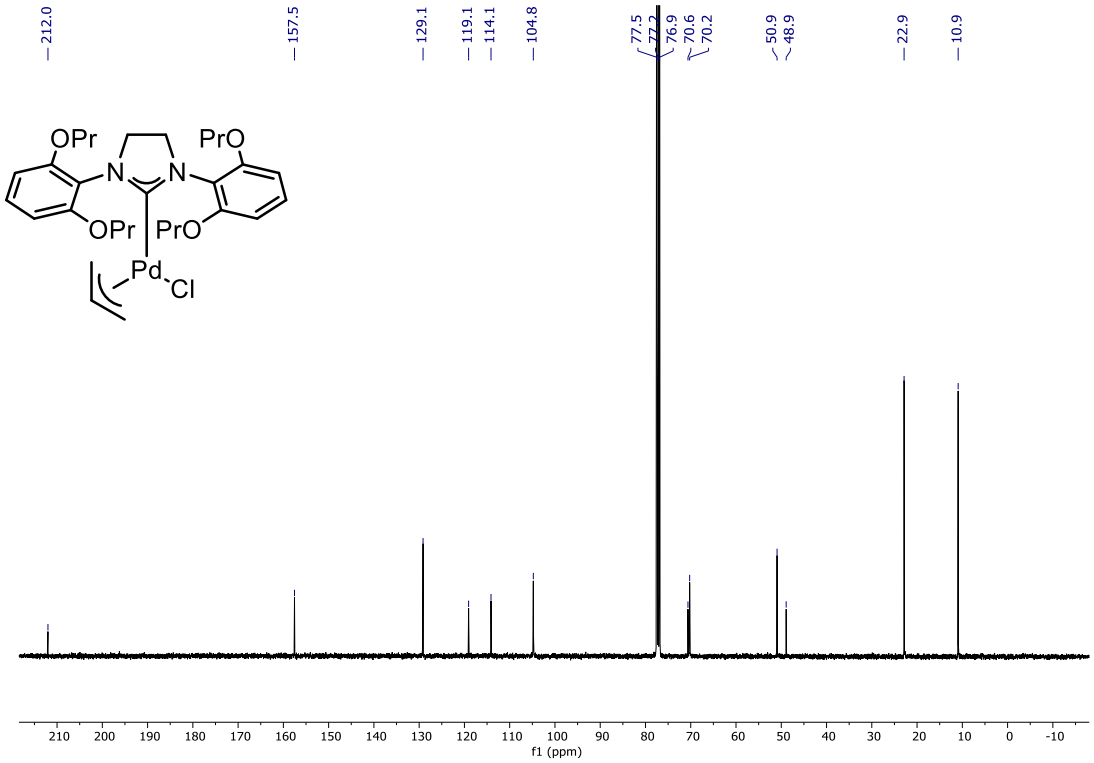

Figure A125: $^{13}C\{^{1}H\}$ NMR spectrum of 3-53 in $CDCl_3$ at 101 MHz

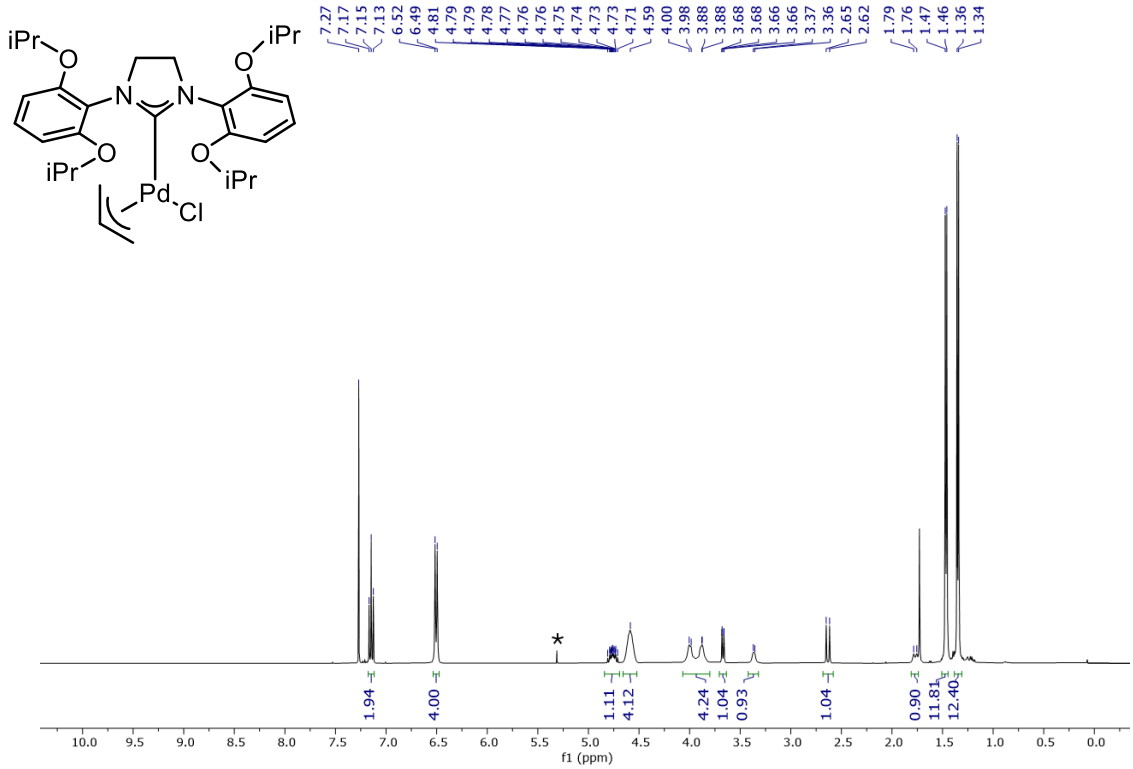

Figure A126: ^{1}H NMR spectrum of 3-54 in $CDCl_3$ at 400 MHz *(*denotes residual CH_2Cl_2)*

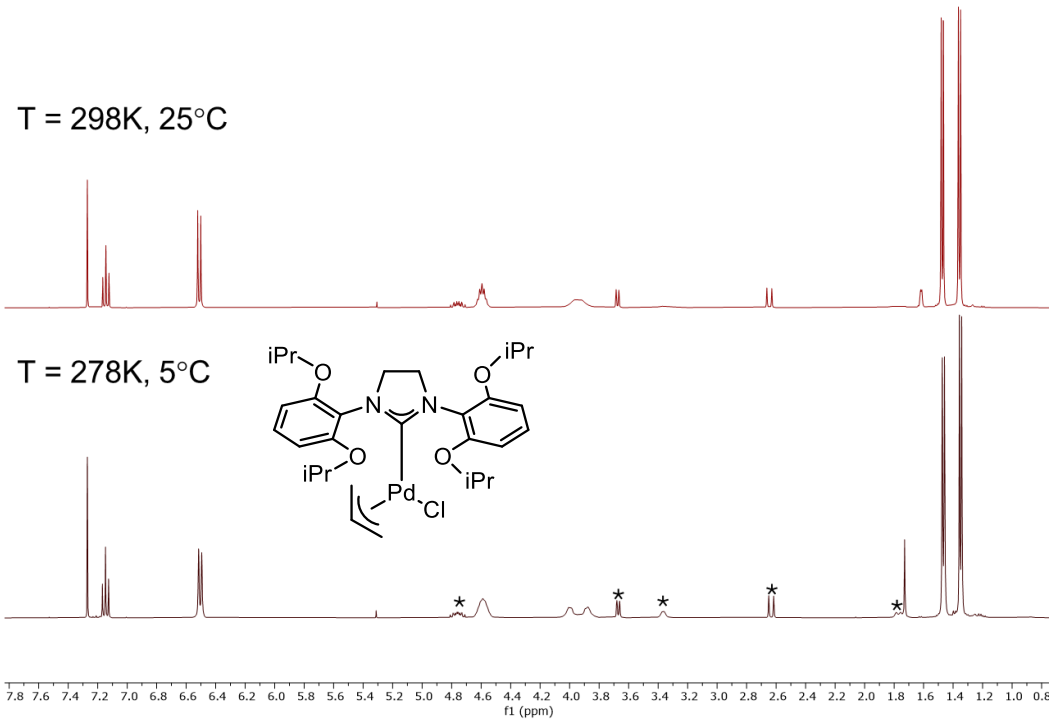

Figure A127: VT-^{1}H NMR spectrum of 3-54 in $CDCl_3$ at 400 MHz *(*denotes allyl peaks)*

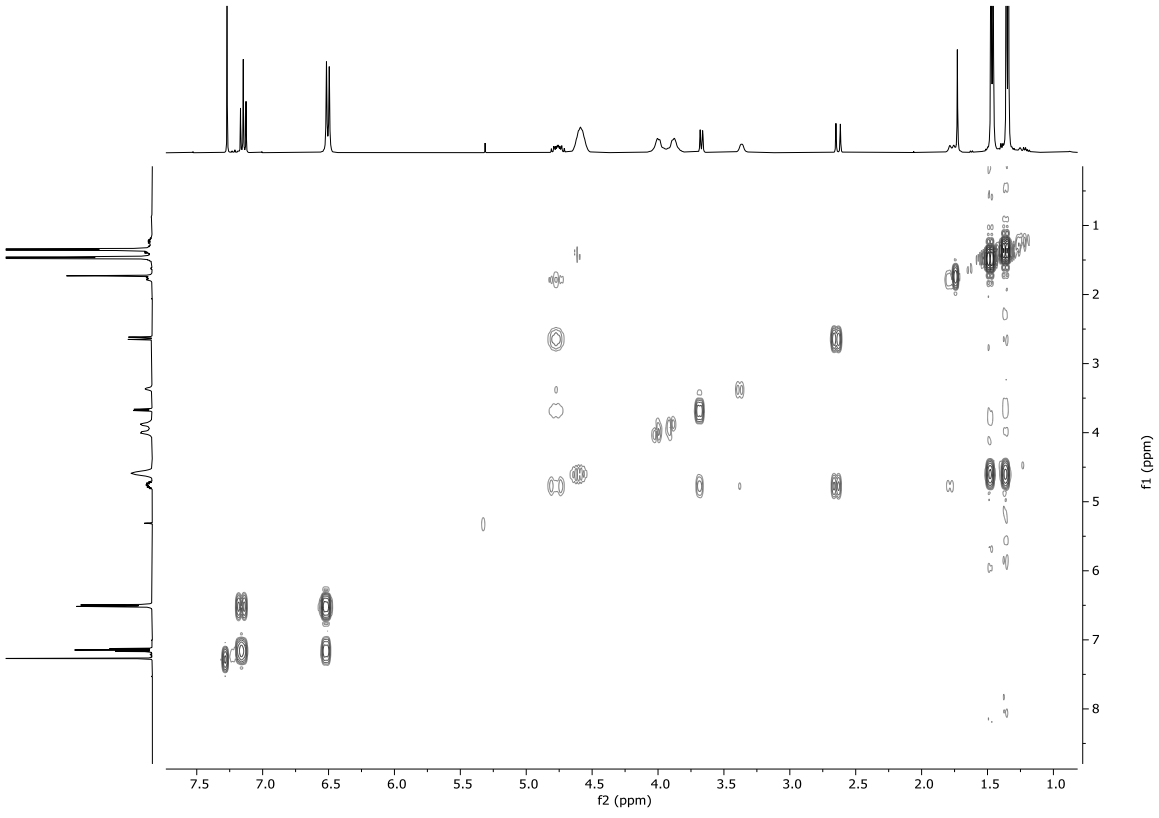

Figure A128: ^{1}H, ^{1}H-COSY NMR (400 MHz) spectrum of 3-54 in $CDCl_3$ at 278 K (5°C)

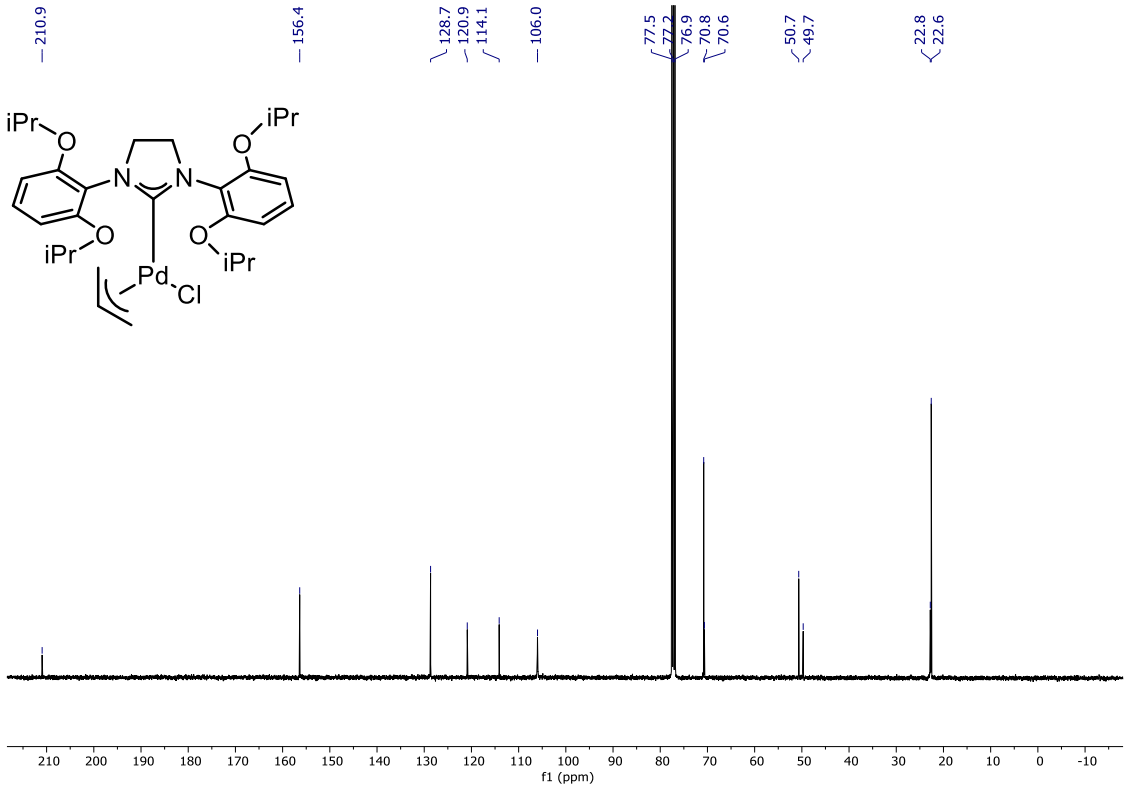

Figure A129: $^{13}C\{^{1}H\}$ NMR spectrum of 3-54 in $CDCl_3$ at 101 MHz

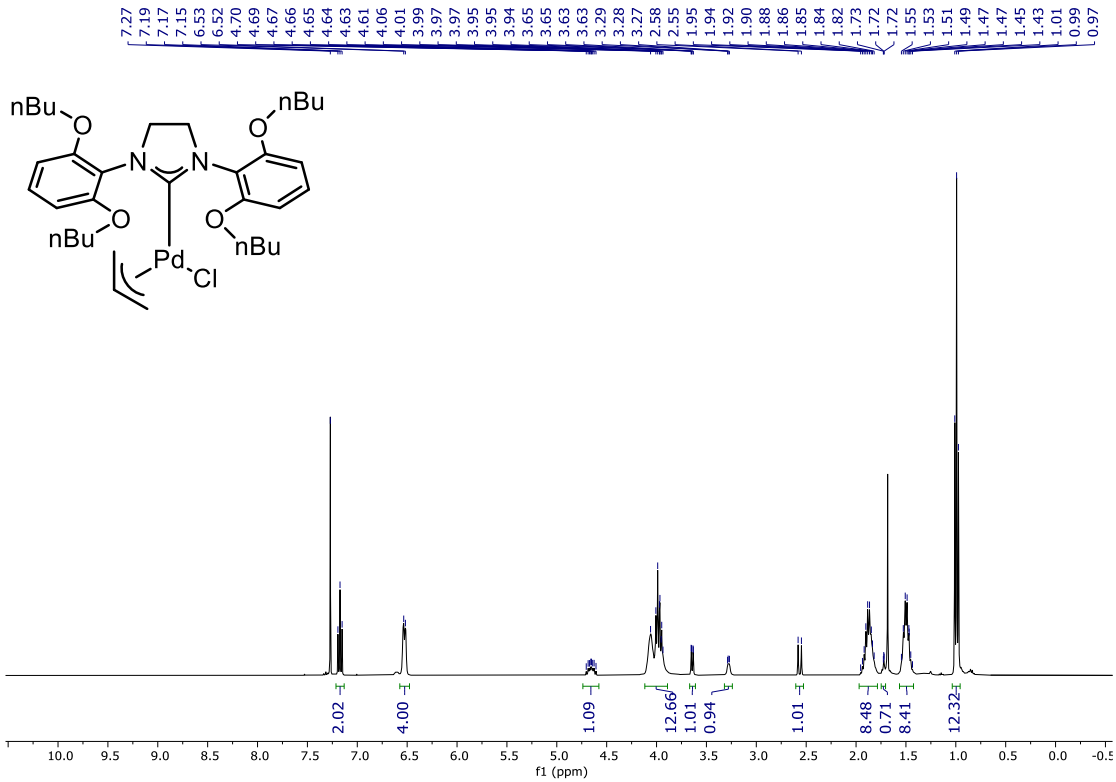

Figure A130: ^{1}H NMR spectrum of 3-55 in $CDCl_3$ at 400 MHz

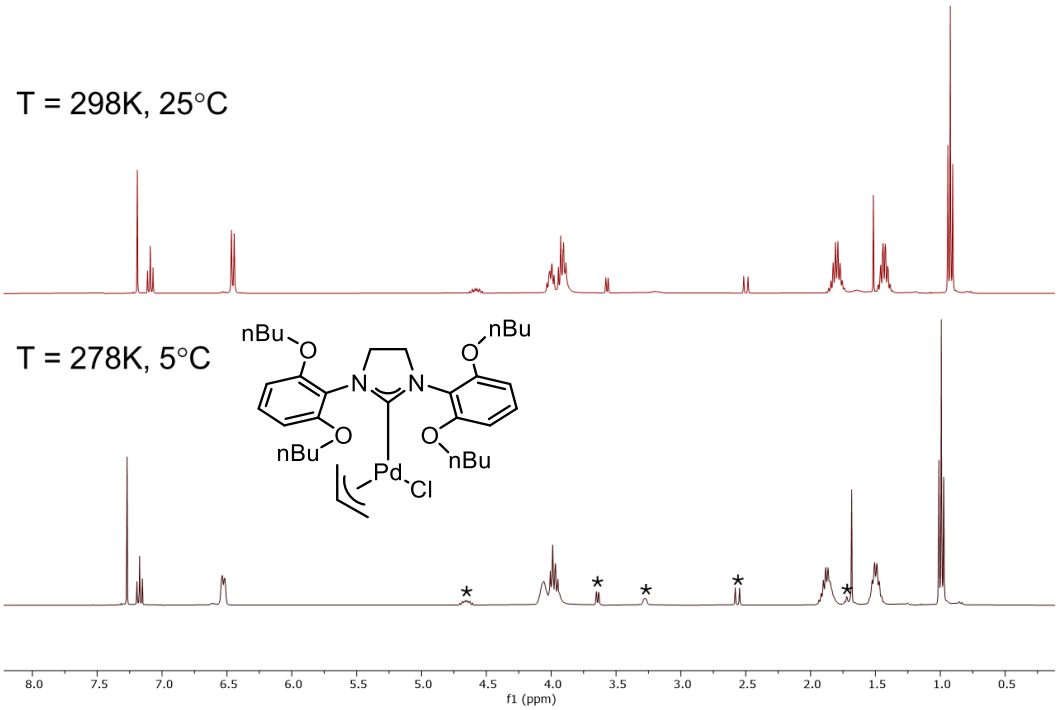

Figure A131: VT-^{1}H NMR spectrum of 11e in $CDCl_3$ at 400 MHz *(*denotes allyl peaks)*

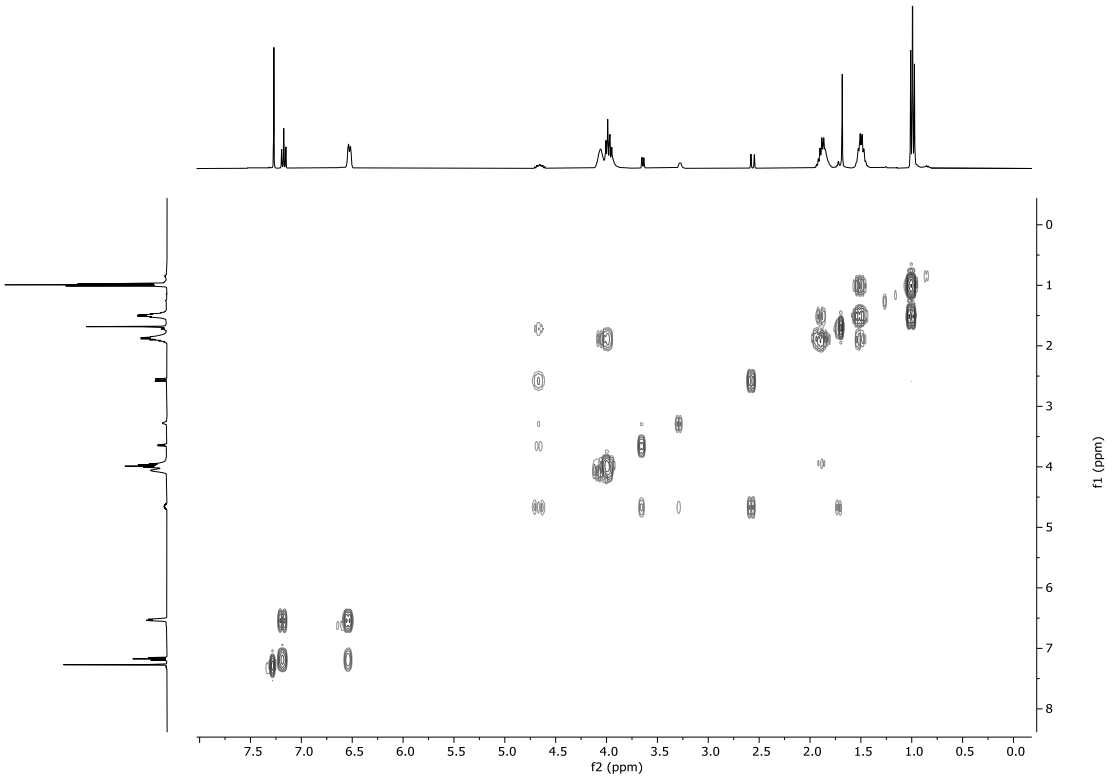

Figure A132: ^{1}H, ^{1}H-COSY NMR (400 MHz) spectrum of 11e in $CDCl_3$ at 278 K (5°C)

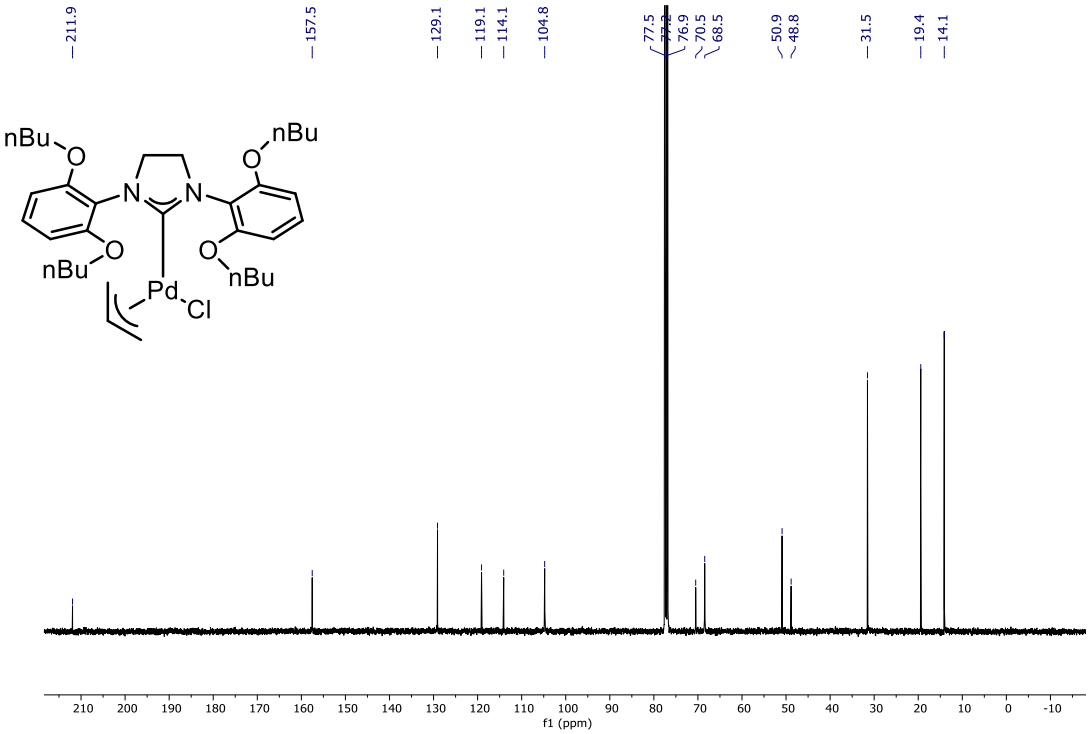

Figure A133: $^{13}C\{^{1}H\}$ NMR spectrum of 3-55 in $CDCl_3$ at 101 MHz

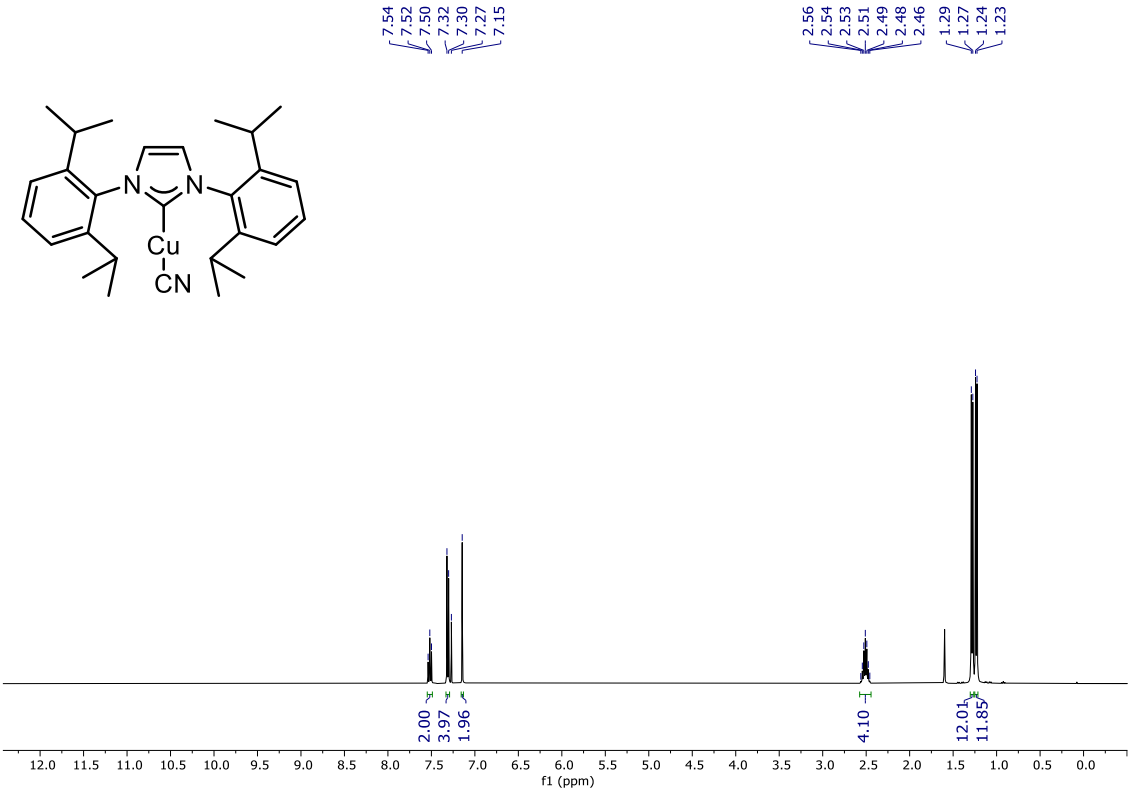

Figure A134: ^{1}H NMR spectrum of 4-1 in $CDCl_3$ at 400 MHz

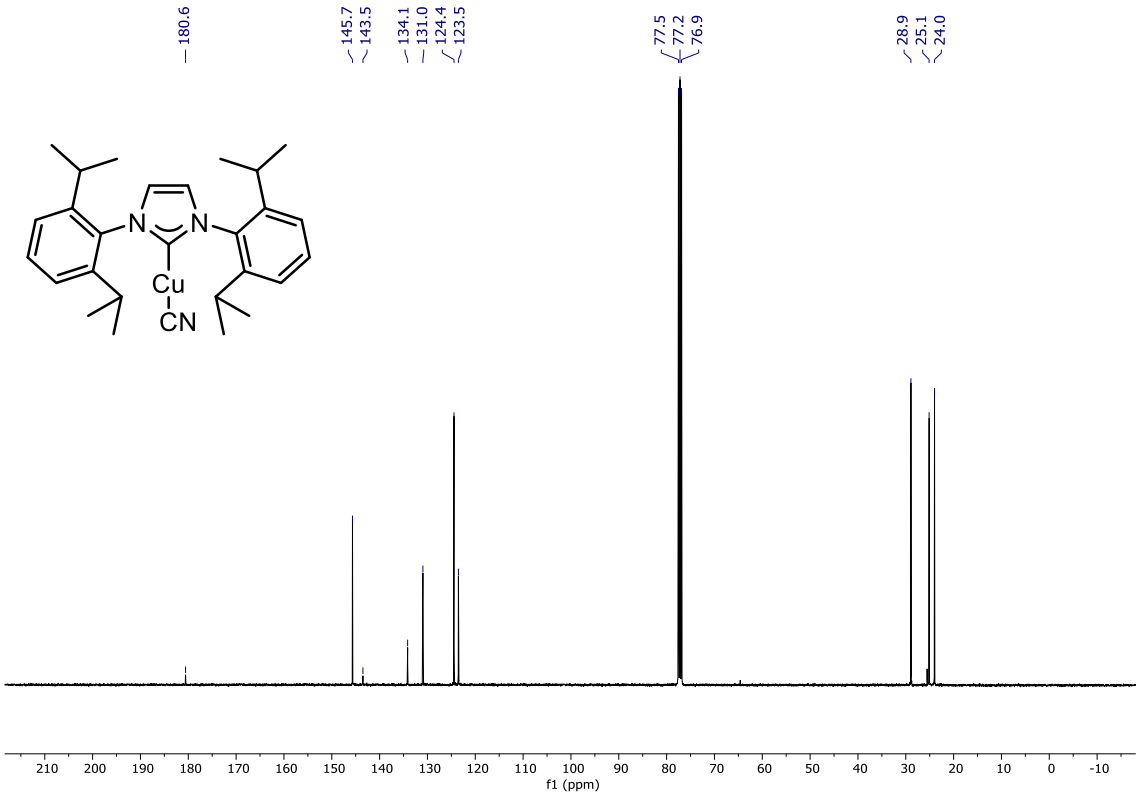

Figure A135: $^{13}C\{^{1}H\}$ NMR spectrum of 4-1 in $CDCl_3$ at 101 MHz

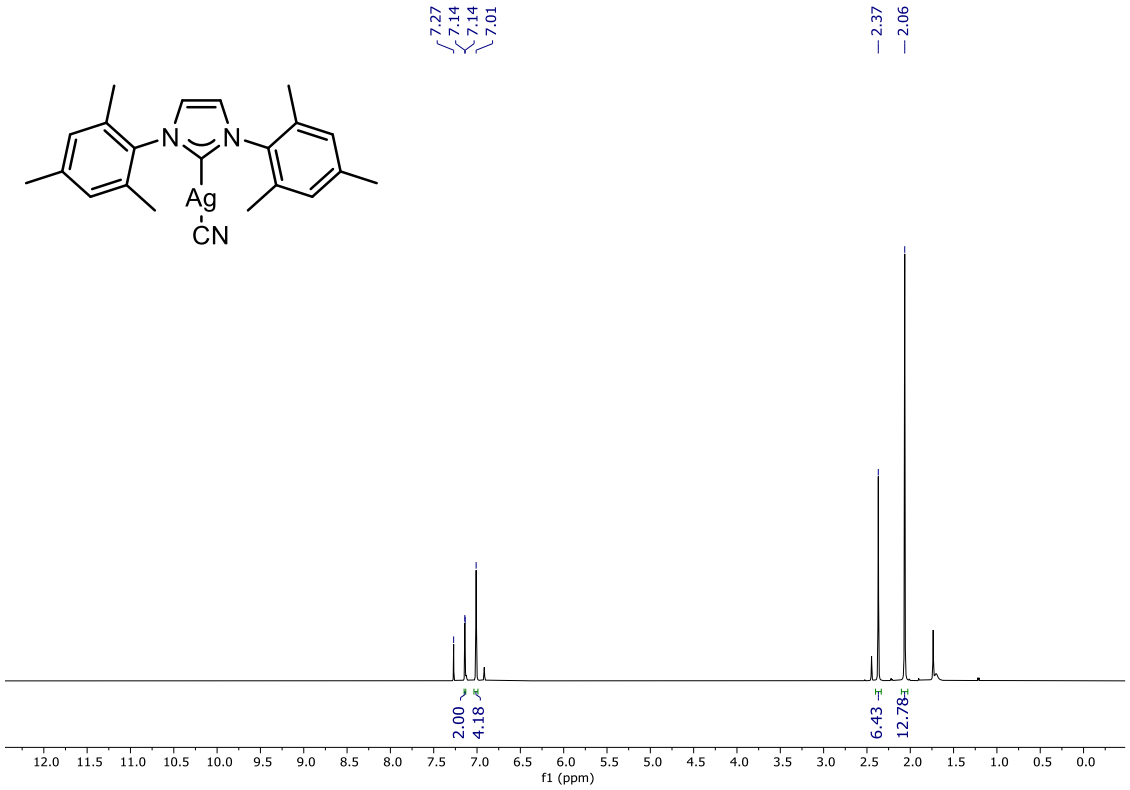

Figure A136: ^{1}H NMR spectrum of 4-9 in $CDCl_3$ at 400 MHz

Figure A137: $^{13}C\{^{1}H\}$ NMR spectrum of 4-9 in $CDCl_3$ at 101 MHz

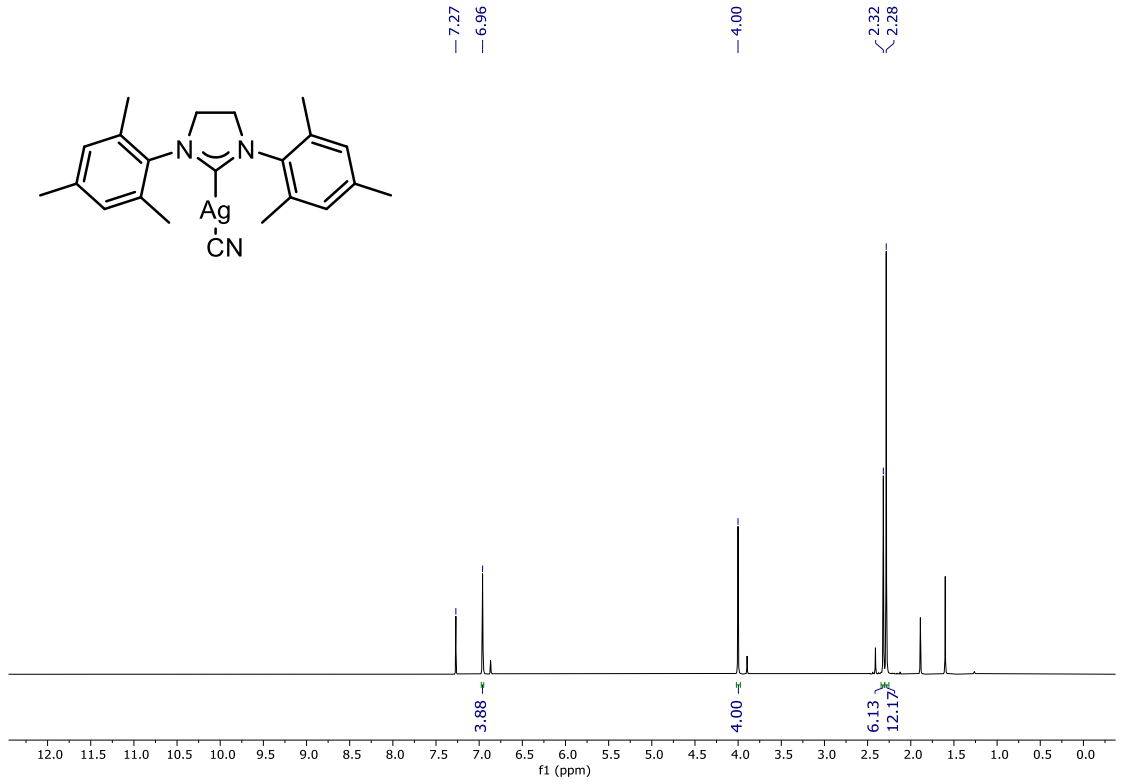

Figure A138: ^{1}H NMR spectrum of 4-10 in $CDCl_3$ at 400 MHz

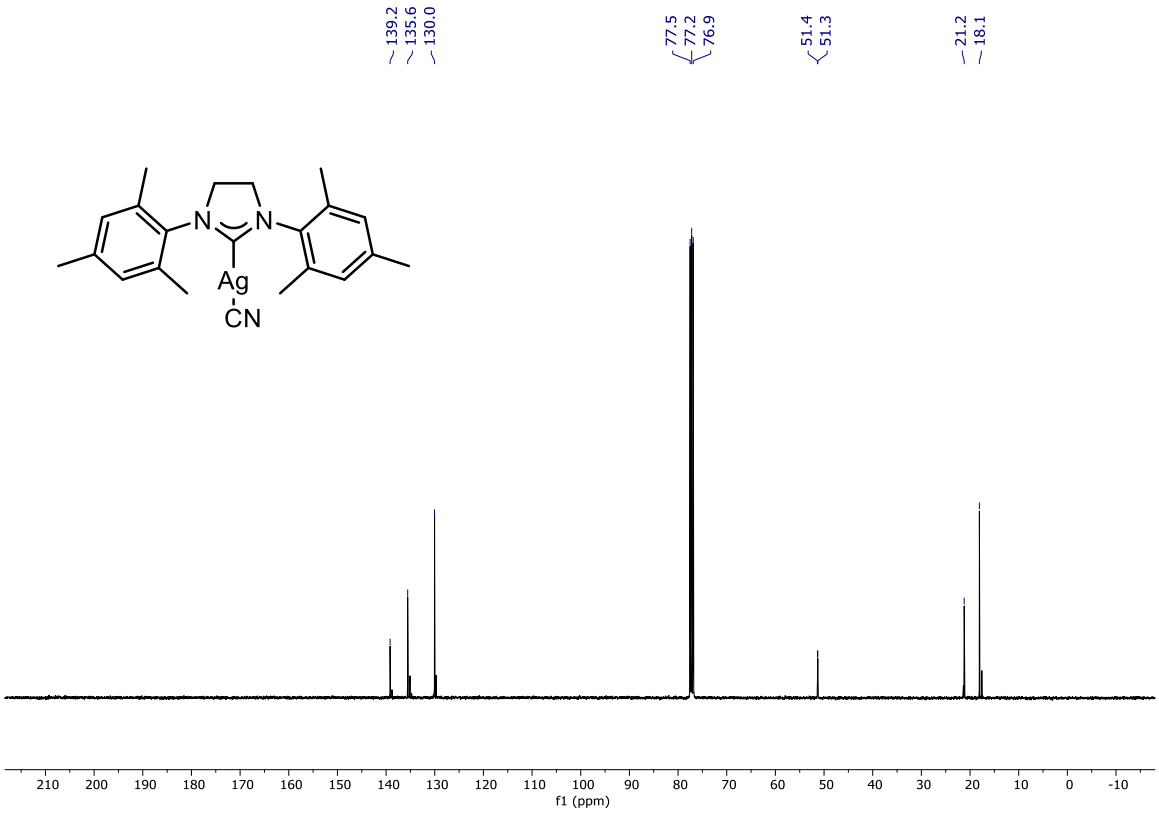

Figure A139: $^{13}C\{^{1}H\}$ NMR spectrum of 4-10 in $CDCl_3$ at 101 MHz

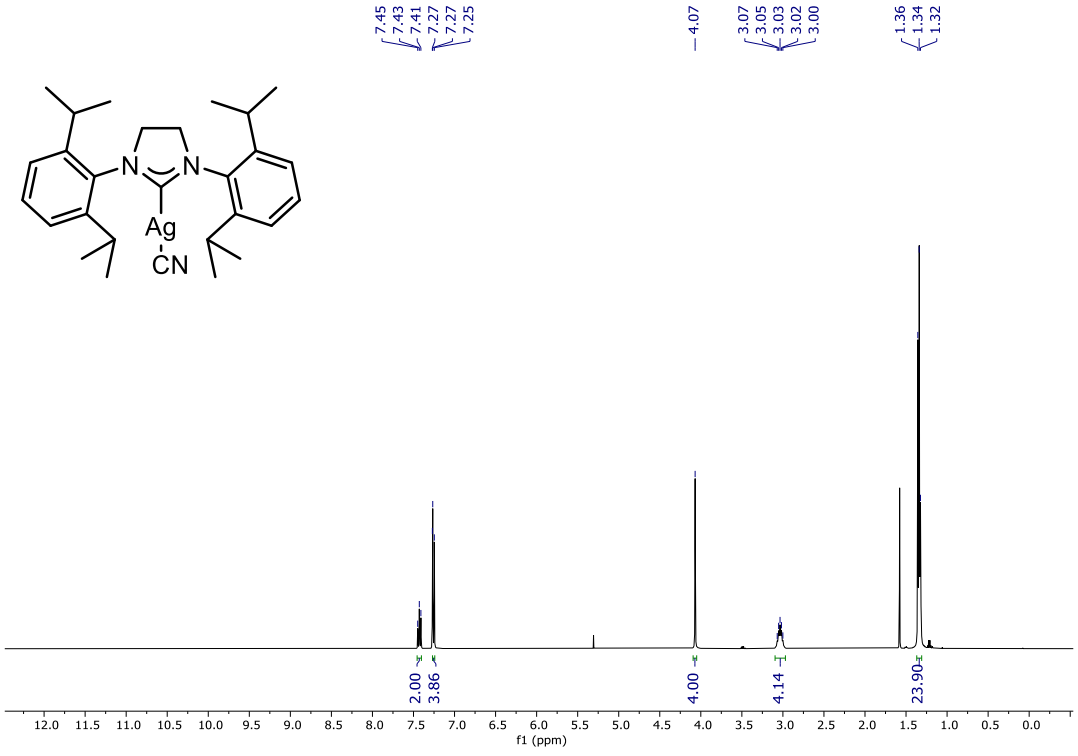

Figure A140: ^{1}H NMR spectrum of 4-11 in $CDCl_3$ at 400 MHz

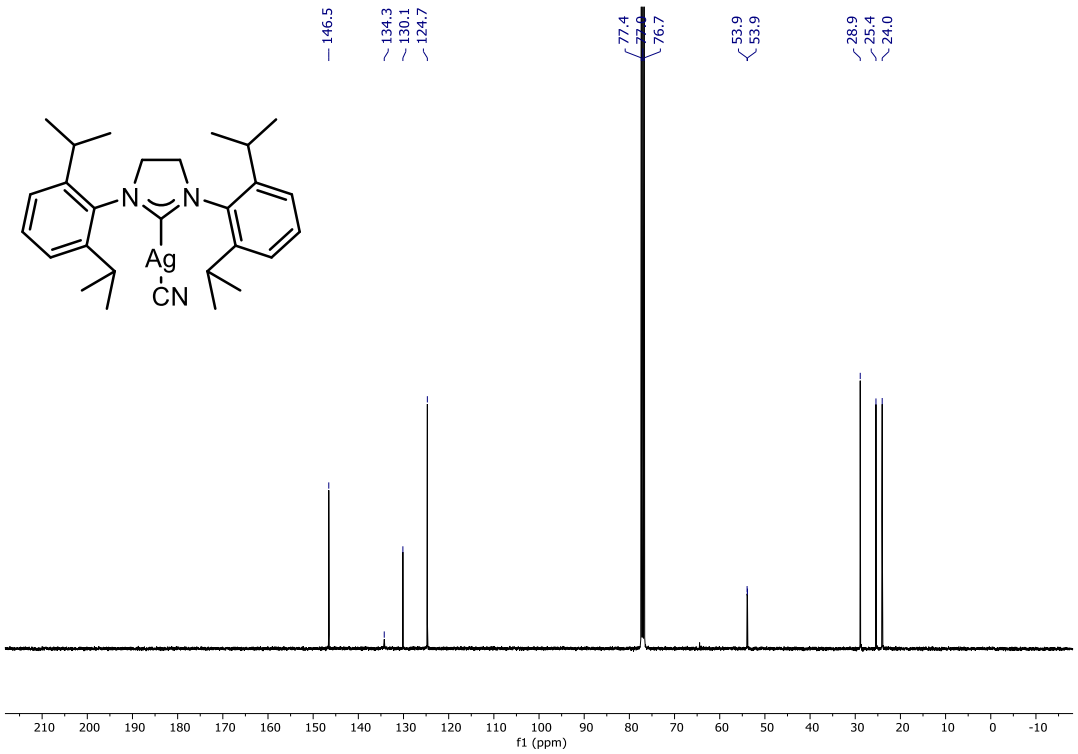

Figure A141: $^{13}C\{^{1}H\}$ NMR spectrum of 4-11 in $CDCl_3$ at 101 MHz

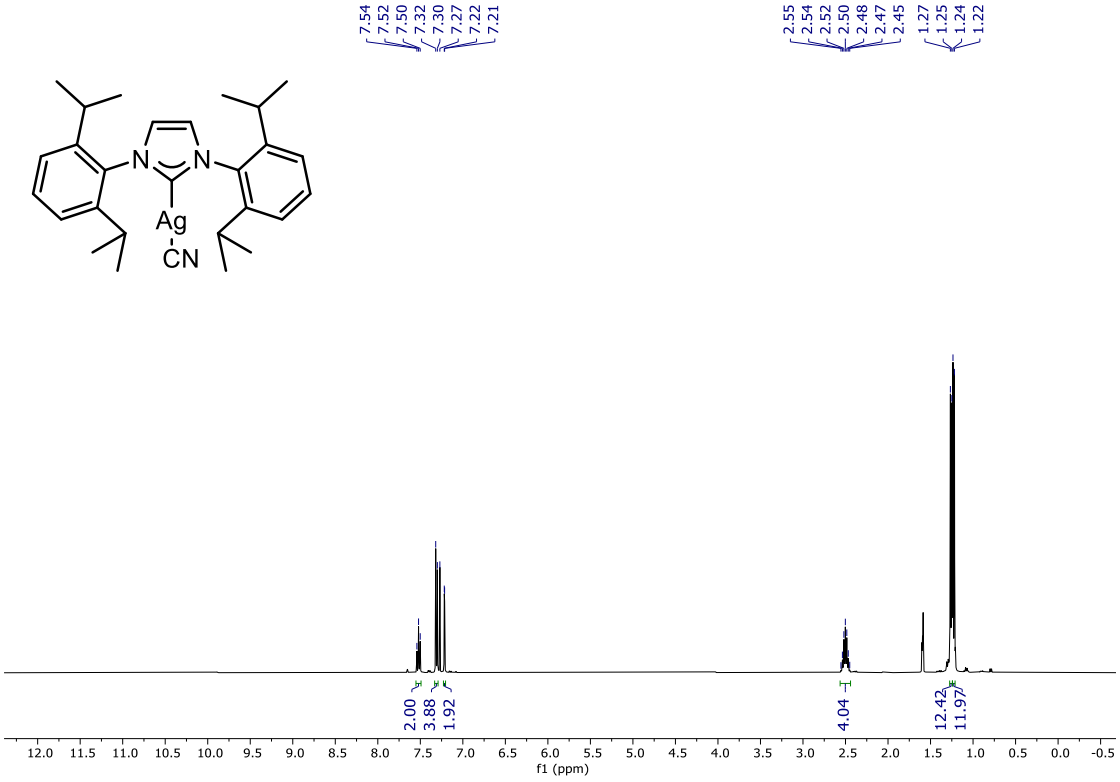

Figure A142: ^{1}H NMR spectrum of 4-16 in $CDCl_3$ at 400 MHz

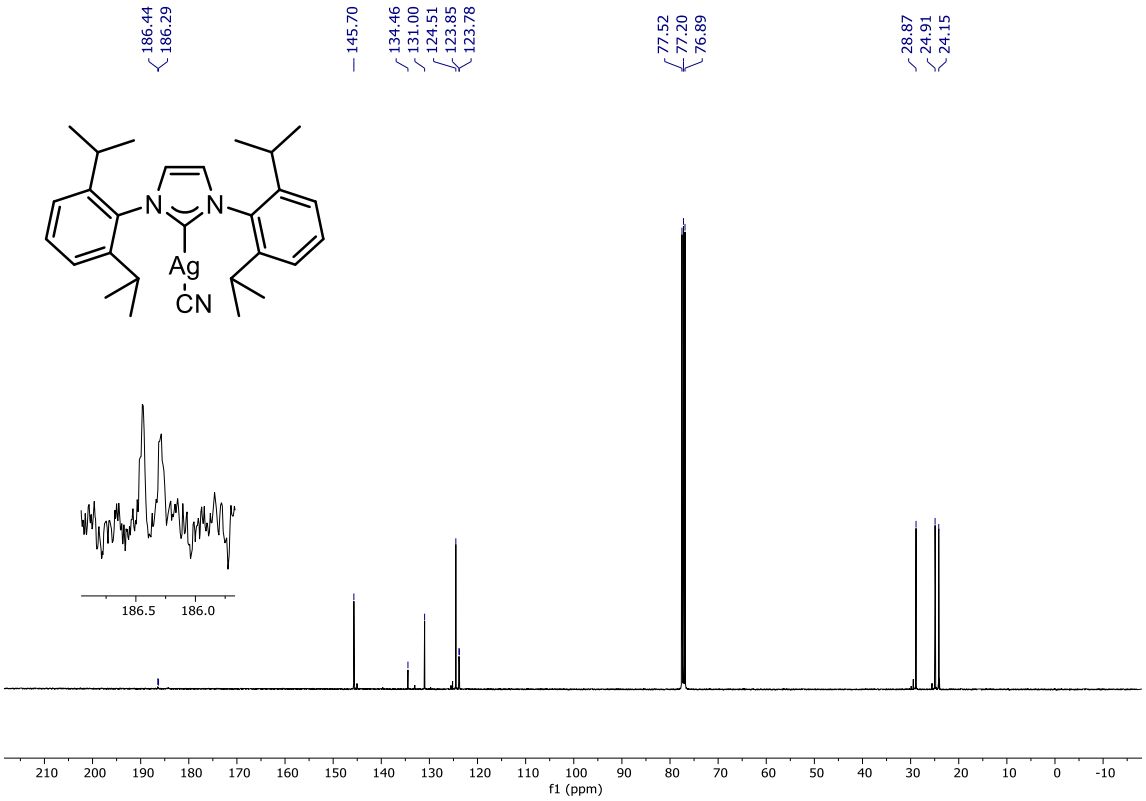

Figure A143: $^{13}C\{^{1}H\}$ NMR spectrum of 4-16 in $CDCl_3$ at 101 MHz

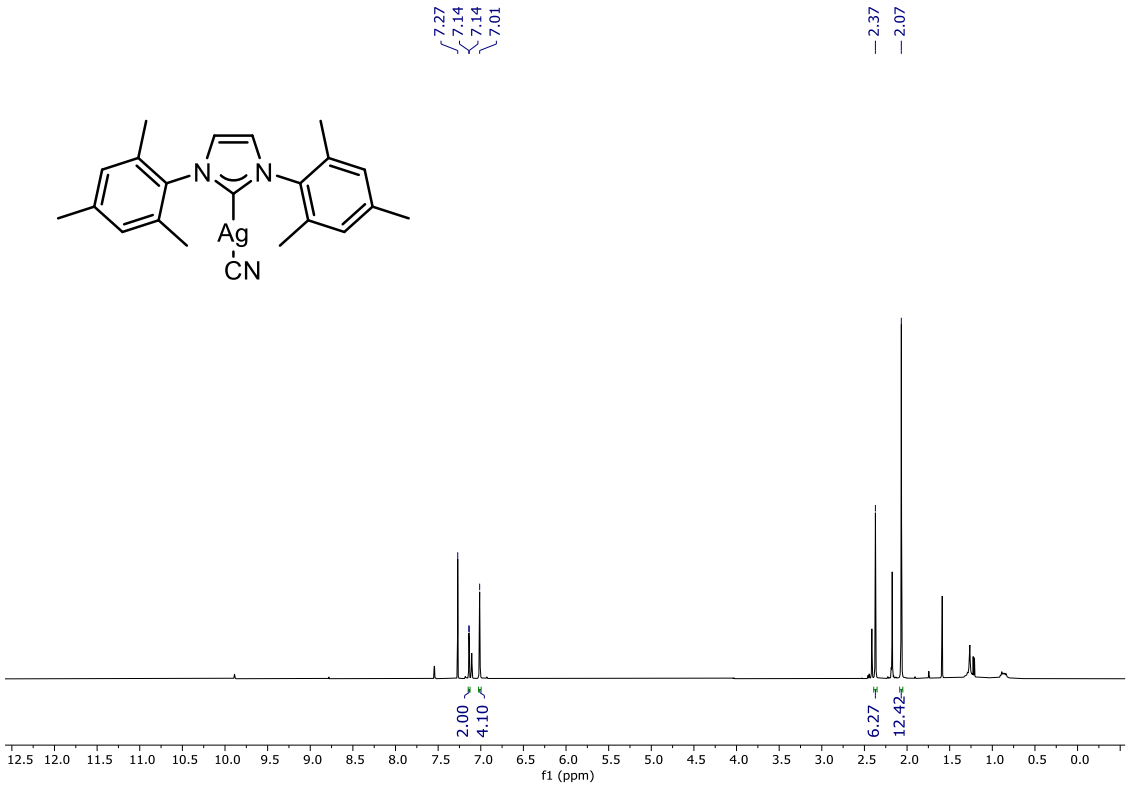

Figure A144: ^{1}H NMR spectrum of 4-17 in $CDCl_3$ at 400 MHz

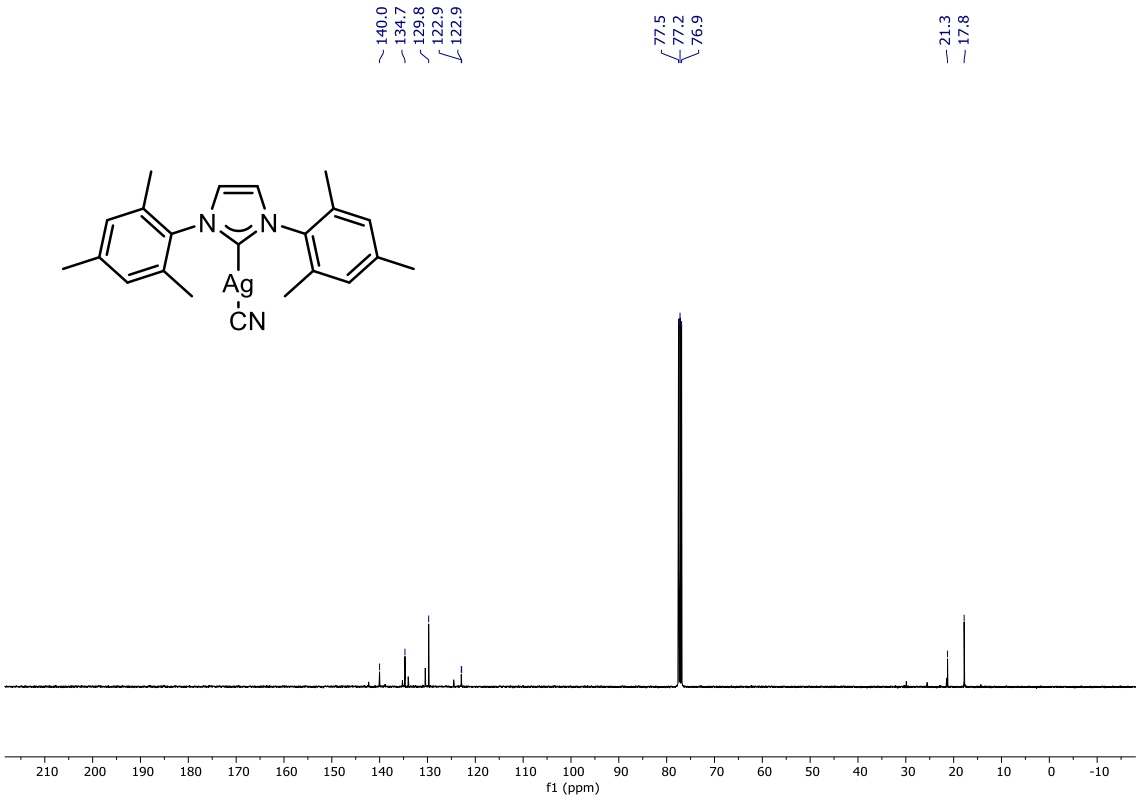

Figure A145: $^{13}C\{^{1}H\}$ NMR spectrum of 4-17 in $CDCl_3$ at 101 MHz

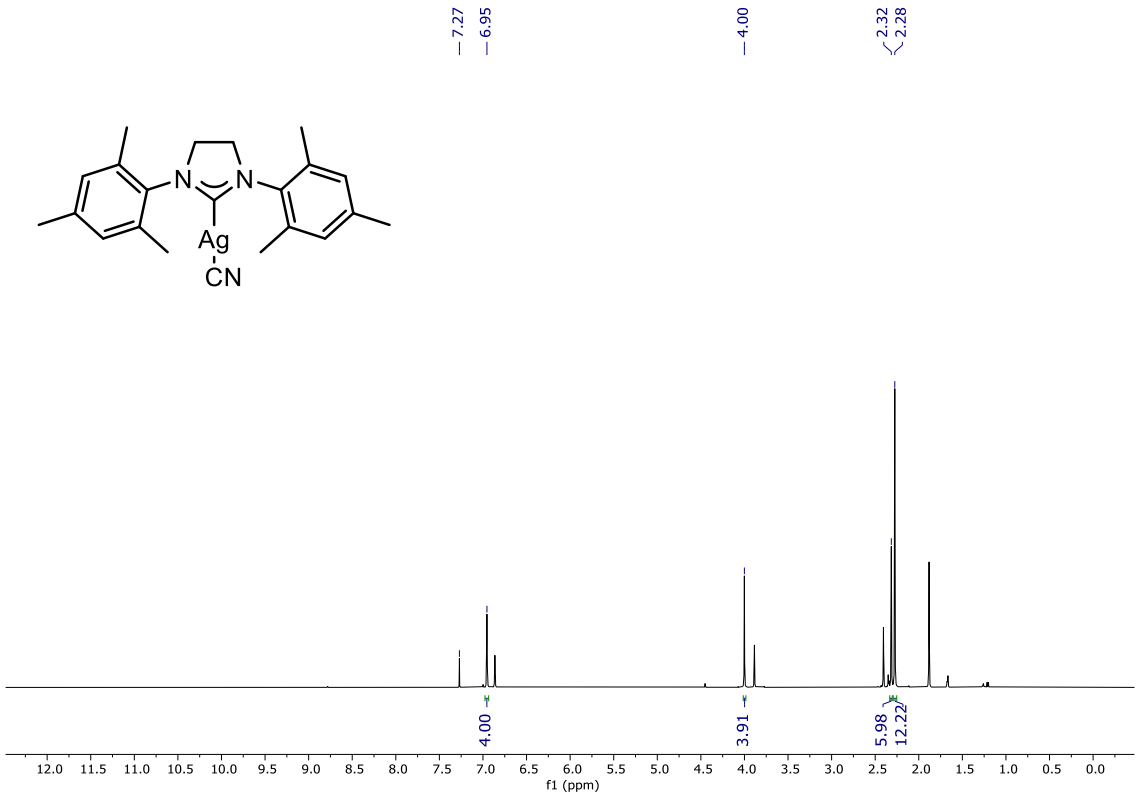

Figure A146: ^{1}H NMR spectrum of 4-18 in $CDCl_3$ at 400 MHz

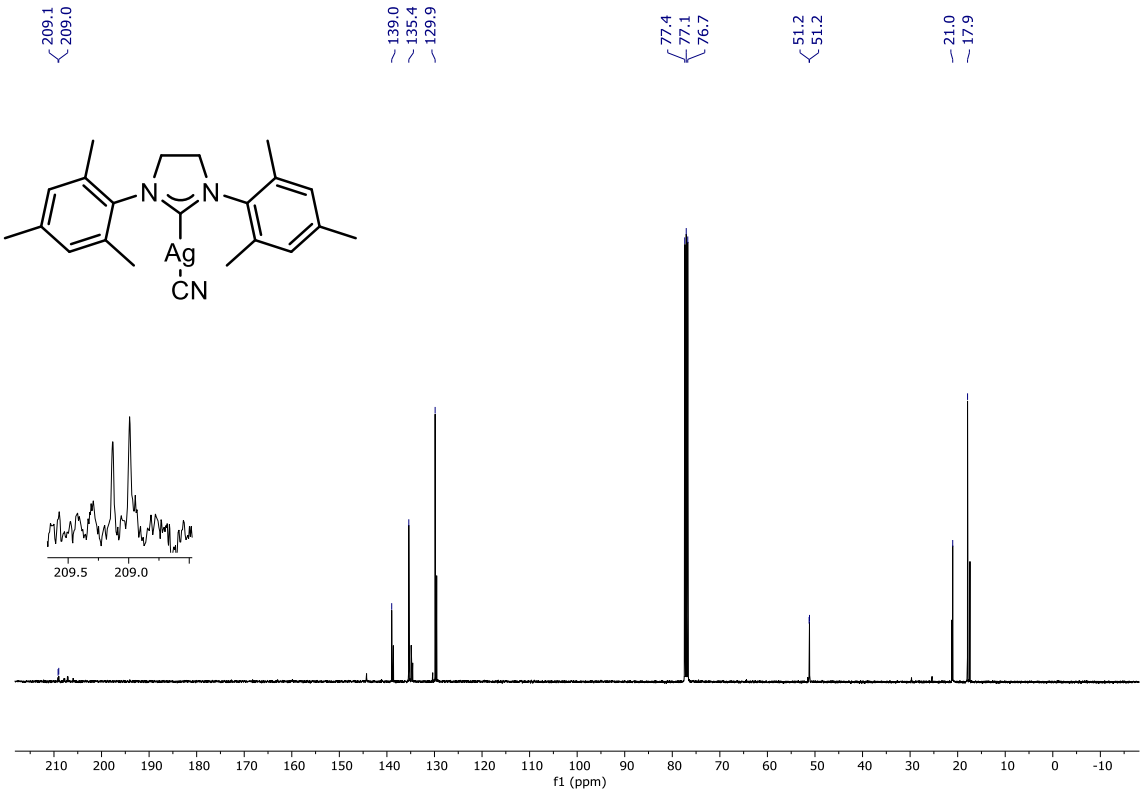

Figure A147: $^{13}C\{^{1}H\}$ NMR spectrum of 4-18 in $CDCl_3$ at 101 MHz

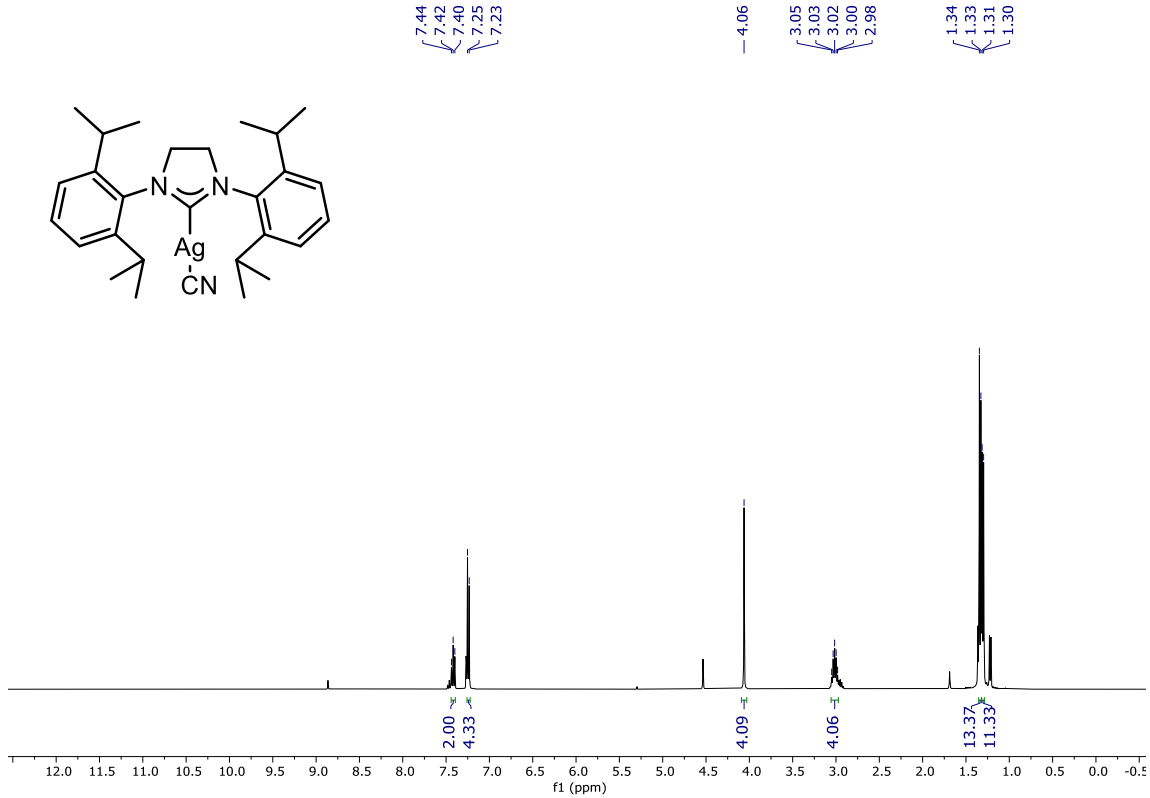

Figure A148: $^{13}C\{^{1}H\}$ NMR spectrum of 4-19 in $CDCl_3$ at 400 MHz

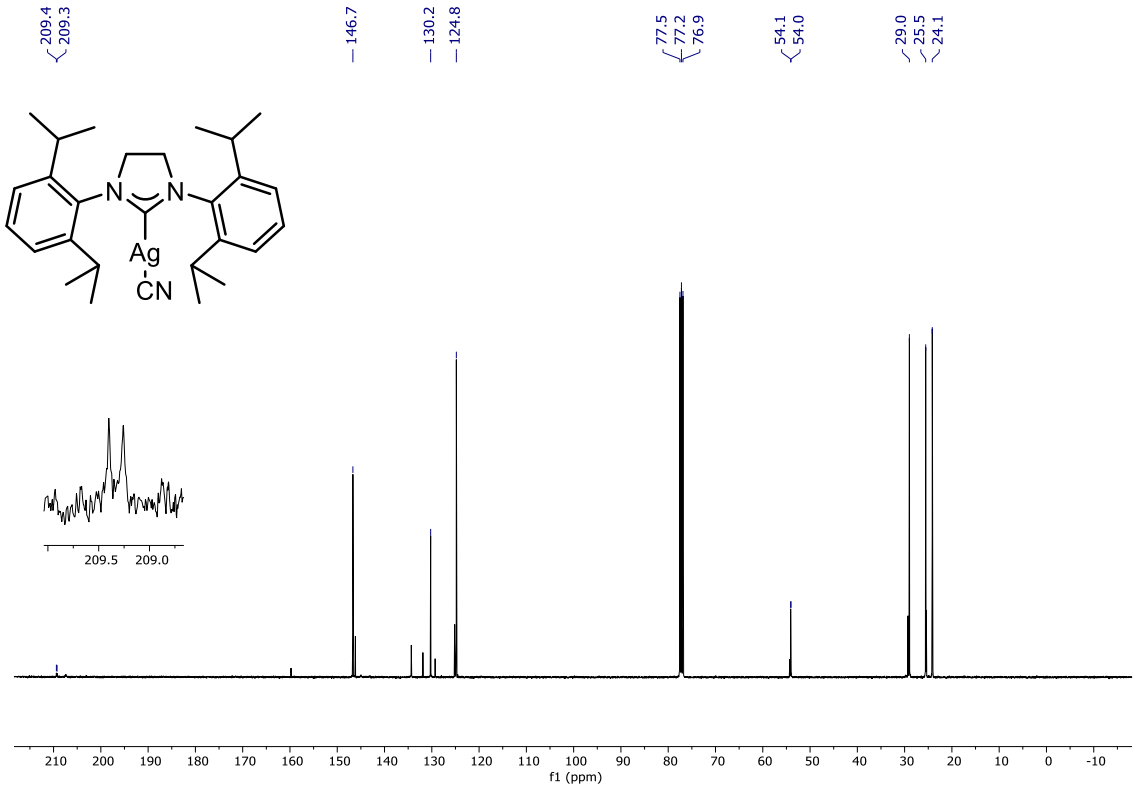

Figure A149: $^{13}C\{^{1}H\}$ NMR spectrum of 4-19 in $CDCl_3$ at 101 MHz

Appendix B: Crystallographic Data

Crystallographic Data for [Cu(NHC)X] in Chapter 3

Complex	**3-33**	**3-34**	**3-35**	**3-36**	**3-44**
Empirical formula	$C_{19}H_{22}Cl_1Cu_1N_2O_4$	$C_{23}H_{30}Cl_1Cu_1N_2O_4$	$C_{27}H_{38}Cl_1Cu_1N_2O_4$	$C_{27}H_{38}Cl_1Cu_1N_2O_4$	$C_{23}H_{30}I_1Cu_1N_2O_4$
Formula weight	441.37	497.48	553.59	553.58	588.93
Temperature	173(2) K	173(2) K	173(2) K	173(2) K	173(2) K
Wavelength	0.71073	0.71073	0.71073	0.71073	0.71073
Crystal System	Monoclinic	Orthorhombic	Orthorhombic	Monoclinic	Monoclinic
Space Group	C 1 2/c 1	P n n a	P b c n	C 2/c	P 21/n
Hall Group	-C 2yc	-P 2a 2bc	-P 2n 2ab	-C 2yc	-P 2yn
Unit Cell Dimensions	a= 16.2946(5) b= 9.5622(3) c= 13.8134(4) α= 90 β= 111.2900(10) γ= 90	a= 9.4420(2) b= 16.0648(4) c= 16.3280(4) α= 90 β= 90 γ= 90	a= 16.1902(8) b= 9.5239(5) c= 18.2825(9) α= 90 β= 90 γ= 90	a= 17.6793(7) b= 9.6888(3) c= 16.5397(5) α= 90 β= 91.1890(10) γ= 90	a= 10.3183(3) b= 14.8253(4) c= 17.3937(5) α= 90 β= 104.7150(10) γ= 90
Volume	2005.41(11)	2476.69(10)	2819.0(2)	2832.50(17)	2573.48(13)
Z	4	4	4	4	4
Density (calculated)	1.462	1.334	1.304	1.298	1.520
F (000)	912.0	1040.0	1168.0	1168.0	1184.0
Crystal Size	0.25 x 0.25 x 0.25 mm^3	0.25 x 0.25 x 0.25 mm^3	0.075 x 0.075 x 0.075 mm^3	0.15 x 0.05 x 0.05 mm^3	0.25 x 0.25 x 0.2 mm^3
Theta range for data collection	2.683 – 33.251	2.492 – 30.501	2.228 – 27.518	2.304 – 28.279	1.831 – 33.142
Index Ranges	-25<=h<=23, -14<=k<=14, -21<=l<=21	-12<=h<=13, -22<=k<=22, -23<=l<=23	-20<=h<=21, -12<=k<=12, -23<=l<=23	-23<=h<=23, -12<=k<=12, -22<=l<=22	-15<=h<=15, -22<=k<=22, -26<=l<=26
Reflections Collected	27879	36516	43300	35182	70687
Independent Reflections/ R_{int}	3853/0.0338	3779/0.0451	3242/0.0912	3520/0.0572	9813
Data / Restraints / Parameters	3853 / 0 / 126	3779 / 0 / 194	3242 / 0 / 162	3520 / 6 / 194	9813 / 0 / 284
Goodness-of-fit on F^2	1.055	1.140	1.278	1.055	1.056

Final R Indices [I>2sigma(I)]	R1 = 0.0326 wR2 = 0.0929	R1 = 0.0592 wR2 = 0.1356	R1 = 0.1086 wR2 = 0.2109	R1 = 0.0365 wR2 = 0.0821	R1 = 0.0434 wR2 = 0.0740
R Indices (all data)	R1 = 0.0442 wR2 = 0.0988	R1 = 0.0785 wR2 = 0.1473	R1 = 0.1329 wR2 = 0.2207	R1 = 0.0539 wR2 = 0.0896	R1 = 0.0676 wR2 = 0.0873
Largest diff. peak and hole (e.Å^{-3})	0.722; -0.347	0.901; -0.810	0.790; -0.986	0.326; -0.279	1.780; -1.147

Crystallographic Data for [Ag(SIPr)CN] in Chapter 4

Complex	**4-11**
Empirical Formula	$C_{27}H_{38}ClN_2$
Formula Weight	559.95
Temperature	173(2) K
Wavelength	0.71073
Crystal System	Orthorhombic
Space Group	P c c n
Hall Group	-P 2ab 2 ac
Unit Cell Dimensions	a= 10.8422(3) b= 12.5514(3) c= 20.1634(5) α= 90 β= 90 γ= 90
Volume	2743.93(12)
Z	4
Density (calculated)	1.292
F (000)	1112.0
Mu (mm^{-1})	0.847
h, k, l_{max}	15, 17, 28
N_{ref}	4212
T_{min}, T_{max}	0.703, 0.746
Theta (max)	30.569

Calculations using SambVca 2.1

Topography maps (**Figure 3-5** in this document) were generated using SambVca 2.1 web application.[54] For complexes 3-33, 3-34, and 3-35 .xyz files were generated using Mercury[156] of the .cif files from the X-ray structures obtained and submitted directly. In the case of 3-36, which displayed some positional disorder in one of the isopropyl groups, two positional isomers were

separated into individual structures (below), and **isomer 2** was submitted to SambVca calculations for simplicity.

Isomer 1:

Cu	8.753850000000	5.146880000000	4.134030000000
Cu	8.753850000000	5.146880000000	4.134030000000
Cl	8.753850000000	3.030560000000	4.134030000000
O	7.869110000000	7.907420000000	7.433820000000
N	9.192400000000	7.823610000000	5.117270000000
O	11.761220000000	6.976130000000	5.047990000000
C	8.753850000000	7.037940000000	4.134030000000
C	9.824230000000	7.348570000000	6.302420000000
C	11.134650000000	6.893580000000	6.258430000000
C	11.742930000000	6.435300000000	7.420100000000
H	12.636210000000	6.112830000000	7.401390000000
C	11.030480000000	6.456620000000	8.602930000000
H	11.447560000000	6.136050000000	9.393930000000
C	9.735670000000	6.925550000000	8.678500000000
H	9.270360000000	6.932870000000	9.506660000000
C	9.124560000000	7.388680000000	7.517000000000
C	7.053180000000	7.980670000000	8.619130000000
H	7.605350000000	8.305940000000	9.386950000000
C	6.481020000000	6.621330000000	8.945890000000
H	5.909080000000	6.322250000000	8.208640000000
H	5.950860000000	6.679500000000	9.768030000000
H	7.212140000000	5.981560000000	9.072970000000
C	5.987960000000	8.996050000000	8.297500000000
H	6.409540000000	9.850420000000	8.068500000000
H	5.406180000000	9.116980000000	9.076650000000
H	5.455190000000	8.680550000000	7.537770000000
C	9.020730000000	9.261520000000	4.853190000000
H	9.881920000000	9.745230000000	4.918330000000
H	8.370210000000	9.667660000000	5.479180000000
O	9.638590000000	7.907420000000	0.834250000000
N	8.315300000000	7.823610000000	3.150800000000
O	5.746480000000	6.976130000000	3.220080000000
C	7.683470000000	7.348570000000	1.965650000000
C	6.373050000000	6.893580000000	2.009640000000
C	4.933250000000	5.836530000000	3.628030000000
H	5.195880000000	5.029450000000	3.098900000000
C	5.764770000000	6.435300000000	0.847970000000
H	4.871490000000	6.112830000000	0.866680000000
C	6.477220000000	6.456620000000	-0.334860000000
H	6.060140000000	6.136050000000	-1.125860000000
C	7.772030000000	6.925550000000	-0.410430000000
H	8.237330000000	6.932870000000	-1.238590000000

C	8.383140000000	7.388680000000	0.751070000000
C	10.454520000000	7.980670000000	-0.351060000000
H	9.902350000000	8.305940000000	-1.118880000000
C	11.026680000000	6.621330000000	-0.677820000000
H	11.598620000000	6.322250000000	0.059430000000
H	11.556830000000	6.679500000000	-1.499960000000
H	10.295560000000	5.981560000000	-0.804900000000
C	11.519740000000	8.996050000000	-0.029430000000
H	11.098160000000	9.850420000000	0.199580000000
H	12.101520000000	9.116980000000	-0.808580000000
H	12.052500000000	8.680550000000	0.730300000000
C	8.486970000000	9.261520000000	3.414880000000
H	7.625780000000	9.745230000000	3.349740000000
H	9.137490000000	9.667660000000	2.788890000000
C	3.467060000000	6.137860000000	3.399830000000
H	3.193720000000	6.883980000000	3.973980000000
H	2.932490000000	5.345920000000	3.617330000000
H	3.325300000000	6.379950000000	2.460810000000
C	5.184210000000	5.588500000000	5.079900000000
H	6.087450000000	5.227060000000	5.197290000000
H	4.527940000000	4.944580000000	5.419010000000
H	5.101870000000	6.430440000000	5.573570000000
C	12.961270000000	6.230870000000	4.742560000000
C	13.557530000000	6.928460000000	3.527160000000
H	12.837770000000	6.943150000000	2.735560000000
H	14.430740000000	6.400310000000	3.205490000000
H	13.823020000000	7.932040000000	3.786490000000
C	12.636280000000	4.835680000000	4.557360000000
H	11.905060000000	4.739660000000	3.782120000000
H	12.243700000000	4.436800000000	5.469330000000
H	13.519330000000	4.297080000000	4.283440000000
H	13.689270000000	6.222290000000	5.526680000000

Isomer 2:

Cu	8.753850000000	5.146880000000	4.134030000000
Cu	8.753850000000	5.146880000000	4.134030000000
Cu	8.753850000000	5.146880000000	4.134030000000
Cl	8.753850000000	3.030560000000	4.134030000000
O	7.869110000000	7.907420000000	7.433820000000
N	9.192400000000	7.823610000000	5.117270000000
O	11.761220000000	6.976130000000	5.047990000000
C	8.753850000000	7.037940000000	4.134030000000
C	9.824230000000	7.348570000000	6.302420000000
C	11.134650000000	6.893580000000	6.258430000000
C	12.574450000000	5.836530000000	4.640040000000
C	11.742930000000	6.435300000000	7.420100000000

H	12.636210000000	6.112830000000	7.401390000000
C	11.030480000000	6.456620000000	8.602930000000
H	11.447560000000	6.136050000000	9.393930000000
C	9.735670000000	6.925550000000	8.678500000000
H	9.270360000000	6.932870000000	9.506660000000
C	9.124560000000	7.388680000000	7.517000000000
C	7.053180000000	7.980670000000	8.619130000000
H	7.605350000000	8.305940000000	9.386950000000
C	6.481020000000	6.621330000000	8.945890000000
H	5.909080000000	6.322250000000	8.208640000000
H	5.950860000000	6.679500000000	9.768030000000
H	7.212140000000	5.981560000000	9.072970000000
C	5.987960000000	8.996050000000	8.297500000000
H	6.409540000000	9.850420000000	8.068500000000
H	5.406180000000	9.116980000000	9.076650000000
H	5.455190000000	8.680550000000	7.537770000000
C	9.020730000000	9.261520000000	4.853190000000
H	9.881920000000	9.745230000000	4.918330000000
H	8.370210000000	9.667660000000	5.479180000000
C	14.040630000000	6.137860000000	4.868240000000
C	12.323480000000	5.588500000000	3.188170000000
O	9.638590000000	7.907420000000	0.834250000000
N	8.315300000000	7.823610000000	3.150800000000
O	5.746480000000	6.976130000000	3.220080000000
C	7.683470000000	7.348570000000	1.965650000000
C	6.373050000000	6.893580000000	2.009640000000
C	4.933250000000	5.836530000000	3.628030000000
H	5.195880000000	5.029450000000	3.098900000000
C	5.764770000000	6.435300000000	0.847970000000
H	4.871490000000	6.112830000000	0.866680000000
C	6.477220000000	6.456620000000	-0.334860000000
H	6.060140000000	6.136050000000	-1.125860000000
C	7.772030000000	6.925550000000	-0.410430000000
H	8.237330000000	6.932870000000	-1.238590000000
C	8.383140000000	7.388680000000	0.751070000000
C	10.454520000000	7.980670000000	-0.351060000000
H	9.902350000000	8.305940000000	-1.118880000000
C	11.026680000000	6.621330000000	-0.677820000000
H	11.598620000000	6.322250000000	0.059430000000
H	11.556830000000	6.679500000000	-1.499960000000
H	10.295560000000	5.981560000000	-0.804900000000
C	11.519740000000	8.996050000000	-0.029430000000
H	11.098160000000	9.850420000000	0.199580000000
H	12.101520000000	9.116980000000	-0.808580000000
H	12.052500000000	8.680550000000	0.730300000000
C	8.486970000000	9.261520000000	3.414880000000

H	7.625780000000	9.745230000000	3.349740000000
H	9.137490000000	9.667660000000	2.788890000000
C	3.467060000000	6.137860000000	3.399830000000
H	3.193720000000	6.883980000000	3.973980000000
H	2.932490000000	5.345920000000	3.617330000000
H	3.325300000000	6.379950000000	2.460810000000
C	5.184210000000	5.588500000000	5.079900000000
H	6.087450000000	5.227060000000	5.197290000000
H	4.527940000000	4.944580000000	5.419010000000
H	5.101870000000	6.430440000000	5.573570000000
H	14.424670000000	6.691090000000	4.036770000000
H	14.582180000000	5.220300000000	4.966850000000
H	14.151170000000	6.715110000000	5.762360000000
H	12.316730000000	4.971590000000	5.214810000000
H	12.585450000000	6.460930000000	2.626800000000
H	11.287760000000	5.365580000000	3.038230000000

“The only way to achieve the impossible is to believe it is possible.” – Lewis Carroll